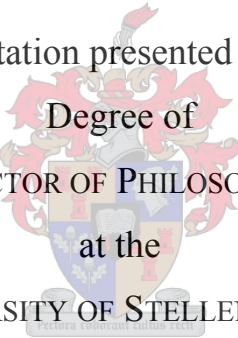


A DFT STUDY OF THE
CATALYTIC HYDROCYANATION
OF ETHYLENE WITH NICKEL COMPLEXES

GRETA HEYDENRYCH

Dissertation presented for the
Degree of
DOCTOR OF PHILOSOPHY
at the
UNIVERSITY OF STELLENBOSCH

The crest of the University of Stellenbosch is centered behind the text. It features a shield with a blue and white design, topped by a crown and surrounded by red and white decorative elements.

Promoter: Prof. Jan L. M. Dillen

Co-promoter: Prof. Helgard G. Raubenheimer

December 2005

DECLARATION

I, the undersigned, hereby declare that the work contained in this dissertation is my own original work and that I have not previously in its entirety or in part submitted it at any university for a degree.

Signature:

Date:

SUMMARY

DFT calculations employing the B3LYP functional were done to investigate the mechanism for the Ni-catalyzed hydrocyanation of ethylene as proposed by Tolman. Although this reaction is an important industrial process, its mechanism has never been studied computationally, apart from calculations pertaining to ligand tailoring.

This study comprises a detailed configurational analysis of each step of the reaction cycle, charge decomposition analysis of pertinent species and analysis of the activation barriers involved at each step. A model ligand, PH_3 , is employed, due to its electronic similarity to the experimental ligand most widely used, $\text{P}(\text{O}-o\text{-tolyl})_3$, and its small size, which makes it amenable for calculations at this level.

It was found that oxidative addition of HCN to the precursor complex $(\text{ethylene})\text{NiL}_2$ ($\text{L}=\text{PH}_3$) can take place in one step and that it is the rate-determining step in the gas phase. The resulting adduct has H^+ (which becomes a hydride) and CN^- coordinated in the *cis* configuration. Ligand dissociation yields three configurations of $(\text{ethylene})\text{-NiHCNL}$, of which only two can participate in the catalytic cycle. It is shown that this is because migration-insertion of ethylene into the Ni-H bond takes place before, or concomitant with, association of a second ethylene molecule, contrary to expectation. This path therefore requires that ethylene and hydrogen are coordinated in the *cis* configuration, something only possible for two of the three isomers of $(\text{ethylene})\text{NiHCNL}$. The calculations support the mechanism of associative reductive elimination and shows that elimination can only take place if the ethyl and cyanide groups are in the *cis* configuration.

Analysis of the energetic profile of the reaction shows that entropy effects play a very important role in the propagation of the cycle, at least in the gas phase.

Preliminary work on the effect of Lewis acids the catalytic cycle is presented, with structural and energetic analysis.

An important general conclusion is that the standard way of representing the energy profile of reactions where intermolecular transitions (as opposed to intramolecular transitions only) take place can be misleading. It will be argued that the implicit assumption that two species which are minimum energy structures on distinct potential energy surfaces will also be an energy minimum on one potential energy surface skews the energy profile of the reaction. The consequence of this is that care must be taken in representing energy profiles for reactions where more than one distinct species participates.

OPSOMMING

Die meganisme, soos deur Tolman voorgestel, van die Ni-gekataliseerde hidrosianering van etileen word ondersoek met behulp van Kohn-Sham elektrondigtheidsteorie (*density functional theory*, DFT) berekening waarin die B3LYP-funksionaal gebruik word. Alhoewel die reaksie 'n belangrike proses is in die industrie, is die volle meganisme nog nooit met behulp van berekening bestudeer nie. Daar is egter wel al werk gedoen aangaande sekere aspekte van die reaksie, byvoorbeeld ligandontwerp.

Hierdie studie behels 'n noukeurige konfigurasionele analise van elke stap van die reaksiesiklus, ladingsverdelingsanalise (*charge decomposition analysis*, CDA) van sekere belangrike spesies asook die analise van die energiestappe betrokke by elke stap. Fosfien is gekies as 'n modelligand, omdat dit elektronies ooreenstem met P(*o*-toliel)₃, die ligand wat meestal in eksperimentele werk gebruik is. Die klein grootte van fosfien maak dit ook geskik vir berekening op hierdie vlak.

Daar is bevind dat die oksidatiewe addisie van HCN aan die voorgangerkompleks (etileen)-NiL₂ (L=PH₃) in een stap kan plaasvind en in die gasfase snelheidsbepalend is. Die adduk (etileen)NiHCNL₂ bevat H⁺ (wat 'n hidried word) en CN⁻ in die *cis*-posisie relatief tot mekaar. Liganddissosiasie lewer drie isomere van (etileen)NiHCNL. Daar is bevind dat slegs twee van dié isomere aan die katalitiese reaksie kan deelneem, omdat die migrasie-inplasing (*migration-insertion*) van etileen in die Ni-H-binding voor, of saam met, die assosiasie van 'n tweede etileen-molekule plaasvind. Dit is slegs moontlik indien waterstof en etileen *cis* teenoor mekaar is, wat geld vir twee van die isomere. Die meganisme van assosiatiewe reduktiewe eliminasië word deur die berekening gerugsteun. Voorts blyk dit vanuit die berekening dat die etiel- en sianiedgroepe *cis* teenoor mekaar moet wees voordat reduktiewe eliminasië van propionitriël kan plaasvind.

Analise van die energetiese profiel van die reaksie toon dat entropie-effekte 'n belangrike rol speel in die voortsetting van die reaksie in die gasfase.

Die invloed van Lewissure op die katalitiese siklus word, met behulp van strukturele en energetiese analise bespreek.

'n Belangrike algemene gevolgtrekking is dat die standaardvoorstelling van die energetiese profiel van reaksies waarin intermolekulêre oorgange (teenoor slegs intramolekulêre oorgange) voorkom, misleidend kan wees. Dit word gestel dat die implisiete aanname dat twee spesies wat minimum-energiestruktuur verteenwoordig op twee verskillende potensiele energie-oppevlaktes ook 'n minimum-energiestruktuur voorstel op een potensiele energie-oppevlaktes, die energieprofiel skeeftrek. Gevolgtrekkings vanuit hierdie energieprofiel van reaksies waar meer as een onderskeibare spesie deelneem, moet dus met omsigtigheid gemaak word.

ACKNOWLEDGMENTS

An endeavor such as this cannot be undertaken alone and I want to thank everyone who helped to ease my way. A profound thank you goes to my promoter, Professor Jan Dillen for many hours of enlightening discussion and explanation. Many thanks too, to Professor Helgard Raubenheimer, my co-promoter, for insightful advice on all questions chemical. Thank you, too, to my colleague and friend, Catharine Esterhuysen, who was always ready to help with some advice. It was a joy to learn from you all. Thank you to Len Barbour, who made his very useful graphics package, Exceed, available to me. To Gerhard Venter, my lab partner, thank you for emergency computer rescue and entertaining conversations, among much else. Without the encouragement and support of my partner, Tinus van Dyk, the road would have been much more bumpier, so thank you to you too. Thank you to my parents, who believe in me. To all my friends, in particular (though in no particular order) Maggie Burger, Thalma Corbett, Yvonne Malan, Tanya de Villiers, Arjan Westra and Marié Roux, who have all shared in my experience of the past few years and can well relate to it all, thank you.

Finally, thank you to the NRF and the University of Stellenbosch for financial support.

ABBREVIATIONS

2M2BN	2-Methyl-3-Butenenitrile
3PN	3-Pentenenitrile
4PN	4-Pentenenitrile
ADN	Adiponitrile
AIM	Atoms In Molecules
BD	Butadiene
B3LYP	Becke-3-parameter Lee-Yang-Parr hybrid functional
BLYP	Becke Lee-Yang-Parr functional
BSSE	Basis Set Superposition Error
CASSCF	Complete Active Space Self-Consistent Field
CC	Coupled Cluster
CCS	Coupled Cluster Singles
CCSD	Coupled Cluster Singles Doubles
CCSDT	Coupled Cluster Singles Doubles Triples
CDA	Charge Decomposition Analysis
CI	Configuration Interaction
CIS	Configuration Interaction singles
CISD	Configuration Interaction Singles and Doubles
CSF	Configuration State Function
DCD	Dewar-Chatt-Duncanson
DFT	Density Functional Theory
ECP	Effective Core Potential
GGA	Generalized Gradient Approximation
GTO	Gaussian Type Orbital
HF	Hartree-Fock
IRC	Intrinsic Reaction Coordinate
KS	Kohn-Sham
LA	Lewis Acid
LANL2DZ	Los Alamos National Laboratories Double Zeta
LCAO	Linear Combination of Atomic Orbitals
LDA	Local Density Approximation

MCSCF	Multi-Configurational Self-Consistent Field
MGN	Methyl Glutaronitrile
MM	Molecular Mechanics
MP	Møller-Plesset
MRCI	Multi-Reference Configuration Interaction
PES	Potential Energy Surface
QM/MM	Quantum mechanics/molecular mechanics
QM/MD	Quantum mechanics/molecular dynamics
SCF	Self-Consistent field
STO	Slater Type Orbital
VWN	Vosko-Wilk-Nusair functional
ZPE	Zero-Point Energy

TABLE OF CONTENTS

I. Introduction	
1. General background	1
2. Brief summary of chapter contents	1
II. Hydrocyanation of Alkenes	
1. Introduction	3
2. Early, non-catalyzed methods	3
3. Early attempts at homogeneous catalysis	4
4. Development of nickel phosphite catalysts	5
(a) Electronic and steric properties of the ligand	5
(b) Three-coordinate nickel complexes	6
(c) Nickel phosphite complexes and olefins	6
(d) Nickel hydrides	7
5. Hydrocyanation of Mono-olefins	10
(a) Hydrocyanation of mono-olefins	10
(b) Mechanism for the hydrocyanation of mono-olefins	11
(c) Hydrocyanation of substituted olefins	14
(d) The effect of Lewis acids	15
6. Hydrocyanation of Butadiene	16
(a) Hydrocyanation of butadiene	16
(b) Mechanism for hydrocyanation of butadiene	16
(c) Isomerization of branched nitriles to linear nitriles	17
(d) Isomerization of other olefins	21
7. Stereospecific Hydrocyanation	22
8. Chelating Ligands	24
9. Other Catalysts	25
10. Conclusion	26
III. Quantum Mechanics and Computational Chemistry	
1. Introduction	27
2. Atomic Units and Notation	27
(a) Atomic Units	27

(b) Notation	28
3. The Potential Energy Surface	29
(a) The Born-Oppenheimer approximation	29
(b) Stationary points on the PES	30
4. The Hartree-Fock Method	31
(a) The Pauli exclusion principle	31
(b) Spin orbitals and spatial orbitals	32
(c) The Hartree product	32
(d) Slater determinants	33
(e) One- and two-electron integrals: notation	35
(f) From spin orbitals to spatial orbitals	35
(g) The Coulomb and exchange operators	37
(h) The Fock operator	37
(i) The Roothaan-Hall equations	38
(j) The charge density	40
(k) The Fock matrix	40
(l) The SCF procedure	41
5. Basis Sets	43
(a) Gaussian-type orbitals	44
(b) Contracted Gaussian functions	44
(c) Polarization functions	46
(d) Diffuse functions	46
(e) Effective core potentials	46
(f) Basis set superposition error	47
6. Ab Initio Methods with Electron Correlation	47
(a) Configuration interaction	48
(b) The Møller-Plesset approach	49
7. Density Functional theory	50
(a) Electron density	50
(b) The Hohenberg-Kohn theorems	51
(c) The Kohn-Sham approach	54
(d) The adiabatic connection	58
(e) The local density approximation	59
(f) The generalized gradient approximation	60

(g) Hybrid functionals	60
(h) Self-interaction	61
(i) DFT calculations	62
(j) Concluding remarks	63
IV. Modeling the Cycle	
1. Introduction	64
(a) General background	64
(b) Chapter layout	66
2. Computational Details	66
(a) Geometry optimizations	66
(b) Electronic structure analysis	66
(c) Atoms in molecules	67
(d) Graphic representations	67
3. Comments on Energetics	67
4. Intramolecular Transitions	69
(a) (Ethylene)Ni(PH ₃) ₂ (1)	69
(b) (Ethylene)Ni(h)(CN)(PH ₃) ₂ (2a-2g)	73
(c) (Ethylene)Ni(H)(CN)PH ₃ (3a-3f)	91
(d) (Ethylene)Ni(ethyl)(CN)PH ₃ (4a-4q)	100
(e) (Ethylene)Ni(ethyl)(CN)(PH ₃) ₂ (5a-5i)	108
5. Intermolecular Transitions	113
(a) (Ethylene)Ni(PH ₃) ₂ (1) to (Ethylene)Ni(h)(CN)(PH ₃) ₂ (2a-2g)	113
(b) (Ethylene)Ni(h)(CN)(PH ₃) ₂ (2a-2g) to (Ethylene)Ni(H)(CN)PH ₃ (3a-3f)	117
(c) (Ethylene)Ni(H)(CN)PH ₃ (3a-3f) to (Ethylene)Ni(ethyl)(CN)PH ₃ (4a-4q)	120
(d) (Ethylene)Ni(ethyl)(CN)PH ₃ (4a-4q) to (Ethylene)Ni(ethyl)(CN)(PH ₃) ₂ (5a-5i)	125
(e) (Ethylene)Ni(ethyl)(CN)(PH ₃) ₂ (5a-5i) to (Ethylene)Ni(PH ₃) ₂ (1)	128
6. The Full Cycle	130
(a) Possible pathways	131

(b) The effect of ZPE, thermal vibrational energy, rotation and translation, and entropy	131
(c) The favored pathway	138
(d) The unproductive pathway	139
(e) The effect of van der Waals stabilizing energy	140
7. Conclusion	141
V. Effects of Lewis Acid Co-Catalysts – A Preliminary Discussion	
1. Introduction	144
2. Computational Details	144
3. Results and Discussion	145
(a) The effect of Lewis acid co-catalysts on the H-CN bond	145
(b) The effect of Lewis acids on the geometries and energetics of the inner pathway	145
4. Conclusion	152
VI. Conclusions	153
References	155

I. INTRODUCTION

1. General background

Nickel catalysts are widely used in a large number of reactions (Montgomery, 2001; Wilke, 1988), such as olefin polymerization (Brookhart, 1999; Keim, 1990), diimidiation (RajanBabu, 1998), hydrometallation (Lautens, 1997), reductive coupling (Montgomery, 2004) and various kinds of cycloadditions (Louie, 2002; Wender, 1997, 1998).

The hydrocyanation of olefins is an industrially important process because nitriles are precursors for a wide variety of chemical goods, from Nylon to painkillers (Rajanbabu, 1996; Tolman, 1985; 1986), as well as steroid production, fertilizers, herbicides, pesticides and anti-bacterials (Hubert, 1983). Due to the importance of hydrocyanation, much experimental work has been done from the middle 1960s to the mid-80s to elucidate the mechanism (Brown, 1974; Hubert, 1983; Jolly, 1974; Tolman, 1985). Recently there has been a resurgence of interest in the subject (Brunkan, 2004; Raetiger, 2004; Van Leeuwen, 2001; Wilting, 2005). However, these studies are experimental, with the exception of Van Leeuwen (2001) who has done molecular mechanics (MM) studies to determine the optimal ligand bite angle for the reductive elimination of RCN from the Ni-catalyst; and Chaumonnot (2004) who has done preliminary density functional theory studies (DFT) on the catalytic isomerization of 2-methyl-3-butenenitrile to 3-pentenenitrile. However, to the knowledge of this author, the hydrocyanation of olefins by nickel catalysts has never been studied extensively by computational methods, which makes this work the first such study. The purpose of this work is to map the potential energy surface for the catalysis of ethylene with a model compound. In addition, some comparisons with respect to different levels of theory and basis sets are made and the lowest energy pathway to complete the reaction is determined. Preliminary work on the effect of a Lewis acid co-catalyst on the energetics of the cycle is included.

2. Brief summary of chapter contents

The following two chapters contain a literature survey on, firstly, hydrocyanation in general with special emphasis on the hydrocyanation of ethylene by means of the ethylene nickel bis[tri(*o*-tolyl) phosphite] catalyst (Chapter 2). Secondly, a brief outline

of quantum mechanics and computational chemistry, especially density functional theory (DFT), follows (Chapter 3).

The results are presented in Chapters 4 and 5. Chapter 4 covers the hydrocyanation of ethylene using a simplified catalyst containing phosphine instead of tri(*o*-tolyl) phosphite. The effect of selected Lewis acids on certain steps of the catalytic cycle is investigated in Chapter 5.

Finally, Chapter 6 contains a summary and conclusion.

II. HYDROCYANATION OF ALKENES

1. Introduction

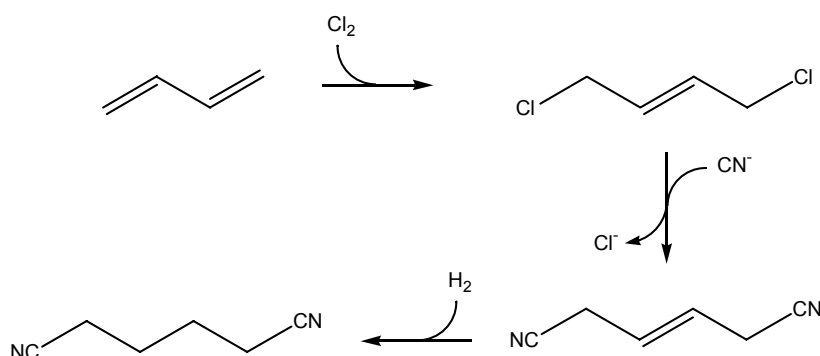
The purpose of this chapter is to highlight the scope of the hydrocyanation reaction. The ordering of material in this chapter is roughly chronological, and based on the extensive review by Tolman (1985). Non-catalyzed methods and early attempts at homogeneous catalysis are discussed first, followed by an overview of the development of the nickel phosphite catalysts, versions of which are currently used in industry. Although this discussion may not pertain directly to the computational work presented later in this study (Chapters 4 and 5), it is important to provide perspective on the details of the catalytic process as it is known today. The hydrocyanation of monoolefins is covered comprehensively, both because much of the initial experimental work on this system and this computational study focus on the hydrocyanation of ethylene. The hydrocyanation of butadiene and other dienes are included in this discussion, not as much because they are directly relevant to the work done in this study, but because butadiene is by far the most important substrate in the industrial process and it is important not to lose sight of that. Stereospecific hydrocyanation and chelating ligands are covered briefly, because much of the current focus on hydrocyanation deals with the development and fine-tuning of these ligands, as exemplified by the work of Van Leeuwen (2004). Finally, alternative catalysts are mentioned cursorily, but it should be noted that they are not widely employed industrially.

2. Early, Non-Catalyzed Methods

Prior to the late 1960s the addition of hydrogen cyanide to butadiene to form adiponitrile (ADP) took place indirectly. The Du Pont company's method (Tolman, 1985) involved the following steps (Scheme 1):

- (i) Sodium chloride was electrolyzed in order to chlorinate butadiene to give 1,4-dichlorobut-2-ene.
- (ii) The chlorinated alkene was then reacted with sodium cyanide, obtained by adding sodium hydroxide to hydrogen cyanide.

(iii) Subsequent hydrogenation yielded ADP. However, due to the high corrosiveness of chlorine and the expense of the electrolysis process, the development of a direct method became imperative.



Scheme 1. Hydrocyanation of butadiene *via* chlorination and hydrogenation

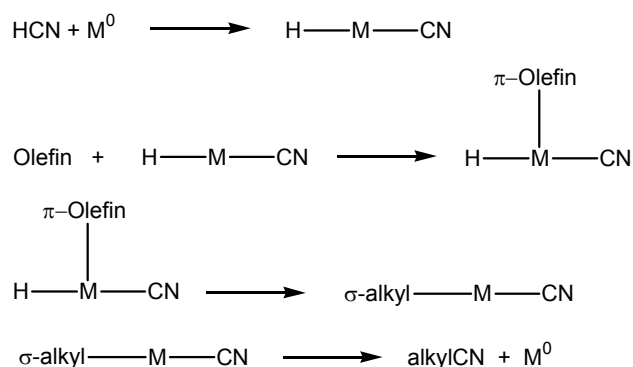
3. Early Attempts at Homogeneous Catalysis

Arthur and Pratt gave the first account of the addition of hydrogen cyanide to unactivated olefins without the use of heterogeneous catalysts in 1954. In the presence of dicobalt octacarbonyl, hydrogen cyanide is added to a wide range of olefins at an average temperature of 130°C and autogenous pressure. Terminal olefins up to 1-butene, conjugated dienes and Diels-Alder adducts of cyclopentadiene give the best results with an average conversion to nitriles of about 60%. Terminal olefins with long side-chains (e.g. octene) and olefins with internal double bonds (e.g. 2-butene) give yields in the order of 10%. It is uncertain what role is played by $\text{Co}_2(\text{CO})_8$, except that a large amount is needed. Moreover, the lack of success in recovering it afterwards makes this method rather unsatisfactory.

The reaction of hydrogen cyanide with bicyclo[2,2,1]heptene with tetrakis(triphenylphosphite) palladium or nickel and additional triphenylphosphite was reported by Brown and Rick (1969) and represent the first example of homogeneous catalysis by a group 10 phosphite catalyst. They also proposed that the mechanism proceeds by oxidative addition of hydrogen cyanide, coordination and insertion by the olefin and reductive elimination of the nitrile. They could not account for the necessity of having excess ligand present and it was left to Taylor and Swift (1972) to propose that this prevents the formation of inactive palladium(II) cyanide by competing for vacant coordination sites on the metal atom. Furthermore, Taylor and Swift discovered the promoting effect of certain Lewis acids as well as the influence of the solvent on the

rate and selectivity of the reaction. The first topic will be discussed throughout this chapter.

The development of the nickel phosphite catalyst and the insight gained in the understanding of the mechanism of hydrocyanation was mostly due to the work of Tolman and his co-workers at Du Pont (Tolman, 1985). The general mechanism for the hydrocyanation of olefins is given by Scheme 2 (Huthmacher, 1996).



Scheme 2. General mechanism for the hydrocyanation of an olefin

More detailed mechanisms of specific examples will be presented later in this chapter.

4. Development of Nickel Phosphite Catalysts

(a) Electronic and steric properties of the ligand

Initial investigation (Tolman, 1970a) focused on the electronic properties of the ligand, since these generally determine the charge on the metal center. It was not expected that the ligand's size would play a significant role. Based on the work by Horrocks and Taylor (1963), an additivity rule was proposed: the substituents on the phosphorus atom of the ligand influence the carbonyl stretch frequency in a monosubstituted complex, $\text{Ni}(\text{CO})_3\text{L}$, in dichloromethane in a predictable manner. By determining the magnitudes of the change in the carbonyl stretch frequency for monosubstituted ligands, a value can be predicted additively for polysubstituted ligands. They found that, although more electron-withdrawing substituents give higher CO stretch frequencies, it cannot be determined whether the reduced electron density on nickel is due to reduced σ -donation by the ligand or increased π -donation by the metal. Steric effects were found to play a negligible role in determining the stretch frequencies, but are essential in determining the stability of the complexes (Tolman, 1970b). Ligand-

competition experiments were carried out in which a ligand L' was added to a solution containing NiL₄ and the mixture was allowed to equilibrate (Equation 1).



From the ³¹P NMR data a relative stability series was compiled which made it clear that there is almost no correlation between the electronic properties of the ligands (as determined in the CO stretch frequency experiment) and the stability of the complexes they form. Instead, the steric bulk of the ligand proved to be decisive. Later calorimetric studies (Tolman, 1976a) supported these results. The now well-known concept of the ligand cone angle (Tolman, 1977) was introduced as a result of these experiments.

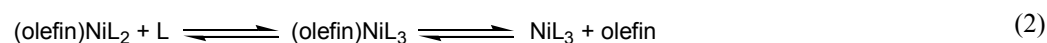
(b) Three-coordinated nickel complexes

Further work showed that the rates of dissociation are generally higher for the phosphines and phosphinites than for phosphites and that the three-coordinated complexes are much more active than the four-coordinated ones (Tolman, 1974a). This led Tolman (1972a) to propose the 16- and 18-electron rule as a heuristic device to aid in the establishment of mechanisms in organometallic catalysis.

The isolation of Ni[P(O-*o*-tolyl)₃]₃ (Tolman, 1970c) made the preparation of the first nitrile complexes of tetravalent nickel possible (Tolman, 1971). Although the nitrile complexes were not isolated, they were unambiguously identified by various spectroscopic techniques. It was found that the formation of nitrile complexes is greatly enhanced by increasing the steric bulk of the ligands.

(c) Nickel phosphite complexes and olefins

The complex (ethylene)Ni[P(O-*o*-tolyl)₃]₃ was first isolated by Wilke (1970). Spectroscopic evidence showed that the Ni-C-bonds are of the same length, indicating π-coordination of the ethylene to the metal atom (Tolman, 1970d). The same study also showed that the ethylene is in the same plane as the nickel and the two phosphorus atoms. This was confirmed by the crystallographic work of Guggenberger (1973). It was shown (Tolman, 1974b) that substitution of the ethylene by another ligand takes place *via* an associative pathway (Equation 2).



Much work was done to determine the effect of the substituents on ethylene on the overall stability of the π-olefin complexes and it was found that steric effects do not

play a significant role whereas electronic effects are decisive – the reverse of what was found for the phosphite ligands. In particular, substituents that tend to lower the energy of the π^* -orbital of the olefin (such as F and CN) stabilize the complex, by facilitating back-bonding (Schrauzer, 1960). Back-bonding (Dewar, 1951; Chatt, 1953) from the metal to the olefin is very important in nickel-olefin complexes (Tolman, 1974c).

(d) Nickel hydrides

Drinkard (1970) was the first to report the synthesis of a pentacoordinated nickel hydride. The synthesis was achieved by the addition of a strong acid to a non-aqueous solution of $\text{Ni}[\text{P}(\text{OC}_2\text{H}_5)_3]_4$ to give $\text{HNi}[\text{P}(\text{OC}_2\text{H}_5)_3]_4^+$. Although the hydride was not isolated, NMR spectroscopy confirmed its formation. Whether its structure is square pyramidal or trigonal bipyramidal could not be established unequivocally, although a trigonal bipyramidal structure seems more probable. The fact that there is only a single ^{31}P resonance can be explained by fast ligand exchange, as is common for complexes of the HML_4 type (Tolman, 1985).

The first isolated pentacoordinated nickel hydride is $\text{HNi}[(\text{C}_6\text{H}_5)_2\text{PCH}_2\text{CH}_2\text{P}(\text{C}_6\text{H}_5)_2]^+$ by Schunn (1970). As in the previous case, this reaction is done in nonaqueous medium, since it is unsuccessful in water.

Tolman (1970e) showed that the protonation of tetracoordinated nickel complexes to yield pentacoordinated complexes is endothermic. The endothermicity of the reaction is offset by the favorable increase in entropy, as solvent molecules that are coordinated to H^+ are released. Furthermore, the oxidation of HNiL_4^+ in acidic medium occurs *via* a tetracoordinate intermediate, HNiL_3^+ . This intermediate was not isolated, but its existence was postulated because the decay of HNiL_4^+ is inhibited by the presence of excess ligand. However, the protonation of NiL_4 also makes ligand dissociation much easier (Tolman, 1970f).

The electronic nature of the phosphorus (donor) ligands has an influence on the ease of protonation. Generally, the more basic the metal atom is, the easier it will be protonated (Shriver, 1970). This was found to be the case for NiL_4 complexes as well. Ligands with electron withdrawing substituents lower the electron density on the metal atom and inhibit protonation. However, the decrease in metal basicity is slower than the decrease in ligand basicity as the electron withdrawing ability of the substitu-

ents on the ligands increase. Thus, in the case of very π -acidic ligands, the metal atom becomes relatively easier to protonate than the ligands (Tolman, 1972b).

Whereas the nickel hydrides discussed so far have been obtained by protonating NiL_4 with strong acids, it was found (Tolman, 1976b) that the addition of a weak acid such as HCN leads to a new class of nickel hydrides of the form HNiL_3CN (equation 3).



NMR-studies of the complexes $\text{HNi}[\text{PPh}(\text{OEt})_2]_3\text{CN}$ and $\text{HNi}[\text{Ph}_2\text{P}(\text{CH}_2)_4\text{PPh}_2]_2\text{CN}$ indicates a trigonal bipyramidal structure (Figure 1).

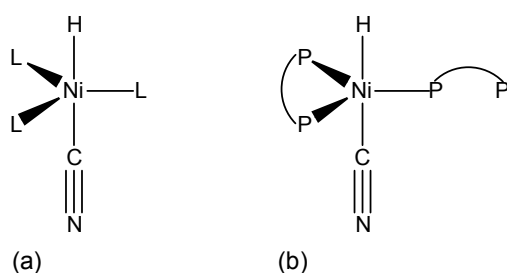
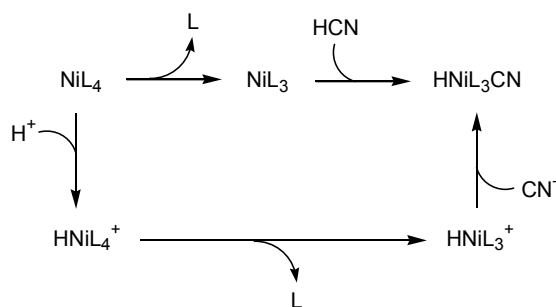


Figure 1. HNiL_2CN with (a) monodentate and (b) bidentate ligands

By X-ray crystallography, the isoelectronic complex $\text{HCo}[\text{PPh}_3]_3$ was found to have a trigonal bipyramidal structure as well (Ibers, 1969), thus providing supporting evidence for the structure of the nickel complex, at least at equilibrium. Variable temperature NMR-work also shows that rapid dissociative exchange of the phosphine ligands takes place, as can be expected for this type of complex (Pearson, 1969). Despite the dissociative exchange, no HNiL_2CN was isolated. In fact, IR-studies show that HNiL_3CN always forms, whether the starting material is NiL_4 or NiL_3 (Tolman, 1976b). Scheme 3 gives two of the possible pathways for the formation of HNiL_3CN from NiL_4 . As it was known that the protonation of NiL_4 is very quick (Tolman, 1970e) and that ligand dissociation takes place much more quickly from HNiL_4 than from NiL_4 (Tolman, 1970f), it was evident that the ionic pathway would be very rapid. This also meant that ligand dissociation would turn out to be the rate-determining step for the molecular pathway.



Scheme 3. The molecular (top) and ionic (bottom) pathways for the formation of HNiL₃CN from NiL₄

It was shown that both steric and electronic factors are important for this process. P(OCH₂CH₂Cl)₃ and P(OEt)₃ are sterically similar, so they compete equally for coordination sites which means that they dissociate from NiL₄ at almost equal rates. (Note that this does not necessarily mean that the activation energy for this step will be the same in both cases.) However, the chlorine containing substituent -OCH₂CH₂Cl is more electronegative than -OEt. Thus, P(OCH₂CH₂Cl)₃ draws much more electronic charge away from the Ni-atom than does P(OEt)₃. The result is that oxidative addition of HCN is much more difficult if L=P(OCH₂CH₂Cl)₃ than if L=P(OEt)₃, and thus less of HNiL₃CN is formed in the former case than the latter. On the other hand, Ni[P(O-*o*-tolyl)₃]₄ and Ni[P(O-*p*-tolyl)₃]₄ are very similar electronically, but differ somewhat sterically. Ni[P(O-*o*-tolyl)₃]₄ dissociates much more easily from NiL₄ due to its steric bulk and hence the first step takes place to a larger extent for Ni[P(O-*o*-tolyl)₃]₄ than for Ni[P(O-*p*-tolyl)₃]₄ so that less HNiL₃CN is formed in the latter case relative to the former.

The ionic pathway is thermodynamically enhanced by the presence of Lewis acids. It is thought that this is because the Lewis acid coordinates to HCN and effectively increases its acid strength, making protonation of NiL₄ more likely than direct HCN addition (Tolman, 1985). The complexes HNi[P(O-*o*-tolyl)₃]₃CN-BPh₃ (Tolman, 1985) and HNi[P(OEt)₃]₃CN-ZnCl₂ (Druliner, 1984) were isolated and characterized. In the latter case the presence of the Ni-CN bond was proven by NMR ¹³C-H coupling experiments and the CN-Zn-coordination was shown by the change in the CN stretch vibrations. This spectroscopic evidence was supported by the crystal structure of CpFe(CO)₂CN-BPh₃ in which the borane is coordinated to the nitrogen atom of the cyano group and the carbon atom of the cyano group to the iron atom (Tolman, 1985). Moreover, the iron complex also displays a trigonal bipyramidal structure (Laing,

1974). However, not all Lewis acids bind with equal ease. The reaction mentioned above with HNiL_3CN goes to completion if BPh_3 , $\text{B}(p\text{-tolyl})_3$ or $\text{B}(\text{CH}_2\text{Ph})_3$ is added in a 1:1 ratio, but this is not the case for $\text{B}(o\text{-tolyl})_3$ and BCy_3 (Tolman, 1985). The degree of interaction as measured by the stretch frequency of the cyano group is determined both by the Lewis acid used and by the phosphite ligand bound to nickel (Druliner, 1984). BPh_3 causes a much higher stretch frequency than either ZnCl_2 or AlCl_3 , presumably because BPh_3 is a better σ -donor due to the phenyl groups attached to B. Furthermore, $\text{HNi}[\text{P}(\text{O}-p\text{-tolyl})_3]_3\text{CN-LA}$ (where LA denotes any Lewis acid) has higher CN stretch frequencies than $\text{HNi}[\text{P}(\text{OEt})_3]_3\text{CN-LA}$, regardless of the LA.

5. Hydrocyanation of Mono-olefins

(a) Hydrocyanation of mono-olefins

In 1974 it was found that (mostly terminal) alkenes and styrene can form complexes with $\text{Ni}(0)$, but that the equilibrium constants for the process decrease as the length of the side-chain or the degree of substitution increase (Tolman, 1974c). A study done to compare the relative rates of hydrocyanation if equal amounts of ethylene and propylene are added to the catalyst simultaneously, shows that hydrocyanation of propylene only begins once all the ethylene has been converted to propionitrile (Tolman, 1985). The addition of hydrogen cyanide to these π -olefin complexes then yields the appropriate nitriles. By labeling hydrogen cyanide with deuterium, NMR-studies showed that α - β -scrambling occurs, which indicates that the addition of hydrogen cyanide to the double bond is reversible.

Generally, the monodentate ligand that gives the best results is $\text{P}(\text{O}-o\text{-tolyl})_3$. With a cone angle of 141° , its steric bulk enhances ligand dissociation to form reactive $16e^-$ species (Tolman, 1977), as well as favoring reductive elimination. Electronically, the ligand's electron donating properties ensure that the charge density on the Ni-atom is high enough to facilitate oxidative addition despite the steric crowding. However, for the hydrocyanation of octene, the ligand $\text{P}(\text{OPh})_3$ in combination with a Lewis acid gives much better results than $\text{P}(\text{O}-o\text{-tolyl})_3$ (with BF_3). In the latter case the product:catalyst ratio is 1:1, and in the former 250:1 (Keim, 1982).

Aryl phosphites tend to be more effective than alkyl phosphites, because they are more electron withdrawing. However, fluorosubstituted alkyl phosphites can increase

the rate of the reaction due to their electron withdrawing properties (Van Leeuwen, 2004).

Steric crowding due to bulky ligands enhance the formation of linear products in most cases (*i.e.* HCN is mostly added to the alkene in an *anti*-Markovnikov-fashion). As an example, the product distribution for the hydrocyanation of propylene is 72% of the linear *n*-butyronitrile and 28% of the branched isobutyronitrile (Tolman, 1984). The linear to branched ratio is even more extreme when branched alkenes are used as substrate. Styrene, however, proves to be an exception. Only 9% of the products is linear 3-phenyl propionitrile, the rest is 2-phenyl propionitrile. This reversal is due to the formation of the stabilized branched alkylnickel cyanide intermediate shown in Figure 2.

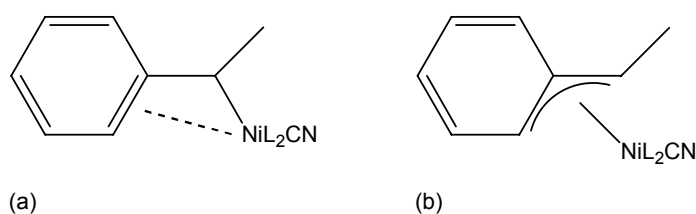


Figure 2. Coordination of styrene to nickel by forming (a) a π -bond and (b) the more extreme allyl nickel complex

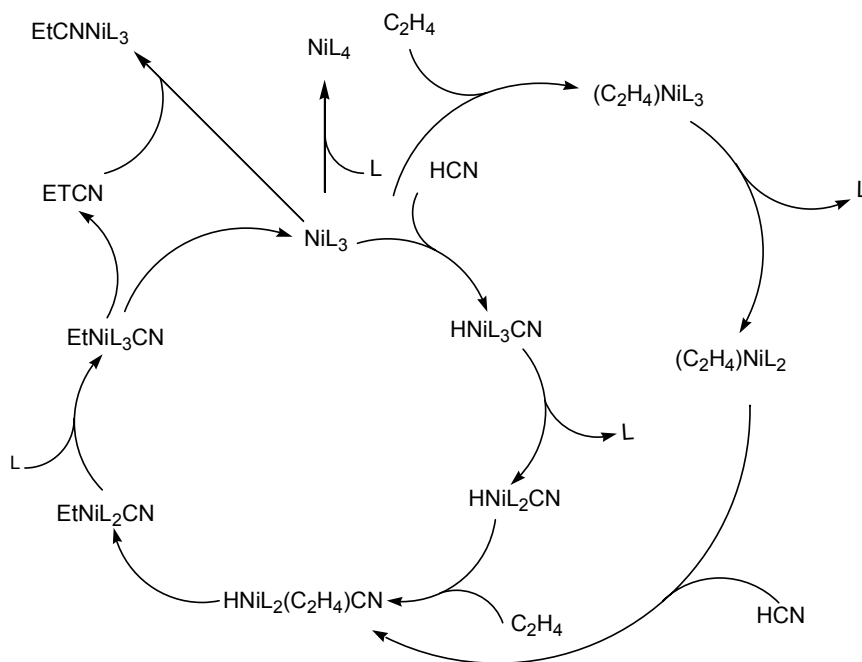
(b) Mechanism for the hydrocyanation of mono-olefins

In the same study (Tolman, 1984), a mechanism for the reaction was proposed based on kinetic studies (Scheme 4). In this mechanism, NiL_3 is taken to be the catalytically active precursor. In later studies specifically dealing with the hydrocyanation of ethylene by McKinney (1985a, b), however, it was shown that the active precursor is (ethylene) $\text{Ni}[\text{P}(\text{O}-o\text{-tolyl})_3]_2$. In Scheme 5, it can be seen that this allows two pathways, the one on the right-hand side being the productive one. As a first step, HCN is added oxidatively to (ethylene) $\text{Ni}[\text{P}(\text{O}-o\text{-tolyl})_3]_2$ (shown in bold) to form a cyano complex. Following the productive pathway (clockwise), one ligand is dissociated followed by ethylene association to form the 16-electron intermediate $(\text{C}_2\text{H}_4)\text{L}(\text{CN})-(\text{C}_2\text{H}_5)\text{Ni}(\text{II})$. This latter step can take place in two ways. The ethylene that is already associated can insert, followed by association of a second molecule of ethylene. However, this would yield a 14-electron intermediate, an occurrence that is deemed unlikely (McKinney, 1985b). Alternatively, the second molecule of ethylene associates first, followed by insertion of either coordinated ethylene. After ligand associa-

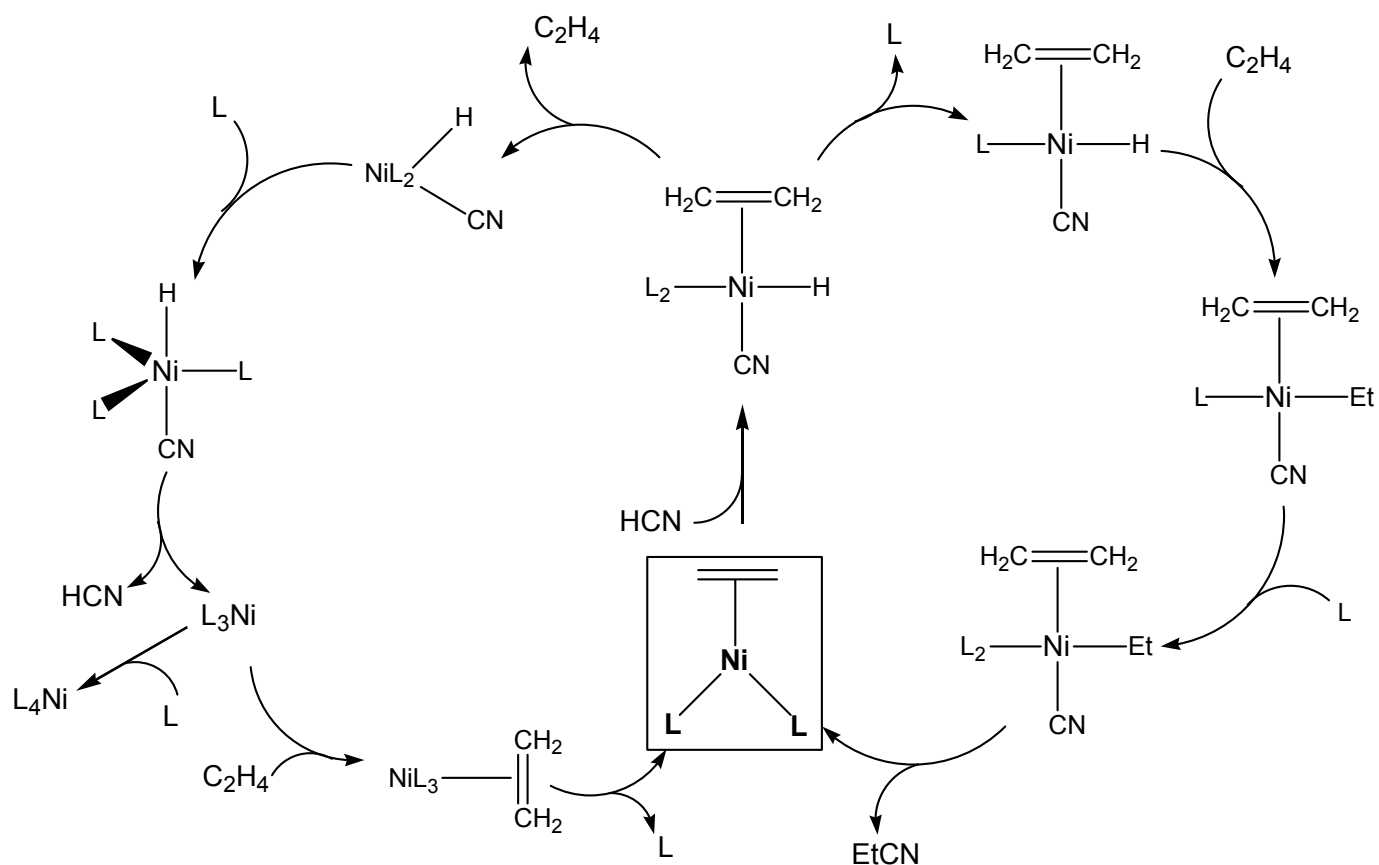
tion to give $(C_2H_4)L_2(CN)(C_2H_5)Ni(II)$, reductive elimination of propionitrile takes place and the cycle is completed.

However, the presence of low concentrations of NiL_4 throughout the reaction suggests an alternative, unproductive pathway (anti-clockwise from the starting point on Scheme 5). After oxidative addition, instead of ligand dissociation, dissociation of ethylene can take place, giving $HNiL_2CN$. Ligand association is then followed by reductive elimination of HCN to give NiL_3 , which will readily take up another ligand to give the relatively unreactive NiL_4 thus terminating the catalyst's lifetime. Alternatively, ethylene association with NiL_3 can take place followed by ligand dissociation to return to the beginning of the cycle.

The intermediate $(C_2H_4)L(CN)(C_2H_5)Ni(II)$ (Figure 3) has been isolated and characterized by NMR. If the concentration of ethylene is less than that of the ligand, the exchange in equation 11 took place with $K \sim 0.1$ at $-40^\circ C$ (McKinney, 1986) as shown in Equation 4. NMR studies also showed that the ligand exchange in this intermediate takes place very rapidly. The transition from one configuration to another probably takes place *via* a five-coordinate unobserved intermediate (Equation 5).



Scheme 4. Hydrocyanation of ethylene as proposed by Tolman (1984), with NiL_3 as the reactive precursor



Scheme 5. Hydrocyanation of ethylene as proposed by McKinney (1985), with $(\text{ethylene})\text{NiL}_2$ as the reactive precursor

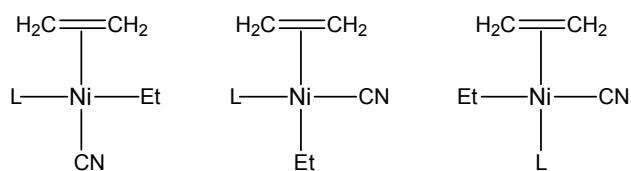
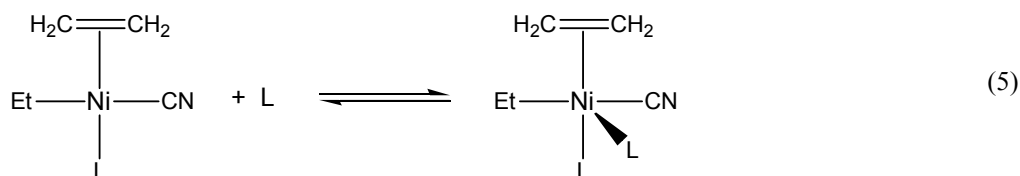
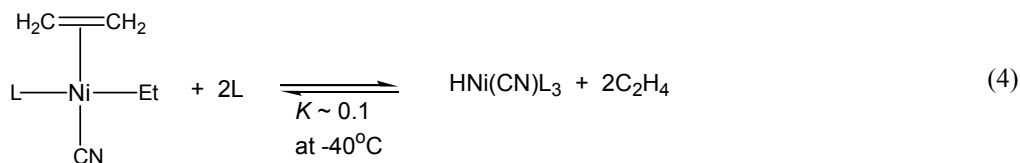


Figure 3. The three configurations of a reactive intermediate of the hydrocyanation of ethylene as proposed by McKinney (1985a)



In the same study, McKinney (1986) finds a second-order rate dependence on the initial concentration of (ethylene)NiL₂ for the formation of propionitrile. The rate of formation of propionitrile is independent of the concentrations of both ethylene and hydrogen cyanide. He discovered that the second-order rate dependence on (ethylene)NiL₂ is indirect and that the rate law should read

$$d[\text{EtCN}]/dt = k[(\text{C}_2\text{H}_4)\text{L}(\text{CN})(\text{C}_2\text{H}_5)\text{Ni}(\text{II})][\text{L}].$$

The apparent second-order dependence is due to the formation of (C₂H₄)L(CN)(C₂H₅)Ni(II) and L which needs to recombine in the last (slow) step to form propionitrile and (ethylene)NiL₂.

The positive entropy of activation for this reaction ($\Delta S^\ddagger = -34 \pm 4$ J/mol) also points to an associative mechanism for the reductive elimination of propionitrile – *i.e.* that (C₂H₄)L(CN)(C₂H₅)Ni(II) needs to recombine with L before reductive elimination of propionitrile. The associative mechanism for the reductive elimination of EtCN is supported by the experimental work of Favero (1976, 1978) and the theoretical work of Tatsumi (1984). The work of the latter is especially interesting, since they conclude that the associative mechanism is preferable to the dissociative mechanism because the nickel fragments left after associative reductive elimination is generally more stable than those left after dissociative reductive elimination. Due to the slowness of the association of the ligand prior to reductive elimination (Tolman, 1985), this is most likely the rate-determining step of the reaction.

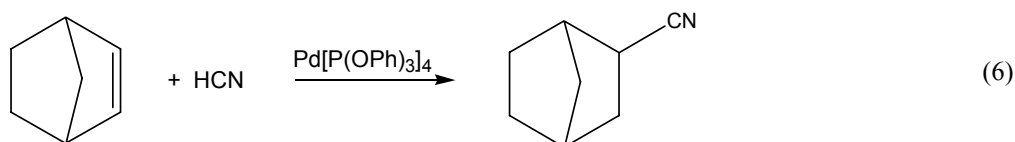
It should be noted that the cyanide ion is a catalyst poison. If the catalyst is used on its own, up to 60% of the added nickel can precipitate as insoluble Ni(CN)₂. If excess ligand is present as well, the percentage drops to 20%, but the overall reaction rate is slowed. The reason for the formation of Ni(CN)₂ with time is probably that an unstable Ni(IV) dicyanide complex forms from the hydrido or alkyl metal cyanide in competition with the hydrocyanation process. The unstable Ni(IV) complex decomposes to Ni(CN)₂ and ethane or hydrogen. The excess ligand prevents this by keeping CN⁻ from coordinating to vacant coordination sites on the metal (Brown, 1974).

(c) Hydrocyanation of substituted olefins

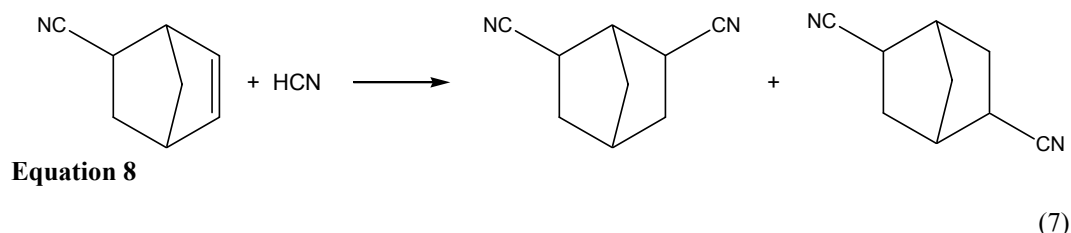
The hydrocyanation of substituted olefins met with mixed success (Tolman, 1985). Generally olefins that are substituted with a halogen, aldehyde, ketone, oxygen or cyanide group on the olefinic carbon readily coordinate with HNiL₃CN, but form sta-

ble allyl cyanide complexes ($RNiL_2CN$) that preclude reductive elimination of the nitrile. An additional reason for the stability of these complexes is that the anti-bonding π^* -orbitals of the olefinic double bonds are lower in energy relative to those of an unsubstituted olefin. This facilitates back-donation from the nickel and stabilizes the metal-olefin π -bond, as mentioned before. In the case of fumaronitrile and maleic anhydride, if the alkene is added before HCN, the resulting electron density on the metal atom is too low to allow oxidative addition of HCN. Cyano-olefins in which there was at least one carbon atom between the olefinic carbon and the cyano group underwent hydrocyanation easily.

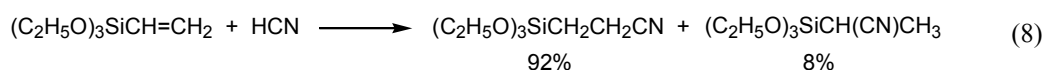
Strained olefins, such as bicyclo[2.2.1]hept-2-ene can undergo hydrocyanation in the presence of $Pd[P(OPh)_3]_4$ (Equation 6). The reaction is stereospecific and only exo-5-cyanobicyclo-[2.2.1]-heptane is formed (Brown, 1974).



Exo-5-cyanobicyclo[2.2.1]hept-2-ene yield dinitriles (Equation 7) in the presence of either $Co_2(CO)_8$ (Arthur, 1954) or zerovalent palladium catalysts (Brown, 1974).



Olefinic silanes undergo hydrocyanation (Equation 8) in the presence of tetrakis(triphenylphosphite)nickel(0) or -palladium(0) (Brown, 1972). However, the nickel complex seems to be less selective for linearity than the palladium complex.



(d) The effect of Lewis acids

In the case of styrene, 1-hexene and propene hydrocyanation, it was found that the addition of different Lewis acids have different effects, although it is not sure why this should be so (Tolman, 1985). $ZnCl_2$ and $AlCl_3$ significantly increase the rate of the reaction (relative to the absence of Lewis acid), but have no effect on the linear to

branched ratio. BPh_3 on the other hand, slows down the reaction rate, but increases the relative amount of linear product that is formed. Other aromatic boranes do just as well in selecting for linearity, but phosphitic boranes do worse than no Lewis acid at all. The reasons for the behavior of the boranes are thought to be both steric and electronic, but McKinney (1989) has shown that the electronic nature of the Lewis acid probably plays a negligible role.

Tolman (1985) also showed that Lewis acids help to extend the lifetime of the catalyst. In coordinating with the cyano group in the complex, the lone pair of the nitrogen atom is tied up and cannot bind to another nickel center to form insoluble polymers.

6. Hydrocyanation of Butadiene

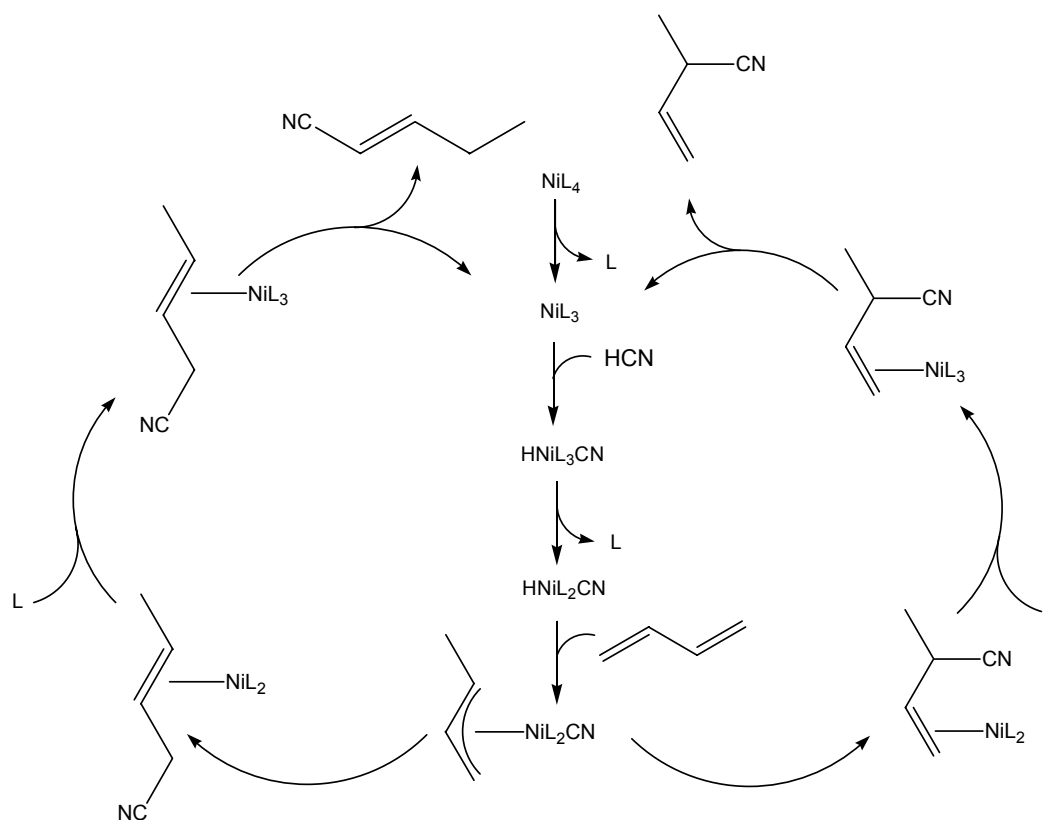
(a) Hydrocyanation of butadiene

Tolman (1985) showed that hydrogen cyanide can be added to butadiene (BD) in the presence of $Ni[P(OR)_3]_4$, with R=alkyl or aryl. The first addition step yields a mixture of the 1,2-addition product 2-methyl-3-butenenitrile (2M3BN) and the 1,4-addition product 3-pentenenitrile (3PN). The reaction takes place in an aromatic or nitrile solvent at temperatures of 50-120° C. It can be executed as a batch process as long as the HCN concentration remains below the BD concentration. The addition of HCN to 3PN only takes place significantly in the presence of a Lewis acid such as $ZnCl_2$. However, if the Lewis acid is added in the first step already, the first addition step remains favored over the second step by a ratio of 20:1.

(b) Mechanism for the hydrocyanation of butadiene

The mechanism for the hydrocyanation of butadiene is given in Scheme 6. The rate-determining steps are the dissociation of a ligand from NiL_4 to give NiL_3 (Tolman, 1970f) as well as the re-arrangement of the allylic complexes to give the π -complexes with 3PN and 2M3BN. The relative amounts of 3PN and 2M3BN that form depend on the ratio of the rate constants of those two steps. This mechanism differs from the mechanism for the hydrocyanation of ethylene in that the active precursor is NiL_3 rather than (ethylene) NiL_2 . Obviously also, the allylic intermediate is likely to be more stable than its counterpart (ethylene)(ethyl) $NiL(CN)$. The last two steps are very different from the mechanism for ethylene as well. Whereas the propionitrile is only formed in the very last step as reductive elimination thereof takes place, the final

product (3PN or 2M3BN) already forms by rearrangement (concomitant with reduction of Ni) in the third to last step after which a ligand is associated and the nitrile is dissociated. These differences are of course due to the remaining double bond of the substrate.

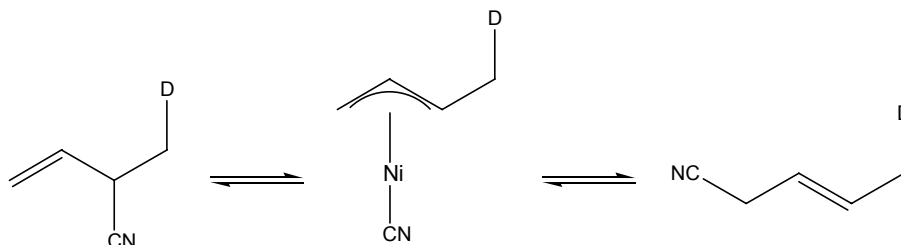


Scheme 6. The catalytic cycle for the hydrocyanation of butadiene

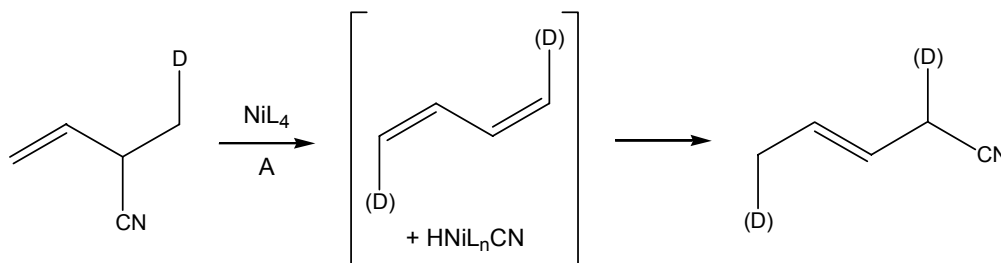
(c) Isomerization of branched nitriles to linear nitriles

As seen in the previous section, the hydrocyanation of butadiene has two main products: 3PN and 2M3BN. ADN is obtained from 3PN *via* isomerization of 3PN to 4PN (4-pentenenitrile) and the preferential *anti*-Markovnikov addition of HCN to 4PN (Tolman, 1984). 2M3BN has to be isomerized to 3PN first, since direct hydrocyanation of the branched nitrile will not give the linear product. The same catalytic system used for hydrocyanation is also suitable for isomerization. During hydrocyanation the selectivity for the formation of these two products are kinetic and isomerization of 2M3BN to 3PN gives the thermodynamic ratio of 93:7 of 3PN:2M3BN (Tolman, 1985). If 3PN and 2M3BN are hydrocyanated separately, ADN and methyl glutaronitrile (MGN) result.

There are two possible mechanisms for isomerization of 2M3BN to 3PN: Rearrangement of the coordinated olefin *via* an allylic intermediate (Scheme 7) or dehydrocyanation followed by rehydrocyanation (Scheme 8).



Scheme 7. Isomerization of 2M3BN to 3PN *via* an allylic intermediate



Scheme 8. Isomerization of 2M3BN to 3PN *via* dehydrocyanation followed by rehydrocyanation. Deuterium labels in parentheses indicate that the deuterium atom could be found at either position.

During the latter process, decomplexation of the olefin may occur, but it could not be observed. The plausibility of these two mechanisms were tested by deuterium-labeling experiments in which the methyl group of 2M3BN was selectively deuterated (Druliner, 1984) before being allowed to isomerize. After isomerization, the 3PN was collected and it was found that the deuterium labels could be found both on the methyl group and the methylene group of 3PN (refer to Scheme 5). This means that the dehydrocyanation mechanism is more plausible, since an allylic rearrangement would not account for the deuterium scrambling. However, recent work done by Sabo-Etienne (2004), supported by 1D and 2D NMR experiments, shows that the allylic mechanism should not be entirely disregarded. After heating a $\text{Ni}(\text{COD})_2/2\text{M3BN}/\text{PPh}_3$ mixture for 30 minutes at 100°C , low temperature ^{31}P spectra of the resulting mixture showed a signal at -4.6 ppm for free phosphine. An AB signal at 32.6 and 23.9 ppm ($J_{\text{P-P}} = 103$ Hz) corresponded to the allyl cyanide complex $\text{Ni}(\eta^3\text{-1-Me-C}_3\text{H}_4)(\text{CN})(\text{PPh}_3)_2$ shown in Figure 4.

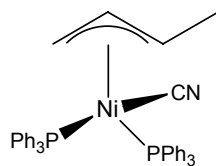
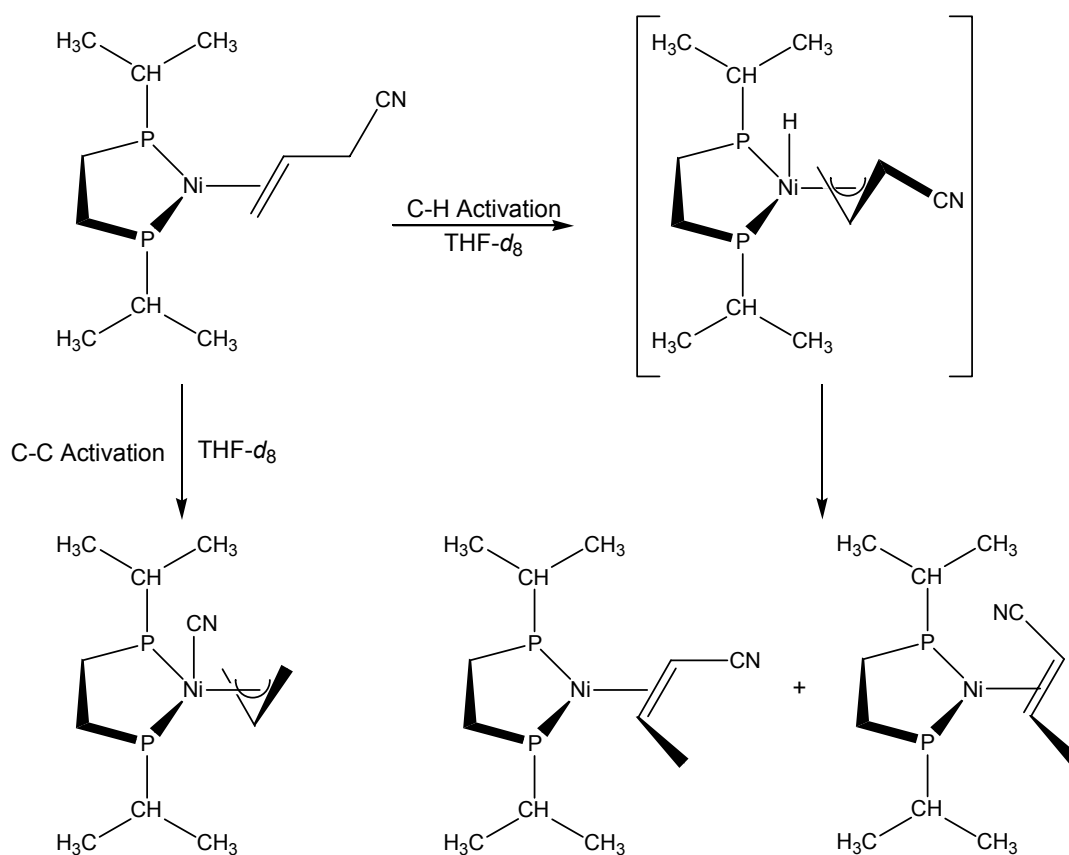


Figure 4. Allylic intermediate observed during the isomerization of 2M3BN to 3PN

Yet, even though the evidence presented by Sabo-Etienne convincingly shows that the allyl cyanide complex can form during the isomerization of 2M3BN, it does not unambiguously convince that the allylic intermediate is involved in the actual catalysis. Moreover, it is well known from the work of Tolman (1970f, 1985) that the η^3 -allylic complex is present both during the hydrocyanation of butadiene and the isomerization of 2M3BN to 3PN. He showed that the reaction is zero-order in the concentration of both butadiene and HCN and that they react in a 1:1 ratio as long as BD is present. This points to the formation of a stable intermediate for the first step of hydrocyanation and that the reductive elimination of 2M3BN or 3PN is the rate-determining step. This stable intermediate was identified as allylic on the basis of IR evidence and NMR studies similar to those performed by Sabo-Etienne. Vogt, *et al.* (2005) also support the allylic rearrangement mechanism, but contend that the allyl species is in equilibrium with its hydrido cyano butadiene species. This might explain the labeling experiment of Druliner. The same study (Vogt, 2005) confirms that the rate-determining step is the reductive elimination of the isomerized substrate.

The coordination of allyl cyanide to (dippe)Ni(0) [dippe=1,2-bis(diisopropylphosphino)ethane] was investigated by Brunkan, *et al.*, (2004). They showed that the activation of the C-CN bond takes place in competition with the activation of a C-H bond (Scheme 9). The C-H bond activated intermediate can rearrange to either *cis*- or *trans*-crotonitrile, both of which are more stable than allylnitrile by some 4-5 kcal per mole, probably because the electron withdrawing CN^- group is bonded directly to an olefinic carbon. This encourages coordination to the relatively electron rich Ni(0) center.

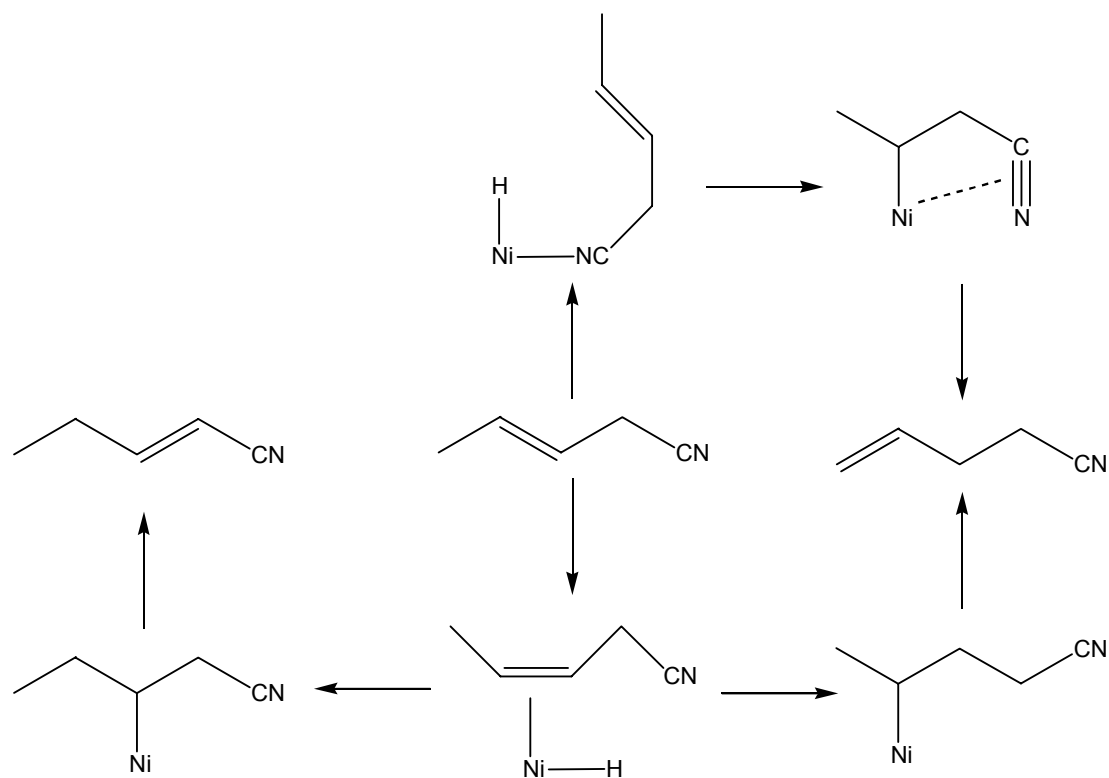
Since it is necessary to isomerize 3PN to 4PN before hydrocyanation to ADN can take place, the discovery that the same catalyst system could perform both functions is very useful industrially (McKinney, 1985a, b). Isomerization of 3PN gives both 2PN, which is conjugated, and the terminal 4PN.



Scheme 9. Competition between C-C- and C-H-activation lead to different products

The thermodynamic preference is for 2PN, and the thermodynamic ratio of 2PN:3PN:4PN is 78.3:20.1:1.6. Also, 4PN:3PN never goes above 1.6:20.1 (Tolman, 1984), but this equilibrium is reached quickly, so that 2PN barely forms. Hence, with the catalyst system of $\text{Ni}[\text{P}(\text{O}-p\text{-tolyl})_3]_4$, HCN and $\text{B}(\text{Ph})_3$ the ratio of 4PN:2PN > 65:1 (McKinney, 1985a, b). When the smaller ligand $\text{P}(\text{OEt})_3$ is used instead of $\text{P}(\text{O}-p\text{-tolyl})_3$, the ratio of 4PN:2PN drops to 17.5:1, indicating that the size of the ligand is rather important. The reason for the kinetic preference for the thermodynamically unfavored 4PN is probably because 3PN preferentially bonds to nickel through the cyano-group rather than π -bonding through its double bond (Tolman, 1985). Binding through the cyano group therefore essentially forces the formation of 4PN rather than 2PN (Scheme 10).

If the catalyst system consists of NiL_4 , HCN and a Lewis acid, the hydride forms quickly and isomerization takes place at a much higher rate than hydrocyanation. Thus the relative rates for the formation of 2PN and 4PN out of 3PN can easily be calculated.



Scheme 10. Contrathermodynamic isomerization of 3PN to 4PN and 2PN.

It was found that the relative rates of formation of 4PN and 2PN is around 65:1, independent of the specific Lewis acid that was used. This, together with the fact that the 4PN:2PN ratio is around 70:1 in the absence of a Lewis acid, indicates that the Lewis acid may accelerate the formation of the active isomerization catalyst, namely HNiL_4LA (LA=Lewis acid), but is not directly involved in the process of isomerization (Tolman, 1985). It is uncertain how a specific Lewis acid influences the rate of the reaction, but BPh_3 was quicker than ZnCl_2 , AlCl_3 and some others. By varying both R and X in a series of R_3SnX promoters, McKinney (1989) showed that it is mainly the steric bulk of the Lewis acid that plays a role and that the electronic effect induced by the promoter is virtually negligible. Lewis acids that are more demanding sterically both favors formation of terminal 4PN over 3PN and the formation of linear ADN over branched MGN during the subsequent hydrocyanation of 4PN.

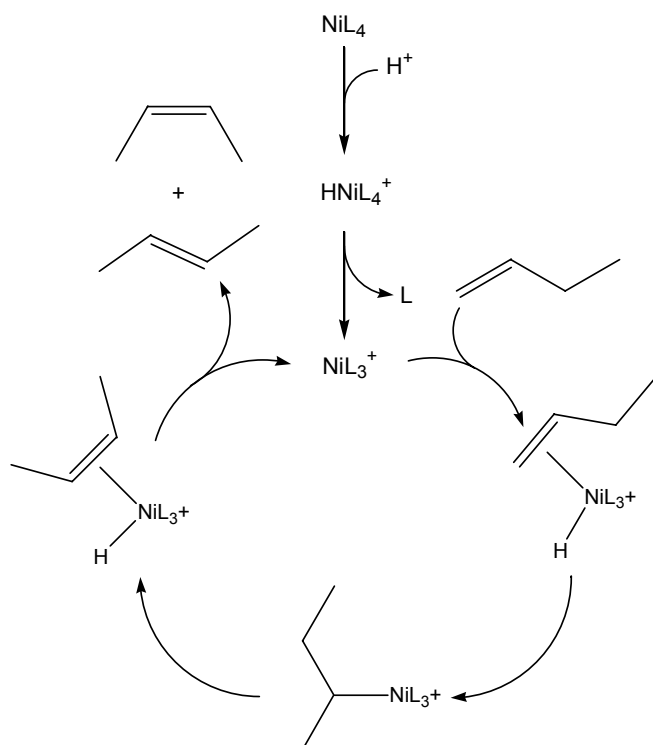
(d) Isomerization of other olefins

It was found (Tolman, 1972c) that the nickel hydride HNiL_4^+ is a very good general olefin isomerization catalyst precursor. The active catalyst is HNiL_3^+ , since an excess of the ligand slows down the reaction. The neutral complexes NiL_4 and NiL_3 are inef-

fective. During the isomerization of 1-butene to 2-butene (Scheme 11), nearly equal amounts of the *cis*- and the *trans*- isomers form initially, but with time the ratio shifts to the equilibrium ratio of 1:3.

The catalyst is poisoned by some dienes, especially butadiene, due to the formation of allyl complexes that are much more stable than any of the isomerization intermediates (Tolman, 1985).

The hydrocyanation reaction has also been successful for a large number of different kinds of dienes (Tolman, 1985).

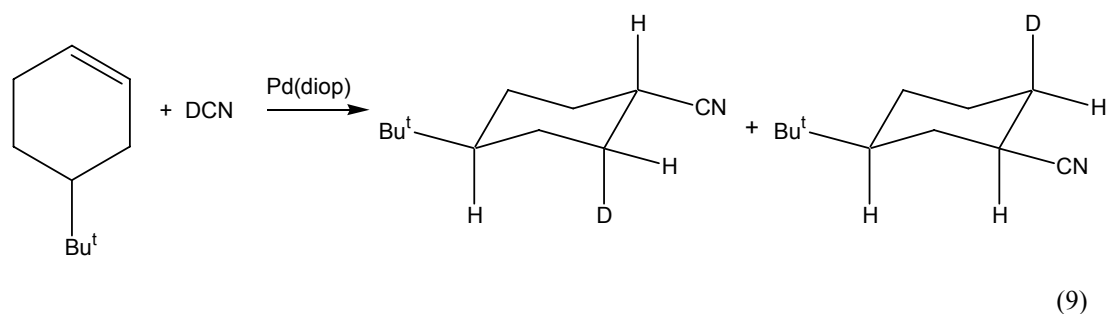


Scheme 11. Isomerization of 1-butene to both *cis*- and *trans*-2-butene

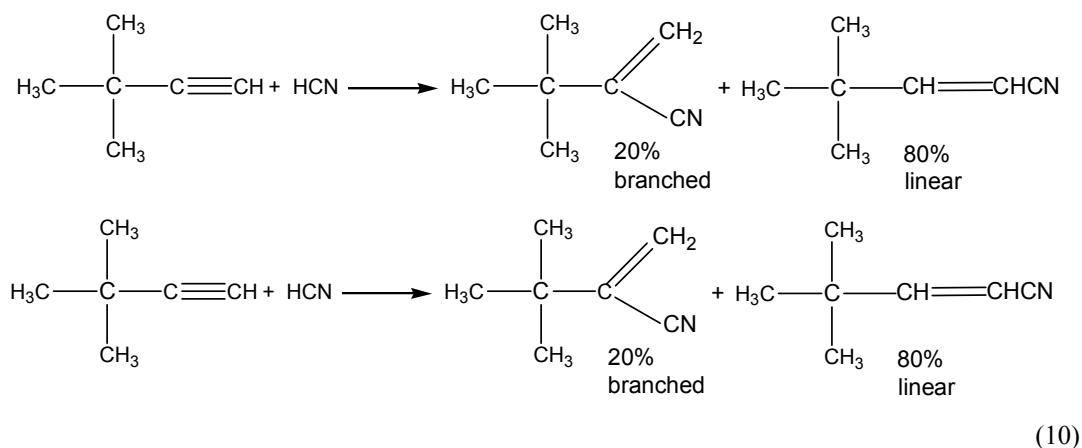
7. Stereospecific Hydrocyanation

The first study of the stereochemistry of hydrocyanation was published by Bäckvall, *et al.* (1981). They found that addition of HCN to the olefinic bond is *cis*.

Jackson (1984) found that deuterium cyanide adds to 4-*t*-butyl-cyclohex-1-ene in the *cis*-fashion to yield only the *syn*-adduct when catalyzed with $\text{Pd}(\text{diop})_2$ (equation 9). However, when other substrates were used, the yields were much lower. Stereoselectivity could, however, be enhanced if a way could be found to enforce some rigidity on the transition state, for example by using a substituted substrate capable of a chelating effect.

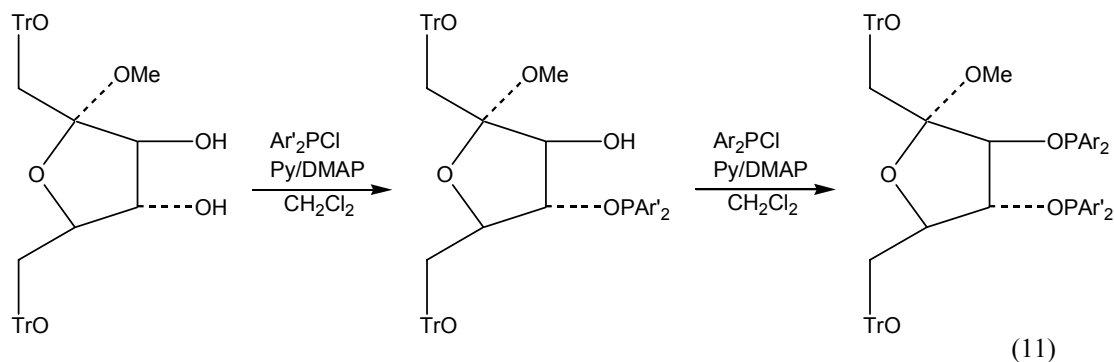


Thus, it was found in the same study that the hydrocyanation of the alkynol gave 80% of the branched nitrile, whereas the same reaction with *t*-butylacetylene gave 80% of the linear nitrile (equation 10).



Addition of HCN to norbornene in the presence of [(*S,S*)-(+)-diop]₂palladium gave norbornane-*exo*-2-carbonitrile with a chemical yield of 91% and an enantiomeric excess of 24% (*R*) as reported by Jackson (1987) and 10% (*R*) as reported by Hodgson (1988).

RajanBabu, *et al.* (1996) have shown that the stereospecificity of a catalyst increases if the ligands contain electron-withdrawing substituents and/or if the substrate have electron-donating substituents. After the chiral atom has been formed, enantioselectivity is also determined by the relative rates of the reductive elimination of the two diastereomers. They derived electronically unsymmetrical bis-3,4-diarylphosphinite ligands from α -D-fructofuranoside (Equation 11) by utilizing the very different reactivities of the 3- and 4-hydroxyl groups of the sugar. By keeping the size of the ligands constant, but varying the electronic properties of the substituents on the phenyl rings, the electronic effects on the stereoselectivity of the catalyst could be observed for the hydrocyanation of 6-methoxy-2-vinylnaphtalene.



They found that electron-donating substituents on the phosphorus aryl groups gave the lowest enantiomeric excesses and that electron deficient substituents caused a higher yield in enantiomeric excess. However the highest yields were found when the C₃-phosphinite was electron-rich relative to the C₄-phosphinite. Reversing the order did not produce the same high results, showing that the “kind” of asymmetry is very important. One drawback, however, of basing ligand design on natural products such as sugars is that often only one diastereomer is freely available.

8.Chelating Ligands

The reductive elimination of alkylnitriles is enhanced by electron-withdrawing phosphite ligands. Generally, catalysts with phosphine ligands do not show much activity (Jackson, 1984). However, Moloy (1998) has shown that chelating diphosphines with large bite angles may accelerate the overall reaction by enhancing reductive elimination of the alkylnitrile. It is probable that the ligand enforces a tetrahedral geometry on the otherwise square-planar complex (Figure 6), which forces the carbon atoms of the alkyl and the cyanide ligands closer to each other and encourages C-C coupling. This mechanism is therefore somewhat different from the case when the ligands are monodentate phosphites and the elimination proceeds *via* an associative mechanism (McKinney, 1985a, b, 1986). The effectiveness of this mechanism is very dependant on the magnitude of the bite angle, with angles of 105-106° the most effective (Kamer, 2001). For a comparison of the most effective ligands for the hydrocyanation of styrene, see Table 1 and Figure 5. However, the enhanced reductive elimination may also be a consequence of the steric bulk that ligands with large bite angles necessarily have. Experiments are underway to test the effectiveness of small bite angle phosphines with bulky substituents (Van Leeuwen, 2004).

Table 1. Nickel-catalyzed hydrocyanation of styrene, using diphosphine ligands

Ligand	β_n (°)	% yield	% branched
Fig. 5a	101	35 - 41	88 - 91
Fig. 5b	105	94 - 95	97 - 98
Fig. 5c	106	69 - 92	96 - 98
Fig. 5d	109	27 - 75	96 - 99
Fig. 5e	138	0.7	83
PPh ₃		0	
dppe	79	<1	~ 40
dppp	87	4 - 11	~ 90
dppb	99	3 - 8	92 - 95
BINAP	85	4	29

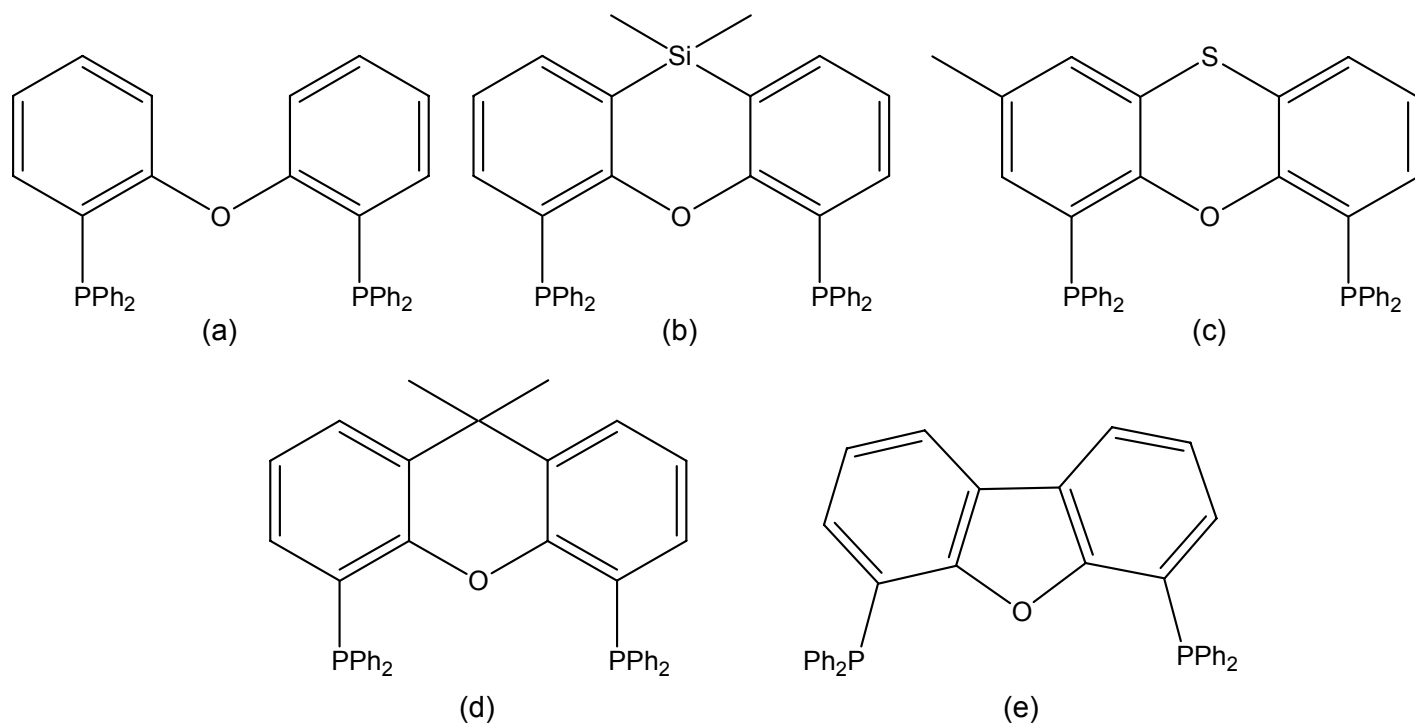


Figure 5. Chelating phosphines used in the hydrocyanation of styrene

9. Other catalysts

Nickel (and other group 12) catalysts are not the only effective catalysts for hydrocyanation. Copper compounds can also catalyze hydrocyanation of olefins (Hubert, 1983) and have the advantage that they are not sensitive to small amounts of water or oxygen. They also tend to be more selective for the 1,4-addition product to butadiene

than the nickel catalysts. However, they can only catalyze the first step of HCN addition to butadiene and are ineffective for the second step. Furthermore, substituted dienes give much lower yields than butadiene itself, limiting the scope of the reaction (Puentes, 1983).

10. Conclusion

It should be clear from this review that the Ni-catalyzed hydrocyanation of alkenes is a very complex reaction system, especially if the substrate is anything other than ethylene. By far the largest fraction of the work discussed here is experimental work and there is certainly a dearth of computational studies devoted to this topic when compared to many other catalytic reaction systems. The work presented in this thesis will represent a first step towards enriching the available knowledge of this system by computational methods.

III. QUANTUM MECHANICS & COMPUTATIONAL CHEMISTRY

1. Introduction

Computational chemistry is a burgeoning field, both with regard to the classical methods of molecular mechanics as well as quantum mechanics. Hybrid quantum mechanics/molecular mechanics (QM/MM) is also very popular. The scope of this chapter is limited to quantum mechanical methods and the focus will be on the methods used in this study. One exception, though, will be a detailed discussion of the Hartree-Fock (HF) methodology, because it gives a good flavor of what quantum mechanics in its application to chemistry is about, without the complication of intricate mathematics.

The chapter layout is as follows: first will be a brief discussion of atomic units and notation. Notation is important, because there seems to be as many different notations as there are treatments of the subject and thus it is important to be clear and consistent in the usage of notation. The potential energy surface (PES) will be the next topic, since an understanding of the PES is essential for any kind of work in computational chemistry. After the treatment of the HF methodology and, very briefly, of correlated *ab initio* methods, the discussion will turn to density functional theory, since this was the methodology of choice for this study.

The work presented here was compiled from a number of general sources, namely: Cramer (2002), Hehre, Radom, Schleyer and Pople (1986), Koch and Holthausen (2000), Levine (2000), Lewars (2003), Szabo and Ostlund (1989). The arrangement of material in this chapter is based on the treatment of Lewars (2003). Details contained in a particular reference will be cited accordingly.

2. Atomic Units and Notation

(a) Atomic units

In SI-units, the Schrödinger equation for the hydrogen atom is written as

$$\left[-\frac{\hbar^2}{2m_e} \nabla^2 - \frac{e^2}{4\pi\epsilon_0 r} \right] \psi = E\psi \quad (1)$$

where $\hbar = h/2\pi$, m_e is the mass of the electron and $-e$ is the charge on the electron. To get from the equation expressed in SI-units to the dimensionless equation, two

reduced variables can be defined as $E_r \equiv E/A$ and $r_r \equiv r/B$ corresponding to energy and length respectively. The constants A and B are products of the Schrödinger equation's constants (in SI-units), \hbar , m_e , e and $4\pi\epsilon_0$, manipulated in such a way that A and B have units of energy and length, respectively. It can be shown that (Levine, 2000)

$$A = \frac{m_e e^4}{(4\pi\epsilon_0)^2 \hbar^2} = \frac{e^2}{4\pi\epsilon_0 a_0} = \frac{e^2}{a_0} \equiv 1 \text{ hartree, and} \quad (2)$$

$$B = \frac{\hbar^2 4\pi\epsilon_0}{m_e e^2} = a_0 \equiv 1 \text{ bohr.} \quad (3)$$

By suitable manipulation (Szabo and Ostlund, 1989), the reduced Schrödinger equation for the hydrogen atom is

$$\left(-\frac{1}{2}\nabla^2 - \frac{1}{r_r}\right)\psi = E_r \psi \quad (4)$$

where the subscript r denotes the reduced variable. Since notation in atomic units is much more concise than the SI equivalent, it will be used throughout. Therefore the subscript “ r ” of r and E will be dropped. An additional advantage of atomic units is that they do not depend on the currently accepted values of the SI-units (Levine, 2000).

(b) Notation

The complete wave function (*i.e.* including both the electrons and the nuclei) will be denoted by Φ , the many-electron wave function by Ψ and the single-electron wave function (molecular orbital) by ψ . Spin orbitals will be denoted by χ and atomic orbitals by ϕ . Integration over three-dimensional space will be denoted by $\int f(\mathbf{r})d\mathbf{r}$ where $f(\mathbf{r})$ is any function of \mathbf{r} . A many-electron operator will be denoted by an italicized capital with a caret, *e.g.* for the Hamiltonian operator, \hat{H} , whereas a one-electron operator will be denoted by an italicized lower-case letter with a hat. Nuclei will be counted by upper case Roman letters and electrons by lower-case Roman letters.

The bracket notation by Dirac is a concise way of writing cumbersome expressions. An inner product can be written as $\langle a|b\rangle$. Dirac saw that the two components of the inner product, $\langle a|$ and $|b\rangle$, can be regarded as separate entities, the latter being a vector and the former being a linear function of vectors (Griffiths, 1995). This notation can be applied to certain expressions as follows:

$$\int f_m^* \hat{A} f_n d\mathbf{r} \equiv \langle f_m | \hat{A} | f_n \rangle \equiv \langle m | \hat{A} | n \rangle \quad (5)$$

and will be used wherever appropriate. In the case of one- and two-electron integrals, a special chemists' notation will be used (see Section 4(e)).

3. The Potential Energy Surface

The potential energy surface (PES) of a non-linear molecule containing N nuclei is a function of both the electronic energy of the molecule and the internuclear repulsion. Only the vibrational degrees of freedom are considered on the PES because the translational and rotational degrees of freedom do not influence the electronic energy of a molecule.

(a) The Born-Oppenheimer approximation

That the electronic energy of a molecule can be described in terms of a potential energy surface is due to the Born-Oppenheimer approximation. According to the Born-Oppenheimer approximation, it is possible to regard the nuclei as stationary relative to the electrons because the nuclei are more than 1 000 times more massive than the electrons. To see the impact of the Born-Oppenheimer approximation, the Hamiltonian operator merits some discussion.

The non-relativistic time-independent Schrödinger equation can be expressed as

$$\hat{H}\Phi = E\Phi \quad (6)$$

where \hat{H} is the Hamiltonian operator for both the nuclei and the electrons and E is the total energy of the system. The Hamiltonian is therefore the operator which, if applied to the wave function, gives the energy of the system. The Hamiltonian for a system consisting of N nuclei and n electrons is

$$\hat{H} = -\sum_{i=1}^n \frac{1}{2} \nabla_i^2 - \sum_{I=1}^N \frac{1}{2M_I} \nabla_I^2 - \sum_{i=1}^n \sum_{I=1}^N \frac{Z_I}{r_{iI}} + \sum_{i=1}^n \sum_{j>i}^n \frac{1}{r_{ij}} + \sum_{I=1}^N \sum_{J>I}^N \frac{Z_I Z_J}{r_{IJ}} \quad (7)$$

where M_I is the ratio of the mass of nucleus I to that of an electron and Z_I is the atomic number of nucleus I . The Laplacian operators ∇_i^2 and ∇_I^2 denote differentiation with respect to the coordinates of electron i and nucleus I respectively. The first term gives the kinetic energy of the electrons and the second term that of the nuclei. The third term represents the Coulomb attraction between the electrons and the nuclei. The fourth and fifth terms denote the Coulomb repulsion between the electrons and the nuclei, respectively.

By separating the motions of the electrons and the nuclei, it is possible to regard the second and the last terms of the Hamiltonian as constants (for fixed nuclei). Thus, one is left with the expression

$$\hat{H}_{\text{elec}} = -\sum_{i=1}^n \frac{1}{2} \nabla_i^2 - \sum_{i=1}^n \sum_{I=1}^N \frac{Z_I}{r_{iI}} + \sum_{i=1}^n \sum_{j>i}^n \frac{1}{r_{ij}} \quad (8)$$

which is the electronic Hamiltonian. If the latter is applied to the Schrödinger equation, the result is the electronic wave function, which describes the motion of the electrons. It depends explicitly on the positions of the electrons, but only parametrically on the nuclear coordinates. If the nuclear coordinates are regarded as being fixed, the total energy of the system is equal to the electronic energy plus the nuclear repulsion. A nuclear Hamiltonian can be generated, which consists of the second and fifth terms of the Hamiltonian given in (7) as well as an expression for the energy of the average field created by the motion of the electrons. This is possible because the electrons move much faster than the nuclei. Thus

$$\hat{H}_{\text{nucl}} = -\sum_{I=1}^N \frac{1}{2M_I} \nabla_I^2 + E_{\text{elec}}(\{\mathbf{r}_I\}) + \sum_{I=1}^N \sum_{J>I}^N \frac{Z_I Z_J}{r_{IJ}} \quad (9)$$

where the last two terms give the expression for the total energy, so that

$$\hat{H}_{\text{nucl}} = -\sum_{I=1}^N \frac{1}{2M_I} \nabla_I^2 + E_{\text{tot}}(\{\mathbf{r}_I\}) \quad (10)$$

where the last term is a potential for the nuclear motion (Szabo and Ostlund, 1989). Thus, due to the Born-Oppenheimer approximation, the nuclei can be seen as moving on a potential energy surface where the energy is given by E_{tot} .

Solving the electronic Schrödinger equation therefore yields the electronic energy, whereas the solution to the nuclear Schrödinger equation provides the translation, rotation and vibration of a molecule. In further discussion the subscripts “elec” and “nucl” will be dropped, because it will be clear from the context which is being referred to.

(b) Stationary points on the PES

Each point on the PES corresponds to a specific arrangement of the nuclei of the molecule related to a specific energy. The energy of a point on the PES can be obtained by a single-point calculation. Arbitrary points on the PES are usually not of much interest, but the stationary points are very important. Stationary points can be obtained by determining where on the PES the gradient, *i.e.* the rate of change of the

electronic energy relative to the arrangement of the nuclear coordinates, is zero. The stationary point can be further characterized by determining the second derivative at that point. The second derivatives are given by the force-constant matrix, also known as the Hessian and given by (Lewars, 2003)

$$\mathbf{H} = \begin{bmatrix} \frac{\partial^2 E}{\partial q_1 \partial q_1} & \frac{\partial^2 E}{\partial q_1 \partial q_2} & \dots & \frac{\partial^2 E}{\partial q_1 \partial q_N} \\ \frac{\partial^2 E}{\partial q_2 \partial q_1} & \frac{\partial^2 E}{\partial q_2 \partial q_2} & \dots & \frac{\partial^2 E}{\partial q_2 \partial q_N} \\ \vdots & \vdots & \ddots & \vdots \\ \frac{\partial^2 E}{\partial q_N \partial q_1} & \frac{\partial^2 E}{\partial q_N \partial q_2} & \dots & \frac{\partial^2 E}{\partial q_N \partial q_N} \end{bmatrix} \quad (11)$$

for a molecule containing N atoms. Although second derivatives are required by some optimization algorithms, they are typically only obtained by approximation, since the calculation of second derivatives are computationally very expensive. To characterize a stationary point, the Hessian needs to be calculated analytically, as happens during a frequency calculation. Diagonalizing the Hessian yields a matrix containing the force constants corresponding to the vibrations of the molecule. If the force constants are mass-weighted, the vibrational frequencies result, with the corresponding columns of the diagonalizing matrix giving the nuclear displacements due to each vibration (Lewars, 2003). If all the force constants (*i.e.* all the elements of the diagonal force constant matrix) are positive, the stationary point is a minimum. If one of the force constants is negative, the stationary point is a one-dimensional saddle point and the frequency associated with the negative force constant is referred to an imaginary frequency. If n of the force constants are negative, the stationary point is an n -dimensional saddle point.

On the lowest energy pathway (also known as the intrinsic reaction coordinate (IRC)) connecting two energy minima, the point of highest energy is the transition structure between the two energy minima. Thus transition structures (connecting two minima) are found at first-order saddle points on the potential energy surface.

4. The Hartree-Fock Method

(a) The Pauli exclusion principle

The description of an electron in terms of its spatial coordinates (\mathbf{r}) is incomplete, because the electron also has spin. Therefore spin functions, $\alpha(\omega)$ and $\beta(\omega)$, are chosen such that they are complete and orthonormal and so that

$$\langle \alpha | \alpha \rangle = \langle \beta | \beta \rangle = 1 \text{ and } \langle \alpha | \beta \rangle = \langle \beta | \alpha \rangle = 0 \quad (12)$$

with α corresponding to “up” and β corresponding to “down”. The electron can now be described in terms of the coordinates $\mathbf{x} = \{\mathbf{r}, \omega\}$ containing both the spatial coordinates and the spin. However, since the electron is a fermion, the wave function needs to be anti-symmetrical with regard to the exchange of the coordinates \mathbf{x} of any two electrons in the system described by the wave function. This is known as the anti-symmetry principle, a more general case of the Pauli exclusion principle. One of the consequences of the Pauli exclusion principle - and therefore also the anti-symmetry principle - is that no two fermions (*i.e.* electrons) may occupy the same state. However, the Hamiltonian does not contain any reference to the spin of an electron and therefore the anti-symmetry principle cannot be upheld by the wave function as it has been expressed up until now. The problem can be solved by the creation of spin orbitals and implementing them in Slater determinants.

(b) Spin orbitals and spatial orbitals

A one-electron spatial orbital only depends on the spatial coordinates of an electron and $|\psi(\mathbf{r})|^2 d\mathbf{r}$ gives the probability of finding an electron in the space element $d\mathbf{r}$. Any two spatial orbitals form an orthonormal set, *i.e.*

$$\langle \psi_i | \psi_j \rangle = \delta_{ij} \quad (13)$$

A spin orbital $\chi(\mathbf{x})$ is the product of a one-electron spatial orbital and a one-electron spin function such that for two spin orbitals

$$\langle \chi_i | \chi_j \rangle = \delta_{ij} \quad (14)$$

Since one spatial orbital can therefore lead to two spin orbitals and no two electrons can occupy the same spin orbital, it means that each spatial orbital can contain two electrons of opposite spin.

(c) The Hartree product

The Hamiltonian for a set of non-interacting electrons can be written as

$$\hat{H} = \sum_{i=1}^n \hat{h}(i) \quad (15)$$

for a system containing n electrons. The operator \hat{h} describes the kinetic and potential energy of the electron. The eigenfunction for \hat{h} can be obtained by

$$\hat{h}(i)\chi_j(\mathbf{x}_i) = \varepsilon_j \chi_j(\mathbf{x}_i) \quad (16)$$

where $\{\chi_j\}$ is a set of one-electron spin orbitals. From this follows that the eigenfunction for \hat{H} is given by

$$\psi^{\text{HP}}(\mathbf{x}_1, \mathbf{x}_2, \mathbf{x}_3, \dots, \mathbf{x}_n) = \chi_i(\mathbf{x}_1)\chi_j(\mathbf{x}_2)\dots\chi_k(\mathbf{x}_n) \quad (17)$$

so that

$$\hat{H}\psi^{\text{HP}} = E\psi^{\text{HP}} \quad (18)$$

where ψ^{HP} is known as the Hartree product. From (15) and (16) it can be seen that the eigenvalue E of (18) is

$$E = \varepsilon_i + \varepsilon_j + \dots + \varepsilon_k \quad (19)$$

(Cramer, 2002). The wave function given by the Hartree product is uncorrelated – *i.e.* the electrons' motions are treated as independent from one another – because

$$\left| \psi^{\text{HP}}(\mathbf{x}_1, \mathbf{x}_2, \dots, \mathbf{x}_n) \right|^2 d\mathbf{x}_1 d\mathbf{x}_2 \dots d\mathbf{x}_n = \left| \chi_i(\mathbf{x}_1) \right|^2 d\mathbf{x}_1 \left| \chi_j(\mathbf{x}_2) \right|^2 d\mathbf{x}_2 \dots \left| \chi_k(\mathbf{x}_n) \right|^2 d\mathbf{x}_n \quad (20)$$

(Szabo and Ostlund, 1989).

(d) Slater determinants

The Hartree product does not satisfy the anti-symmetry principle, for instance a two-electron Hartree product can be written as

$$\Psi_{1,2}^{\text{HP}}(\mathbf{x}_1, \mathbf{x}_2) = \chi_i(\mathbf{x}_1)\chi_j(\mathbf{x}_2) \text{ or} \quad (21a)$$

$$\Psi_{2,1}^{\text{HP}}(\mathbf{x}_1, \mathbf{x}_2) = \chi_j(\mathbf{x}_1)\chi_i(\mathbf{x}_2) \quad (21a)$$

with (21a) and (21b) not exactly equivalent. The electrons are not indistinguishable and the anti-symmetry principle is violated, since the sign of the Hartree product does not change upon exchanging the coordinates of the electrons. On the other hand, if a linear combination is made of the two Hartree products so that

$$\Psi(\mathbf{x}_1, \mathbf{x}_2) = \frac{1}{\sqrt{2}} [\chi_i(\mathbf{x}_1)\chi_j(\mathbf{x}_2) - \chi_j(\mathbf{x}_1)\chi_i(\mathbf{x}_2)] \quad (22)$$

where $1/\sqrt{2}$ is a normalization factor, it follows that

$$\Psi(\mathbf{x}_1, \mathbf{x}_2) = -\Psi(\mathbf{x}_2, \mathbf{x}_1) \quad (23)$$

and if $i=j$, the wave function disappears. For a system containing n electrons, this adapted wave function can also be written in the form of a determinant, so that

$$\Psi(\mathbf{x}_1, \mathbf{x}_2, \dots, \mathbf{x}_n) = \frac{1}{\sqrt{n!}} \begin{vmatrix} \chi_i(\mathbf{x}_1) & \chi_j(\mathbf{x}_1) & \cdots & \chi_k(\mathbf{x}_1) \\ \chi_i(\mathbf{x}_2) & \chi_j(\mathbf{x}_2) & \cdots & \chi_k(\mathbf{x}_2) \\ \vdots & \vdots & \ddots & \vdots \\ \chi_i(\mathbf{x}_n) & \chi_j(\mathbf{x}_n) & \cdots & \chi_k(\mathbf{x}_n) \end{vmatrix} \quad (24)$$

where $1/\sqrt{n!}$ is a normalization factor. Writing the wave function in this form means that the electrons are indistinguishable, since a specific electron is not assigned to a specific spin orbital anymore. The anti-symmetry principle is also obeyed, since the exchange of the coordinates of any two electrons implies the exchange of two rows of the determinant, which changes the sign of the wave function. This kind of wave function is known as a Slater determinant. The determinant notation can become rather cumbersome and can be shortened by using Dirac notation:

$$\Psi(\mathbf{x}_1, \mathbf{x}_2, \dots, \mathbf{x}_n) = \left| \chi_i(\mathbf{x}_1) \chi_j(\mathbf{x}_2) \dots \chi_k(\mathbf{x}_n) \right\rangle \quad (25)$$

If $\mathbf{x}_1, \mathbf{x}_2, \dots, \mathbf{x}_n$ always follows in the same order, the notation can be abbreviated even further to

$$\Psi(\mathbf{x}_1, \mathbf{x}_2, \dots, \mathbf{x}_n) = \left| \chi_i \chi_j \dots \chi_k \right\rangle \quad (26)$$

The introduction of the Slater determinant and consequent anti-symmetrizing of the wave function introduces the correlation of the motion of electrons with parallel spin. Electrons with opposite spin still move independently of each other. The introduction of correlation can be shown as follows: for a two-electron Slater determinant

$$\Psi(\mathbf{x}_1, \mathbf{x}_2) = \left| \chi_i \chi_j \right\rangle \quad (27)$$

containing two electrons of opposite spins in different spin orbitals so that

$$\chi_1(\mathbf{x}_1) = \psi_1(\mathbf{r}_1)\alpha(\omega_1) \text{ and } \chi_2(\mathbf{x}_2) = \psi_2(\mathbf{r}_2)\beta(\omega_2) \quad (28)$$

the expansion of the determinant yields

$$|\Psi|^2 d\mathbf{x}_1 d\mathbf{x}_2 = \frac{1}{2} |\psi_1(\mathbf{r}_1)\alpha(\omega_1)\psi_2(\mathbf{r}_2)\beta(\omega_2) - \psi_1(\mathbf{r}_2)\alpha(\omega_2)\psi_2(\mathbf{r}_1)\beta(\omega_1)|^2 d\mathbf{r}_1 d\mathbf{r}_2 \quad (29)$$

The probability that electron 1 will be between \mathbf{r}_1 and $d\mathbf{r}_1$ at the same time that electron 2 will be in $d\mathbf{r}_2$ at \mathbf{r}_2 is given by

$$P(\mathbf{r}_1, \mathbf{r}_2) d\mathbf{r}_1 d\mathbf{r}_2 = \int |\Psi|^2 d\omega_1 d\omega_2 d\mathbf{r}_1 d\mathbf{r}_2 = \int \frac{1}{2} [|\psi_1(\mathbf{r}_1)|^2 |\psi_2(\mathbf{r}_2)|^2 + |\psi_2(\mathbf{r}_1)|^2 |\psi_1(\mathbf{r}_2)|^2] d\mathbf{r}_1 d\mathbf{r}_2 \quad (31)$$

The probability takes this form because the electrons are indistinguishable (Szabo and Ostlund, 1989). If the electrons have identical spin, then the probability that electron 1 will be in $d\mathbf{r}_1$ at \mathbf{r}_1 at the same time that electron 2 will be in $d\mathbf{r}_2$ at \mathbf{r}_2 is given by

$$\begin{aligned} P(\mathbf{r}_1, \mathbf{r}_2) d\mathbf{r}_1 d\mathbf{r}_2 &= \int |\Psi|^2 d\omega_1 d\omega_2 d\mathbf{r}_1 d\mathbf{r}_2 \\ &= \frac{1}{2} \left[|\psi_1(\mathbf{r}_1)|^2 |\psi_2(\mathbf{r}_2)|^2 + |\psi_2(\mathbf{r}_1)|^2 |\psi_1(\mathbf{r}_2)|^2 \right] \\ &\quad - \left[\psi_1^*(\mathbf{r}_1) \psi_2(\mathbf{r}_1) \psi_2^*(\mathbf{r}_2) \psi_1(\mathbf{r}_2) + \psi_1(\mathbf{r}_1) \psi_2^*(\mathbf{r}_1) \psi_2(\mathbf{r}_2) \psi_1^*(\mathbf{r}_2) \right] \end{aligned} \quad (30)$$

where the third term on the right hand side is due to the exchange correlation between electrons of parallel spin. If $\mathbf{r}_1 = \mathbf{r}_2$, the probability reduces to zero, *i.e.* it is not possible to find two electrons of parallel spin in the same space simultaneously. Therefore a hole, known as a Fermi hole, exists around each electron, limiting the extent of approach between two electrons of parallel spin.

(e) One- and two-electron integrals: notation

Two kinds of integrals are used in the Hartree-Fock approximation. One-electron integrals are integrated over the space-spin coordinates of one electron, whereas two-electron integrals are integrated over the space-spin coordinates of two electrons. Both are used in the HF approximation. The expanded expressions for these integrals are cumbersome, and therefore an abbreviated notation will be employed here. The notation in this study is after that of Szabo and Ostlund (1989), specifically the chemists' notation, and the reader is referred to Table 2.2 of the first edition (Revised) of Szabo and Ostlund's text.

Before the HF approximation can be discussed in detail, it is important to show how integrals formulated in terms of spin orbitals can be converted to integrals formulated in terms of spatial orbitals, the topic of the next section.

(f) From spin orbitals to spatial orbitals

It is necessary to convert the integrals of spin orbitals to the integrals of spatial orbitals to reduce the number of variables and expedite the calculations. Moreover, chemists are accustomed to viewing molecules and their properties in terms of spatial orbitals.

For an n -electron system containing an even number of electrons, the ground state minimal basis Hartree-Fock wave function can be written as

$$|\Psi_0\rangle = |\chi_1\chi_2\chi_3\chi_4\cdots\chi_{n-1}\chi_n\rangle = |\psi_1\bar{\psi}_1\psi_2\bar{\psi}_2\cdots\psi_{n/2}\bar{\psi}_{n/2}\rangle \quad (31)$$

where

$$\chi_1(\mathbf{x}) \equiv \psi_1(\mathbf{x}) = \psi_1(\mathbf{r})\alpha(\omega) \text{ and } \chi_2(\mathbf{x}) \equiv \bar{\psi}_1(\mathbf{x}) = \psi_1(\mathbf{r})\beta(\omega) \quad (32)$$

so that a spatial orbital with a bar always indicates occupation by an electron of β spin (Levine, 2000). In this specific case, the spatial orbitals are restricted to be the same for α and β spins, so that each spatial orbital contains two electrons of opposite spin. Of course, unrestricted spins are also possible, but will not be discussed here. In terms of the spin orbitals, the energy of the ground state can be expressed as

$$E_0 = \sum_a^n [a|\hat{h}|a] + \frac{1}{2} \sum_a^n \sum_b^n [aa|bb] - [ab|ba] \quad (33)$$

where \hat{h} is the single-electron Hamiltonian

$$\hat{h}(i) = -\frac{1}{2} \nabla_i^2 - \sum_A \frac{Z_A}{r_{iA}} \quad (34)$$

and a and b represent occupied HF spin orbitals. Due to the restriction on spin, the sum over spin orbitals for single-electron integrals can be reduced to a sum over spatial orbitals as

$$\sum_a^n \chi_a = \sum_a^{n/2} \psi_a + \sum_{\bar{a}}^{n/2} \bar{\psi}_a \quad (35)$$

The expression for the two-electron integrals is

$$\sum_a^n \sum_b^n \chi_a \chi_b = \sum_a^n \chi_a \sum_b^n \chi_b = \sum_a^{n/2} (\psi_a + \bar{\psi}_a) \sum_b^{n/2} (\psi_b + \bar{\psi}_b) = \sum_a^{n/2} \sum_b^{n/2} \psi_a \psi_b + \bar{\psi}_a \psi_b + \psi_a \bar{\psi}_b + \bar{\psi}_a \bar{\psi}_b \quad (36)$$

Using (36), the first term in (33) can be reduced to

$$\sum_a^n [a|\hat{h}|a] = \sum_a^{n/2} [a|\hat{h}|a] + \sum_{\bar{a}}^{n/2} [\bar{a}|\hat{h}|\bar{a}] = 2 \sum_a^{n/2} [\psi_a|\hat{h}|\psi_a] \quad (37)$$

and the second term to

$$\begin{aligned} & \frac{1}{2} \sum_a^n \sum_b^n [aa|bb] - [ab|ba] \\ &= \frac{1}{2} \left\{ \begin{aligned} & \sum_a^{n/2} \sum_b^{n/2} [aa|bb] - [ab|ba] + \sum_a^{n/2} \sum_b^{n/2} [aa|\bar{b}\bar{b}] - [a\bar{b}|\bar{b}a] + \sum_a^{n/2} \sum_b^{n/2} [\bar{a}\bar{a}|bb] - [\bar{a}b|b\bar{a}] \\ & + \sum_a^{n/2} \sum_b^{n/2} [\bar{a}\bar{a}|\bar{b}\bar{b}] - [\bar{a}\bar{b}|\bar{b}\bar{a}] \end{aligned} \right\} \quad (38) \\ &= \sum_a^{n/2} \sum_b^{n/2} 2(\psi_a \psi_a | \psi_b \psi_b) - (\psi_a \psi_b | \psi_b \psi_a) \end{aligned}$$

where the round brackets indicate two-electron integrals over spatial orbitals.

Comparing these results with (33), it can be seen that

$$E_0 = 2 \sum_a (a|\hat{h}|a) + \sum_{ab} 2(aa|bb) - (ab|ba) \quad (39)$$

where the round brackets indicate two-electron integrals over spatial orbitals. Since the notation shows clearly that spatial orbitals are used, the upper limit of the summations ($n/2$) is not shown.

(g) The Coulomb and exchange operators

The purpose of the HF approximation is to find the set of spin orbitals that will minimize (*i.e.* provide the closest approximation to the exact minimum) the ground state energy of a system containing n electrons. The interaction between the electrons is described by the Hamiltonian. The variational principle (Szabo and Ostlund, 1989) can be used to show that the HF energy will always be higher than the exact energy. Therefore, the spin orbitals giving the lowest energy will be the most accurate description of the system. It is possible to use the variational method (Levine, 2000) to vary the spin orbitals systematically, subject to the constraint that they remain orthonormal.

The relevant equation is

$$f(1) = \hat{h}(1) + \sum_a^{n/2} 2\hat{J}_a(1) - \hat{K}_a(1) \quad (40)$$

where

$$\hat{J}_a(1) = \int \psi_a^*(2) r_{12}^{-1} \psi_a(2) d\mathbf{r}_2 \quad \text{and} \quad (41)$$

$$\hat{K}_a(1)\psi_i(1) = \left[\int \psi_a^*(2) r_{12}^{-1} \psi_i(2) \right] \psi_a(1) d\mathbf{r}_2 \quad (42)$$

Equation (41) defines the Coulomb operator, which is used to calculate the average electrostatic potential acting on the electron in ψ_a . Equation (42) defines the exchange operator. Whereas the Coulomb operator is local, the exchange operator is nonlocal and arises due to the anti-symmetry of the wave function with respect to electron exchange.

(h) The Fock operator

The Hartree-Fock equation in its eigenvalue form is

$$\left[\hat{h}(1) + \sum_{b \neq a} 2\hat{J}_b(1) - \sum_{b \neq a} \hat{K}_b(1) \right] \mu_a(1) = \varepsilon_a \mu_a(1) \quad (43)$$

where ε_a is the orbital energy of spin orbital χ_a . The restricted summation over $b \neq a$ is necessary to prevent unphysical self-interaction. However, in the HF formalism, the term representing self-interaction is

$$[\hat{J}_a(1) - \hat{K}_a(1)]\chi_a(1) = 0 \quad (44)$$

which, being equal to zero, can be added to (43). This will eliminate the restriction on the summation and enable the definition of a Fock operator

$$\hat{f}(1) = \hat{h}(1) + \sum_b \hat{J}_b(1) - K_b(1) \quad (45)$$

which simplifies the Hartree-Fock equations to

$$\hat{f}\psi_a = \varepsilon_a\psi_a \quad (46)$$

The Hamiltonian operator $\hat{h}(1)$ is also known as the core-Hamiltonian because it describes the kinetic and potential energy of electron (1) due to the field of the nuclei. The last two terms in the definition of the Fock operator are also known as the Hartree-Fock potential $\hat{v}^{\text{HF}}(1)$. The Hartree-Fock potential describes both the electrostatic interaction between electron (1) and the other electrons (in an averaged way) and the effect of exchange as described earlier.

Generally, the Hartree-Fock equations cannot be solved exactly. Typically, therefore, the exact spin functions are approximated by a linear basis set expansion. Due to the variational theorem, as the size of the basis set increases, so will the accuracy of the spin functions and the energy obtained. Theoretically, an infinite basis set will yield the exact spin functions and energy. In practice this limit, the Hartree-Fock limit, can be approached by increasing the size of the basis set as much as is practically feasible, and extrapolating from there.

(i) The Roothaan-Hall equations

The Hartree-Fock equation is an eigenvalue-like equation where applying the Fock operator to the wave function yields the energy. However, the Fock operator depends on the Coulomb and exchange operators which, in their turn, depend on the wave function. Thus, the Hartree-Fock equation is a pseudo-eigenvalue equation, which needs to be solved iteratively, and therefore an initial guess of the wave function is necessary. This can be done by expressing the wave function as a set of known basis functions (also sometimes called atomic orbitals, although they do not need to have the same form as hydrogenic atomic orbitals) which remain fixed during the variation of the wave function so that

$$\psi_i = \sum_{\mu=1}^K C_{\mu i} \phi_{\mu} \quad \text{with } i = 1, 2, \dots, K \quad (47)$$

The added advantage of introducing the basis set is that the differential equation can be converted to a set of matrix equations which is much more amenable to computerized solving. However, since the basis set expansion is limited by the computing capacity, the exact wave function can only be approximated. A factor in

the choice of basis set is therefore to have the smallest number of basis functions span the largest fraction of the space spanned by the exact molecular orbital. Because the basis functions are known, the molecular orbital is calculated by finding the set of expansion coefficients that provide the best fit of the basis functions onto the molecular orbital. In the case of Hartree-Fock optimizations, this means that the set of expansion coefficients resulting in the lowest energy of the system gives the best approximation, because the variational theorem is valid in the Hartree-Fock approximation. Equation (47) can be substituted into the Hartree-Fock equation to give

$$\hat{f}(1) \sum_v C_{vi} \phi_v(1) = \varepsilon_i \sum_v C_{vi} \phi_v(1) \quad (48)$$

Multiplying by $\phi_\mu^*(1)$ on the left and integrating gives

$$\sum_v C_{vi} \int \phi_\mu^*(1) \hat{f}(1) \phi_v(1) d\mathbf{r}_1 = \varepsilon_i \sum_v C_{vi} \int \phi_\mu^*(1) \phi_v(1) d\mathbf{r}_1 \quad (49)$$

which is a matrix equation.

The expression

$$S_{\mu\nu} = \int \phi_\mu^*(1) \phi_\nu(1) d\mathbf{r}_1 \quad (50)$$

represents the elements of the overlap matrix \mathbf{S} which is a $K \times K$ Hermitian (*i.e.* a self-adjoint) matrix. The elements on the diagonal ($S_{\mu\mu}$) are equal to one, because the overlap of an orbital with itself is complete. The magnitudes of the off-diagonal elements (which are all smaller than one) give an indication of the extent of overlap (and linear dependence) between the two relevant orbitals – a larger value implying a larger overlap.

A Fock matrix \mathbf{F} can be defined, with elements

$$F_{\mu\nu} = \int \phi_\mu^*(1) \hat{f}(1) \phi_\nu(1) d\mathbf{r}_1 \quad (51)$$

This matrix is also a Hermitian matrix and can be regarded as a matrix representation of the Fock operator with a set of basis functions $\{\phi_\mu\}$ (Szabo and Ostlund, 1989).

It is now possible to write the Hartree-Fock equation as a matrix equation so that

$$\sum_v F_{\mu\nu} C_{vi} = \varepsilon_i \sum_v S_{\mu\nu} C_{vi} \equiv \mathbf{FC} = \varepsilon \mathbf{SC} \quad (52)$$

where

$$\mathbf{C} = \begin{bmatrix} C_{11} & C_{12} & \cdots & C_{1K} \\ C_{21} & C_{22} & \cdots & C_{2K} \\ \vdots & \vdots & & \vdots \\ C_{K1} & C_{K2} & \cdots & C_{KK} \end{bmatrix} \quad (53)$$

and $\boldsymbol{\varepsilon}$ is a diagonal matrix of the orbital energies. Equation (52) is known as the Roothaan-Hall equations (Lewars, 2000).

(j) The charge density

The probability of finding an electron in a space $d\mathbf{r}$ is $|\psi_a(\mathbf{r})|^2 d\mathbf{r}$ for a wave function $\psi_a(\mathbf{r})$. The function $|\psi_a(\mathbf{r})|^2$ is known as the probability distribution function or the charge density $\rho(\mathbf{r})$. Integration of the charge density over all space gives the number of electrons in the system. The molecular orbital expansion of (47) can be inserted into the expression for charge density

$$\begin{aligned} \rho(\mathbf{r}) &= 2 \sum_a^{n/2} \psi_a^*(\mathbf{r}) \psi_a(\mathbf{r}) \\ &= 2 \sum_a^{n/2} \sum_v^{\kappa} C_{va}^* \phi_v^*(\mathbf{r}) \sum_{\mu}^{\kappa} C_{\mu a} \phi_{\mu}(\mathbf{r}) \\ &= \sum_{\mu\nu}^{\kappa} \left[2 \sum_a^{n/2} C_{\mu a} C_{va}^* \right] \phi_{\mu}(\mathbf{r}) \phi_{\nu}^*(\mathbf{r}) \\ &= \sum_{\mu\nu}^{\kappa} P_{\mu\nu} \phi_{\mu}(\mathbf{r}) \phi_{\nu}^*(\mathbf{r}) \end{aligned} \quad (54)$$

where $\mathbf{P} = [P_{\mu\nu}]$ is the density matrix. The Fock operator can be expressed in terms of the density matrix so that

$$\hat{f}(\mathbf{r}_1) = \hat{h}(\mathbf{r}_1) + \frac{1}{2} \sum_{\lambda\sigma} P_{\lambda\sigma} \left[\int \phi_{\sigma}^*(\mathbf{r}_2) (2 - \hat{P}_{12}) r_{12}^{-1} \phi_{\lambda}(\mathbf{r}_2) d\mathbf{r}_2 \right] \quad (55)$$

(l) The Fock matrix

The elements of the Fock matrix can be expressed as

$$\begin{aligned} F_{\mu\nu} &= \int \phi_{\mu}^*(1) \hat{f}(1) \phi_{\nu}(1) d\mathbf{r}_1 \\ &= \int \phi_{\mu}^*(1) \hat{h}(1) \phi_{\nu}(1) d\mathbf{r}_1 + \sum_a^{n/2} \int \phi_{\mu}^*(1) [2J_a(1) - K_a(1)] \phi_{\nu}(1) d\mathbf{r}_1 \\ &= H_{\mu\nu}^{\text{core}} + \sum_a^{n/2} 2(\mu\nu|aa) - (\mu a|a\nu) \end{aligned} \quad (56)$$

where $H_{\mu\nu}^{\text{core}}$ are the elements of the core-Hamiltonian matrix \mathbf{H}^{core} . The core Hamiltonian matrix is the means of calculating the kinetic energies and nuclear attractions of the electrons. If the basis set is known, these calculations only need to be done once, because it will remain constant throughout the energy optimization (but of course not the geometry optimization).

The linear expansion of the molecular orbitals can now be substituted into the second term on the right hand side of (56) to give

$$\begin{aligned} \sum_a^{n/2} 2(\mu\nu|aa) - (\mu a|a\nu) &= \sum_a^{n/2} \sum_{\lambda\sigma} C_{\lambda a} C_{\sigma a}^* [2(\mu\nu|\sigma\lambda) - (\mu\lambda|\sigma\nu)] \\ &= \sum_{\lambda\sigma} P_{\lambda\sigma} [(\mu\nu|\sigma\lambda) - \frac{1}{2}(\mu\lambda|\sigma\nu)] = G_{\mu\nu} \end{aligned} \quad (57)$$

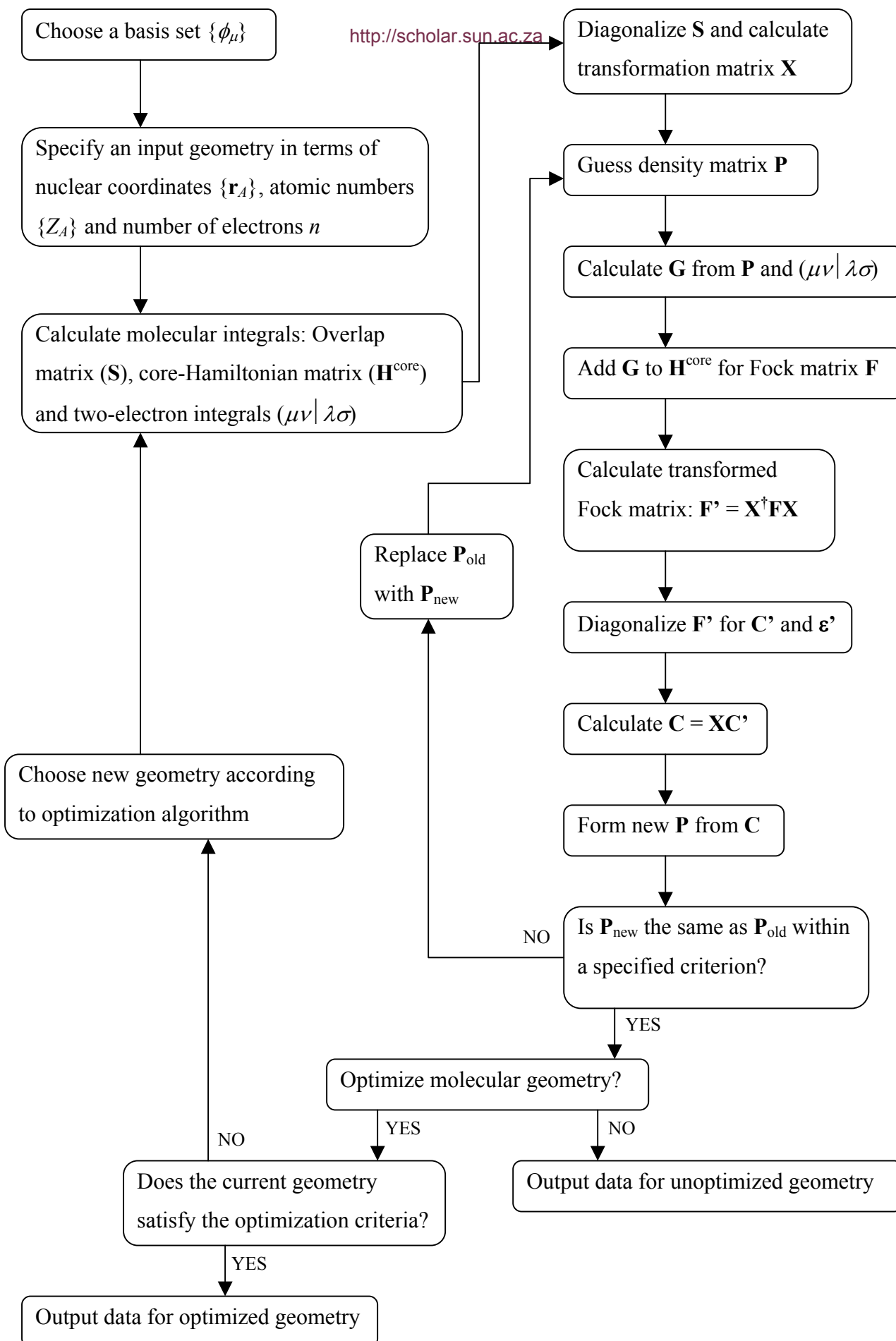
Thus, the Fock matrix can be expressed as the sum of a one-electron part and a two-electron part so that

$$F_{\mu\nu} = H_{\mu\nu}^{\text{core}} + G_{\mu\nu} \quad (58)$$

The Roothaan-Hall equations are non-linear because \mathbf{F} depends on the density matrix \mathbf{P} , thus they need to be solved iteratively, as mentioned before. Moreover, the basis set is not orthogonal (*i.e.* \mathbf{S} is not a unitary matrix), therefore \mathbf{F} cannot simply be diagonalized. So in order to solve the Roothaan-Hall equations, the basis set needs to be orthogonalized before diagonalization of the Fock matrix can yield the eigenvectors \mathbf{C} and the eigenvalues ε . The first step of the procedure is to find a transformation matrix \mathbf{X} that will transform a non-orthogonal set of functions to an orthogonal set. There are many way of doing this, each with its own advantages and disadvantages (Szabo and Ostlund, 1989; Levine, 2000).

(m) The SCF procedure

Finding the Hartree-Fock solution by means of the Roothaan-Hall equations is called the self-consistent field (SCF) procedure and is shown schematically in the diagram on the next page (Szabo and Ostlund, 1989; Cramer, 2002) within the framework of geometry optimization. Geometry optimization is a process in which the energy of a system, expressed as a function of the nuclear coordinates, is minimized. The choice of basis set is very important and will be discussed shortly. The process of energy minimization is iterative because the Roothaan-Hall equations are nonlinear. Due to this non-linearity, convergence does not always take place.



Diagrammatic representation of the SCF procedure for energy and geometry optimization

After SCF convergence has taken place, the energy of the system can be obtained. The orbital energies are given by the eigenvalues of the transformed Fock matrix, \mathbf{F}' . The total electronic energy for the ground state is given by

$$E_0 = 2 \sum_a^{n/2} h_{aa} + \sum_a^{n/2} \sum_b^{n/2} 2J_{ab} - K_{ab} \quad (59)$$

Given that

$$\varepsilon_a = f_{aa} = h_{aa} + \sum_b^{n/2} 2J_{ab} - K_{ab} \quad (60)$$

it follows that

$$E_0 = \sum_a^{n/2} (h_{aa} + f_{aa}) = \sum_a^{n/2} (h_{aa} + \varepsilon_a) \quad (61)$$

By substituting the basis function expansion into (61), the following expression is obtained for the energy:

$$E_0 = \frac{1}{2} \sum_{\mu} \sum_{\nu} P_{\nu\mu} (H_{\mu\nu}^{\text{core}} + F_{\mu\nu}) \quad (62)$$

The total energy for the system is obtained by adding the energy due to the nuclear-nuclear repulsion to the electronic energy so that

$$E_{\text{tot}} = E_0 + \sum_A \sum_{B>A} \frac{Z_A Z_B}{r_{AB}} \quad (63)$$

The optimal geometry of a molecule occurs at the minimum of the total energy as expressed above.

Many other molecular properties can also be calculated, such as the dipole and quadrupole moments and different kinds of population analyses (Levine, 2000; Szabo and Ostlund, 1989).

5. Basis Sets

A basis set is a linear expansion of a molecular orbital. Although the basis functions can be of any mathematical form, they are usually chosen to be atom-centered. The chosen basis functions must be amenable to efficient computation while giving a good description of chemical behavior. For a variational approach, larger basis sets will yield more accurate results than smaller basis sets, all other things being equal. However, they are also more expensive computationally, so a trade-off has to be made between accuracy and efficiency. Since a molecular orbital is made up of a linear

combination of the (usually) atom-centered functions, this is called the linear combination of atomic orbitals (LCAO) approach.

(a) Gaussian type orbitals

Functions of the form

$$g = ae^{-ar} \quad (64)$$

are called Slater-type orbitals (STOs) and they represent hydrogenic orbital behavior the best. However, there is no way to evaluate the two-electron integrals analytically, so they have to be solved numerically. This makes a calculation using STOs very time-consuming and unpractical in most cases. An analytical solution to the two-electron integrals is possible if the orbital function is changed to a Gaussian-type orbital (GTO), which has the form

$$g = ae^{-ar^2} \quad (65)$$

However, GTOs are not as well-behaved as STOs, especially close to the nucleus, where they taper off to a maximum gradually instead of forming a cusp. The radial decay is also too rapid to mirror the behavior of a hydrogenic orbital accurately. One way to solve these problems is to use several GTOs to replace one STO. The extra computation necessary is more than offset by the time-difference in solving two-electron integrals analytically rather than numerically. Therefore, GTOs are the basis functions used in most applications.

The equation for a GTO given above can be expanded somewhat to

$$\varphi(x, y, z; i, j, k) = \left(\frac{2\alpha}{\pi}\right)^{3/4} \left[\frac{(8\alpha)^{i+j+k} i! j! k!}{(2i)!(2j)!(2k)!}\right]^{1/2} x^i y^j z^k e^{-\alpha(x^2+y^2+z^2)} \quad (66)$$

where α controls the width of the Gaussian type orbital (GTO) and i, j , and k are nonnegative integers that give an indication of the shape of the GTO. If $i = j = k = 0$ then the orbital has spherical symmetry. If one and only one of the indices i, j , and k equals one, the GTO is a p -like orbital; if the sum of the indices is two it is a Cartesian d -like GTO, of which there are six because there are six possible combinations of having three integer indices sum to two. The Cartesian d -like GTOs can be recombined to give the five canonical d -orbitals required to span all the possible values for the z -component of the orbital angular momentum $l = 2$.

(b) Contracted Gaussian functions

The computational efficiency of GTOs can be combined with the good behavior of STOs by combining the GTOs in a linear fashion in such a way that the new function

resembles an STO. Such a function is known as a contracted Gaussian function and is expressed as

$$\varphi_{\mu}^{\text{CGF}} = \sum_{p=1}^L d_{p\mu} g_p(\alpha_{p\mu}) \quad (67)$$

where $\alpha_{p\mu}$ and $d_{p\mu}$ are contraction coefficients and L is the length of the contraction. The contraction coefficients are chosen to optimize the shape of the basis function and to ensure normalization. The individual Gaussian functions in the contraction are called primitive Gaussians. The degree of contraction (L) is determined by the number of GTOs used as primitive basis functions. The STO is better described the more primitives are used, but evaluation of the two-electron integral becomes more complicated, so a balance is needed. The use of contracted basis functions also solves the problem of representing the radial nodes of higher energy orbitals in that the coefficients may be chosen to have negative values.

The first generation of basis sets combined GTOs in a straightforward manner to yield basis sets designated as STO- M G where $M=3$ is the optimum number of GTOs for speed and accuracy.

STO- M G basis sets are minimal or single- ξ basis sets, which means that there is only one basis function (which may consist of a number of primitives) per orbital type on each atom. It is possible to expand the size of a basis set without increasing the number of primitives that are used. This is known as decontraction and consists of splitting the primitives that are contracted into one basis function. Thus, instead of having one basis function consisting of three primitives, it is possible to keep two of the primitives in one basis function and to use the third primitive as a basis function on its own, with the necessary readjustment of the normalization coefficients. A basis set with two basis functions per orbital type is a double- ξ basis set, one with three functions per orbital type is triple- ξ and so forth. However, since it is the valence orbitals that vary the most chemically, only the valence orbitals are usually decontracted. Such basis sets are called split-valence or valence-multiple- ξ basis sets. These basis sets are among the most commonly used and include the 3-21G, 6-31G and 6-311G. The number before the hyphen indicates the number of primitives used for the core basis functions and the numbers after the hyphen the number of primitives used for the valence basis functions. Thus, the 6-31G is a double-valence basis set with 6 primitives for each core orbital and 3 + 1 primitives – *i.e.* two functions – for

the valence orbitals. Since these basis sets are not minimal, they are not optimized to fit STOs, but to minimize the energy (according to the variational principle).

(c) Polarization functions

Atom-centered GTOs are useful from a chemical point of view, but are not always that flexible mathematically when molecular geometries have to be optimized. One way to improve the flexibility of the basis set without sacrificing much by way of chemical sense is to add polarization functions representing orbitals of a higher angular momentum than the functions describing the valence orbitals. So, for oxygen, a *d*-function can be added to better describe the bonding by the *s*- and *p*-orbitals. Likewise, *p*-orbitals can be added to hydrogen to describe its bonding better.

It is prudent to add a set of polarization functions for each decontraction, to ensure that the basis set remains balanced. Thus, a balanced double- ξ basis set should also contain *d*-functions on heavy atoms and *p*-functions on H and a triple- ξ basis set should have a set of *f*- and two sets of *d*-functions on the heavy atoms as well as one *d*- and two *p*-functions on H and He.

(d) Diffuse functions

Diffuse functions have very small orbital exponents, which means that their electron density decreases very slowly (relative to the other basis functions in the set) as the distance from the nucleus increases. Diffuse functions can be added to basis sets as their use warrants. Typically, the outermost electrons of anions, excited states and supermolecular complexes are weakly bound. The basis set should therefore be able to handle significant electron density away from the nucleus and this is done by adding diffuse functions.

(e) Effective core potentials

For heavier atoms, there are so many electrons that computations can become very time-consuming. Since the core electrons do not participate in chemical reactions, it increases efficiency without appreciable loss of accuracy if the inner electrons can be replaced by an analytical function (known as an effective core potential, or ECP) that describes their effect. Thus, the valence electrons can be seen as being under the influence of the nucleus-plus-core-electrons. ECPs typically take into account not only Coulomb effects, but also the Pauli exclusion principle and relativistic effects and can therefore be rather complex.

(f) Basis set superposition error

The basis set superposition error (BSSE) occurs especially in computations dealing with weak interactions between molecular fragments (say A and B). The reason for this is that each fragment has access to the basis functions on the other fragment, something that would not be possible were the fragments completely isolated. The net effect is that the interaction between the two fragments will seem to lower the energy of the system by more than is really the case, because the calculation is effectively done with a bigger basis set than specified.

One remedy for the problem is to use ghost orbitals in what is known as the counterpoise method. The ghost orbitals are placed on ghost atoms (no nucleus and no electrons) situated in the same position relative to the isolated fragment as the second fragment, *e.g.* in calculating the energy of isolated B, ghost orbitals for A are placed at the same coordinates as A in the dimer AB. This method, however, is not always successful. Another solution is to use very big basis sets, so that the BSSE will be relatively smaller, but this is not always practical when larger systems are considered.

6. Ab Initio methods with Electron Correlation

The HF-approach of treating each electron as if it moves in an averaged field due to the other electrons is useful, as it speeds up the calculation, but it also has some disadvantages. Among these is that the total amount of electron repulsion is systematically overestimated so that HF-energies are always higher than what they should be. Electrons repel each other both due to the Pauli exclusion principle and due to electrostatic interactions. HF calculations take into account the Pauli exclusion principle, but tend to overestimate its effect (*i.e.* it increases the average distance between electrons due to the exclusion principle). This overestimation is offset by the underestimation of the electrostatic repulsion, so that, overall, electrons tend to be too close to each other in the HF approximation.

Another reason why HF energies tend to be too high is that the basis set can never represent the molecular orbitals perfectly. Thus, the energies obtained by HF calculations will steadily decrease as the size of the basis set is increased (variational principle), until, at the hypothetical infinite basis set, a limit, known as the HF limit, is reached. The energy at this limit is higher than the exact energy due to HF's lack of electron correlation.

The electron correlation energy can be calculated in principle by subtracting the HF energy (in the HF limit) from the exact energy. As such, it is a negative quantity and is also sometimes known as the dynamic correlation energy. This distinguishes it from so-called static correlation energy which typically arises in problems where a single determinant approach is unsuitable, because the system can be represented by other determinants of similar energy. This is the case in the energy minimization of biradicals. Dynamic electron correlation can usually be obtained by configuration interaction (CI) or the Møller-Plesset (MP) approach. Multi-reference configuration interaction can be used for static electron correlation.

The closed-shell HF approach limits the whereabouts of the electrons to the $n/2$ orbitals (for a n -electron system) of the lowest energy. Both the CI and MP approaches make higher energy orbitals available for occupation so that the allowable space in which the electrons are contained is increased, resulting in a lowering of the energy. The two methods use quite different mathematical approaches to realize this, which will be discussed below.

(a) Configuration interaction

Configuration interaction (CI) can be seen as improving on the HF wave function by adding Slater determinants that correspond to different excited states to the Slater determinant for the ground state (which is the one used by a straightforward HF calculation) and forming a wave function consisting of a linear combination of Slater determinants:

$$\Psi = c_0|\Psi_0\rangle + \sum_{ar} c_r^a |\Psi_r^a\rangle + \sum_{\substack{a<b; \\ r<s}} c_{rs}^{ab} |\Psi_{rs}^{ab}\rangle + \sum_{\substack{a<b<c; \\ r<s<t}} c_{rst}^{abc} |\Psi_{rst}^{abc}\rangle + \sum_{\substack{a<b<c<d; \\ r<s<t<u}} c_{rstu}^{abcd} |\Psi_{rstu}^{abcd}\rangle + \dots \quad (68)$$

where $|\Psi_0\rangle$ is the HF determinant. The determinant $|\Psi_r^a\rangle$ arises by replacing spin orbital χ_a (filled in the ground state) by spin orbital χ_r (unfilled in the ground state), thus representing a singly excited electronic state. The third and fourth terms represent doubly and triply excited states respectively. These determinants are also known as configuration state functions (CSFs) and correspond to idealized electronic configurations. A CI calculation in which all the possible CSFs and their constants are calculated is known as a full CI calculation and is only possible for the smallest of molecules. Usually only the singly (known as CIS – CI singles) and doubly (known as CISD – CI singles and doubles) excited matrices are used.

Instead of obtaining the matrices and their constants in the manner strictly analogous to HF, it is also possible to optimize the constants of the basis functions within each matrix (instead of doing it just once and modifying slightly for each new determinant). This is known as multiconfigurational SCF (MCSCF). The most widely used version of MCSCF is complete active space SCF (CASSCF) in which the most important orbitals for the reaction (the active space) is chosen beforehand. It is clear that some chemical knowledge of the process needs to be known prior to the implementation of this method. Multi-reference CI (MRCI) builds on MCSCF in the same sense that CI builds on HF in that more determinants are generated from the already existing CSFs.

The coupled cluster (CC) method also generates excited determinants, but does it *via* an excitation operator so that

$$\Psi = \left(1 + \hat{T} + \frac{\hat{T}^2}{2!} + \frac{\hat{T}^3}{3!} + \dots \right) \Psi_{\text{HF}} = e^{\hat{T}} \Psi_{\text{HF}} \quad (69)$$

where $\hat{T} = \hat{T}_1 + \hat{T}_2 + \dots$, and the subscript of the operator indicates how many electrons are promoted to virtual spin orbitals. Again, there are different extents to which electrons can be promoted as implemented in the CC singles (CCS), CC singles and doubles (CCSD) and CC singles doubles and triples (CCSDT) methods. It is also possible to approximate the triples contribution, in which case the method is called CCSD(T).

Just like the HF approach, full CI is both variational and size consistent (*i.e.* a non-interacting dimer A-A would have exactly twice the energy of one monomer A). Unfortunately, the truncated methods are not variational or size consistent.

(b) The Møller-Plesset approach

The Møller-Plesset (MP) approach is based on general perturbation theory. The foundation of a perturbation method is that if a simple system can be handled well by a mathematical technique and a more complicated system is still similar to the simple system, then the more complicated system can be handled by a somewhat altered (perturbed) version of the technique used to deal with the simple system.

The MP method is implemented at a number of different levels, designated as MP0, MP1, MP2, etc. MP0 and MP1 are never used. MP0 is simply the sum of the one-electron orbital energies, whereas MP1 is the MP0 energy plus the correction due to the Coulomb and exchange integrals – *i.e.* the HF energy. The first improvement of

the HF energy is obtained by the MP2 method which is the HF energy plus an electronic perturbation term. The perturbation term, $E^{(2)}$, is the sum of the energy gained by promoting pairs of electrons to unoccupied MOs. For a two-electron system, the MP2 energy correction of the HF energy is given by

$$E^{(2)} = \frac{\left[\int d\mathbf{r}_1 d\mathbf{r}_2 \psi_1^*(1) \psi_1^*(1/r_{12}) \psi_2(1) \psi_2(2) \right]}{2(\varepsilon_1 - \varepsilon_2)} \quad (70)$$

where the operator $(1/r_{12})$ indicates the Coulombic interaction between the electrons over distance; and ψ_1 is the occupied orbital and ψ_2 the unoccupied orbital. The energy difference $\varepsilon_1 - \varepsilon_2$ is negative (because ψ_1 is lower in energy than ψ_2). The larger its absolute value becomes, the more difficult it is for the excitation to take place, so the absolute value of $E^{(2)}$ will also be less. In MP calculations the virtual orbitals are also optimized and not just the occupied orbitals as in HF calculations.

Higher levels of MP calculations involve the interaction of doubly excited states with each other (MP3), and single, double, triple and quadruple excitations (MP4). MP2 and MP4 are the methods most commonly employed.

7. Density Functional Theory

(a) Electron density

For a system containing n electrons the probability that an electron is in the space-volume element $d\mathbf{x}_1$ at \mathbf{x}_1 while another electron is in the space-volume element $d\mathbf{x}_2$ at \mathbf{x}_2 and so forth up to electron n is given by

$$\Phi(\mathbf{x}_1, \mathbf{x}_2, \mathbf{x}_3, \dots, \mathbf{x}_n) \Phi^*(\mathbf{x}_1, \mathbf{x}_2, \mathbf{x}_3, \dots, \mathbf{x}_n) d\mathbf{x}_1, d\mathbf{x}_2, d\mathbf{x}_3, \dots, d\mathbf{x}_n \quad (71)$$

The probability of finding an electron in the space-volume element $d\mathbf{x}_1$ at \mathbf{x}_1 while all the other electrons may be anywhere is given by averaging over all the other electrons' space-spin coordinates, so that

$$\rho(\mathbf{x}_1) = n \int \Phi(\mathbf{x}_1, \mathbf{x}_2, \mathbf{x}_3, \dots, \mathbf{x}_n) \Phi^*(\mathbf{x}_1, \mathbf{x}_2, \mathbf{x}_3, \dots, \mathbf{x}_n) d\mathbf{x}_2, d\mathbf{x}_3, \dots, d\mathbf{x}_n \quad (72)$$

which is the electron density. The function $\rho(\mathbf{x}_1)$ is also known as the reduced density function for a single electron in an n -electron system.

The probability of finding an electron in the space-volume element $d\mathbf{x}_1$ at \mathbf{x}_1 while another electron is simultaneously in the space-volume element $d\mathbf{x}_2$ at \mathbf{x}_2 and all the other electrons may be anywhere is given by the reduced pair density function

$$\rho_2(\mathbf{x}_1, \mathbf{x}_2) = n(n-1) \int \Phi(\mathbf{x}_1, \mathbf{x}_2, \mathbf{x}_3, \dots, \mathbf{x}_n) \Phi^*(\mathbf{x}_1, \mathbf{x}_2, \mathbf{x}_3, \dots, \mathbf{x}_n) d\mathbf{x}_3, \dots, d\mathbf{x}_n \quad (73)$$

The reduced pair density function can be extended to a second-order or two-electron reduced density matrix $\gamma(\mathbf{x}_1, \mathbf{x}_2; \mathbf{x}_1', \mathbf{x}_2')$ so that

$$\gamma(\mathbf{x}_1, \mathbf{x}_2; \mathbf{x}_1', \mathbf{x}_2') = n(n-1) \int \Phi(\mathbf{x}_1, \mathbf{x}_2, \mathbf{x}_3, \dots, \mathbf{x}_n) \Phi^*(\mathbf{x}_1', \mathbf{x}_2', \mathbf{x}_3, \dots, \mathbf{x}_n) d\mathbf{x}_3, \dots, d\mathbf{x}_n \quad (74)$$

If $\mathbf{x}_1 = \mathbf{x}_1'$ and $\mathbf{x}_2 = \mathbf{x}_2'$ then $\gamma(\mathbf{x}_1, \mathbf{x}_1; \mathbf{x}_1', \mathbf{x}_1') = \rho_2(\mathbf{x}_1, \mathbf{x}_2)$. In addition, interchanging \mathbf{x}_1 and \mathbf{x}_2 or \mathbf{x}_1' and \mathbf{x}_2' will change the sign of γ . This means, therefore, that two electrons of the same spin cannot be in the same volume-element simultaneously – electrons show exchange (or Fermi) correlation. The charge on the electrons also prevents them from coming too close to each other. Therefore, the motion of electrons shows correlation due to charge as well, known as Coulomb correlation.

(b) The Hohenberg-Kohn theorems

Hohenberg and Kohn proved two theorems – an existence and a variational theorem – that in principle established density functional theory (DFT) as a valid and reliable approach to calculating molecular properties.

The First Hohenberg-Kohn theorem states that the ground-state electron density of a molecule can uniquely determine its ground-state energy, wave function and other electronic properties, provided that the ground state is nondegenerate. The ground-state wave function is an eigenfunction of the electronic Hamiltonian, which can be expressed as

$$\hat{H} = -\frac{1}{2} \sum_{i=1}^n \nabla_i^2 + \sum_{i=1}^n v(\mathbf{r}_i) + \sum_i \sum_{j>i} \frac{1}{r_{ij}} \quad (75)$$

where

$$v(\mathbf{r}_i) = -\sum_A \frac{Z_A}{r_{iA}} \quad (76)$$

is called the external potential. The external potential is the potential energy resulting from the interaction between the electron and the fixed nuclei. Hohenberg and Kohn have shown that the ground-state electron density determines the external potential as well as the number of electrons (Levine, 2000).

Integration of the electron density over all space gives the number of electrons. To show that the ground state electron probability density (expressed as $\rho_0(\mathbf{r}_i)$) also determines the external potential, it can be supposed that this is not so and that two different (by more than an additive constant) external potentials $v_a(\mathbf{r}_i)$ and $v_b(\mathbf{r}_i)$ can be determined by one electron density $\rho_0(\mathbf{r}_i)$. Then \hat{H}_a and \hat{H}_b are the two n -electron Hamiltonians for v_a and v_b with $\psi_{0,a}$ and $\psi_{0,b}$ their ground-state normalized wave

functions and $E_{0,a}$ and $E_{0,b}$ their ground-state energies. The wave functions have to be different because their Hamiltonians differ by more than an additive constant. However, given that the ground state is nondegenerate, only one normalized wave function can give the exact energy of the ground state. Any other normalized ground-state wave function will give an energy that is higher. Thus

$$E_{0,a} < \langle \psi_{0,b} | \hat{H}_a | \psi_{0,b} \rangle = \langle \psi_{0,b} | \hat{H}_a + \hat{H}_b - \hat{H}_b | \psi_{0,b} \rangle = \langle \psi_{0,b} | \hat{H}_a - \hat{H}_b | \psi_{0,b} \rangle + \langle \psi_{0,b} | \hat{H}_b | \psi_{0,b} \rangle \quad (77)$$

But since \hat{H}_a and \hat{H}_b only differ by their external potentials, it follows that

$$E_{0,a} < \left\langle \psi_{0,b} \left| \sum_{i=1}^n [v_a(\mathbf{r}_i) - v_b(\mathbf{r}_i)] \right| \psi_{0,b} \right\rangle + E_{0,b} \quad (78)$$

It can be shown that

$$\int d\mathbf{r} \psi^* \sum_{i=1}^n B(\mathbf{r}_i) \psi = \int \rho(\mathbf{r}) B(\mathbf{r}) d\mathbf{r} \quad (79)$$

for any function B of the spatial coordinates of an electron (Levine, 2000). Since the external potential is the function of the spatial coordinates of an electron, it follows that

$$E_{0,a} < \int \rho_{0,b}(\mathbf{r}) [v_a(\mathbf{r}_i) - v_b(\mathbf{r}_i)] d\mathbf{r} + E_{0,b} \quad (80)$$

The converse also holds

$$E_{0,b} < \int \rho_{0,a}(\mathbf{r}) [v_b(\mathbf{r}_i) - v_a(\mathbf{r}_i)] d\mathbf{r} + E_{0,a} \quad (81)$$

But according to the initial assumption, $\rho_{0,a} = \rho_{0,b}$ so that

$$E_{0,a} + E_{0,b} < E_{0,b} + E_{0,a} \quad (82)$$

which is false. Therefore, the initial assumption – that two different (by more than an additive constant) external potentials $v_a(\mathbf{r}_i)$ and $v_b(\mathbf{r}_i)$ can be determined by one electron density $\rho_0(\mathbf{r}_i)$ – is false.

This theorem shows that the ground state energy is a functional of the electron density. Thus

$$E_0 = E_v[\rho_0] = \bar{T}[\rho_0] + \bar{V}_{Ne}[\rho_0] + \bar{V}_{ee}[\rho_0] \quad (83)$$

where the subscript v shows the dependence of E_0 on the external potential and where the bars indicate average values. From

$$\hat{V}_{Ne} = \sum_{i=1}^n v(\mathbf{r}_i) \quad (84)$$

where the external potential is defined as in (76). From (79) it follows that

$$\bar{V}_{Ne} = \left\langle \psi_0 \left| \sum_{i=1}^n v(\mathbf{r}_i) \right| \psi_0 \right\rangle = \int \rho_0(\mathbf{r}) v(\mathbf{r}) d\mathbf{r} \quad (85)$$

Thus $\bar{V}_{Ne}[\rho_0]$ is known, while $\bar{T}[\rho_0]$ and $\bar{V}_{ee}[\rho_0]$ remain unknown. The latter two functionals can be combined so that

$$F[\rho_0] = \bar{T}[\rho_0] + \bar{V}_{ee}[\rho_0] \quad (86)$$

where the functional $F[\rho_0]$ – known as the Hohenberg-Kohn functional – is not dependent on the external potential. This means that the Hohenberg-Kohn functional is universal to all systems. As shown earlier (98), $\bar{V}_{ee}[\rho_0]$ can be decomposed into a classical Coulomb part and a non-classical part containing the exchange-correlation hole function. Since the ground state density determines the Hamiltonian used for all excited states too, it can be said that the excited states are formally dependent on the ground state density. Moreover, only the ground state density can be used to determine the external potential of a system. However, other functionals than the ones just defined are necessary to determine the properties of the excited states and thus, DFT is mainly seen as a ground state theory.

While the first Hohenberg-Kohn theorem proves that the ground state electron density is necessary and sufficient to determine all the properties of interest, the second theorem proves that the electron density is variational – *i.e.* that only the exact ground state density will deliver the lowest energy. This can be proved by constructing a trial functional ρ_{tr} for an n -electron system such that

$$\int \rho_{tr}(\mathbf{r}) d\mathbf{r} = n \text{ and } \rho_{tr}(\mathbf{r}) \geq 0 \forall \mathbf{r} \quad (87)$$

This electron density determines the external potential v_{tr} , which determines the wave function ψ_{tr} corresponding to ρ_{tr} . From the variation theorem it follows that

$$\left\langle \psi_{tr} \left| \hat{H} \right| \psi_{tr} \right\rangle = \left\langle \psi_{tr} \left| \hat{T} + \hat{V}_{ee} + \sum_{i=1}^n v(\mathbf{r}_i) \right| \psi_{tr} \right\rangle \geq E_0 = E_v[\rho_0] \quad (88)$$

From (85) and given that the average kinetic and potential energies are functionals of the electron density

$$\bar{T}[\rho_{tr}] + \bar{V}_{ee}[\rho_{tr}] + \int \rho_{tr} v(\mathbf{r}) d\mathbf{r} \geq E_v[\rho_0] \quad (89)$$

Here, the functionals are the same as in (83), although the electron densities differ. Thus, from (89)

$$E_v[\rho_{tr}] \geq E_v[\rho_0] \quad (90)$$

for any $\rho_{tr} \neq \rho_0$, which proves that no trial density function can give a ground state energy lower than that given by the exact ground-state density function.

Although these two theorems show that the exact ground state electron density gives the ground state energy and that the exact electron density functionals are variational, it says nothing of how to obtain the exact functionals. Specifically, the Hohenberg-Kohn functional is not exactly known and there is no systematic way to improve the available functionals. Moreover, since the variational theorem only holds for the exact functionals, the approximate functionals (which means that the Hamiltonian is an approximation too) cannot be regarded as variational. The reason for this is that only approaches that employ exact Hamiltonians are variational.

(c) The Kohn-Sham approach

The Kohn-Sham approach provides a way to solve chemical problems by means of DFT. Central to their scheme is the concept of the non-interacting reference system, in which the quantities that need to be calculated are broken down in such a way that as much as possible of the energy of the system can be calculated without any approximations. Thus, only a small part of the total energy needs to be calculated by approximate methods.

The non-interacting reference system consists of n electrons that experience an external potential $v_s(\mathbf{r}_i)$ such that the ground state electron density $\rho_s(\mathbf{r})$ will be identical to that of the real system where electrons do interact – *i.e.* $\rho_s(\mathbf{r}) = \rho_0(\mathbf{r})$, where the subscripts s and 0 denote the non-interacting reference system and the real system respectively. Since the electrons do not interact with each other in the reference system, the Hamiltonian can be expressed as

$$\hat{H}_s = \sum_{i=1}^n \left[-\frac{1}{2} \nabla_i^2 + v_s(\mathbf{r}_i) \right] \equiv \sum_{i=1}^n \hat{h}_i^{\text{KS}} \quad (91)$$

where the subscript s refers to the reference system and \hat{h}_i^{KS} denotes the one-electron Kohn-Sham Hamiltonian which does not contain any electron-electron interactions, as expected. Due to this non-interaction, the ground state wave function can be described by a determinant similar to the Slater determinant so that

$$\Phi^{\text{KS}} = \frac{1}{\sqrt{n}} \begin{vmatrix} \chi_1^{\text{KS}}(\mathbf{x}_1) & \chi_2^{\text{KS}}(\mathbf{x}_1) & \chi_n^{\text{KS}}(\mathbf{x}_1) \\ \chi_1^{\text{KS}}(\mathbf{x}_2) & \chi_2^{\text{KS}}(\mathbf{x}_2) & \chi_n^{\text{KS}}(\mathbf{x}_2) \\ \chi_1^{\text{KS}}(\mathbf{x}_n) & \chi_2^{\text{KS}}(\mathbf{x}_n) & \chi_n^{\text{KS}}(\mathbf{x}_n) \end{vmatrix} \quad (92)$$

where the superscripts KS indicate that this is a Kohn-Sham system and the χ_i^{KS} for $i=1, 2, 3, \dots, n$ are Kohn-Sham spin orbitals. These spin orbitals, like their HF analogs, can be decomposed into a spatial part and a spin part so that

$$\chi_i^{\text{KS}} = \varphi_i^{\text{KS}} \sigma \quad (93)$$

where σ is a spin function with either up or down spin. As in the HF approach, the spatial portions of the spin orbitals can be obtained by the pseudo-eigenvalue equation

$$\hat{h}^{\text{KS}} \varphi_i^{\text{KS}} = \varepsilon_i^{\text{KS}} \varphi_i^{\text{KS}} \quad (94)$$

Now the external potential upon which the Hamiltonian depends must be chosen in such a way that $\rho_s(\mathbf{r}) = \rho_0(\mathbf{r})$ will hold.

The ground state energy of a system containing n electrons can be written as

$$E_0 = E_v[\rho_0] = \bar{T}[\rho_0] + \bar{V}_{\text{Ne}}[\rho_0] + \bar{V}_{\text{ee}}[\rho_0] = F[\rho_0] + \bar{V}_{\text{Ne}}[\rho_0] \quad (95)$$

where the latter term depends on the system and the first term is the universal Kohn-Sham functional

$$F[\rho_0] = \bar{T}[\rho_0] + V_{\text{ee}}[\rho_0] \quad (96)$$

While neither of these terms can be expressed as explicit functionals of the ground state density, it is possible to write both in terms of the non-interacting electron density ρ_s , in order to compute as much as possible of the energy exactly. However, this approach will not account for the electronic interaction encountered in the real system, even though a large part of the energy will be calculated exactly.

Thus, a quantity $\Delta\bar{T}[\rho_0]$ can be defined as

$$\Delta\bar{T}[\rho_0] \equiv \bar{T}[\rho_0] - \bar{T}[\rho_s] \quad (97)$$

where

$$\bar{T}[\rho_s] = -\frac{1}{2} \sum_{i=1}^n \langle \varphi_i^{\text{KS}} | \nabla^2 | \varphi_i^{\text{KS}} \rangle \quad (98)$$

It can be shown that $\Delta\bar{T}[\rho_0] \geq 0$. A second quantity $\Delta\bar{V}_{\text{ee}}[\rho_0]$ can be defined as

$$\Delta\bar{V}_{\text{ee}}[\rho_0] = \bar{V}_{\text{ee}}[\rho_0] - \bar{V}_{\text{ee}}[\rho_s] \quad (99)$$

where

$$\bar{V}_{ee}[\rho_s] = \frac{1}{2} \int \frac{\rho(\mathbf{r}_1)\rho(\mathbf{r}_2)}{r_{12}} d\mathbf{r}_1 d\mathbf{r}_2 \quad (100)$$

which is the classical expression for the electrostatic interaction between two electrons that are smeared out in an average density. Thus (83) can now be written as

$$\begin{aligned} E_v[\rho_0] &= \bar{V}_{Ne}[\rho_0] + \bar{T}[\rho_0] + \bar{V}_{ee}[\rho_0] \\ &= \int \rho(\mathbf{r})v(\mathbf{r})d\mathbf{r} + \bar{T}[\rho_s] + \frac{1}{2} \int \int \frac{\rho(\mathbf{r}_1)\rho(\mathbf{r}_2)}{r_{12}} d\mathbf{r}_1 d\mathbf{r}_2 + \Delta\bar{T}[\rho_0] + \Delta\bar{V}_{ee}[\rho_0] \end{aligned} \quad (101)$$

The first three terms on the right hand side can be calculated exactly and constitute the bulk of the contribution to the energy of the system. The functionals in the last two terms are unknown and are defined as the exchange-correlation functional so that

$$E_{XC}[\rho_0] \equiv \Delta\bar{T}[\rho_0] + \Delta\bar{V}_{ee}[\rho_0] \quad (102)$$

Contained in these two terms are the kinetic correlation energy (the first term on the right-hand side), the exchange energy (from anti-symmetry), the Coulombic correlation energy and a correction for self-interaction. The self-interaction arises because the electrons in this expression are smeared out in space, so they can interact with their own charges – which is unphysical.

The energy of the ground state, E_0 , can be found from the electron density by means of the Kohn-Sham orbitals, because they are related by

$$\rho_0 = \rho_s = \sum_{i=1}^n |\varphi_i^{\text{KS}}|^2 \quad (103)$$

where the KS-orbitals must be orthonormal. Therefore

$$E_0 = -\sum_A Z_A \int \frac{\rho(\mathbf{r}_1)}{r_{1A}} d\mathbf{r}_1 - \frac{1}{2} \sum_{i=1}^n \langle \varphi_i^{\text{KS}}(1) | \nabla_1^2 | \varphi_i^{\text{KS}}(1) \rangle + \frac{1}{2} \int \frac{\rho(\mathbf{r}_1)\rho(\mathbf{r}_2)}{r_{12}} d\mathbf{r}_1 d\mathbf{r}_2 + E_{XC}[\rho] \quad (104)$$

It can be shown that the Kohn-Sham orbitals that will minimize the ground state energy will satisfy the equation

$$\left[-\frac{1}{2} \nabla_1^2 - \sum_A \frac{Z_A}{r_{1A}} + \int \frac{\rho(\mathbf{r}_2)}{r_{12}} d\mathbf{r}_2 + v_{XC}(1) \right] \varphi_i^{\text{KS}}(1) = \left[-\frac{1}{2} \nabla_1^2 - v_s(1) \right] \varphi_i^{\text{KS}}(1) = \varepsilon_i^{\text{KS}} \varphi_i^{\text{KS}}(1) \quad (105)$$

where $v_{XC}(1)$ is defined as

$$v_{XC}(1) = \frac{\delta E_{XC}[\rho(\mathbf{r})]}{\delta \rho(\mathbf{r})} \quad (106)$$

and is known as the exchange-correlation potential. The expression denoted by $v_s(1)$ is the external potential of the non-interacting system.

The functional derivative can easily be found from $E_{xc}[\rho_0]$ (if the latter were known) (Levine, 2000). In addition, the one-electron Kohn-Sham operator of (105) plays the same role in solving the Kohn-Sham equations as the Fock operator in solving the Hartree-Fock equations. The main difference is that the exchange operator contained in the Hartree-Fock operator is now replaced by the exchange-correlation potential, which handles both exchange and correlation.

The potential $v_s(\mathbf{r})$ of the non-interacting Kohn-Sham reference system – *i.e.* the Kohn-Sham potential – is local because it only depends on the value of \mathbf{r} at a single point in space. However, its dependency on the density is likely to be non-local and complex.

It is also important to note that the exchange-correlation energy in the Kohn-Sham scheme is not exactly the same as the exchange and correlation in the Hartree-Fock scheme (Koch and Holthausen, 2000). The primary reason for this is that the Hartree-Fock ground state electron density is not exact, since it is derived from the non-exact wave function. On the other hand, the Kohn-Sham ground state electron density is exact by definition.

A common perception is that the Kohn-Sham orbitals do not have any physical meaning because they cannot be related to a wave function in the same sense as the Hartree-Fock orbitals. However, it has been shown that the Kohn-Sham orbitals do resemble the Hartree-Fock orbitals and that they could therefore be used at least for qualitative applications. Moreover, the Hartree-Fock orbitals neither reflect the effects of correlation nor do they yield the exact density; the Kohn-Sham orbitals are based on the exact density and on a one-electron potential that includes all the non-classical effects. The orbital energies indeed have no physical meaning, though with the exception of the orbital energy of the highest occupied Kohn-Sham orbital. This energy is equal to the negative of the molecular ionization energy, given that the exact functional was used to obtain it.

The Kohn-Sham scheme can be extended to unrestricted systems, as discussed in detail in Koch and Holthausen, 2000.

(d) The adiabatic connection

Most of the contributions to the electronic energy of a system can be determined exactly, leaving only the exchange functional as an unknown. However, unlike the Hartree-Fock wave function approach, it is not possible to improve systematically on approximate functionals, primarily because they are not variational. A way to obtain good approximations to the exact exchange functional needs to be obtained. Before that, it is necessary to find a way to connect the non-interacting reference system to the real interacting system and this is done by means of the adiabatic connection.

The Hamiltonian for an n -electron system can be written as

$$\hat{H} = \sum_{i=1}^n \left(-\frac{1}{2} \nabla_i^2 + v_{ext}^\lambda(\mathbf{r}_i) \right) + \lambda \sum_i^n \sum_{j>i}^n \frac{1}{r_{ij}} \quad (107)$$

where λ is the coupling strength parameter. If $\lambda = 0$, the system is non-interacting and $v_{ext}^{\lambda=0} = v_s$; if $\lambda = 1$ the system is fully interacting and $v_{ext}^{\lambda=1} = v_0$. As the value of λ is varied between 0 and 1, the external potential adapts to keep the reference electron density equal to the exact density. The path connecting the various external potentials connected to the values of λ is a smooth and continuous trajectory called the adiabatic connection. The energy of the interacting system is therefore given by the definite integral

$$E_{\lambda=1} - E_{\lambda=0} = \int_0^1 dE_\lambda \quad (108a)$$

$$\text{therefore } E_{\lambda=1} = E_{\lambda=0} + \int_0^1 dE_\lambda \quad (108b)$$

The change in energy for an infinitesimal change in the coupling strength parameter is given by the expectation value of

$$d\hat{H} = dv_{ext}^\lambda + d\lambda \sum_i^n \sum_{j>i}^n \frac{1}{r_{ij}} \quad (109)$$

where the kinetic energy term disappears because it is not influenced by a change in λ . From (106) and (108) it follows that

$$E_{\lambda=1} - E_{\lambda=0} = \int \rho(\mathbf{r}) [v_{ext}^{\lambda=1} - v_{ext}^{\lambda=0}] d\mathbf{r} + \frac{1}{2} \int \frac{\rho(\mathbf{r}_1)\rho(\mathbf{r}_2)}{r_{12}} d\mathbf{r}_1 d\mathbf{r}_2 + \frac{1}{2} \int d\lambda \frac{\rho(\mathbf{r}_1)h_{XC}^\lambda}{r_{12}} d\mathbf{r}_1 d\mathbf{r}_2 \quad (110)$$

Since

$$E_{\lambda=0} = \bar{T}[\rho_s] + \int \rho_s(\mathbf{r}) v[\rho_s] d\mathbf{r} \quad (111)$$

and a coupling-strength integrated exchange-correlation hole can be defined as

$$\bar{h}_{xc}(\mathbf{r}_1; \mathbf{r}_2) \equiv \int h_{xc}^\lambda(\mathbf{r}_1; \mathbf{r}_2) d\lambda \quad (112)$$

the energy of the real and interacting system can be written as

$$E_{\lambda=1} = \bar{T}[\rho_s] + \int \rho(\mathbf{r}) v_{\text{eff}} d\mathbf{r} + \frac{1}{2} \int \frac{\rho(\mathbf{r}_1)\rho(\mathbf{r}_2)}{r_{12}} d\mathbf{r}_1 d\mathbf{r}_2 + \frac{1}{2} \int \frac{\rho(\mathbf{r}_1)\bar{h}_{xc}(\mathbf{r}_1; \mathbf{r}_2)}{r_{12}} d\mathbf{r}_1 d\mathbf{r}_2 \quad (113)$$

where the exchange energy is given by the last term on the right-hand side. Thus, integration over the coupling strength parameter transfers $\Delta\bar{T}[\rho_0]$ from the kinetic energy term to the hole function.

(e) The local density approximation

The idea of the uniform electron gas is central to the local density approximation (LDA). The uniform electron gas is an infinite-volume system of neutral charge containing an infinite number of interacting electrons that move against the background of a smeared-out positive charge. The electron density is nonzero and constant throughout. In a system where ρ varies infinitesimally slowly with a change in position, the exchange energy is given by

$$E_{xc}^{\text{LDA}}[\rho] = \int \rho(\mathbf{r}) \varepsilon_{xc}(\rho) d\mathbf{r} \quad (114)$$

where $\varepsilon_{xc}(\rho)$ is the one-electron exchange-correlation energy for an electron in a uniform electron gas. The functional derivative (Levine, 2000) of E_{xc}^{LDA} is

$$v_{xc}^{\text{LDA}} = \frac{\delta E_{xc}^{\text{LDA}}}{\delta \rho} = \varepsilon_{xc}(\rho(\mathbf{r})) + \rho(\mathbf{r}) \frac{\partial \varepsilon_{xc}(\rho)}{\partial \rho} \quad (115)$$

Equations (114) and (115) are known as the local density approximation to finding the energy. Formally, the one-electron correlation-exchange energy can be split into exchange and correlation energies where the exchange part is given by

$$\varepsilon_x(\rho) = -\frac{3}{4} \left(\frac{3}{\pi}\right)^{1/3} (\rho(\mathbf{r}))^{1/3} \quad (116)$$

known as the Slater exchange and the correlation part by

$$\varepsilon_c(\rho) = \varepsilon_c^{\text{VWN}}(\rho) \quad (117)$$

where the superscript VWN indicates a known, but very complicated function derived by Vosko, Wilk and Nusair in 1980 (Koch and Holthausen, 2000). The function is not exact, but was obtained by interpolation from accurate numerical quantum Monte Carlo simulations of the homogeneous electron gas.

(f) The generalized gradient approximation

Since the LDA depends on the properties of a uniform electron gas, one can hardly expect it to give accurate results for systems where the electron density shows considerable variation, *i.e.* most systems of chemical interest. The generalized gradient approximation (GGA) also considers the gradient of the electron density and as such incorporates changes in the density. A generic expression for a GGA-functional is

$$E_{XC}^{GGA}[\rho_\alpha, \rho_\beta] = \int F(\rho_\alpha, \rho_\beta, \nabla\rho_\alpha, \nabla\rho_\beta) d\mathbf{r} \quad (118)$$

where ρ_α and ρ_β indicate the electron densities of electrons with opposite spins and ∇ symbolizes the gradient of the electron density. As with the LDA, the exchange-correlation energy is split into exchange and correlation parts so that

$$E_{XC}^{GGA} = E_X^{GGA} + E_C^{GGA} \quad (119)$$

which are generally modeled separately. Modeling is based on the known behavior of the exact functionals as well as the addition of some empirical parameters to fit data.

Commonly used GGA exchange functionals include Perdew and Wang's 1986 (without empirical parameters) and 1991 functionals and Becke's 1988 functional. Functionals by Lee, Yang and Parr; Perdew and Becke are commonly used correlation functionals. Exchange and correlation functionals can be used in any combination, with the BLYP-combination a popular one. The B denotes Becke's 1988 exchange functional and LYP is the Lee-Yang-Parr exchange functional. Something to keep in mind is that the form of a specific functional (especially if it includes empirical parameters) does not aid in understanding the underlying physics, which is probably too complex to be captured by a single mathematical expression of reasonable simplicity anyway. Also, GGA functionals are sometimes called non-local. Mathematically speaking, they are as local as LDA functionals because the value of the functional at \mathbf{r} only depends on the density at that point. Therefore, the label non-local is best avoided lest confusion arises.

(g) Hybrid functionals

An accurate expression for the exchange energy should increase the overall accuracy of the exchange-correlation functional because the exchange contribution to the exchange-correlation energy is typically much higher than the correlation contribution. An obvious route therefore would be to substitute the approximate density functional exchange by the exact Hartree-Fock exchange given as

$$E_x = -\frac{1}{4} \sum_{i=1}^n \sum_{j=1}^n \langle \phi_i^{\text{KS}}(1) \phi_j^{\text{KS}}(2) | 1/r_{12} | \phi_j^{\text{KS}}(1) \phi_i^{\text{KS}}(2) \rangle \quad (120)$$

However, the exact exchange hole of the density functional approach is delocalized, as is the exact correlation hole. When they are combined (the separation is only formal anyway), most of their errors cancel so as to give an exact localized total hole. The approximate exchange and correlation holes of the LDA and GGA are also localized to give a localized (approximate) total hole. The Hartree-Fock exchange hole, being exact, is delocalized. Combining the exact delocalized exchange with the approximate localized correlation will not lead to a canceling of errors. Therefore, in order to have the advantage of the exact Hartree-Fock exchange with the localized nature of the approximate exchange hole, the exchange hole is represented by a mixture of the Hartree-Fock exchange and the approximate density functional exchange.

The first generation hybrid exchange-correlation functionals simply contain half Hartree-Fock exchange-correlation and half density functional exchange-correlation and are known as half-and-half functionals. The next step is to weight the contributions from Hartree-Fock and density functional exchange by introducing empirical parameters. The very popular B3LYP functional is an example of an empirically weighted hybrid functional and is expressed as a combined exchange-correlation functional

$$E_{\text{XC}}^{\text{B3LYP}} = (1 - a_0 - a_X) E_X^{\text{LSDA}} + a_0 E_X^{\text{exact}} + a_X E_X^{\text{B88}} + (1 - a_C) E_C^{\text{VWN}} + a_C E_C^{\text{LYP}} \quad (121)$$

where E_X^{exact} is defined in equation (120) and the empirical parameters $a_0 = 0.20$, $a_X = 0.72$ and $a_C = 0.81$ were found by fitting experimental molecular atomization energies.

Hybrid functionals are very popular due to their flexibility and reasonably accurate results at a fairly low computational cost. Currently, the most widely-used functional and the one employed for geometry optimizations in this study is the B3LYP functional.

It will probably not be possible to improve on these functionals without introducing higher-order density derivatives (Levine, 2000), but this will significantly increase the computing time.

(h) Self-interaction

For a one-electron system the electrostatic repulsion should be zero, *i.e.* the term

$$\bar{V}_{ee}[\rho_s] = \frac{1}{2} \int \frac{\rho(\mathbf{r}_1)\rho(\mathbf{r}_2)}{r_{12}} d\mathbf{r}_1 d\mathbf{r}_2 \quad (122)$$

should vanish. However, this is not the case. In the Hartree-Fock scheme, this is not a problem, because the self-interaction is cancelled by the exchange term. In a density functional scheme, the exchange functionals are approximate, so the self-interaction error is not corrected completely. This holds not only for one-electron systems, but also for systems containing many electrons. Moreover, the only correlation functional that gives zero correlation for one-electron systems is the LYP functional (Koch and Holthausen, 2000). A self-interaction corrected scheme due to Perdew and Zunger does exist, but unfortunately the external potential is orbital dependent and therefore the scheme is not of much practical use in large systems.

The error due to self-interaction is most severe in cases where a molecule splits to form two identical radicals and a non-integer number of electrons need to be transferred. Since this study does not deal with homologous bond breaking, the issue of self-interaction will be kept in mind, but not of concern here.

(i) DFT calculations

DFT calculations also follow an SCF procedure as in HF calculations. Where the density matrix forms the starting guess in HF, the electron density is the initial guess in DFT. The initial guess for a molecular system is typically a superposition of the individual atomic densities. The initial electron density is used to generate an initial external potential, which is in turn used to obtain the initial Kohn-Sham (KS) orbitals. The KS molecular orbitals are represented as a basis set of atomic orbitals, so that it really is the orbital coefficients that are guessed. Thus a set of equations similar to the Roothaan-Hall equations is obtained. This process is iterated until the exchange-correlation potential reaches self-consistence with respect to the KS orbitals. The ground state energy can be obtained from the converged electron density. Analytic first and second derivatives of the KS DFT energy can be obtained, so geometry optimizations and frequency calculations can be done in a manner similar to the HF procedure.

While the procedure for DFT calculations is very similar to that for Hartree-Fock calculations, there is one big difference, which lies in evaluating the two-electron integrals of the Coulomb term. For HF calculations, these two-electron integrals need to be calculated explicitly because they are needed for both the classical Coulomb energy and the exchange energy. However, since the exchange and correlation in DFT

is obtained by approximation, explicit evaluation of two-electron integrals become redundant. The density can be expanded (approximately) into an auxiliary basis set which is atom-centered, so that

$$\rho(\mathbf{r}) \approx \tilde{\rho}(\mathbf{r}) = \sum_{\kappa}^K c_{\kappa} \omega_{\kappa}(\mathbf{r}) \quad (123)$$

where the tilde indicates an approximate density and the auxiliary basis set is symbolized by $\{\omega\}$. Alternatively, the two-electron integrals can be solved numerically as points on a grid. A weighted summation over all the grid points leads to the Coulomb contribution (Koch and Holthausen, 2000).

(k) Concluding remarks

It is generally agreed that DFT provides more accurate results for organometallic systems than *ab initio* methods of similar computational cost (see, for example Ziegler, 2005). Specific examples pertaining to the work in this study will be mentioned in context of the discussions in the next two chapters.

IV. MODELING THE CATALYTIC CYCLE

1. Introduction

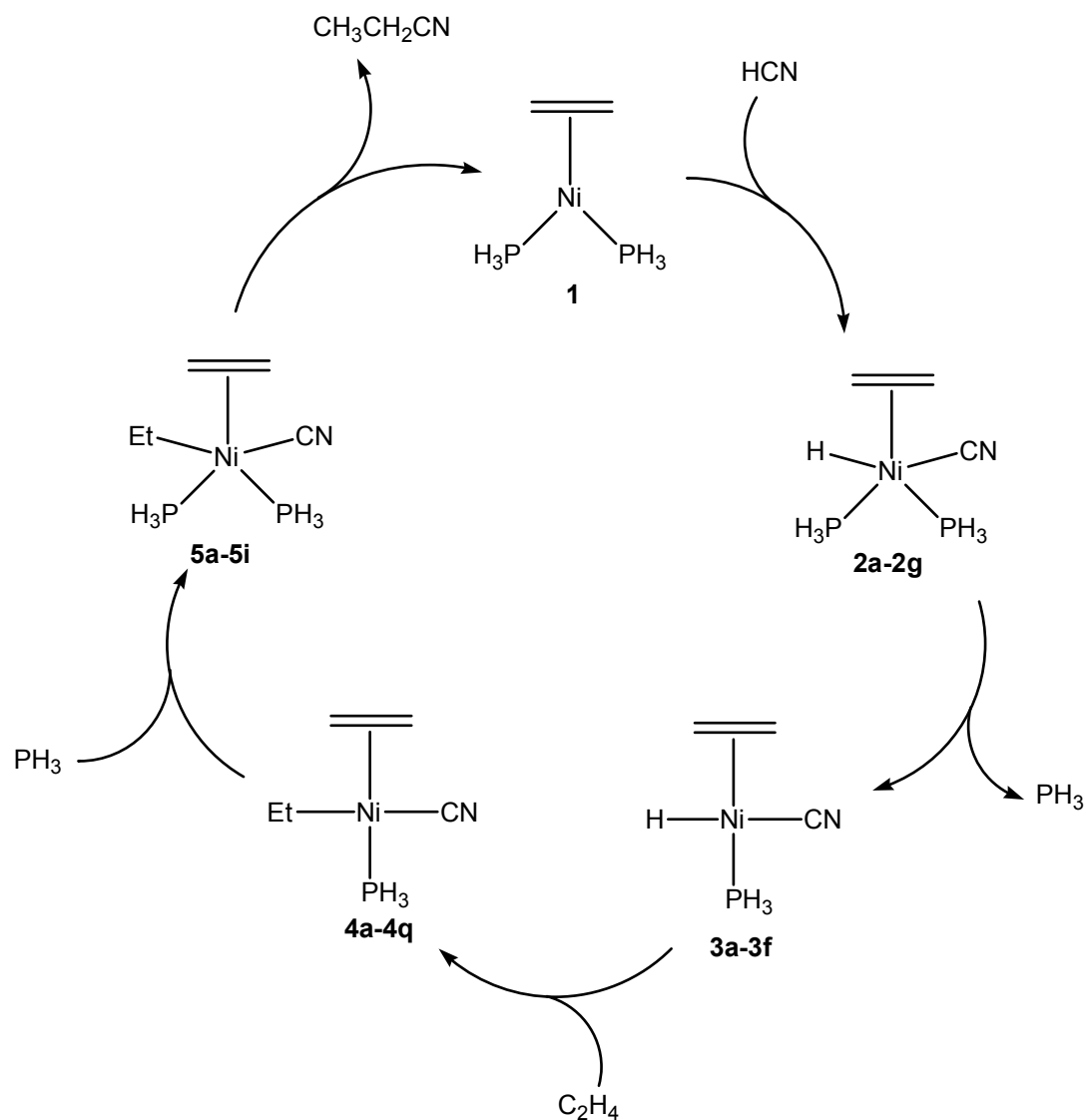
(a) General background

To the best knowledge of the author, this is the first computational study to treat the complete cycle for the catalytic hydrocyanation of ethylene as proposed by Tolman and McKinney (Tolman, 1985). Work on the isomerization of coordinated butadiene has been done (Sabo-Etienne, 2004), but not in the context of the complete cycle. Work on ligand optimization for hydrocyanation by means of molecular mechanics (MM) has been done by the group of Van Leeuwen (2004). The work of both groups has been discussed in Chapter 2.

A schematic representation of a proposed catalytic cycle for the hydrocyanation of ethylene with a model catalyst is given in Scheme 1. The reactive 16-electron fragment, (ethylene)Ni(PH₃)₂ (**1**), undergoes oxidative addition of HCN to form (ethylene)Ni(H)(CN)(PH₃)₂ (**2**). After ligand dissociation to form a square planar complex (**3**), association and insertion of ethylene occurs (**4**). It will be shown that it is the coordinated ethylene that inserts in the Ni-H bond with concomitant association of a second ethylene molecule. Subsequent ligand association yields (ethylene)Ni(ethyl)-(CN)(PH₃)₂ (**5**), which then undergoes irreversible reductive elimination of acetonitrile to complete the cycle (Tolman, 1985).

The ligand used in the commercial process of Du Pont, P(O-*o*-tolyl)₃, is very bulky and therefore not amenable to calculation at the QM level used in this study, so phosphine was substituted. The electronic behavior of phosphine is closer to that of P(O-*o*-tolyl)₃ than the behavior of P(OMe)₃ (which was also considered as a model ligand for this study), as based on the carbonyl stretch frequencies that these ligands induce in complexes of the type Ni(CO)₃L (see Chapter 2 for more details), whereas the cone angles of both candidate molecules are significantly less than that of P(O-*o*-tolyl)₃ (Tolman, 1977; Table 1). This, and the computational advantages of using phosphine, means that phosphine as model ligand is the best practical choice. However, the steric properties of the phosphorus ligand could be much more important than its electronic behavior (Tolman, 1985). Therefore, this study should be seen as a basis for further work using a more realistic ligand employing quantum mechanics/molecular mechanics (QM/MM) or quantum mechanics/molecular

dynamics (QM/MD) methods. The substrate investigated is ethylene, even though it is not the most important substrate in the commercial process (Tolman, 1985). This is to avoid the complications of isomerization and multiple possible routes that a larger substrate brings.



Scheme 1. The catalytic hydrocyanation of ethylene using the model ligand phosphine

Table 1. Electronic and steric differences between possible model ligands (Tolman, 1977)

	Electronic parameter [cm^{-1}]*	Cone angle [degrees]
$\text{P}(\text{O}-o\text{-tolyl})_3$	2084.1	141
$\text{P}(\text{OCH}_3)_3$	2079.5	107
PH_3	2083.2	87

* $\nu(\text{CO})$ frequencies; see text for details

(b) Chapter layout

The next section covers the computational details and methods employed in this study. A brief discussion on the calculation and presentation of the relative energies of species in a catalytic cycle will follow. This is necessary because there are different ways of presenting the energetics of a cycle in which several species partake and these will be explicitly delineated to avoid ambiguity. Section 4 presents the details of all the intramolecular energy minima and the transition structures that connect them, while Section 5 contains the details of the intermolecular transitions. The energetics of the full cycle is discussed in the next section, followed by the conclusions and possibilities for further study.

2. Computational details

(a) Geometry optimizations and energy calculations

All the computations described in this chapter were performed with the Gaussian 03 (Revision B.05) suite of programs (Frisch, 2003). Geometries were optimized by using the nonlocal hybrid functional B3LYP (Becke, 1983, 1988; Lee, 1988) which is known to give reliable descriptions of the geometries of transition metal complexes and the associated potential energy surfaces of catalytic processes (Ziegler, 2005). The basis set used for all geometry optimizations and frequency calculations is the ECP LANL2DZ (Dunning, 1976; Hay, 1985a-c) on Ni and 6-31G(d) (Hehre, 1986) on all other atoms (henceforth referred to as BS1). The nature of stationary points were verified by frequency calculations in all cases, with minima having no imaginary frequencies and transition states having one and only one imaginary frequency. Each transition state was further tested by examining the geometry changes along the eigenvector associated with its imaginary frequency. Zero-point energy (ZPE) corrections were obtained from the frequency calculations done with the B3LYP functional and BS1 basis set. The ZPE scaling factor was obtained from the literature (Scott, 1996; Foresman, 1996).

(b) Electronic structure analysis

Charge decomposition analysis (CDA) is a technique developed by the group of Frenking (1995). CDA entails the calculation of the bonding interactions in a transition metal complex according to the Dewar-Chatt-Duncanson (DCD) bonding model (Dewar, 1951; Chatt, Duncanson, 1953). The complex can be regarded as

consisting of two fragments, namely the donating fragment A and the back-donating fragment B, so that the interaction between the two fragments consists of donation from A to B, back-donation from B to A, as well as some interelectronic repulsion in the bonding region. A value for the donation from A to B is obtained by calculating the mixing of occupied orbitals of A with unoccupied orbitals of B (denoted by d in the data). The back-donation is obtained by calculating the mixing of B's occupied orbitals with the empty orbitals of A (denoted by b) and the last component – interelectronic repulsion or charge polarization – by the mixing of occupied orbitals of A with occupied orbitals of B (denoted by r). The sum of the r -terms is always negative, since filled orbitals will repel each other. However, an individual term may be positive or negative, depending on charge accumulation or charge depletion, respectively, in that area. The relevant r -terms as well as the total quantities will be represented but not discussed, since this is a slippery concept with respect to the DCD bonding model.

(c) Atoms in molecules

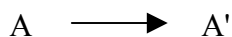
The theory of atoms in molecules (AIM) developed by Bader (1990) was used to present some of the results. Specifically, the electron densities of a few geometries were plotted using the AIMPAC suite of programs (Bader, 1990).

(d) Graphic representations

The graphic representations of molecules were mostly done with the Exceed program package developed by Barbour (2003).

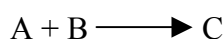
3. Comments on Energetics

The relative energies of the components of a reaction can be compared in various ways. If the reaction consists of an intramolecular rearrangement (*i.e.* the connectivity remains the same and no bonds are broken or formed) of the kind



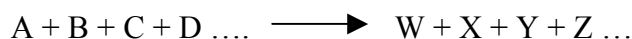
the energy comparison is direct, since both A and A' can be regarded as minimum energy structures on the same potential energy surface. The energy of the transition structure connecting the two minima will always be higher than the energies of either minimum energy structure.

When the reaction is of the kind



A and B can be bound together in a van der Waals complex, which can then be regarded as a minimum on the same potential energy surface as C. The situation is now the same as in the intramolecular case. It is important, though, to ensure that the transition structure does lead to the “correct” van der Waals complex, because there are many possible van der Waals complexes for the system. This kind of system is exemplified by the computational work of Rzepa (2005) on the ring-opening polymerization of *rac*-lactide catalyzed by a single-site β -diketiminato magnesium complex.

When the reaction is of the kind



as is typical for a catalytic cycle such as described in this study, the situation becomes much more complicated. Ideally, one would want all the reactant molecules (and all the product molecules) to be on the same potential energy surface as a well-defined minimum energy structure – *i.e.* a van der Waals complex consisting of not only two, but all the participating molecules. However, the computational task of finding the exact initial arrangement that would give rise to all the subsequent arrangements and the transition structures connecting them is probably intractable. The standard solution for this scenario is to regard all the components of the reaction as infinitely separated in space, without any interaction at all and to add up their separate energies. The disadvantage is that the assumption – given that all the molecules are at a minimum on their respective potential energy surfaces – is implicitly made that the infinitely separated ensemble represents a minimum energy structure on the potential energy surface where the reaction takes place. In reality, the ensemble cannot be defined as a minimum, or any other kind of stationary point, for that matter. Thus it becomes difficult to describe the energetics of the catalytic cycle completely and without internal inconsistencies, since one is not dealing anymore with well-defined minimum energy structures connected by transition structures as represented by one-dimensional saddle points on the potential energy surface. This is shown by Radom and Chan (2005) in their work on base-catalyzed hydrogenation. The cycle consists of an associative step (where formaldehyde is associated with sodium methoxide), followed by insertion of a hydrogen molecule in the resulting metallacycle, intramolecular rearrangement and dissociation (of methanol and sodium methoxide). A transition structure was found for the insertion and rearrangement step, but not for

the association and dissociation steps – which are typically problematic in this approach.

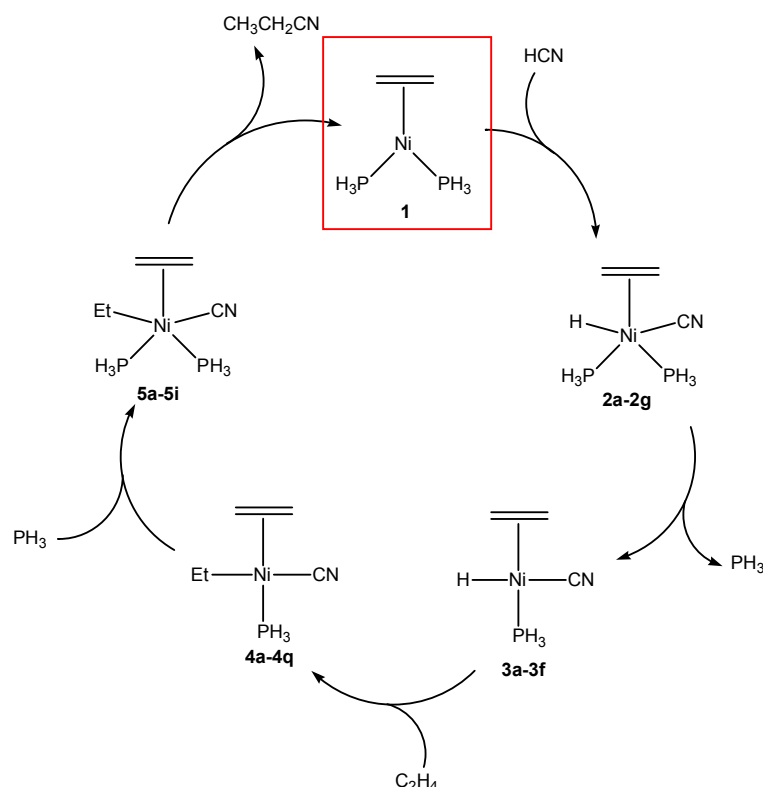
The work by Shaik *et al.*, on the role of anionic palladium(0) complexes in cross-coupling reactions is an example of a combination of the “infinite separation” approach and the “van der Waals” approach. An aryl halide (Ar-X) is oxidatively added to a palladium(II) chloride complex. Internal rearrangement takes place, the halide is replaced by a nucleophile (Nu⁻), followed by reductive elimination of Ar-Nu. Throughout their calculation, they regard the complete ensemble as a van der Waals complex (or a cluster, to use their terminology). Most notably, transition states were obtained for each rearrangement, except the complete dissociation of chloride, the only step in which a sum of components were considered, rather than a van der Waals complex. The work of Bottoni *et al.*, (2005) is similar to that of Shaik’s group in that all the intermediates except one (in this case a precursor to an association) are regarded as van der Waals complexes. The review of Frenking *et al.*, (2000) gives numerous further examples of catalytic cycles where transition structures were only obtained as long as no association or dissociation takes place – *i.e.* only where one can be sure that the two points on the potential energy surface connected by the transition structure are minimum energy structures and the energies of the infinitely separated molecules can be seen as additive constants for that reaction only.

The approach taken in this study is to consider each step in the catalytic cycle separately, so the “van der Waals complex” technique could be employed. The method of “infinite separation” is used to study the complete cycle. Thus, the energies of transition structures that arise due to intermolecular reactions – as opposed to intramolecular rearrangements – were disregarded in the holistic view.

4. Intramolecular Transitions

(a) (Ethylene)Ni(PH₃)₂ (1)

(Ethylene)Ni(PH₃)₂ (Figure 1), a coordinatively unsaturated 16-electron complex, is the starting point of the catalytic cycle (Scheme 2).



Scheme 2. The catalytic cycle, indicating the position of **1**

The Ni-C bonds are 2.003 Å each and the Ni-P bonds slightly longer at 2.193 Å each. The C-C-axis of the π -coordinated ethylene is in the plane of the molecule and no minimum energy structure could be obtained with ethylene out of the plane. There are only two crystal structures of similar compounds, namely (acrylonitrile)Ni(O-tri-*o*-tolyl)₃ and (ethylene)Ni(O-tri-*o*-tolyl)₃ (Guggenberger, 1973). For both these structures, the coordinated olefin is in the plane of the molecule. Figure 1 (**TS(1-1)**) shows the transition structure that results when the ethylene is rotated out of the plane. The energy of the transition structure is 13.34 kcal/mol higher than that of the minimum energy structure. (All energies include ZPE corrections unless stated otherwise.) For **TS(1-1)** the Ni-C bonds are slightly longer than for the minimum geometry, at 2.112 Å each, with the Ni-P bonds at 2.202 Å each. Table 2 summarizes the relevant bond lengths and angles for the two crystal structures and for **1** and **TS(1-1)**. Average values were used for the bond lengths of the crystal structures. The calculated Ni-C bond lengths are within the range of the equivalent bond lengths of the two crystal structures, whereas the calculated Ni-P bond lengths are somewhat longer.

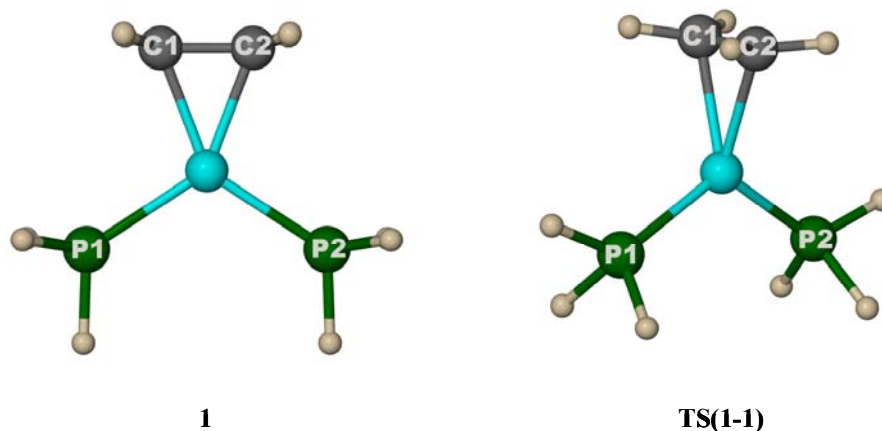


Figure 1. Minimum energy and transition structures for complex **1**

Table 2. Selected bond lengths (Å) and angles (°) for complex **1** and similar crystal structures (Guggenberger, 1973)

	Ni-C [Å]	Ni-P [Å]	C-Ni-C [°]	P-Ni-P [°]
1	2.003	2.193	41.1	113.1
TS(1-1)	2.112	2.202	38.0	116.5
(acrylonitrile)Ni(O-tri- <i>o</i> -tolyl) ₃	1.964	2.109	43.5	110.3
(ethyl)Ni(O-tri- <i>o</i> -tolyl) ₃	2.020	2.095	42.5	116.3

To establish why a minimum structure could not be obtained with ethylene out of the plane of the molecule a CDA analysis was performed on both **1** and **TS(1-1)**. The relevant data is summarized in Table 3.

Table 3. Charge components for selected MOs of **1** and **TS(1-1)***

Complex	Donor	<i>d</i>	<i>b</i>	<i>r</i>
1	Ethylene to Ni	0.262	0.004	0.169
	Phosphine to Ni	0.240	0.019	0.047
	Ni to Phosphine	0.098	0.122	-0.162
	Ni to Ethylene	0.012	0.308	-0.122
TS(1-1)	Phosphine to Ni	0.124	0.015	0.156
	Ethylene to Ni	0.179	0.014	-0.057
	Ni to Ethylene	-0.002	0.146	-0.028
	Ni to Phosphine	0.123	0.078	-0.194

**d* indicates the amount of donation from fragment A to fragment B, *b* indicates the amount of back-donation from fragment B to fragment A, and *r* indicates the amount of electronic repulsion between fragments A and B. This notation will be used throughout. Also, refer to section 2.

Only the orbitals with the biggest contributions to either donation or back-donation are represented here. The total amount of donation from ethylene to Ni is 0.525 electrons for **1** and 0.471 electrons for **TS(1-1)**, whereas the amount of back-donation is 0.321 electrons for the former and 0.158 electrons for the latter. The relevant orbitals are shown in Figure 2.

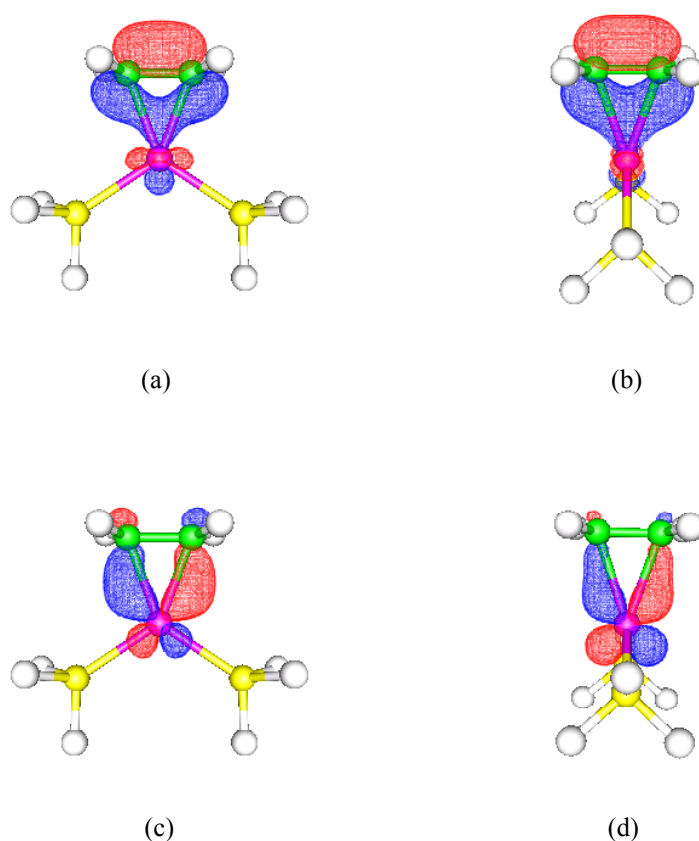


Figure 2. Molecular orbitals of (a) **1** and (b) **TS(1-1)** mostly involved in donating from ethylene to Ni. Molecular orbitals of (c) **1** and (d) **TS(1-1)** mostly involved in back-donating from Ni to ethylene.

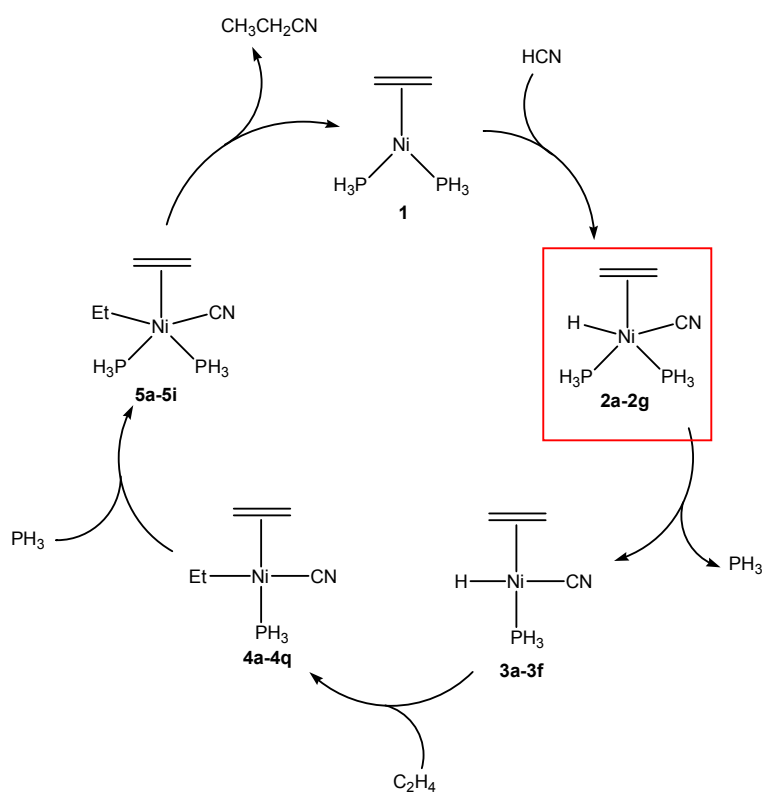
Figures 2(a) and 2(b) show that in both cases, although much of the electron density of the orbital is concentrated on ethylene, there is significant delocalization in the direction of the Ni-atom. From Table 3 it should be evident that although the extent of donation from ethylene to the Ni-fragment is almost the same for both complexes, the amount of back-donation is significantly less for **TS(1-1)** than it is for **1**. This can also be seen from Figure 2(c) and (d) – the back-donation to ethylene is much more

pronounced in (c) than in (d), keeping in mind that both orbitals are represented at the same level of electron density. This diminished back-donation from ethylene to Ni in **TS(1-1)** explains why this complex is not an energy minimum, but a transition structure.

The total amount of donation from phosphine to Ni is 0.824 electrons for **1** and 0.694 electrons for **TS(1-1)**, whereas the amount of back-donation is 0.319 electrons for the former and 0.258 electrons for the latter. The donation from phosphine to Ni is also shown in Table 3. Both the donation and back-donation is somewhat less for **TS(1-1)** than for **1** and this correlates with the longer bond lengths for Ni-P in the transition structure.

(b) (Ethylene)Ni(H)(CN)(PH₃)₂ (**2a-2g**)

After oxidative addition of HCN, an 18-electron complex, (Ethylene)Ni(H)(CN)(PH₃)₂ is formed (Scheme 3).



Scheme 3. The catalytic cycle, indicating the position of **2**

Seven different minimum energy configurations have been identified, as shown in Figure 3.

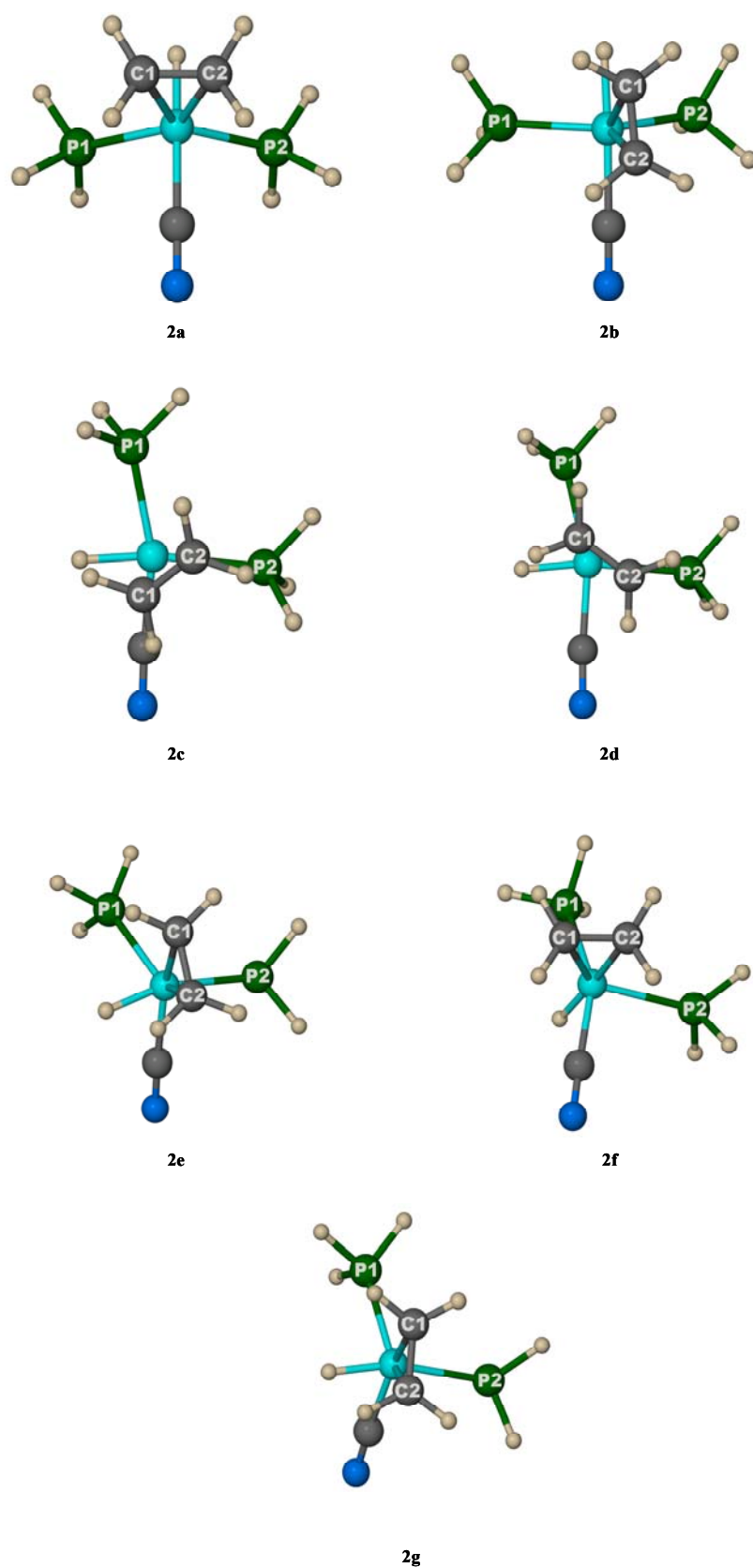


Figure 3. Minimum energy structures for complex 2

Selected bond lengths and angles for the various configurations are summarized in Table 4 and the relative energies of the geometries are summarized in Table 5. A thorough search on the Cambridge Crystallographic Database has yielded no crystal structure suitable for comparison with **2**. The only similar structures have geometries that are very constrained by the ligands (such as chelating phosphines, *etc.*). Such structures cannot be fruitfully compared to the geometries obtained here.

Table 4. Selected bond lengths (Å) and angles (°) for complex **2**

	2a	2b	2c	2d	2e	2f	2g
Ni-C1	2.192	2.402	3.170	3.373	2.175	2.223	2.175
Ni-C2	2.192	2.368	3.728	3.462	2.146	2.235	2.146
Ni-P1	2.249	2.228	2.207	2.206	2.335	2.237	2.335
Ni-P2	2.249	2.230	2.296	2.296	2.327	2.434	2.327
Ni-CN	1.929	1.909	1.857	1.858	1.885	1.867	1.885
Ni-H	1.489	1.497	1.476	1.478	1.459	1.483	1.459
C-Ni-C	36.4	33.0	20.3	22.5	37.1	35.7	37.2
P-Ni-P	116.9	130.2	107.5	107.4	101.6	103.1	101.6
P2-Ni-CN	90.8	91.6	88.9	88.9	86.2	92.8	86.2
P1-Ni-H	86.3	84.8	82.3	82.1	85.6	79.7	85.6

Table 5. Energies of minimum energy and transition structures for **2** relative to **2a**

Complex	Energy [kcal/mol]	Complex	Energy* [kcal/mol]
2a	0.00	TS(2a-2b)	2.81 (2.81)
2b	2.74	TS(2b-2f)	16.98 (14.24)
2c	5.93	TS(2c-2d)	6.13 (0.20)
2d	6.07	TS(2c-2e)	7.74 (1.81)
2e	7.29	TS(2d-2f)	8.02 (1.95)
2f	7.59	TS(2f-2g)	10.17 (2.88)
2g	7.29		

* Values in parentheses indicate the barrier height relative to the lowest minimum energy geometry of the pair connected by the transition structure

Structures **2a** and **2b** both have a trigonal bipyramidal-like configuration with H-Ni-CN as the axis; the major difference between the two structures is in the orientation of the coordinated ethylene molecule. In **2a** the C-C-axis of ethylene is in the trigonal plane, whereas it is perpendicular to the trigonal plane in **2b**. The energy of **2b** is 2.74

kcal/mol higher than that of **2a** with a barrier of 2.81 kcal/mol (relative to **2a**) separating them. Structures **2c** and **2d** are both square pyramidal, with ethylene at the apex of the pyramid. Again, the difference in the orientation of the ethylene constitutes the biggest difference between the two geometries. The energy difference between the two geometries is 0.14 kcal/mol, with **2c** having the lower energy. The energy barrier between the two geometries is 0.20 kcal/mol relative to **2c**. Notable is the very long distance between Ni and ethylene for both these configurations, indicating that **2c** and **2d** are perhaps best regarded as square planar complexes of HNiCN(PH₃)₂ in a van der Waals complex with ethylene. CDA results (see below) show that there is indeed very little interaction between ethylene and Ni for **2c** and **2d**. It must be noted, however, that for both **2c** and **2d** an AIM electron density analysis yields bond critical points for the Ni-C1 bonds, though not for the Ni-C2 bonds. This very loose interaction with ethylene explains the small energy difference between the two complexes, as well as the almost negligible energy barrier between them. Structure **2e** is a distorted trigonal bipyramid with H-Ni-P2 as the axis. The H-atom is bent away from the axis in the direction of the CN-ligand. The trigonal plane is somewhat distorted in the direction of H. Structure **2f** is a trigonal bipyramid with the axis defined by ethylene-Ni-CN, but distorted somewhat to resemble a square pyramid with P2 at the apex and ethylene perpendicular to the distorted square. Structure **2g** is a square pyramid with P2 at the apex. The base of the pyramid is distorted away from the apical phosphine. The ethylene is oriented parallel to the square plane.

Complexes **2a** to **2g** are all minimum energy geometries that can be connected *via* the transition structures shown in Figure 4. Selected bond lengths and angles for the various transition structures are summarized in Table 6. The interconnecting paths are shown in Scheme 2 and energies (in kcal/mol) relative to **2a** are presented in Table 5. It should be noted that although visual inspection suggests that there might be other transition structures possible, none could be found. Structure **2a** has the lowest energy. As mentioned earlier, there is a 2.81 kcal/mol barrier (TS(**2a-2b**)) to the rotation of ethylene for **2a** to **2b**. A study by Bäckvall *et al.* (1981) proposed that the most favorable configuration of **2** might be **2b**. With the aid of NMR they found that DCN adds > 90% *cis* to an olefinic double bond. They proposed a mechanism in which this is most likely if **2** is in the **2b** configuration.

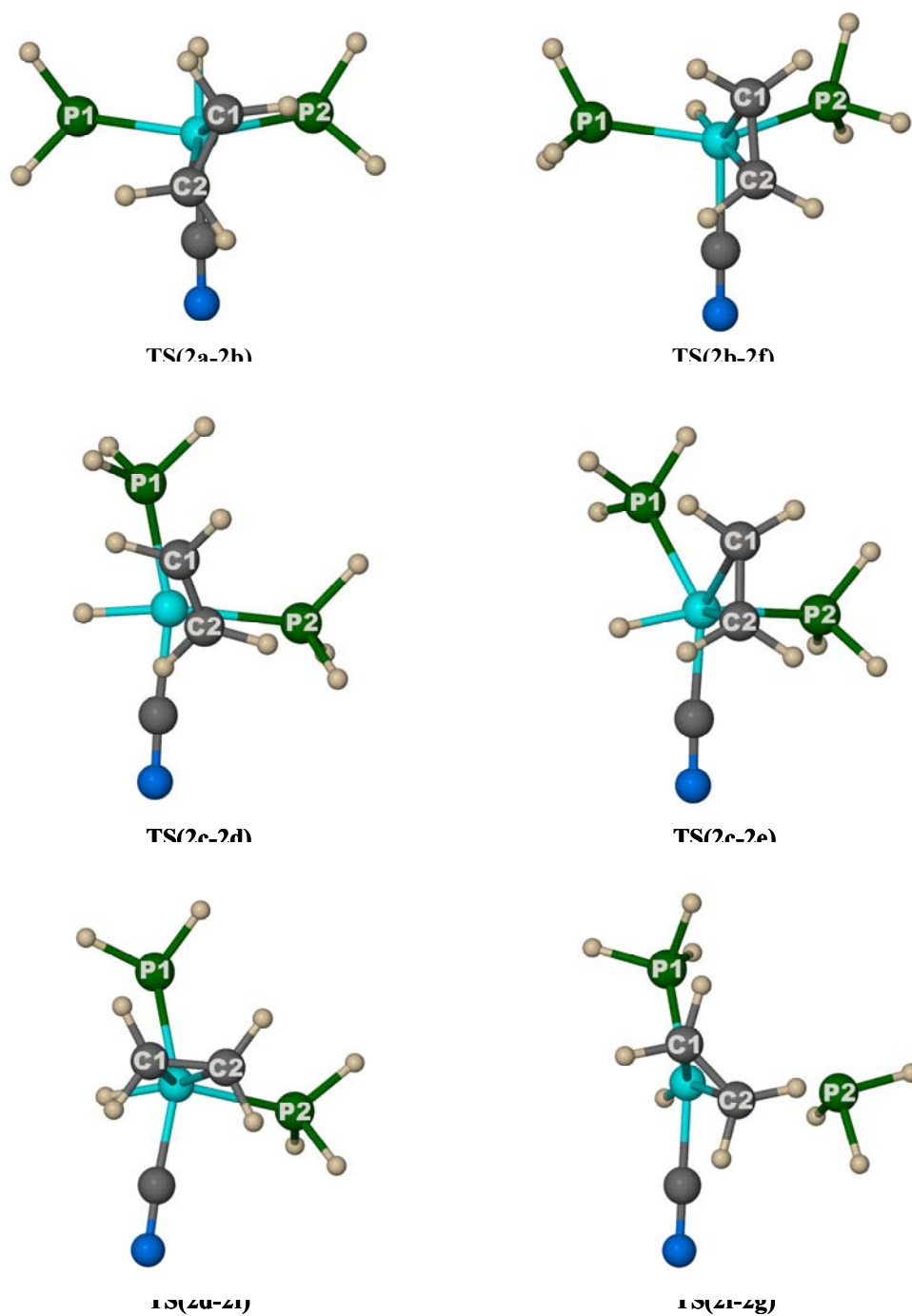
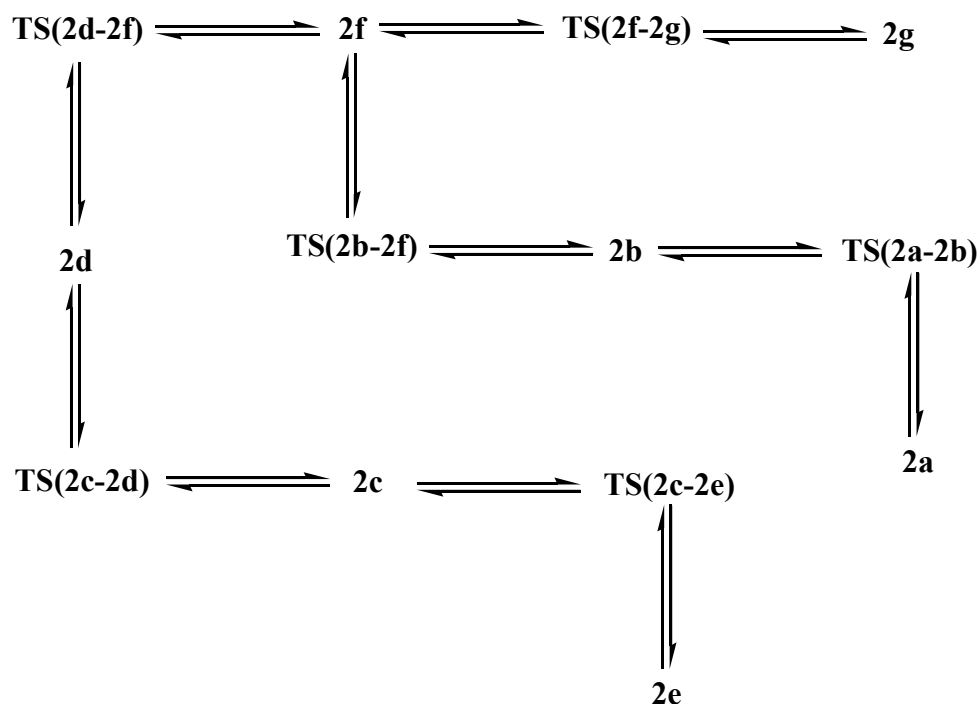


Figure 4. Transition structures connecting the minima of complex 2

Table 6. Selected bond lengths (Å) and angles (°) for the transition structures of complex **2**

	2a-2b	2b-2f	2c-2d	2c-2e	2d-2f	2f-2g
Ni-C1	2.414	2.203	4.023	2.452	2.320	2.246
Ni-C2	2.390	2.145	3.405	2.354	2.367	2.274
Ni-P1	2.229	2.219	2.208	2.241	2.221	2.228
Ni-P2	2.223	2.219	2.295	2.304	2.349	3.019
Ni-CN	1.911	1.978	1.857	1.872	1.861	1.859
Ni-H	1.497	1.488	1.476	1.470	1.487	1.468
C-Ni-C	32.7	36.9	18.4	32.6	33.7	35.0
P-Ni-P	130.6	145.5	107.5	104.3	103.5	94.1
P2-Ni-CN	90.9	99.1	88.9	87.5	89.5	87.7
P1-Ni-H	84.1	74.8	82.4	81.2	79.7	79.6



Scheme 2. Interconnecting pathway for the minimum energy and transition structures of **2**

However, it will be shown in a later section that, although **2b** is quite low in energy relative to the other configurations of **2**, it most likely does not play a very important role in the catalytic cycle, since the oxidative addition of HCN takes place such that H and CN are *cis* to each other, as in **2e** or **2f**. The *cis* oxidative addition has also been found for other systems, such as the oxidative addition of alkyl chlorides to Pt (Bickelhaupt, 1995; Thiel, 2005). The arrangement of ligands of **2a** and **2b**

correspond to expectation, at least on steric grounds. Phosphine and ethylene both occupy more space than either CN or H, so that they are found in the equatorial positions. Generally, more electronegative ligands are expected to occupy the axial positions (Wulfsberg, 1987). However, in this case, the electronegativities are so similar that it probably plays no role. Structure **2b** is connected to **2f** via a Berry-pseudorotation (**TS(2b-2f)**) of 14.24 kcal/mol (relative to **2b**). Complex **2f** is the minimum energy structure with the highest relative energy and is connected to **2d** and **2g** via transition structures of 1.95 kcal/mol relative to **2d** and 2.88 kcal/mol relative to **2g**. **TS(2d-2f)** is a distortion of the square pyramid **2c** with ethylene apical to **2f** which is intermediate between a trigonal pyramidal structure with ethylene-Ni-CN as axis and a square pyramidal structure with P2 apical. **TS(2f-2g)** shows the rotation of the coordinated ethylene that is necessary to convert **2f** to **2g**. Structure **2c** is connected to **2d** (as discussed, see above) and **2e**. **TS(2c-2e)** is intermediate between the square pyramid of **2c** and the distorted trigonal bipyramid of **2e**. The relatively high energies of both **2e** and **2f** are probably due to the axial position of ethylene. Ethylene is bulkier than either H (equatorial in **2e**) or CN (equatorial in **2f**), therefore it is more likely to be found in the equatorial plane of the complex, as in **2a** and **2b**. Indeed, the activation energy for the transition from **2f** to **2b** is 9.39 kcal/mol, whereas the reverse transition, from **2b** to **2f** is 14.24 kcal/mol.

A CDA analysis was done for all seven minimum structures and their interconnecting transition structures. The data is summarized in Tables 7 and 8. Only the orbitals with the biggest contribution to either donation or back-donation are represented here.

Since the biggest difference between **2a** and **2b** is the orientation of the π -coordinated ethylene, one expects this to reflect in the CDA data and this is indeed the case, although the effect is somewhat smaller than anticipated. From Table 8 it is clear that both the donation and back-donation between ethylene and the Ni-fragment is more for **2a** than for **2b**, which means that the higher stability of **2a** relative to **2b** can be ascribed to the different orientations of the π -coordinated ethylene. In fact, the back-donation from ethylene is almost negligible for **2b**. The total amount of donation and back-donation between both phosphines and the Ni-fragment is also shown in Table 8. Again, the amount of donation is a bit more for **2a** than for **2b**, but the reverse is true for the back-donation. In addition, the Ni-P bonds of **2a** are somewhat longer than those of **2b**.

Table 7. Charge components for selected MOs of **2** and its interconnecting transition structures

Complex	Donor	<i>d</i>	<i>b</i>	<i>r</i>
2a	Ethylene to Ni	0.127	0.009	-0.020
	Phosphine to Ni	0.198	0.025	-0.089
	Phosphine to Ni	0.201	0.024	0.133
2b	Ethylene to Ni	0.096	0.003	-0.017
	Phosphine to Ni	0.192	0.029	-0.096
	Phosphine to Ni	0.204	0.019	0.132
2c	Ethylene to Ni	0.050	-0.002	0.001
	Phosphine1 to Ni	0.084	0.008	0.006
	Phosphine2 to Ni	0.217	0.012	-0.305
2d	Ethylene to Ni	0.062	-0.002	0.013
	Phosphine1 to Ni	0.206	0.011	-0.322
2e	Ethylene to Ni	0.113	0.008	-0.030
	Ni to Ethylene	0.029	0.094	-0.083
	Phosphine2 to Ni	0.105	0.011	-0.059
2f	Ethylene to Ni	0.114	0.007	-0.076
	Phosphine1 to Ni	0.113	-0.001	0.067
	Phosphine2 to Ni	0.093	0.002	-0.007
2g	Ethylene to Ni	0.113	0.008	-0.030
	Phosphine1 to Ni	0.089	0.014	-0.115
	Phosphine2 to Ni	0.175	-0.010	-0.395
TS(2a-2b)	Ethylene to Ni	0.097	0.003	-0.014
	Phosphine to Ni	0.135	0.022	-0.099
	Phosphine to Ni	0.217	0.081	0.126
TS(2b-2f)	Ethylene to Ni	0.098	0.027	-0.043
	Ethylene to Ni	0.036	0.010	-0.018
	Ni to Ethylene	-0.005	0.114	-0.088
	Phosphine to Ni	0.190	-0.001	0.015
	Phosphine to Ni	0.183	0.029	0.060
TS(2c-2d)	Ethylene to Ni	0.059	-0.003	0.006
	Phosphine1 to Ni	0.075	0.007	0.004
	Phosphine2 to Ni	0.205	0.010	-0.321
TS(2c-2e)	Ethylene to Ni	0.131	-0.001	0.067
	Phosphine2 to Ni	0.137	0.022	-0.174
TS(2d-2f)	Ethylene to Ni	0.125	0.001	0.028
	Ni to Ethylene	0.009	0.074	-0.067
	Phosphine1 to Ni	0.105	0.016	-0.174
	Phosphine2 to Ni	0.110	0.012	-0.172
TS(2f-2g)	Ethylene to Ni	0.138	0.004	-0.072
	Phosphine1 to Ni	0.145	0.002	0.023
	Ni to Phosphine1	0.001	0.044	-0.031

Table 8. Total amounts of donation and back-donation for **2** and its transition structures

Complex	Donor	<i>d</i>	<i>b</i>	<i>r</i>
2a	Ethylene	0.463	0.105	-0.257
	Phosphine	0.939	0.194	-0.471
2b	Ethylene	0.412	0.065	-0.217
	Phosphine	0.900	0.204	-0.405
2c	Ethylene	0.135	0.013	-0.006
	Phosphine	0.797	0.294	0.054
2d	Ethylene	0.131	0.013	-0.045
	Phosphine	0.794	0.289	-0.657
2e	Ethylene	0.459	0.151	-0.269
	Phosphine	0.820	0.158	-0.668
2f	Ethylene	0.442	0.130	-0.236
	Phosphine	0.743	0.184	-0.715
2g	Ethylene	0.459	0.151	-0.269
	Phosphine	0.820	0.158	-0.668
TS(2a-2b)	Ethylene	0.400	0.061	-0.209
	Phosphine	0.911	0.228	-0.416
TS(2b-2f)	Ethylene	0.473	0.151	-0.314
	Phosphine	0.853	0.198	-0.348
TS(2c-2d)	Ethylene	0.126	0.005	-0.042
	Phosphine	0.789	0.289	-0.656
TS(2c-2e)	Ethylene	0.395	0.055	-0.218
	Phosphine	0.911	0.273	-0.613
TS(2d-2f)	Ethylene	0.412	0.080	-0.222
	Phosphine	0.862	0.256	-0.654
TS(2f-2g)	Ethylene	0.425	0.114	-0.228
	Phosphine	0.437	0.177	-0.553

These differences are so slight, though, that they probably have very little influence on the relative energies of the two complexes and the data should not be over-interpreted. Turning now to **TS(2a-2b)**, it can be seen that the total amounts of donation and back-donation between ethylene and the Ni-fragment is lower for the transition structure than for either of the two minimum structures, whereas the donation from the phosphines to Ni is intermediate between **2a** and **2b** and the back-donation more than either of the two minima. The diminished bonding between ethylene and Ni was expected for this structure. The MOs most involved in donation from ethylene to Ni for **2a**, **2b** and **TS(2a-2b)** are shown in Figure 5.

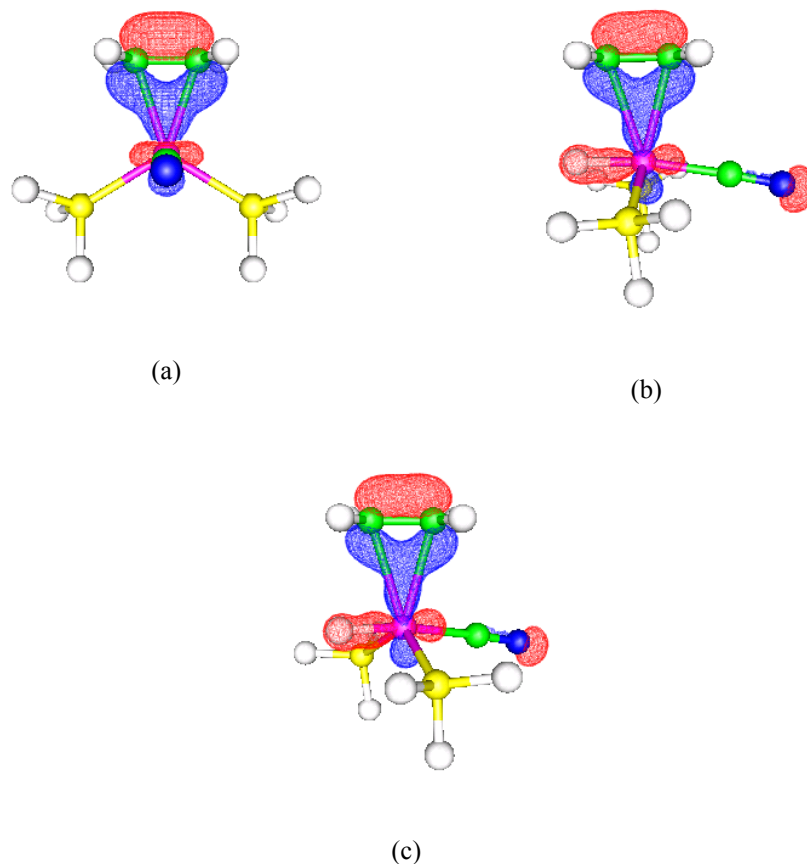


Figure 5. Donation from ethylene to Ni for (a) **2a** (b) **2b** (c) **TS(2a-2b)**

No significant amount of back-donation could be assigned to any specific MO either from the CDA data or from the graphical representation of the occupied MOs. It can be seen in Figure 5 that the electron density between Ni and ethylene is somewhat higher for **2a** than for **2b** and **TS(2a-2b)**. Additionally, some delocalization to H and to CN takes place for the latter two complexes. All three representations are at an isovalue of 0.08/-0.08 au. Although the bonding between phosphine and Ni does not play a significant role in the relative energies of these complexes, there is an interesting discrepancy in the data. The CDA data shows that phosphine certainly donates to Ni, as expected, but this could not be correlated with the orbital shapes (Figure 6). Here, it can be seen clearly that each orbital seem to be centered on Ni, contrary to expectation. Nothing found in the literature either supports or contradicts this finding (Takano, 2000; Cheung, 2003), which certainly warrants further investigation. Again, the back-donation could not be ascribed to any specific orbital.

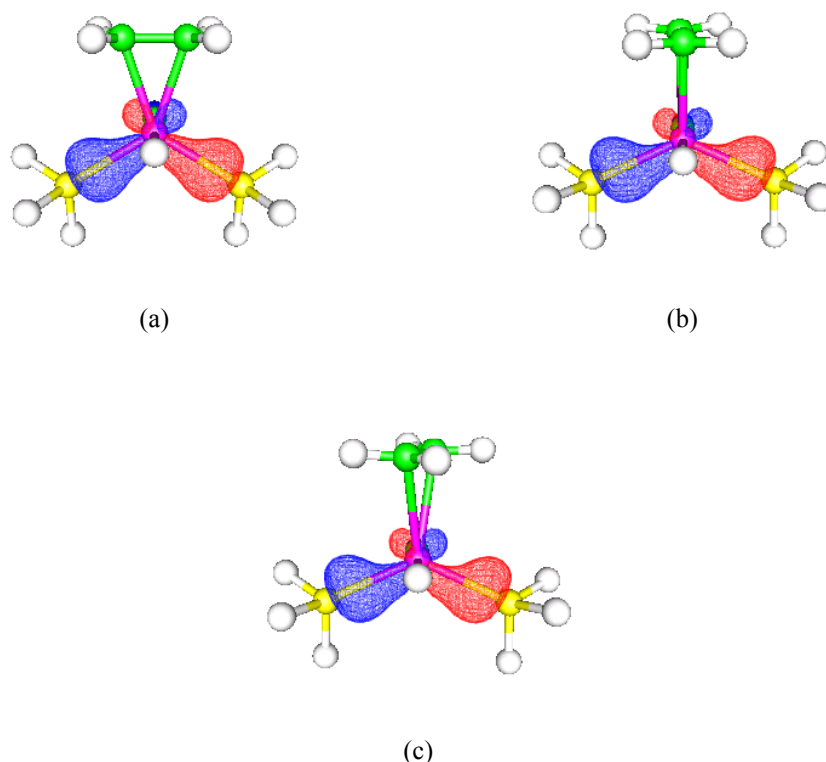


Figure 6. Molecular orbital 23 for (a) **2a** (b) **2b** (c) **TS(2a-2b)**

Complex **2b** can convert to **2f** via the transition state **TS(2b-2f)**. The primary difference between the two geometries is that P1 and H has exchanged their positions (refer to Figure 3) and that **2f** can be seen as a distorted trigonal bipyramid with ethylene-Ni-H the axis, whereas **2b** is a trigonal bipyramid with H-Ni-CN the axis. This is also reflected in the transition state where H is in a position that is intermediate between its position in **2b** and in **2f**. Thus, the expectation is that there will be some difference in the extent to which the two phosphines are bound as well as some difference in the coordination of the ethylene, although the latter will most likely play a less important role than the former. The molecular orbitals for donating from ethylene to Ni for **2b**, **2f** and **TS(2b-2f)** are all presented in Table 7 and Figure 7. For the two minimum structures no specific orbital could be associated with back-donation from Ni to ethylene, but for the transition structure the back-donation is concentrated in one MO, although the graphical representation of said orbital does not seem to show this.

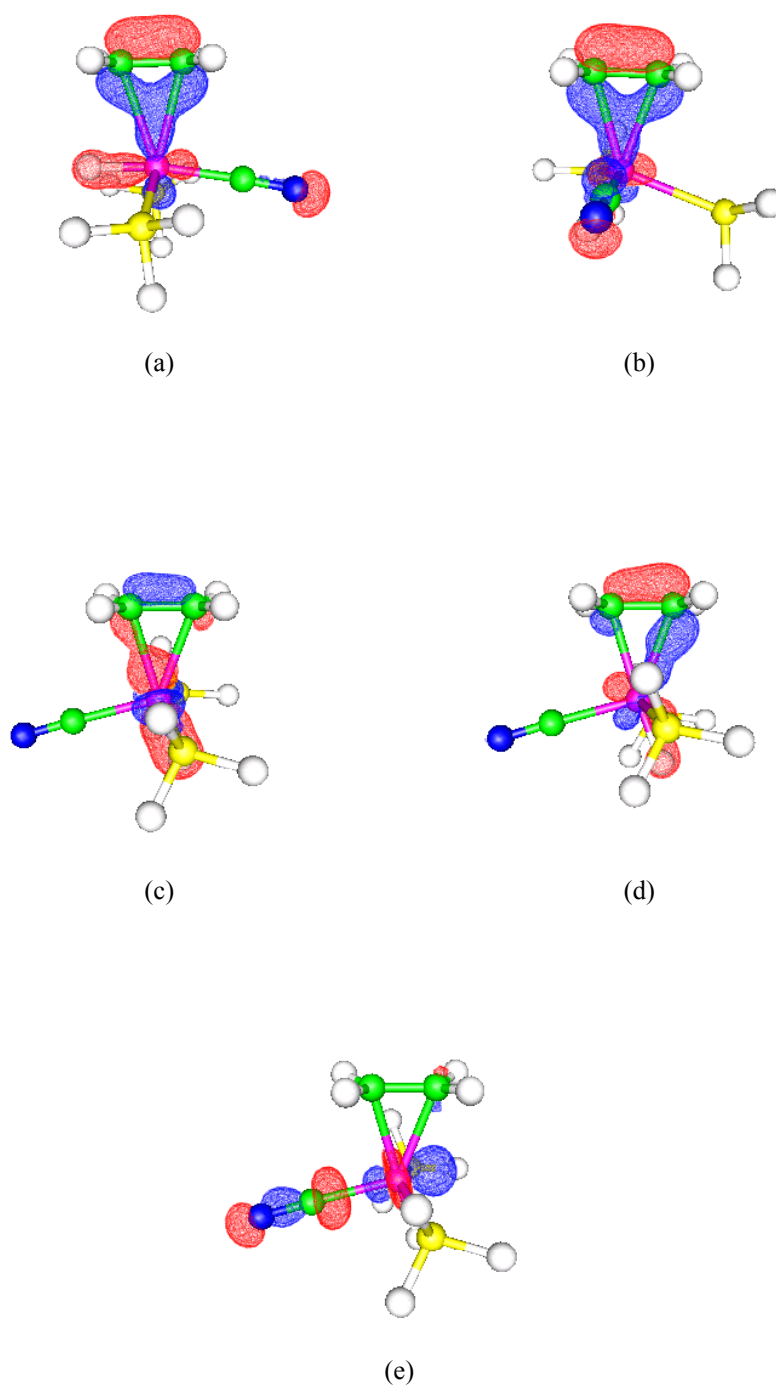


Figure 7. Molecular orbitals showing donation from ethylene to Ni for (a) **2b** (b) **2f** (c) **TS(2b-2f)** (d) **TS(2b-2f)**. (e) Molecular orbital 32 of **TS(2b-2f)**

It is clear from Figure 7(a) that the MO of **2b** donating to Ni from ethylene is also delocalized over CN and H – which are both in the same plane as ethylene itself. Figure 7(b) shows that this delocalization only extends over CN in the case of **2f**, with CN being perpendicular to the plane of the ethylene.

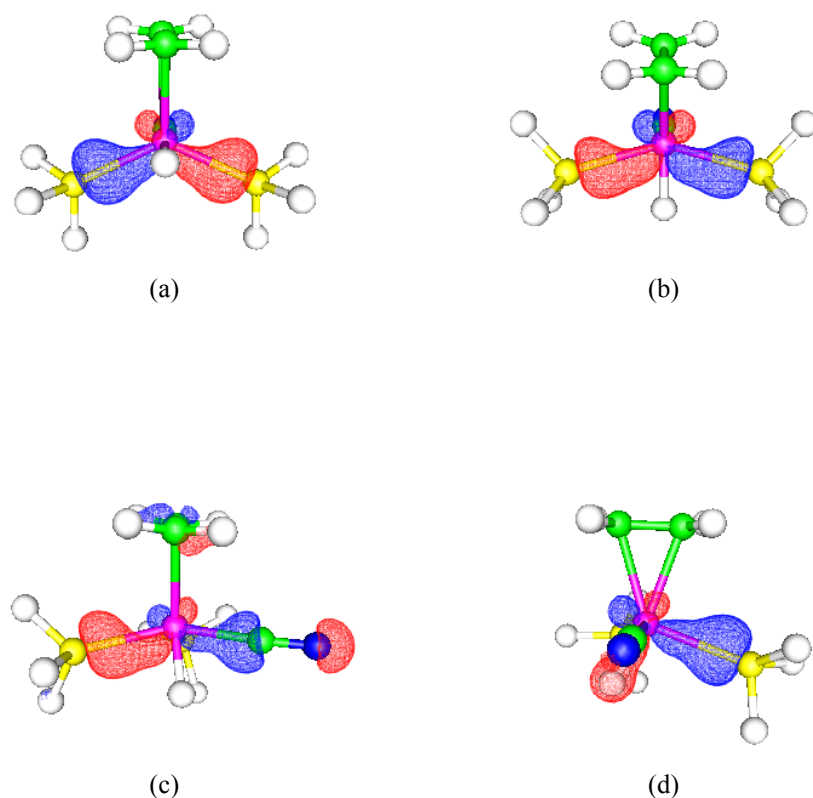


Figure 8. Molecular orbitals showing donation from phosphine to Ni for (a) **2b** (b) **TS(2b-2f)** (c) **2f** (Ni-P1) (d) **2f** (Ni-P2)

It is possible that the reduced delocalization of the latter orbital leads to its slightly higher contribution for donation from ethylene to Ni than the corresponding orbital of **2b**. The total amount of donation (Table 8) from ethylene to Ni is slightly more for **2f** than for **2b**, and the back-donation in the latter case is significantly less – almost negligible. For the transition state the amount of donation is more than for either of the minima, and the amount of back-donation is intermediate. Interestingly, though, the donation in this case is distributed over two orbitals, as shown in Figures 7(c) and 7(d). The Ni-C bond lengths for this structure differ by about 0.05 Å, but this is also the case for **2f**. The increased asymmetry of the transition structure relative to the two minima may play a role in the asymmetry of the MOs. Note also that there is no delocalization to CN. The total amount of back-donation from Ni to ethylene for **TS(2b-2f)** is 0.130 electrons (Table 8), of which 0.114 (Table 7) electrons are concentrated in one MO. However, inspection of Figure 7(e) reveals no electron

density between ethylene and nickel. All the images of Figure 7 were rendered with an isovalue of 0.08/-0.08, except 7(d) which was rendered at 0.085/-0.085. Having said this, the overall the ethylene-Ni interaction for all three complexes seem very similar, so that it probably plays a very small role in the observed energy difference (4.85 kcal/mol) between **2b** and **2f**. Therefore, it is probably the large difference in phosphine coordination that will play the decisive role with regard to the energy difference. The relevant MOs for donation from phosphine as presented in Table 7 are shown in Figure 8. Again, although the CDA data shows that the electron density in these orbitals contribute to phosphine to Ni donation, the orbitals seem to be centered on Ni. The total amount of donation and back-donation is significantly more for **2b** than for **2f**, and this is also reflected in their Ni-P bond lengths, especially for Ni-P2 where there is a difference in lengths of 0.2 Å.

Turning now to **2f**, **2g** and **TS(2f-2g)**, what is immediately apparent (Figure 3) are the different orientations of ethylene for the two minimum structures as well as the longer Ni-P bond lengths for **2g** (Table 4). H is also in a slightly different position in **2g**. The MOs listed in Table 7 are shown in Figure 9. The total amount of donation from ethylene to Ni as well as the total amount of back-donation is almost the same for both minimum structures and slightly less for the transition structure and this is also reflected in Figure 9 as well as the Ni-C bond lengths for the relevant complexes. The total amount of donation from phosphine to Ni follows a similar pattern for both **2f** and **2g**, with the contribution from Ni-P2 donation slightly less than that of Ni-P1 in both cases. This is expected, since Ni-P2 is slightly longer than Ni-P1 for both complexes. The main contributors to phosphine-Ni donation for **2f** are listed in Table 7. Interestingly, even though the total amounts of donation and back-donation are similar for both minimum structures, this similarity does not occur at the MO level. It is much harder to attribute the donation to a specific MO in the case of **2g**. Again the graphic representations show Ni-centered MOs instead of the expected phosphorus centered MOs. However, although the amount of donation from P1 to Ni for **TS(2f-2g)** is comparable to what is seen for the two minimum structures, the amount of donation from P2 to Ni is so slight (0.055) electrons as to be negligible. Thus, it is likely that the transition of **2f** to **2g** is accompanied by a reversible ligand dissociation.

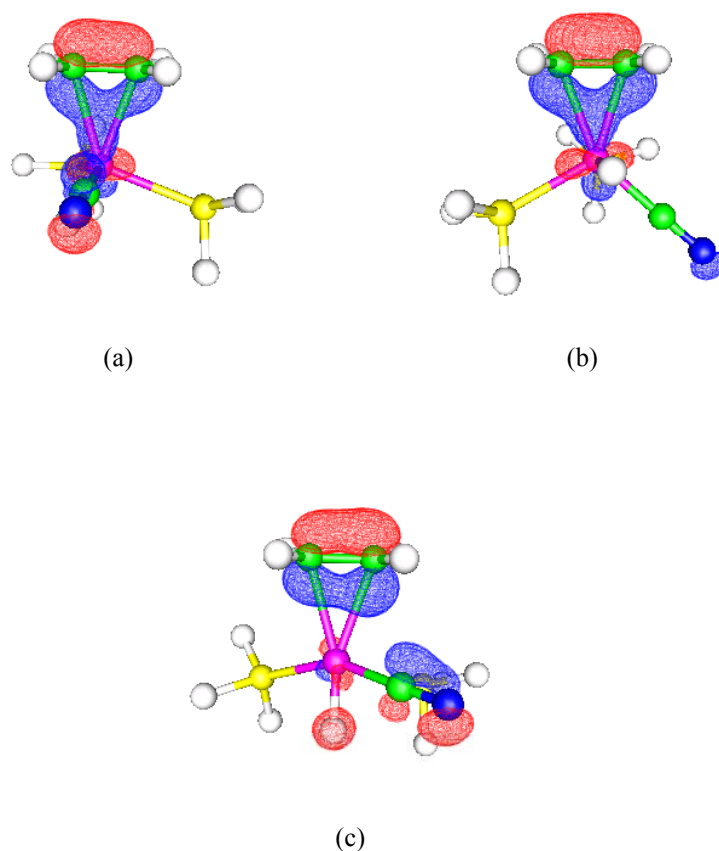


Figure 9. Molecular orbitals showing donation from ethylene to Ni for (a) **2f** (b) **2g** (c) **TS(2f-2g)**

Structure **2f** is also connected to **2d** via **TS(2d-2f)**. Although the total amount of donation from P2 to Ni is somewhat more (0.425 *vs.* 0.369 electrons), it is not possible to assign this electron transfer to a specific MO. As before, the orbitals seem to be Ni-centered. The total amounts of donation and back-donation for the Ni-P bonds are the similar for all three structures, as expected, because the major difference between these structures lie in the orientation of ethylene as well as the Ni-C bond distances. The Ni-C bond distances for **2d** are ~ 3.42 Å, for **2f** ~ 2.23 Å and ~ 2.34 Å for the transition structure. The difference between the two minimum structures is quite dramatic and the total amounts of donation from ethylene to Ni, shown in Table 8, shows why this is so. The total amount of donation differ by a factor of 3.5 for the two complexes and is intermediate for the transition structure.

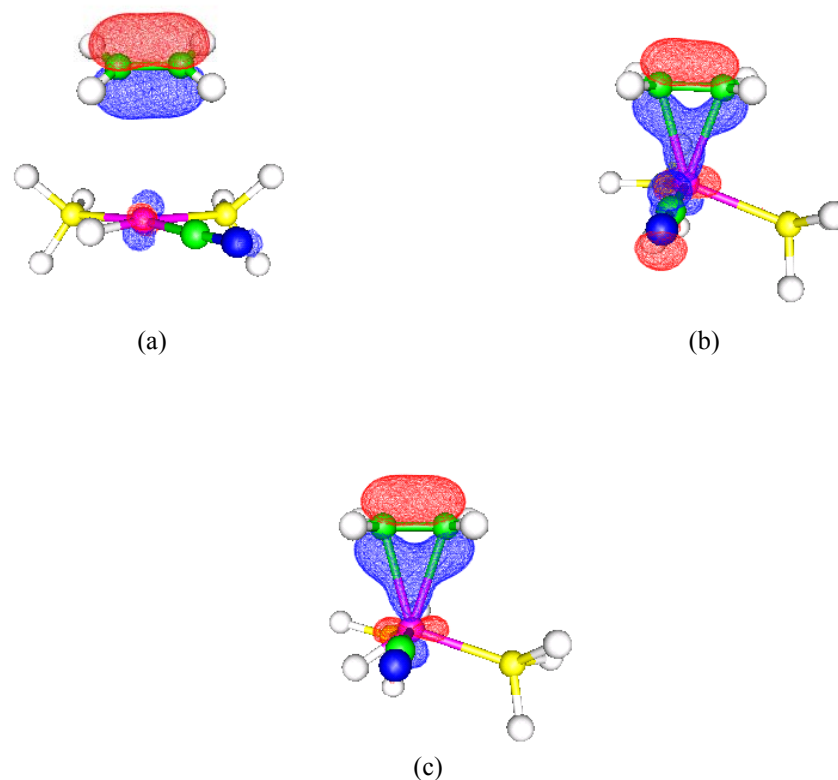


Figure 10. Molecular orbitals showing donation from ethylene to Ni for (a) **2d** (b) **2f** (c) **TS(2d-2f)**

The back-donation follows the same trend, except that the difference between the two minimum structures are even more amplified here. The relevant MOs are shown in Figure 10, and the differences between them are evident, most notably the much diminished electron density between the ethylene and Ni in Figure 10(a). The energy difference between the minimum structures is around 1.5 kcal/mol, with **2d** having the lower energy. Structure **2f** is a very distorted trigonal bipyramid, whereas **2d** is essentially a square planar complex with ethylene associated loosely. This is probably why **2d** is slightly stabilized over **2f**. By rotating the loosely coordinating ethylene of structure **2d** it is possible to obtain **2c** which is also square planar with ethylene loosely coordinated in a different orientation than in **2d**. For both complexes, the Ni-C bond lengths are more than 3 Å, which is well over the sum of the van der Waals radii of Ni and C at 2.33 Å.

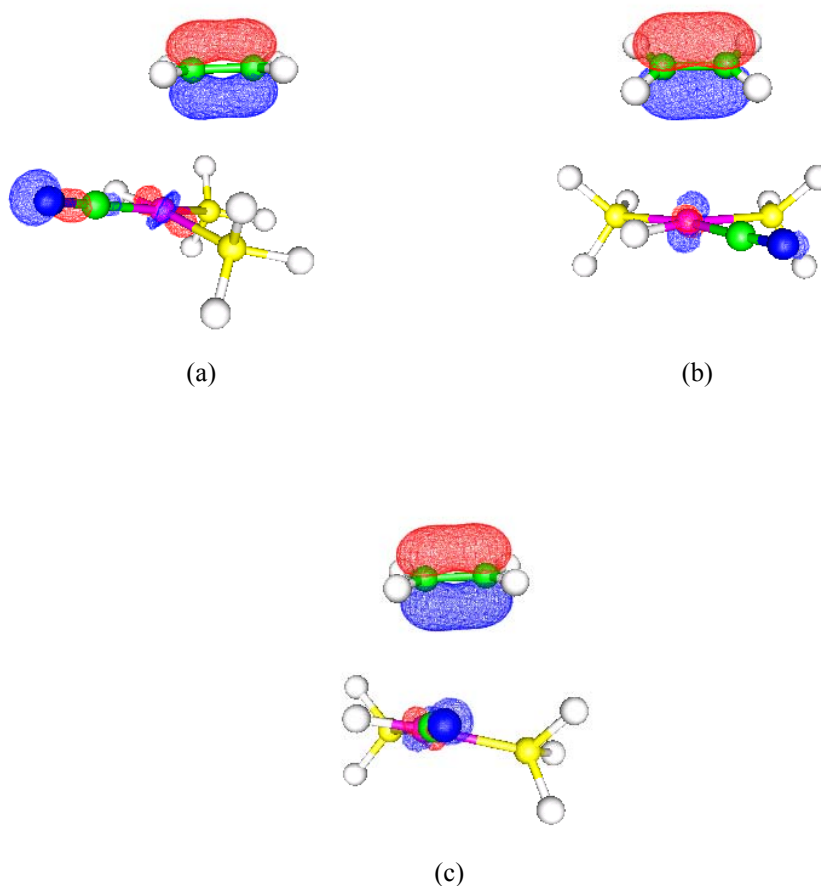


Figure 11. Molecular orbitals showing donation from ethylene to Ni for (a) **2c** (b) **2d** (c) **TS(2c-2d)**

It is expected that the coordination of the phosphines will be very similar for both structures as well as the transition structure and this is indeed the case. The relevant orbitals are presented in Table 7. As for **2d** the amount of donation from P2 to Ni is somewhat more than that of P1, but could not be assigned to a specific orbital. Since the coordination of the phosphines for **3d** has already been discussed, nothing will be added here. The MOs contributing the most to donation from ethylene to Ni, such as it is, are listed in Table 7. The total amount at ~ 0.13 electrons is very low in each case and the amount of back-donation negligible. Given the long Ni-C-bonds this is of course not unexpected. The molecular orbitals showing the donation is presented in Figure 11. Note the almost absent electron density between Ni and ethylene in all three cases (at the $\pm 0.08e$ cut-off level).

The final intramolecular transition for complex **2** is that between **2c** and **2e**. The primary difference between these two geometries is that whereas **2c** is square planar with ethylene very loosely associated at the apex of the molecule, **2e** is a very distorted trigonal bipyramid with ethylene much more closely associated as can be seen from the bond lengths presented in Table 4. As for **2c**, the amount of donation from P2 to Ni is more than that of P1, but cannot be assigned to a specific MO. The orbitals involved in Ni-ethylene interaction are all represented in Figure 12, which clearly shows the big difference between **2c** and **2e** in terms of ethylene coordination.

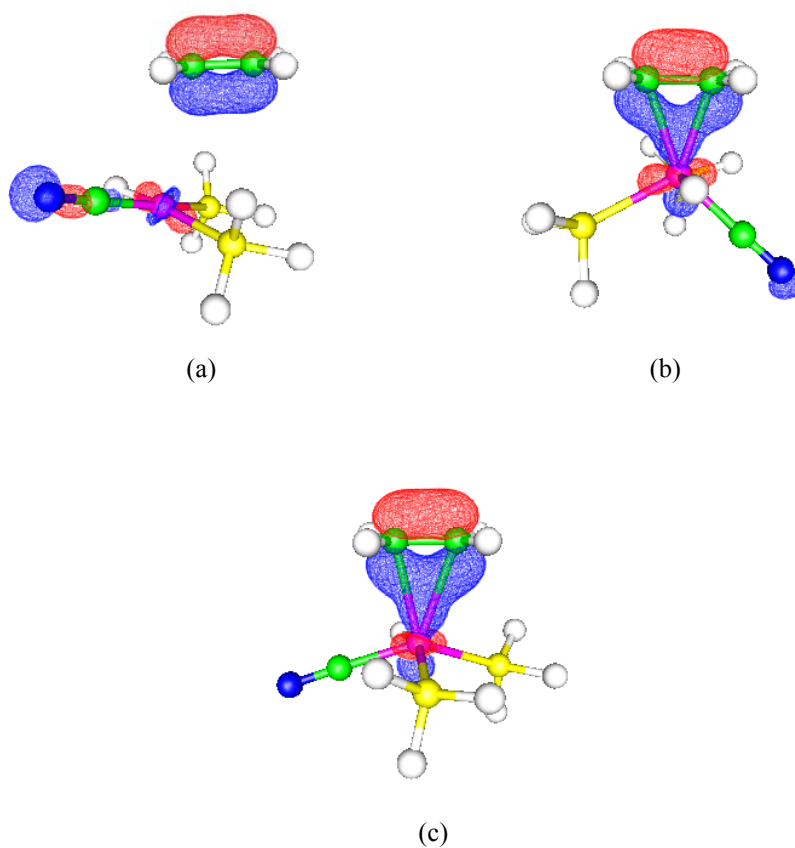
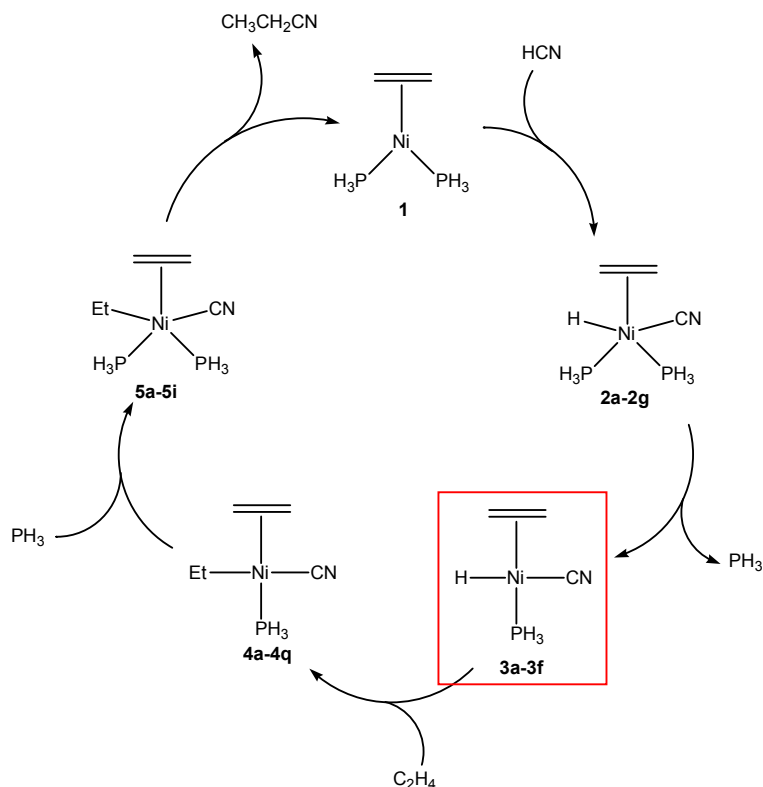


Figure 12. Molecular orbitals showing donation from ethylene to Ni for (a) **2c** (b) **2e** (c) **TS(2c-2e)**

(c) (Ethylene)Ni(H)(CN)PH₃ (3a-3f)

After ligand dissociation, it is postulated that (ethylene)Ni(H)(CN)PH₃ forms (Tolman, 1985), although the complex has never been isolated (Scheme 4).



Scheme 4. The catalytic cycle, indicating the position of **3**

Three minimum energy configurations, each with two conformations (the C-C-axis of ethylene either in the plane or perpendicular to the plane of the molecule) have been found, as shown in Figure 13. Relevant bond lengths and angles are summarized in Table 9.

Table 9. Selected bond lengths (Å) and angles (°) for complex **3**

	3a	3b	3c	3d	3e	3f
Ni-C1	1.909	2.151	2.186	2.254	1.888	2.173
Ni-C2	2.194	2.151	2.191	2.254	2.190	2.173
Ni-P	2.156	2.376	2.212	2.237	2.281	2.193
Ni-H	1.763	1.463	1.465	1.473	1.763	1.500
Ni-CN	1.900	1.851	1.856	1.851	1.840	1.924
C1-Ni-C2	42.1	37.0	36.3	35.0	42.7	36.6
C1-C2-Ni-X*	180.0	90.1	180.0	-91.6	180	-90.3

*X=H for **3a**, **3b**, **3e** and **3f**; X=CN for **3c** and **3d**

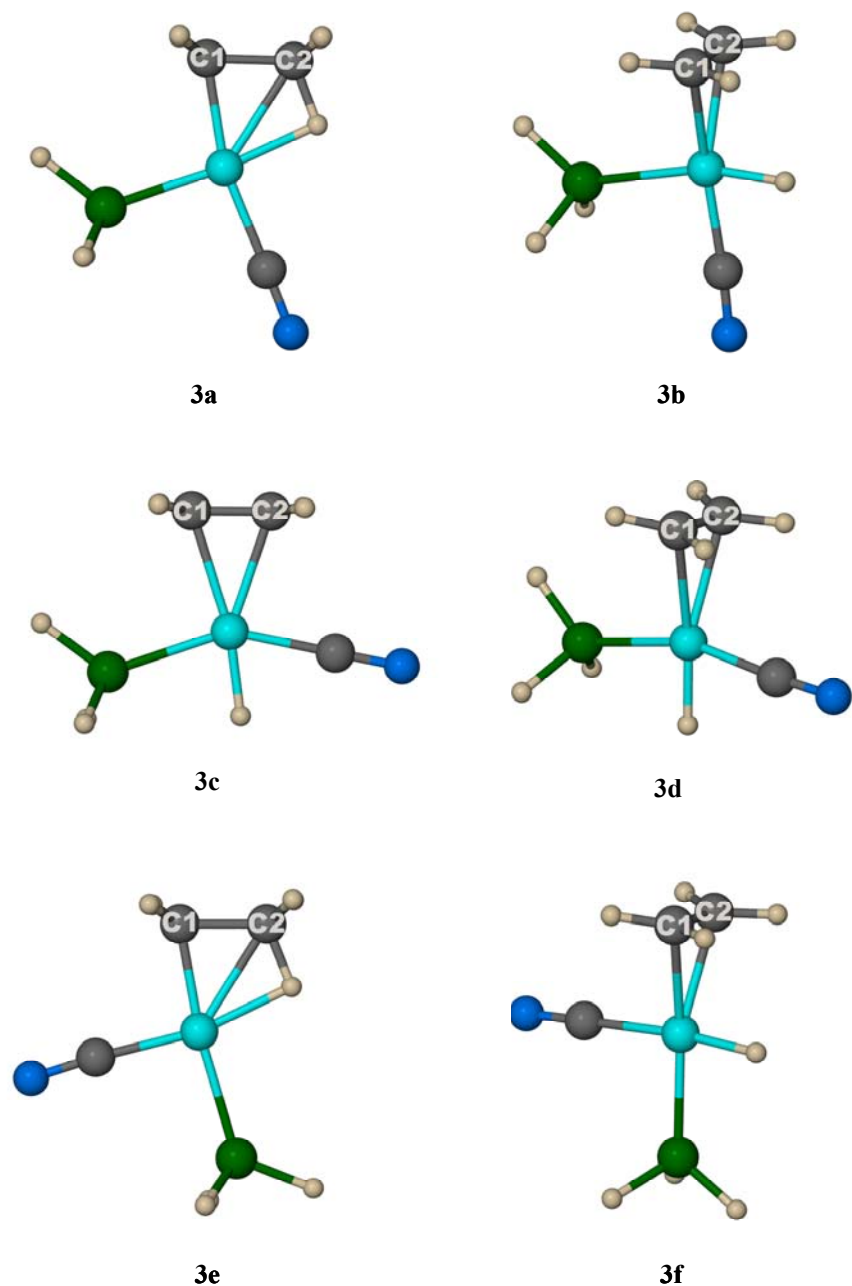


Figure 13. Minimum energy structures for complex 3

All six complexes are square planar and differ only in the relative positions of the ligands and the orientation of the coordinated ethylene. For structures **3a** and **3b**, CN is *trans* to ethylene, for **3c** and **3d**, H is *trans* to ethylene and for **3e** and **3f**, PH₃ is *trans* to ethylene. The C-C-axis of ethylene is parallel to the plane of the complex in

structures **3a**, **3c** and **3e**, whereas it is perpendicular to the plane in complexes **3b**, **3d** and **3f**.

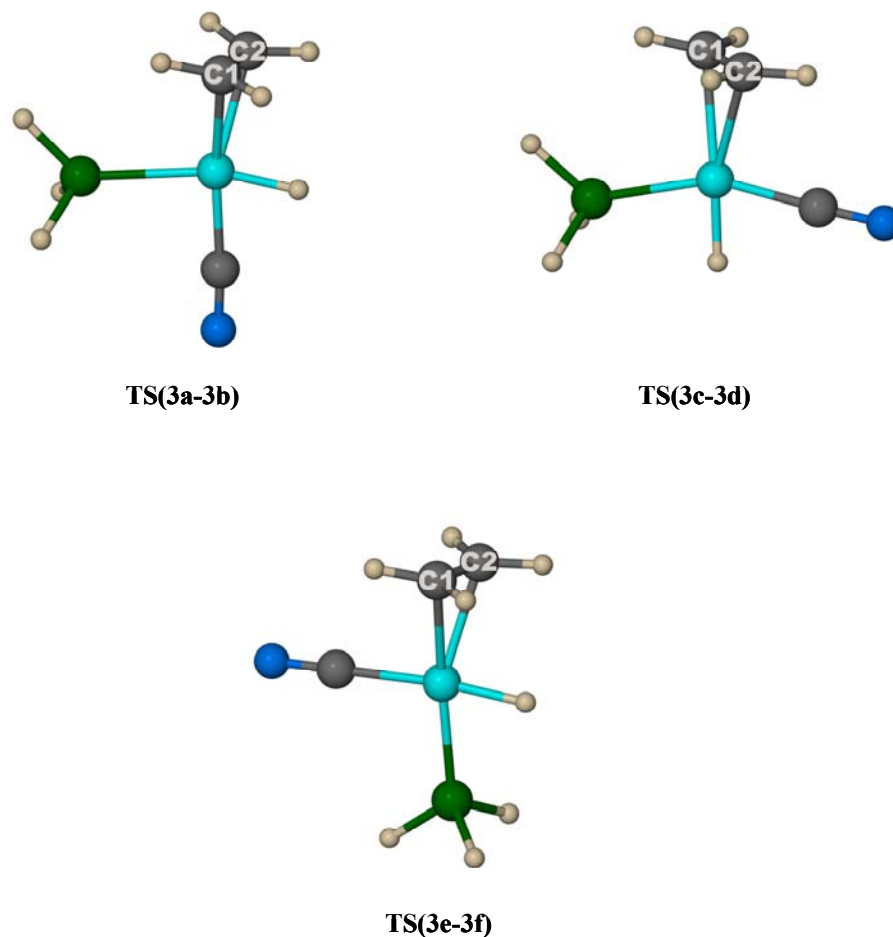


Figure 14. Transition structures for complex **3**

Transition structures (shown in Figure 14) were obtained for the pairs **3a** and **3b**, **3c** and **3d**, and **3e** and **3f** where the major difference between the pairs are the orientation of the ethylene. Relevant bond lengths and angles for the transition structures are summarized in Table 10. The energies of the minimum and transition structures relative to **3e** are shown in Table 11. Complexes **3a** and **3e** have much lower energy than the other complexes in this series, due to interaction of the hydrogen with coordinated ethylene. Also, the transition structure **TS(3e-3f)** has slightly lower energy than **3f**. However, when the free energy is considered, the energy of **3f** is lower than the energy of **TS(3e-3f)** by 1.60 kcal/mol.

Table 10. Selected angles (°) and bond lengths (Å) for the transition structures of complex **3**

	TS(3a-3b)	TS(3c-3d)	TS(3e-3f)
Ni-C1	2.150	2.237	2.186
Ni-C2	2.150	2.253	2.182
Ni-P	2.372	2.230	2.179
Ni-H	1.463	1.469	1.512
Ni-CN	1.851	1.852	1.909
C1-Ni-C2	37.0	35.2	36.4
C1-C2-Ni-X*	100.1	129.3	-105.4

*X=H for **TS(3a-3b)** and **TS(3e-3f)**; X=CN for **TS(3c-3d)**

Table 11. Energies of minima and transition structures of **3** relative to **3e**

Complex	Energy [kcal/mol]	Complex	Energy* [kcal/mol]
3a	1.32	3f	14.82
3b	15.94	TS(3a-3b)	16.39 (15.07)
3c	14.44	TS(3c-3d)	15.43 (0.99)
3d	14.94	TS(3e-3f)	14.63 (14.53)
3e	0.00		

*Values in parentheses gives the energy barrier with respect to the lowest energy minimum of the pair connected by the transition structure.

A CDA analysis was done on these structures and the results are summarized in Tables 12 and 13. From Table 13 it is clear that the total amount of electron donation from ethylene to Ni is similar for all the geometries, including the transition states, except for **3a** and **3e** where it is somewhat more. Back-donation from Ni is significantly more for the latter two complexes in comparison to the other geometries. With the exception of **3e**, back-donation from Ni to ethylene could not be ascribed to any single MO. The orbitals for donation from ethylene to Ni are shown in Figures 15 and 16. Figure 15 shows that ethylene is certainly π -coordinated when ethylene is perpendicular to the plane or almost so as in the case of the transition structures. The electron density between ethylene and Ni is somewhat diminished for **3d** and **3f** as is also reflected in the CDA data and this correlates well with the calculated bond lengths. From Figure 16 it can be seen that, when ethylene is in the plane of the molecule, its coordination is very unsymmetrical, especially for **3a** and **3e**. The position of H *cis* to ethylene definitely plays a role in this as there is significant electron density between H and the C atom adjacent to it (Figure 17).

Table 12. Charge components for selected MOs of **3**

Complex	Donor	<i>d</i>	<i>b</i>	<i>r</i>
3a	Ethylene to Ni	0.177	0.076	-0.290
	Phosphine to Ni	0.365	0.035	-0.212
	Cyanide to Ni	0.116	-0.001	-0.210
3b	Ethylene to Ni	0.103	0.013	-0.051
	Phosphine to Ni	0.106	0.002	-0.032
	Cyanide to Ni	0.163	-0.014	0.189
3c	Ethylene to Ni	0.145	0.013	-0.082
	Phosphine to Ni	0.169	0.004	-0.014
	Cyanide to Ni	0.134	-0.010	-0.108
3d	Ethylene to Ni	0.098	-0.002	-0.084
	Phosphine to Ni	0.122	0.002	0.043
	Cyanide to Ni	0.119	-0.005	-0.081
3e	Ethylene to Ni	0.094	0.019	-0.135
	Ni to Ethylene	0.052	0.126	-0.199
	Phosphine to Ni	0.225	0.014	-0.040
	Cyanide to Ni	0.196	0.010	-0.113
3f	Ethylene to Ni	0.214	0.004	-0.089
	Phosphine to Ni	0.183	0.023	-0.083
	Cyanide to Ni	0.158	-0.011	-0.184
TS(3a-3b)	Ethylene to Ni	0.103	0.014	-0.061
	Phosphine to Ni	0.117	0.007	0.042
	Cyanide to Ni	0.165	-0.015	0.196
TS(3c-3d)	Ethylene to Ni	0.124	0.005	-0.079
	Phosphine to Ni	0.143	0.004	0.015
	Cyanide to Ni	0.124	-0.007	-0.098
TS(3e-3f)	Ethylene to Ni	0.182	0.015	-0.073
	Phosphine to Ni	0.169	0.027	-0.099
	Cyanide to Ni	0.204	-0.015	-0.199

Table 13. Total amounts of donation and back-donation for **3**

Complex	Donor	<i>d</i>	<i>b</i>	<i>r</i>
3a	Ethylene	0.545	0.427	-0.354
	Cyanide	0.703	0.015	-0.217
	Phosphine	0.510	0.190	-0.236
3b	Ethylene	0.433	0.097	-0.232
	Cyanide	0.732	0.064	-0.197
	Phosphine	0.372	0.111	-0.284
3c	Ethylene	0.424	0.147	-0.271

Table 13. *Continued*

Complex	Donor	<i>d</i>	<i>b</i>	<i>r</i>
3d	Cyanide	0.668	0.059	-0.242
	Phosphine	0.397	0.159	-0.360
	Ethylene	0.414	0.076	-0.208
3e	Cyanide	0.685	0.052	-0.211
	Phosphine	0.372	0.310	-0.342
	Ethylene	0.513	0.423	-0.351
3f	Cyanide	0.708	0.066	-0.178
	Phosphine	0.376	0.111	-0.297
	Ethylene	0.451	0.080	-0.217
TS(3a-3b)	Cyanide	0.669	-0.004	-0.269
	Phosphine	0.521	0.180	-0.247
	Ethylene	0.431	0.104	-0.234
TS(3c-3d)	Cyanide	0.733	0.064	-0.199
	Phosphine	0.370	0.114	-0.285
	Ethylene	0.415	0.102	-0.227
TS(3e-3f)	Cyanide	0.686	0.061	-0.222
	Phosphine	0.379	0.144	-0.356
	Ethylene	0.448	0.089	-0.217
	Cyanide	0.659	0.003	-0.257
	Phosphine	0.530	0.209	-0.249

Moreover, in all the reported crystal structures in which ethylene and hydrogen are coordinated *cis* to each other to a metal center (Zr in all cases), the average H-C bond distance is 1.016 (\pm 0.106) Å while the average H-M distance is 2.123 (\pm 0.058) Å. The earliest such example is a zirconocene complex reported in 1986 by Erker and co-workers. There have been many subsequent reports (Arndt, 2003; Horacek, 2004), but no similar Ni-containing structures could be found. It may well be that the increased interaction of H with ethylene draws some electron density way from the carbon atoms, thus facilitating enhanced back-donation from Ni to ethylene. In addition, this causes the ethylene to be coordinated more like an ethyl group, hence the asymmetry in the electron density between ethylene and Ni. For **3c** too the donation is asymmetrical and the position of CN *cis* to ethylene may well have an effect here, perhaps due to electron delocalization to CN. In all the cases donation from cyanide to Ni is \sim 0.7 electrons, with insignificant back-donation.

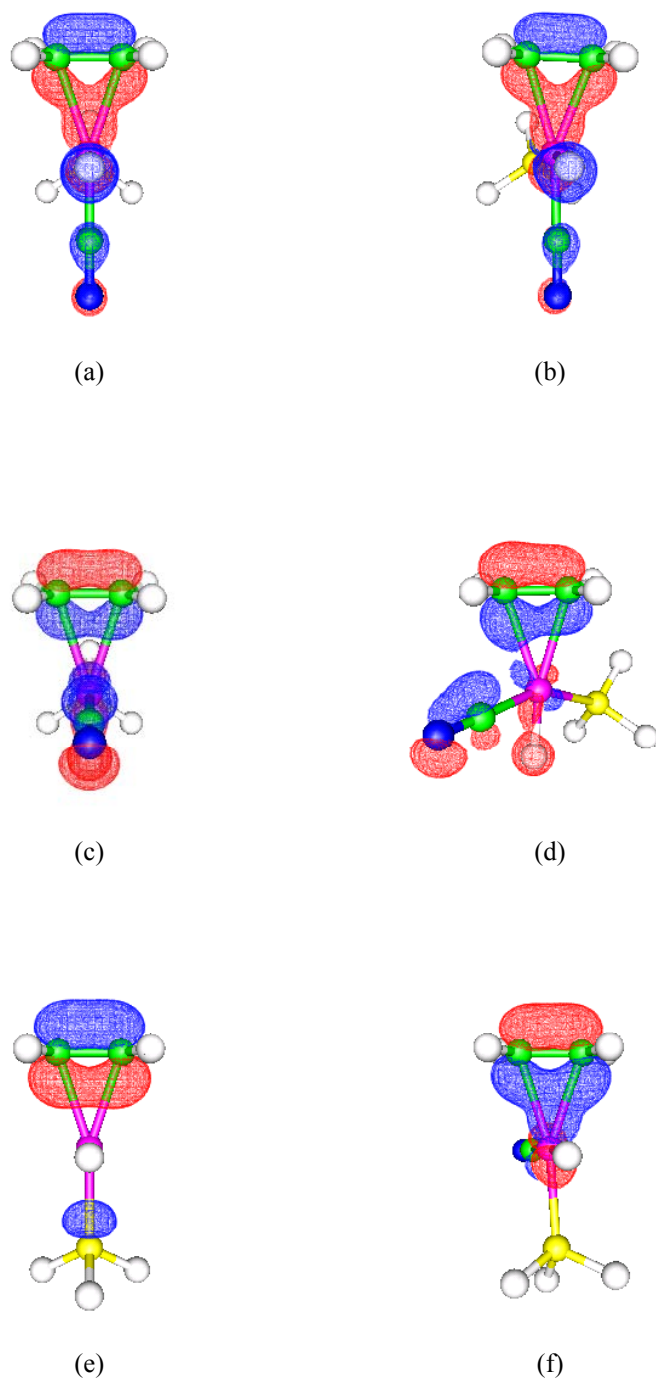


Figure 15. Molecular orbitals showing donation from ethylene to Ni for (a) **3b** (b) **TS(3a-3b)** (c) **3d** (d) **TS(3c-3d)** (e) **3f** (f) **TS(3e-3f)**

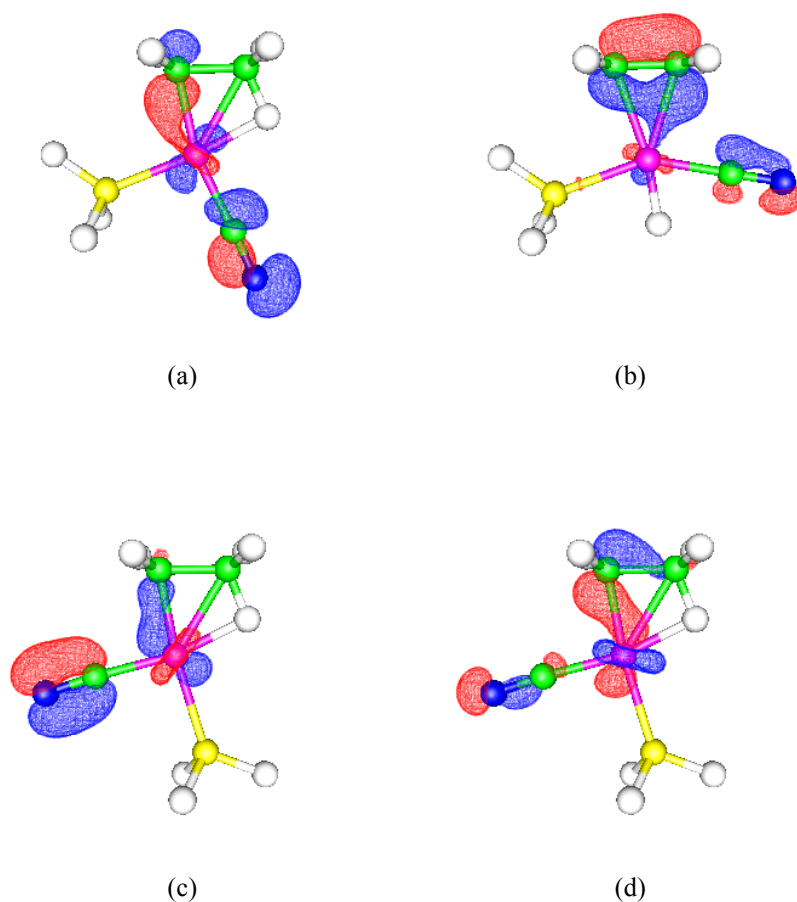


Figure 16. Molecular orbitals showing donation from ethylene to Ni for (a) **3a** (b) **3c** (c) **3e** and back-donation from Ni to ethylene for (d) **3e**

This, of course, is not surprising, since CN, unlike CO, is a strong enough σ -donor that back-donation from Ni is not necessary to stabilize the bond (Cotton, 1988). The relevant orbitals are presented in Table 12. In the case of **3b**, **3c**, **3d**, **3f**, **TS(3a-3b)** and **TS(3c-3d)**, other orbitals also seem to contribute significantly to donation from cyanide to Ni, based on the CDA data, but the graphical representation of these orbitals do not bear this out. Donation from phosphine is considerably less than from cyanide, but in each case the back-donation is somewhat more, especially for **3d** and **TS(3c-3d)**, but could not be ascribed to any specific orbitals. Notably though, the

donation from phosphine to Ni for **3a** and **3e** is somewhat more than for the other geometries. This is brought about by the diminished electron density on Ni due to its increased back-donation to ethylene as discussed. Again, as for **2**, however, the orbitals most involved in donation from phosphine to Ni seem to be Ni-centered. The relevant orbitals are presented in Table 12.

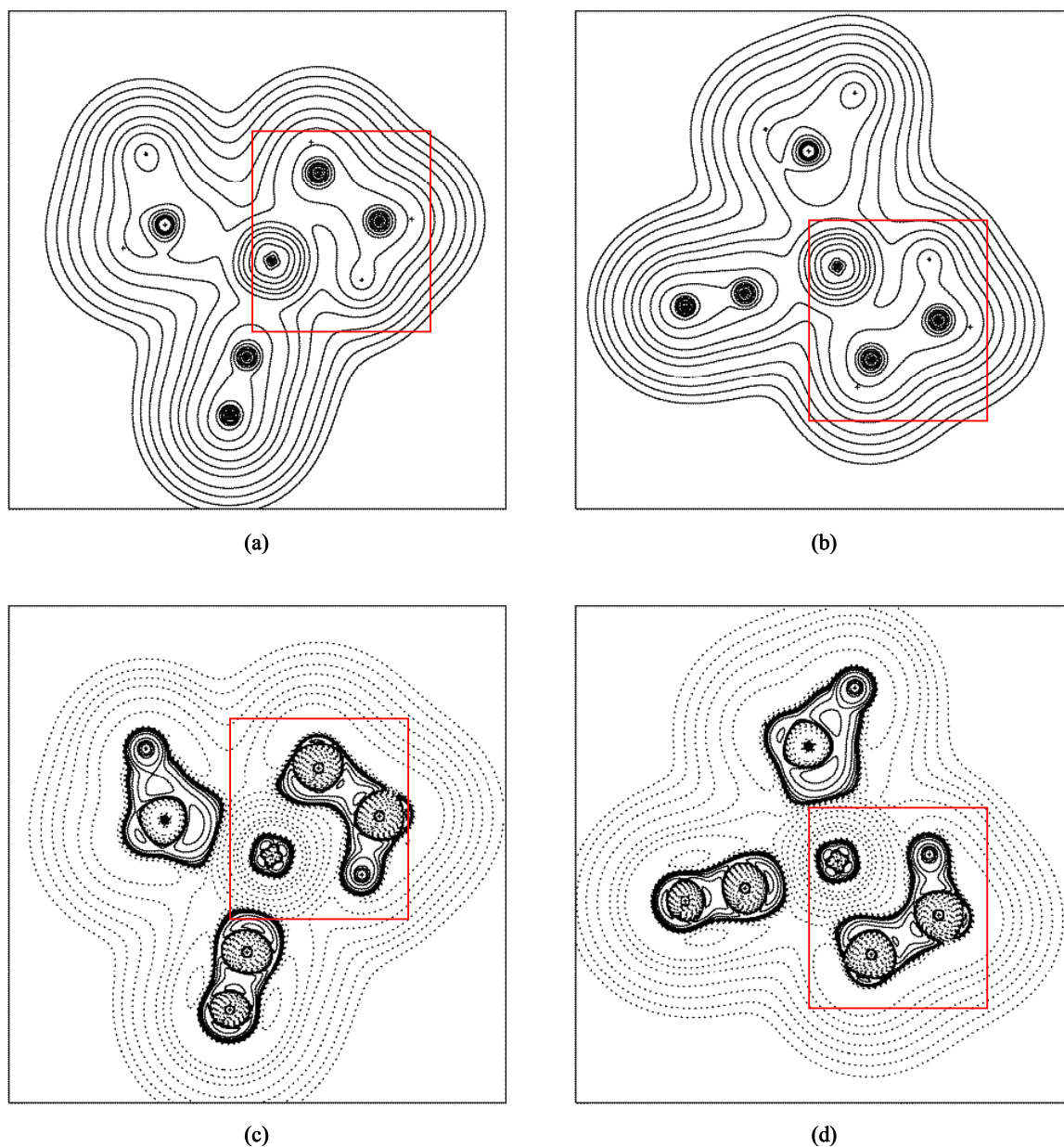
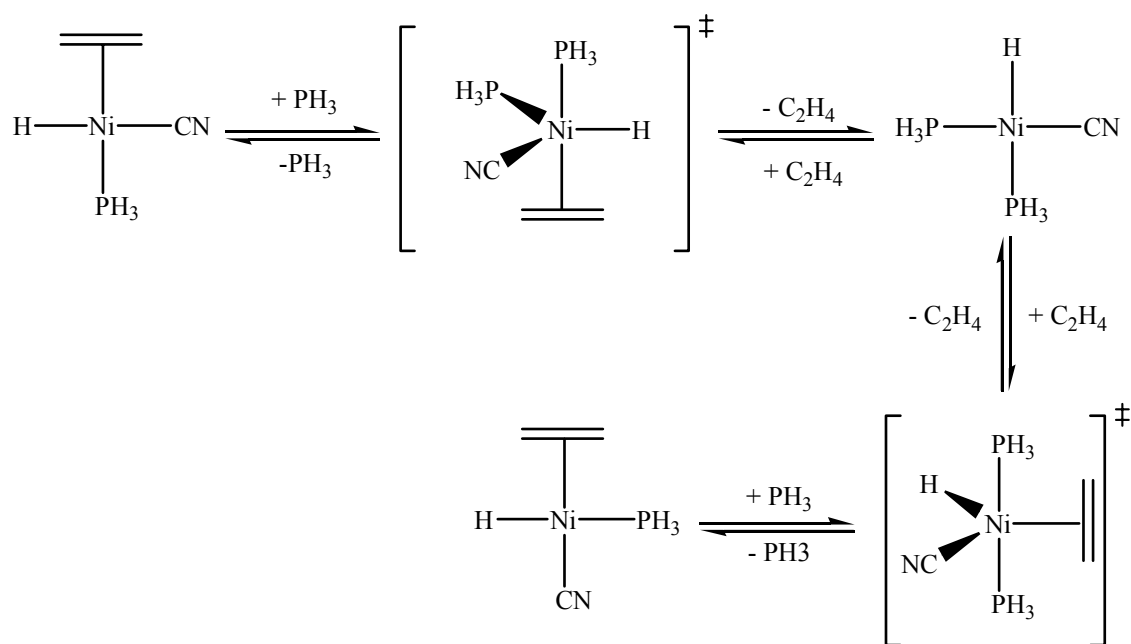


Figure 17. Electron density plot of (a) **3a** (b) **3e**. Laplacian of (c) **3a** (d) **3e**. Of interest are the areas in the red squares. In (c) and (d) the solid lines show areas of electron build-up and dotted lines indicate areas of electron depletion.

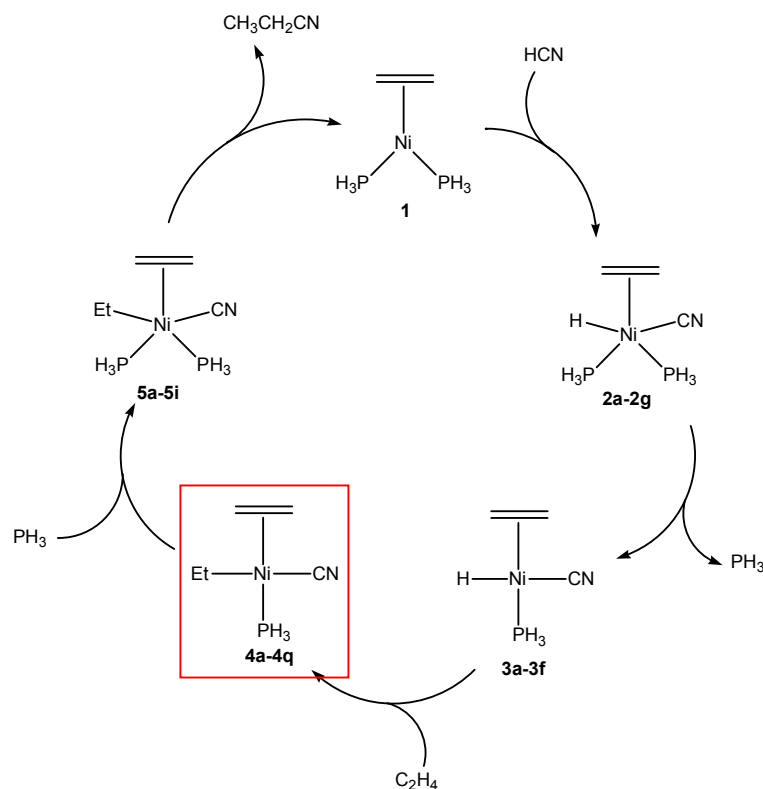
The transition between two isomers of **3** should readily take place in solution as shown by NMR studies of $(C_2H_4)L(CN)(C_2H_5)Ni$ (McKinney, 1985, 1986). Generally, the isomerization of a square planar complex (see Scheme 5) involves the association of a solvent molecule (or, since the ligand is present in excess in this reaction (Tolman, 1985), most likely a molecule of phosphine) with subsequent rearrangement to a trigonal bipyramidal transition structure. Dissociation of a substituent leads to a square planar intermediate and reassociation of the substituent leads to a different trigonal bipyramidal transition structure. Finally, dissociation of a ligand gives the new isomer (Cotton, 1998). However, the postulated transition states need to be found by potential energy surface scans – a very expensive technique. Since McKinney (1985) has shown that equilibration among the isomers takes place more quickly than the catalytic reaction, finding these transition structures will not add much to the understanding of the catalytic cycle.



Scheme 5. Postulated transition between two geometries of **3**

(d) (Ethylene)Ni(ethyl)(CN)PH₃ (4a-4q)

After coordination and insertion (see Section **5(c)**) of a second ethylene molecule, the result is (ethylene)Ni(ethyl)(CN)PH₃ – a complex that contains both π -bonded ethylene and a σ -bonded ethyl group (Scheme 6).



Scheme 6. The catalytic cycle, showing the position of **4**

As for **3**, all the geometries are square planar. Again, the major differences between the geometries are the relative orientations of the ligands and the orientation of the π -coordinated ethylene, so that there are six configurations representing energy minima. The additional conformations for each configuration are due to the different possible orientations of the σ -bonded ethyl group. Figure 18 shows the geometries as represented by the lowest energy conformation of each of the six configurations. Transition structures were found for the rotation of both π -bonded ethylene and σ -bonded ethyl, but not for changes in the relative positions of the ligands for the same reasons as stated in Section 4(c). The pathways connecting the various energy minima and transition structures are shown in Schemes 7, 8 and 9. It is also indicated whether the transition is due to rotation of π -coordinated ethylene or rotation around the σ -bonded ethyl group. Relevant bond lengths and angles for the minimum and transition structures are summarized in Table 14 and Table 15 respectively. The energies relative to **4d** are presented in Table 16. From these tables it should be clear that there are many pairs of conformations that are mirror-images (but not enantiomers) of each other – connected by transition structures.

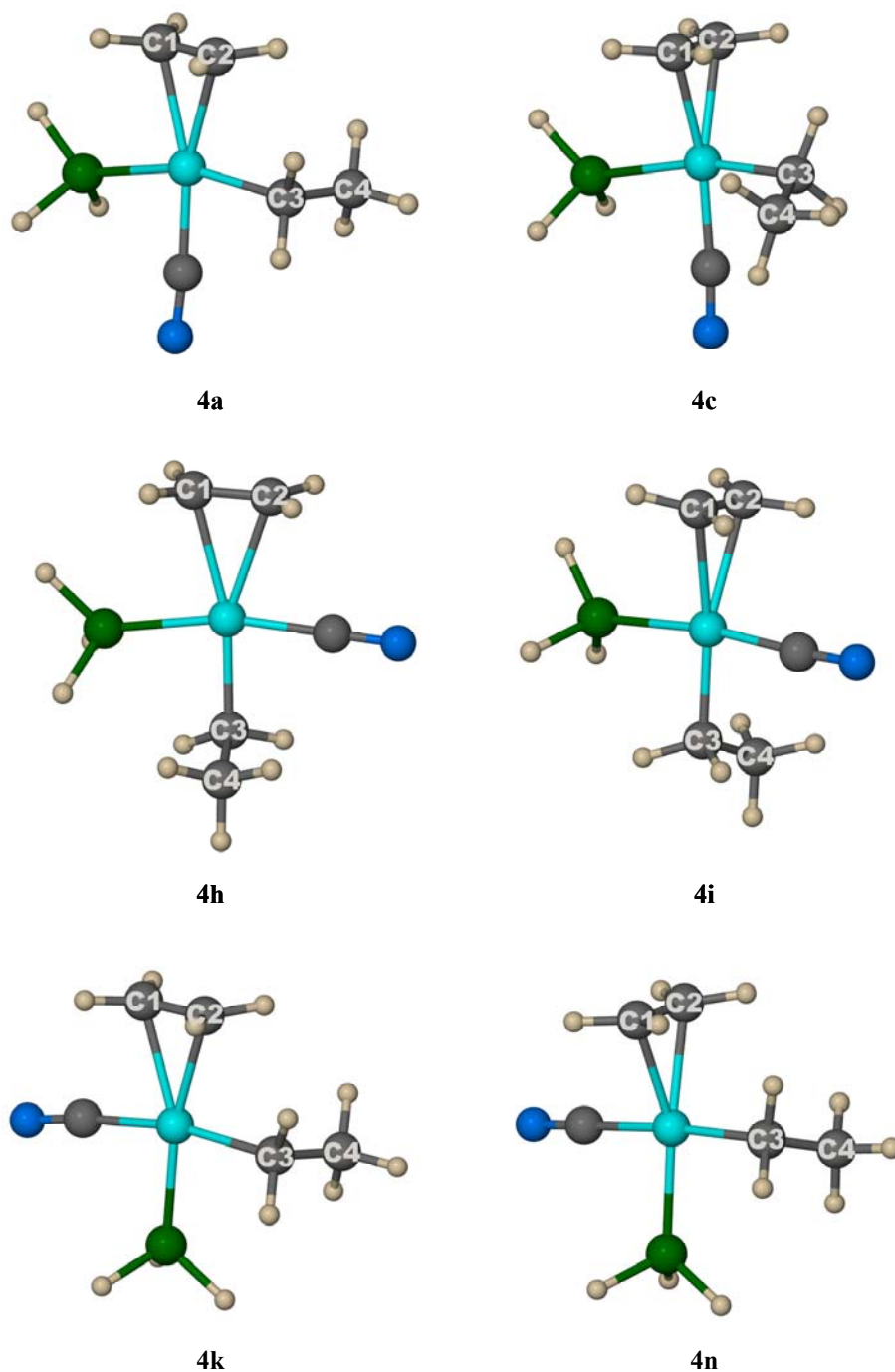
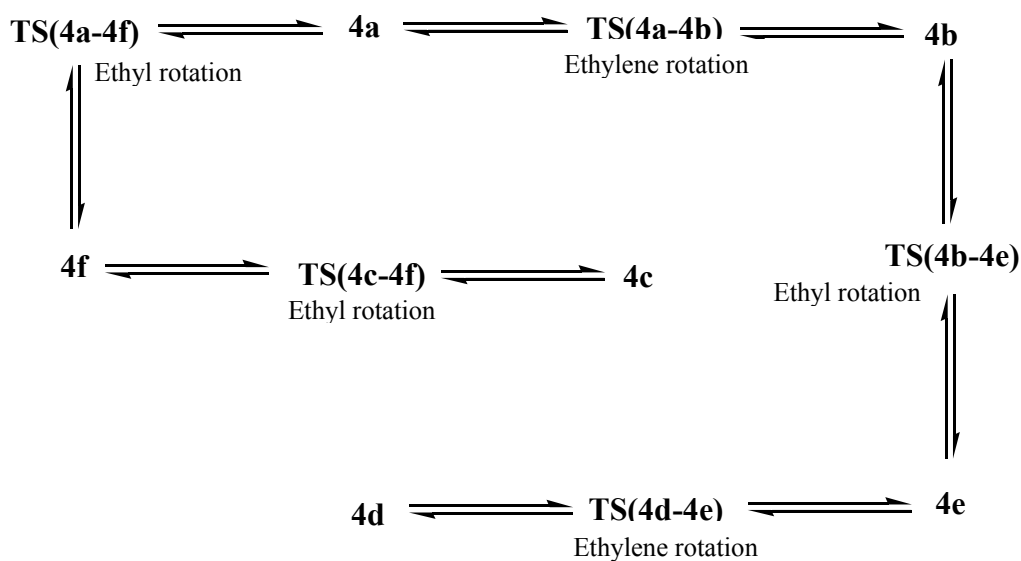
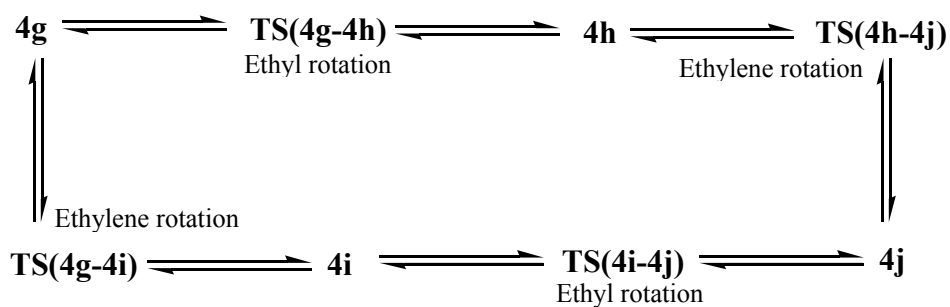


Figure 18. Selected minimum energy structures for complex 4

Note that the optimizations were obtained without any symmetry constraints, so that the term “mirror image” should not be interpreted in the strict group theoretical sense of the word. Thus, each energy minimum, with the exception of **4m**, has a mirror image. The small discrepancies in the energies of a mirror-image pair arise from the lack of symmetry constraints during optimization.



Scheme 7. Interconnecting pathway for the minimum and transition structures of **4a** to **4f**



Scheme 8. Interconnecting pathway for the minimum and transition structures of **4g** to **4j**

Table 14. Selected bond lengths (Å) and angles (°) for complex **4**

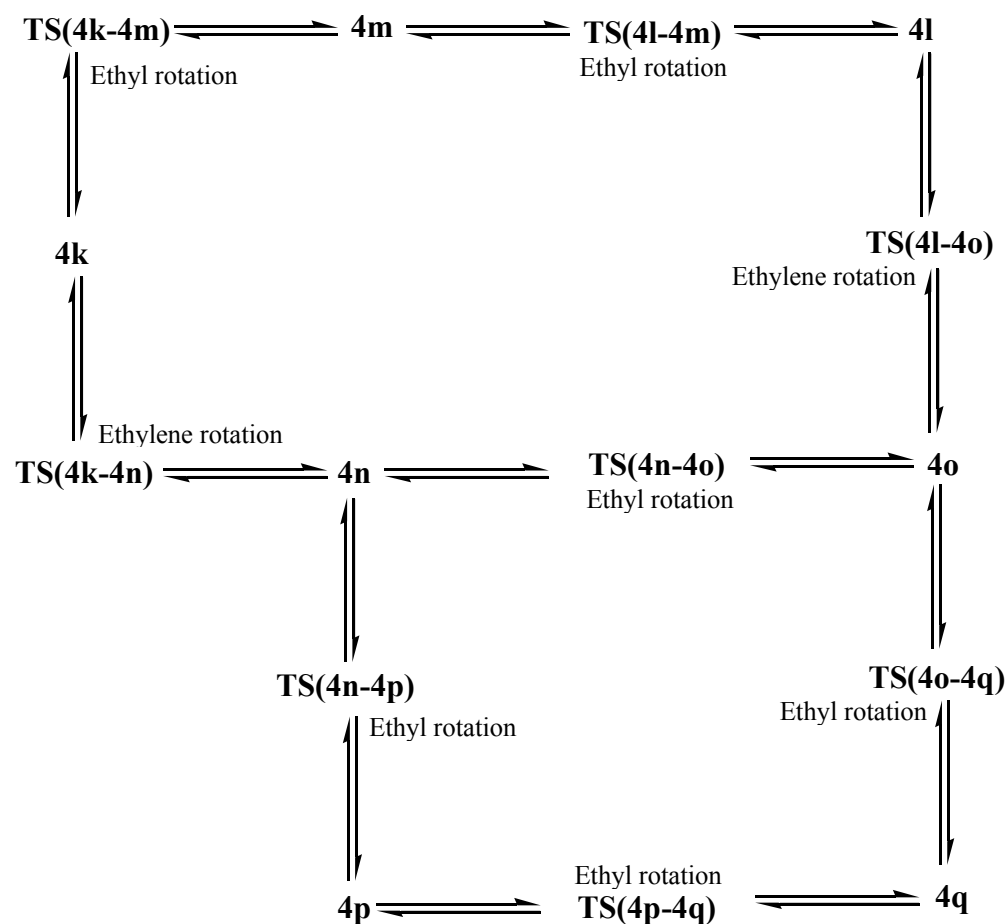
	4a	4b	4c	4d	4e	4f
Ni-C1	2.213	2.213	2.158	2.158	2.173	2.180
Ni-C2	2.205	2.205	2.158	2.158	2.179	2.173
Ni-P	2.328	2.328	2.418	2.419	2.424	2.425
Ni-CN	1.855	1.855	1.875	1.875	1.868	1.868
Ni-Et	2.019	2.020	1.956	1.956	1.969	1.969
C1-C2-Ni-X	-10.5	10.4	95.3	90.2	101.2	83.4
CH ₃ -CH ₂ -Ni-Y	92.9	-92.8	-75.8	75.9	137.2	-137.2

Table 14. *Continued*

	4g	4h	4i	4j	4k	4l
Ni-C1	2.337	2.339	2.316	2.314	2.229	2.229
Ni-C2	2.331	2.339	2.316	2.316	2.188	2.188
Ni-P	2.232	2.232	2.252	2.252	2.198	2.198
Ni-CN	1.877	1.877	1.872	1.872	1.924	1.924
Ni-Et	1.995	1.995	1.982	1.982	2.017	2.016
C1-C2-Ni-X	-174.5	-179.3	-91.5	-88.8	-7.6	7.5
CH ₃ -CH ₂ -Ni-Y	-83.5	81.9	-82.1	82.9	84.6	-84.8
	4m	4n	4o	4p	4q	
Ni-C1	2.229	2.187	2.184	2.198	2.224	
Ni-C2	2.153	2.185	2.189	2.224	2.198	
Ni-P	2.214	2.214	2.216	2.214	2.214	
Ni-CN	1.924	1.943	1.943	1.946	1.946	
Ni-Et	2.030	1.970	1.970	1.982	1.982	
C1-C2-Ni-X*	0.1	91.3	91.3	101.5	79.6	
CH ₃ -CH ₂ -Ni-Y**	-169.3	79.9	-80.1	139.8	-139.4	

* X=PH₃ for **4a-4f**; X=CN for **4g-4q**

** Y=CN for **4a-4j**; Y=PH₃ for **4k-4q**



Scheme 9. Interconnecting pathway for the minimum and transition structures of **4k** to **4q**

Table 15. Selected bond lengths (Å) and angles (°) for the transition structures of complex 4

	TS(4a-4b)	TS(a/b-f/e)	TS(4c-4f)	TS(4d-4e)	TS(g/h-i/j)
Ni-C1	2.199	2.275	2.191	2.196	2.446
Ni-C2	2.164	2.271	2.196	2.191	2.420
Ni-P	2.329	2.354	2.426	2.426	2.272
Ni-CN	1.869	1.838	1.864	1.864	1.859
Ni-Et	2.049	2.011	1.967	1.967	1.980
C1-C2-Ni-X*	0.1	0.3	83.9	100.4	179.9
CH ₃ -CH ₂ -Ni-Y**	-179.9	0.0	-115.4	115.4	0.0
	TS(4g-4h)	TS(4i-4j)	TS(4k-4m)	TS(4k-4h)	TS(4l-4m)
Ni-C1	2.432	2.358	2.238	2.255	2.238
Ni-C2	2.436	2.358	2.168	2.211	2.168
Ni-P	2.251	2.267	2.209	2.193	2.209
Ni-CN	1.994	1.874	1.925	1.927	1.925
Ni-Et	1.881	1.982	2.029	2.010	2.029
C1-C2-Ni-X*	-173.0	-89.4	5.3	16.5	-5.3
CH ₃ -CH ₂ -Ni-Y**	175.4	180.0	151.4	86.0	-151.4
	TS(4l-4o)	TS(4n-4o)	TS(4n-4p)	TS(4o-4q)	TS(4p-4q)
Ni-C1	2.246	2.240	2.223	2.240	2.184
Ni-C2	2.211	2.240	2.240	2.223	2.184
Ni-P	2.219	2.205	2.207	2.207	2.228
Ni-CN	1.927	1.947	1.946	1.946	1.949
Ni-Et	2.010	1.973	1.980	1.980	1.983
C1-C2-Ni-X*	-16.6	90.1	100.0	80.7	90.3
CH ₃ -CH ₂ -Ni-Y**	-86.0	0.0	112.1	-112.1	180.0

*X=PH₃ for **TS(4a-4b)**, **TS(a/b-f/e)**, **TS(4c-4f)** and **TS(4d-4e)**; X=CN for all the others

Y=PH₃ for **TS(4k-4m), **TS(4k-4n)**, **TS(4l-4m)**, **TS(4l-4o)**, **TS(4n-4o)**, **TS(4n-4p)** and **TS(4o-4q)**; Y=CN for all the others

Table 16. Energies relative to **4c** for the minimum and transition structures of complex 4

Structure	Energy [kcal/mol]	Structure	Energy* [kcal/mol]
4a	5.65	4q	3.09
4b	5.65	TS(4a-4b)	17.34 (11.69)
4c	0.00	TS(4a/b-4f/e)	15.42 (12.94)
4d	0.00	TS(4c-4f)	9.55 (9.55)
4e	2.49	TS(4d-4e)	9.55 (9.55)
4f	2.48	TS(4g-4h)	15.43 (11.27)
4g	4.22	TS(4g/h-4i/j)	13.85 (12.13)
4h	4.16	TS(4i-4j)	11.81 (10.09)

Table 16. *Continued*

Structure	Energy [kcal/mol]	Structure	Energy* [kcal/mol]
4i	1.72	TS(4k-4m)	15.38 (10.47)
4j	1.74	TS(4k-4n)	12.59 (7.68)
4k	4.91	TS(4l-4m)	15.38 (10.47)
4l	4.91	TS(4l-4o)	12.59 (11.88)
4m	8.43	TS(4n-4o)	10.34 (9.63)
4n	0.71	TS(4n-4p)	10.02 (9.31)
4o	0.71	TS(4o-4q)	10.02 (9.31)
4p	3.09	TS(4p-4q)	10.26 (7.17)

*The value in parentheses is the energy barrier with respect to the lowest minimum energy conformation of the pair connected by the transition structure

A CDA analysis was done on selected geometries, namely **4a**, **4c**, **4h**, **4i**, **4k** and **4n**. The results are presented in Tables 17 and 18. Donation from phosphine could not be assigned to a specific MO, but overall, the trends are the same as found for complex **3** and the conclusions derived there also hold here. A notable exception, though, is seen with donation from ethylene to Ni for **4a** (which corresponds to **3a**) and **4k** (which corresponds to **3e**). For both **3a** and **3e** H is *cis* to ethylene. The resulting interaction between H and ethylene results in electron density being drawn away from ethylene, so that there is significant back-donation from Ni to ethylene; this diminished electron density on Ni causes increased donation from phosphine. Since in **4a** and **4k** H is replaced by ethyl, this cannot happen here and the back-donation from Ni to ethylene is significantly diminished relative to **3a** and **3e** respectively. The donation from phosphine to Ni also decreases somewhat. Another interesting aspect of the ethylene to Ni donation in **4k** in particular, is that there are two orbitals (see Table 17) contributing to the donation, shown in Figure 19 giving the same net result as for the other geometries where only one orbital is primarily involved.

Table 17. Charge components for selected MOs of complex **4**

Complex	MO	<i>d</i>	<i>b</i>	<i>r</i>
4a	Ethylene to Ni	0.140	0.014	-0.087
	Phosphine to Ni	0.124	0.018	-0.138
	Cyanide to Ni	0.139	0.011	-0.102
4c	Ethylene to Ni	0.122	0.010	-0.073
	Phosphine to Ni	0.107	0.009	-0.139
	Cyanide to Ni	0.129	0.010	-0.060
4h	Ethylene to Ni	0.146	0.008	-0.052
	Cyanide to Ni	0.102	0.008	-0.036
4i	Ethylene to Ni	0.116	0.001	0.029
	Phosphine to Ni	0.145	0.021	-0.215
	Cyanide to Ni	0.129	0.004	-0.054
4k	Ethylene to Ni	0.120	0.030	-0.168
	Ethylene to Ni	0.070	0.027	-0.015
	Phosphine to Ni	0.186	0.024	-0.022
	Cyanide to Ni	0.130	0.001	-0.126
4n	Ethylene to Ni	0.113	-0.000	-0.065
	Phosphine to Ni	0.109	0.018	-0.052
	Cyanide to Ni	0.215	-0.015	-0.294

Table 18. Total amounts of donation and back-donation for complex **4**

Complex	Donor	<i>d</i>	<i>b</i>	<i>r</i>
4a	Ethylene	0.435	0.162	-0.290
	Cyanide	0.720	0.080	-0.267
	Phosphine	0.423	0.161	-0.368
4c	Ethylene	0.447	0.126	-0.265
	Cyanide	0.726	0.058	-0.219
	Phosphine	0.350	0.117	-0.341
4h	Ethylene	0.425	0.113	-0.257
	Cyanide	0.665	0.052	-0.264
	Phosphine	0.358	0.177	-0.402
4i	Ethylene	0.430	0.079	-0.218
	Cyanide	0.377	0.045	-0.232
	Phosphine	0.355	0.144	-0.356
4k	Ethylene	0.459	0.181	-0.275
	Cyanide	0.701	0.031	-0.311
	Phosphine	0.510	0.238	-0.314
4n	Ethylene	0.469	0.107	-0.237
	Cyanide	0.707	0.010	-0.253
	Phosphine	0.527	0.214	-0.262

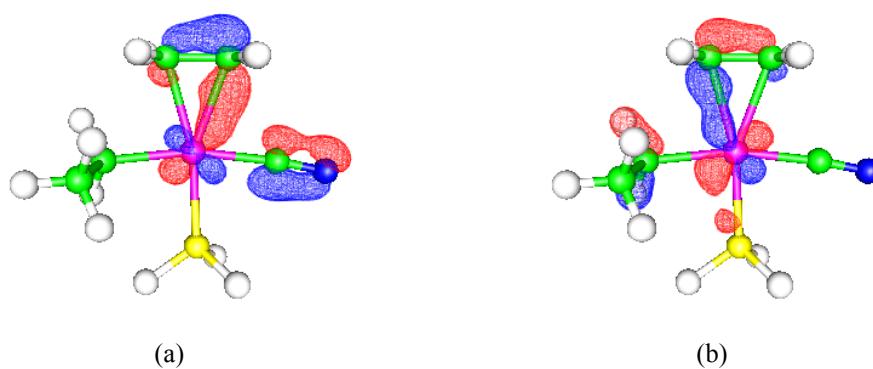
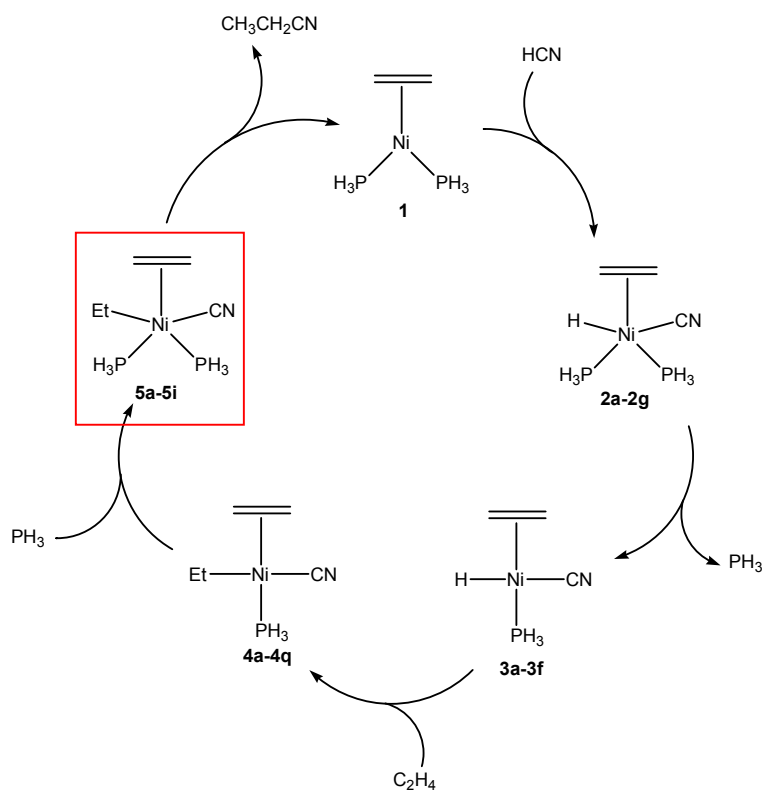


Figure 19. Donation from ethylene to Ni for **4k**, (a) MO 28 (b) MO 31

(e) (Ethylene)Ni(ethyl)(CN)(PH₃)₂ (5a-5i)

After ligand association, (Ethylene)Ni-(ethyl)(CN)(PH₃)₂ is formed (Scheme 10).



Scheme 10. The catalytic cycle, showing the position of **5**

Table 19. Comparative data for complexes **2** and **5**, with bond lengths in Å and angles in °

	2a	2e	2f	2g
Ni-C1	2.192	2.175	2.230	2.175
Ni-C2	2.192	2.146	2.235	2.146
Ni-P1	2.249	2.335	2.237	2.335
Ni-P2	2.249	2.327	2.434	2.327
Ni-CN	1.929	1.885	1.867	1.885
Ni-H	1.489	1.459	1.483	1.459
P1-Ni-P2	116.9	101.6	103.1	101.6
C1-C2-Ni-X*	6.4	172.9	-83.2	-172.9
	5a	5e	5g	5i
Ni-C1	2.252	2.180	2.272	2.435
Ni-C2	2.252	2.147	2.325	2.346
Ni-P1	2.258	2.440	2.248	3.368
Ni-P2	2.258	2.378	2.579	2.233
Ni-CN	1.950	1.892	1.882	1.879
Ni-Et	2.000	1.995	2.016	1.996
P1-Ni-P2	123.5	98.9	100.3	93.6
C1-C2-Ni-X*	4.9	175.8	-86.6	175.8

*X=P1 for **2a** and **5a**; X=CN for all the others

The optimized geometries were found by assuming that they would be similar to those of **2** (see Table 19 for comparative data), with the biggest difference being the replacement of H by ethyl. Table 19 shows that the geometries remain roughly the same, with a general lengthening of bonds for **5** relative to **2**. Moreover, the P-Ni-P angles of **5a** and **5i** are about 10° smaller/larger than those of their complex **2** counterparts. Ignoring geometry differences due to the variable orientation of the σ -coordinated ethyl group for the moment, four configurations of minimum energy were obtained, as shown by the lowest energy conformation of each in Figure 20. Selected bond lengths and angles are summarized in Table 20. Apart from transition structures obtained by varying the orientation of ethyl within a group, the only transition structures that could be found are those between **5g** and **5i**. Other possibilities were tried, but yielded no positive results. The main difference between **5g** and **5i** is in the orientation of π -bound ethylene as shown clearly in Figure 21, together with the two possible transition structures.

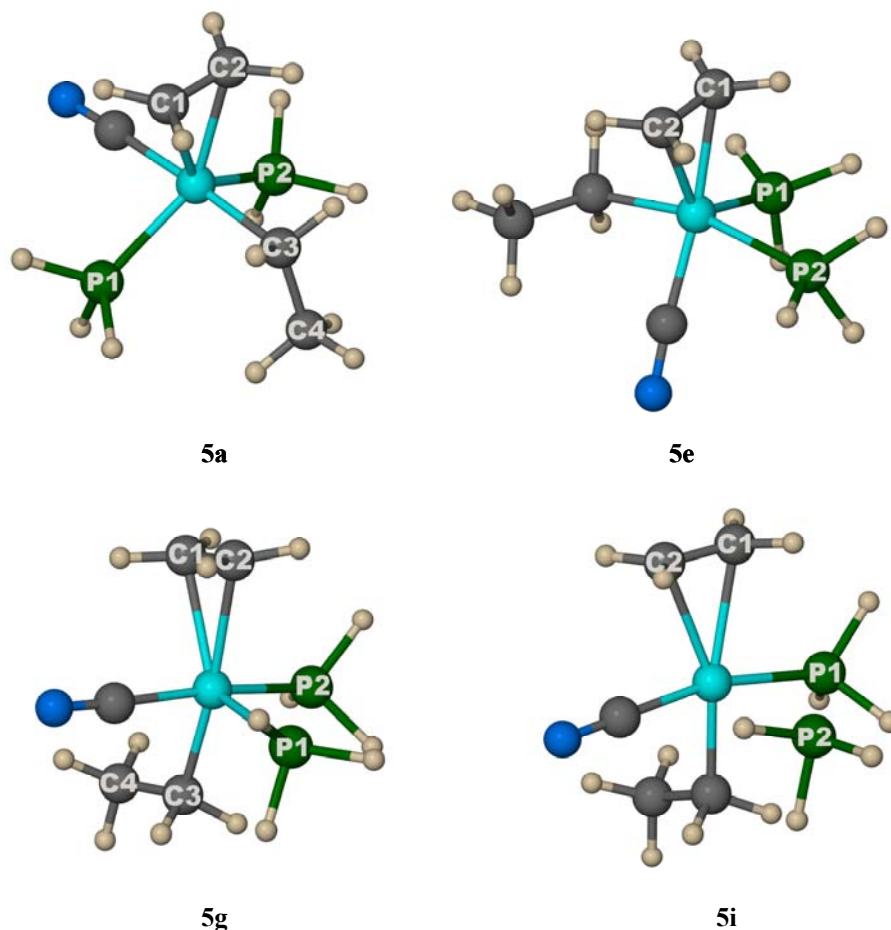


Figure 20. Selected minimum structures for complex **5**

Table 20. Selected bond lengths (Å) and angles (°) for complex **5**

	5a	5b	5c	5d	5e
Ni-C1	2.252	2.202	2.219	2.210	2.180
Ni-C2	2.252	2.219	2.202	2.168	2.147
Ni-P1	2.258	2.272	2.276	2.361	2.440
Ni-P2	2.258	2.276	2.272	2.367	2.378
Ni-CN	1.950	1.954	1.954	1.894	1.892
Ni-Et	2.000	2.009	2.009	1.996	1.995
C1C2NiX*	4.9	18.2	-5.0	175.6	175.8
CH ₃ CH ₂ NiY*	61.8	-174.2	-70.6	-61.2	59.8
	5f	5g	5h	5i	
Ni-C1	2.178	2.272	2.304	2.435	
Ni-C2	2.141	2.325	2.372	2.346	
Ni-P1	2.396	2.248	2.224	3.368	
Ni-P2	2.283	2.579	2.464	2.233	
Ni-CN	1.904	1.882	1.881	1.879	
Ni-Et	2.002	2.016	2.037	1.996	
C1C2NiX*	170.8	-86.6	-88.8	175.8	
CH ₃ CH ₂ NiY*	-174.7	78.2	-76.2	83.4	

*X=Y=P1 for **5a-5c**; X=Y=CN for all the others

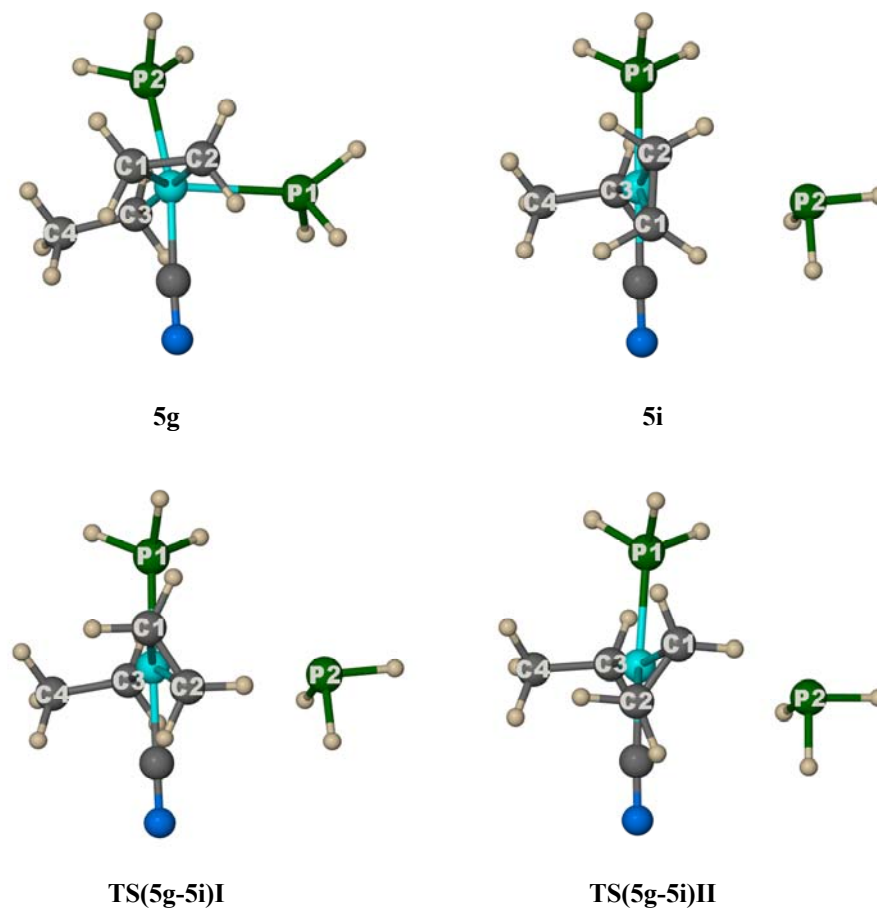


Figure 21. Transition structures between **5g** and **5i**

Table 21. Selected bond lengths and angles for the transition structures of complex **5**

	TS(5a-5b)	TS(5a-5c)	TS(5d-5e)	TS(5d-5f)
Ni-C1	2.187	2.179	2.139	2.163
Ni-C2	2.179	2.187	2.150	2.163
Ni-P1	2.280	2.307	2.381	2.395
Ni-P2	2.307	2.280	2.437	2.458
Ni-CN	1.963	1.963	1.902	1.899
Ni-Et	2.023	2.023	2.015	2.010
C1C2NiX*	6.5	16.0	-5.6	0.4
CH ₃ CH ₂ NiY*	118.9	-6.2	6.1	-127.1
	TS(5g-5h)	TS(5i-5i)I	TS(5i-5i)II	
Ni-C1	2.320	2.409	2.426	
Ni-C2	2.399	2.411	2.438	
Ni-P1	2.265	3.413	3.288	
Ni-P2	2.505	2.267	2.258	
Ni-CN	1.869	1.862	1.875	
Ni-Et	2.022	1.990	1.995	
C1C2NiX*	-87.4	-2.8	-11.9	
CH ₃ CH ₂ NiY*	-109.9	-13.6	-151.2	

*X=Y=P1 for **TS(5a-5b)** and **TS(5a-5c)**; X=Y=CN for all the others

Transition structures were obtained for the rotation of the σ -bonded ethyl groups (see Table 12 for selected bond lengths and angles) and the energies relative to **5a** of the minimum and transition structures are presented in Table 22.

Table 22. Relative energies of minimum and transition structures of complex **5** relative to **5a**

Structure	Energy [kcal/mol]	Structure	Energy* [kcal/mol]
5a	0.00	5i	9.69
5b	0.93	TS(5a-5b)	4.00 (4.00)
5c	0.93	TS(5a-5c)	4.00 (4.00)
5d	5.60	TS(5d-5e)	9.31 (3.82)
5e	5.49	TS(5d-5f)	9.06 (3.46)
5f	6.61	TS(5g-5h)	10.11 (2.18)
5g	7.93	TS(5i-5iI)	12.76 (3.07)
5h	9.23	TS(5i-5iII)	13.60 (3.91)

*Values in parentheses indicate the magnitude of the barrier relative to the lowest energy minimum of the pair connected by the transition structure.

A CDA analysis was done for selected minimum structures of complex **5** and the results are summarized in Tables 23 and 24.

Table 23. Charge components for selected MOs of **5**

Complex	MO	d	b	r
5a	29	0.214	0.038	-0.105
	32	0.101	-0.003	0.015
5e	32	0.080	0.007	-0.057
	38	0.192	0.017	-0.291
5g	31	0.143	0.026	-0.225
	39	0.103	0.027	-0.139
	40	0.109	0.003	-0.377
5i	31	0.151	0.008	-0.046
	31	0.114	0.016	-0.193

Comparison with the data obtained for the equivalent geometries of complex **2** shows that the trends for **2** and **5** are similar, down to the relative amounts donated by each phosphine for the nonsymmetrical geometries (this data is not presented). The only exception is **5i** where the total amount of donation from phosphine to Ni is very low.

Table 24. Total amounts of donation and back-donation for **5**

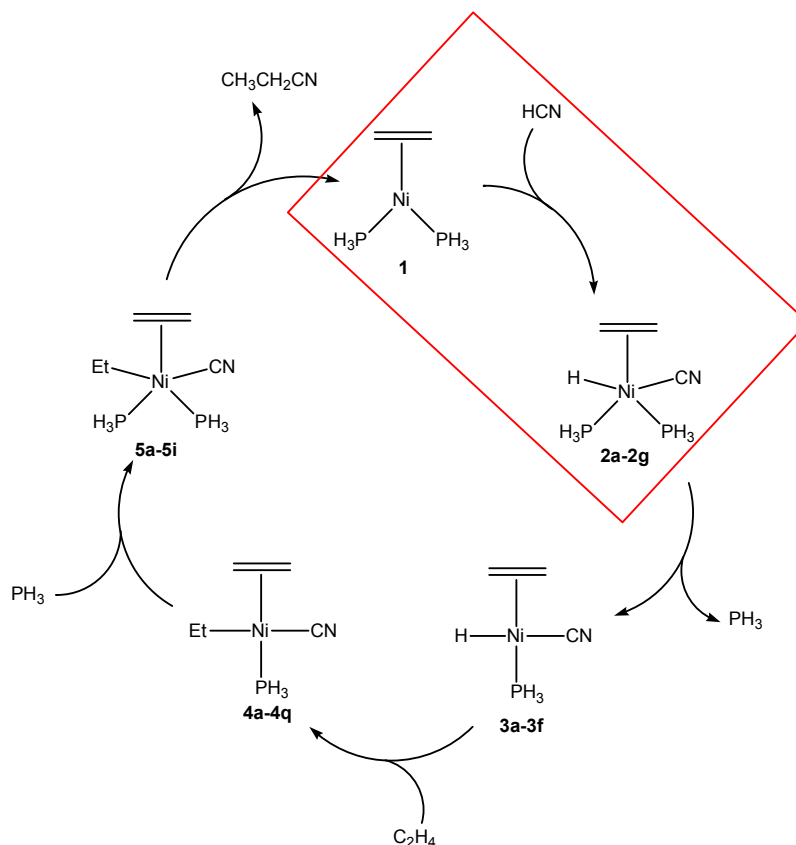
Complex	Donor	<i>b</i>	<i>d</i>	<i>r</i>
5a	Ethylene	0.459	0.092	-0.261
	Phosphine	0.977	0.268	-0.540
5e	Ethylene	0.470	0.183	-0.288
	Phosphine	0.707	0.139	-0.780
5g	Ethylene	0.446	0.112	-0.235
	Phosphine	0.618	0.192	-0.729
5i	Ethylene	0.432	0.111	-0.254
	Phosphine	0.363	0.161	-0.475

This is because there is no donation from P2 to Ni so, essentially, **5i** can be seen as a Van der Waals complex of **4h** and phosphine.

5. Intermolecular Transitions

(a) (Ethylene)Ni(PH₃)₂ (**1**) to (Ethylene)Ni(H)(CN)(PH₃)₂ (**2a-2g**)

Oxidative addition of hydrogen cyanide to complex **1** yields complex **2** (Scheme 11). Since there are at least seven different conformations of **2** that correspond to energy minima, there are at least seven potential transition structures for this reaction. Two transition structures were obtained (other attempts having failed), **TS(1-2e)** and **TS(1-2f)**, to **2e** and **2f**, respectively, shown in Figure 22. Note that in both **2e** and **2f** H and CN are *cis* relative to each other, as has also been observed in similar calculations (Thiel, 2005). The relative energies of these structures are summarized in Table 25. The energies are given as non-ZPE-corrected, with the ZPE-corrected energies in parentheses. Note that the Van der Waals complex of **1** and HCN is stabilized by 1.33 (0.86) kcal/mol relative to **1** and HCN at infinite separation. There is not a very big energy difference between the transition structures and the minima **2e** and **2f**. This is not unexpected, since the minimum conformations are similar to the transition structures. The ZPE-corrected energy, but not the uncorrected energy, of the transition structure is somewhat lower than that of the minimum conformation, therefore the uncorrected energies are also presented. The reason for this discrepancy is that the determination of ZPE-corrections only takes into account real components of the force constant, which means that a whole degree of freedom is lost for transition structures in which one component of the force constant has to be imaginary.



Scheme 11. The catalytic cycle, showing the position of the transition from **1** to **2**

Table 25. Relative energies for **1** to **2** and the van der Waals complex formed by **1** and HCN (**1**-HCN) relative to **1** + HCN; ZPE-corrected energies in parentheses

Complex	Energy [kcal/mol]	Complex	Energy [kcal/mol]
1 + HCN	0.00 (0.00)	TS(1-2f)	14.50 (13.16)
1 -HCN (van der Waals complex)	-1.33 (-0.86)	2e	13.31 (13.23)
TS(1-2e)	14.21 (12.93)	2f	14.01 (13.53)

Moreover, for more complicated molecules, the different vibrational modes are not independent, which means that neglect of one mode may influence one or more of the other modes as well. Thus ZPE-corrected energies for a transition structure may sometimes turn out to be lower than the ZPE-corrected energies of one (or both) of its associated minimum structures, as is the case here.

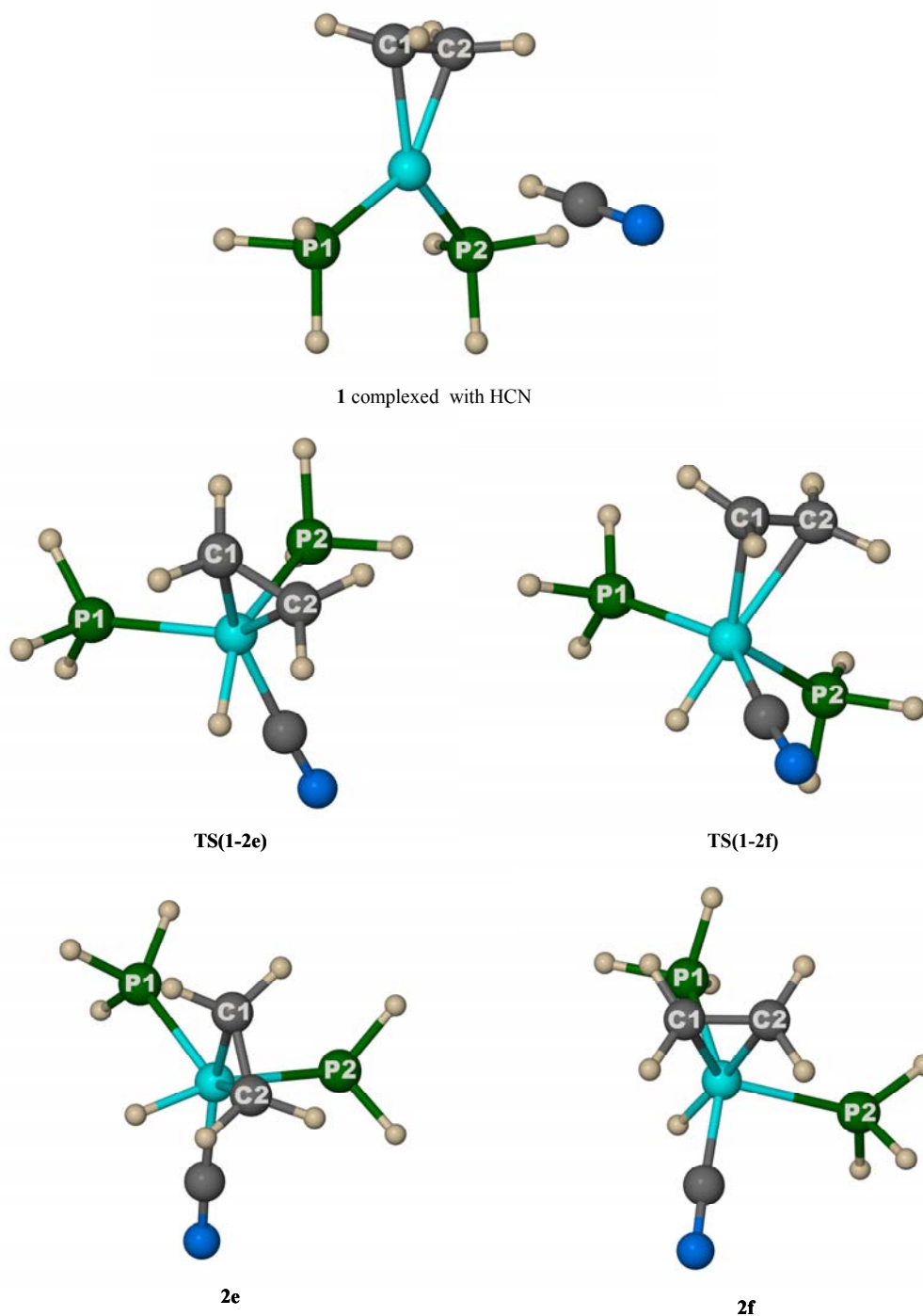


Figure 22. Transition of **1** to complexes **2e** and **2f**

This is a problem that has not received much attention in the literature, although some authors do suggest that the energy due to an imaginary translation ($RT/2$) could be added to the enthalpy of the transition structure to compensate for the lost degree of freedom (Dillen, 1995; Ermer, 1981).

The geometries were obtained by systematically scanning the H-CN distance in complexes **2e** and **2f**. Relaxing the structure obtained at the energy maximum of the scan yielded the transition structure. Relaxing the structure one or two steps before the maximum gave **2e** or **2f**, while relaxing the structure one or two steps beyond the maximum gave **1** complexed with HCN in both cases as shown in Figure 22. The H-CN distances are 2.071 Å and 2.032 Å for **2e** and **2f**, respectively. For the corresponding transition structures, the H-CN distances are 1.654 Å and 1.693 Å; and it is 1.082 Å in the **1**-HCN complex. The Ni-CN bond angles in **2e** and **2f** are 176.8° and 176.7° respectively, while those of the corresponding transition structures are 175.2° and 175.0°. Interestingly, the Ni-CN bond shortens somewhat to 1.871 Å in **TS(1-2e)** from 1.885 in **2e**. The corresponding change for **2f** is 1.867 Å for the minimum and 1.863 Å for the transition structure. The Ni-H bond, on the other hand, lengthens to 1.479 Å in **TS(1-2e)** from 1.459 in **2e**. The corresponding change for **2f** is 1.483 Å for the minimum and 1.493 Å for the transition structure. All these bond lengths together with selected bond angles are summarized in Table 26.

Table 26. Selected bond lengths (Å) and angles (°) for the transition of **1** to **2**

	1 -HCN	2e	TS(1-2e)	2f	TS(1-2f)
Ni-H	2.383	1.459	1.479	1.483	1.493
Ni-CN	3.457	1.885	1.871	1.867	1.863
H-CN	1.082	2.071	1.654	2.032	1.693
Ni-C-N	173.5	176.8	175.2	176.7	175.0
H-C-N	179.3	140.2	135.6	138.7	135.6

A CDA analysis was done for **TS(1-2e)**, **TS(1-2f)** and **1**-HCN; the results are presented in Tables 27 and 28. The total amounts of ethylene and phosphine donation to Ni is similar in both transition structures and in **2e** and **2f**, whereas the amount of donation from cyanide is somewhat less for the transition structures, as expected. (The total amounts of donation from CN are 0.728 and 0.703 for **2e** and **2f** respectively.) Curiously, though, this does not correlate with the observed changes in bond lengths, but the discrepancy is so slight that it is probably negligible. The orbitals with the largest components of donation (and back-donation) are shown in Table 27. The appearance of the orbitals for the transition structures is very similar to those of the corresponding energy minima.

Table 27. Charge components for selected orbitals of **TS(1-2e)**, **TS(1-2f)** and **1-HCN**

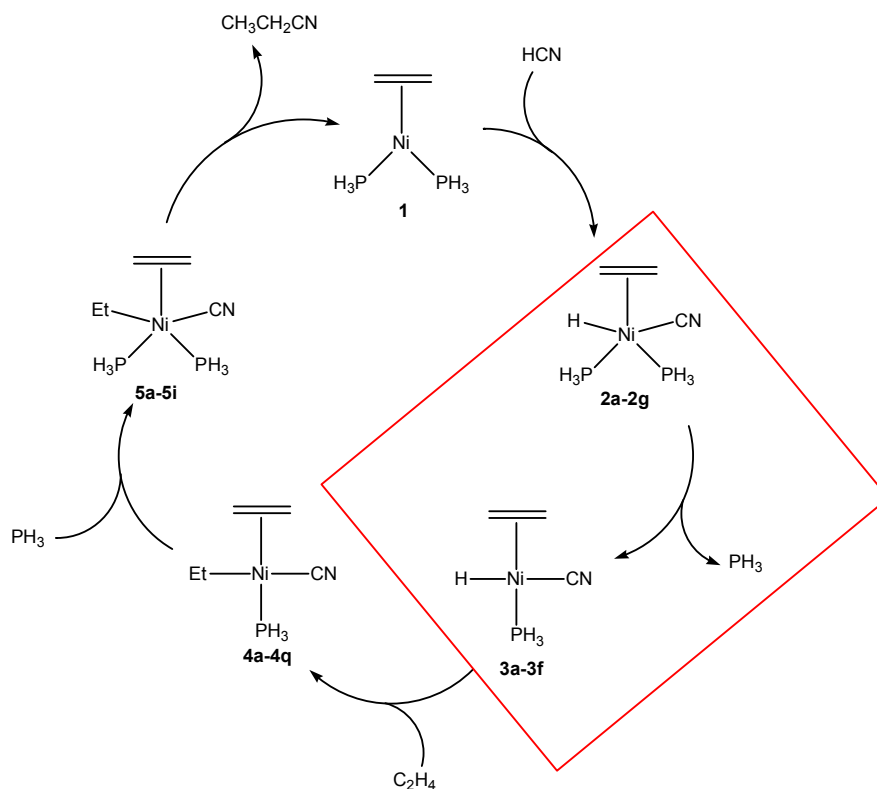
Complex	Donor	<i>d</i>	<i>b</i>	<i>r</i>
TS(1-2e)	Ethylene to Ni	0.104	0.008	-0.029
	Phosphine1 to Ni	0.114	0.016	-0.117
	Phosphine2 to Ni	0.181	-0.006	-0.360
	Cyanide to Ni	0.162	0.007	-0.228
TS(1-2f)	Ethylene to Ni	0.120	0.006	-0.052
	Phosphine1 to Ni	0.090	0.001	0.067
	Phosphine2 to Ni	0.093	0.004	-0.029
	Cyanide to Ni	0.116	0.005	-0.161
1-HCN	Ethylene to Ni	0.183	0.017	-0.176
	Ni to Ethylene	0.008	0.295	-0.127
	Phosphine to Ni	0.249	0.022	0.048
	Phosphine to Ni	0.239	0.003	0.169
	Ni to Phosphine	0.093	0.109	-0.160

Table 28. Total amounts of donation and back-donation for **TS(1-2e)**, **TS(1-2f)** and **1-HCN**

Complex	Donor	<i>d</i>	<i>b</i>	<i>r</i>
TS(1-2e)	Ethylene	0.462	0.155	-0.250
	Cyanide	0.680	0.060	-0.210
	Phosphine	0.808	0.164	-0.626
TS(1-2f)	Ethylene	0.454	0.137	-0.237
	Cyanide	0.672	0.062	-0.288
	Phosphine	0.790	0.177	-0.668
1-HCN	Ethylene	0.560	0.319	-0.266
	Phosphine	0.838	0.315	-0.331

(b) (Ethylene)Ni(H)(CN)(PH₃)₂ (2a-2g) to (Ethylene)Ni(H)(CN)PH₃ (3a-3f)

The dissociation of a ligand from complex **2** yields complex **3** (Scheme 12). Again, because there are at least seven energy minima for **2**, there are several possibilities for a transition structure between **2** and **3**. However, the search for a transition structure was limited to ligand dissociation from **2a**, **2e**, **2f** and **2g**. Complex **2a** was considered a starting point for this reaction because it is the lowest energy conformation for complex **2** and therefore most of the molecules would be in that conformation at equilibrium in the gas phase for non-interacting theoretical structures. However, since catalytic reactions do not necessarily take place at this equilibrium, other configurations of **2** were also considered as starting points for this transition.



Scheme 12. The catalytic cycle, showing the position of the transition of **2** to **3**

Complexes **2e** and **2f** were considered, because there is a transition from **1** directly to either **2e** or **2f**. Complex **2g** was considered too, because of its very similar geometry to **2f**, but no transition state for the dissociation of phosphine could be obtained.

A transition structure was obtained for ligand dissociation from **2a** to **3f**. No transition structures could be obtained for ligand dissociation from **2e**, **2f** or **2g**, but it was established that ligand dissociation from these three geometries lead to **3a**, **3d** and **3c**, respectively. The transition structure and van der Waals complex obtained for the ligand dissociation of **2a** is shown in Figure 23. Selected bond lengths and angles are presented in Table 29 and the energies relative to **2a** in Table 30. It is clear that, during transition, distortion of the trigonal bipyramidal **2a** to a square pyramidal geometry with phosphine at the apex takes place with the lengthening of the Ni-P bond.

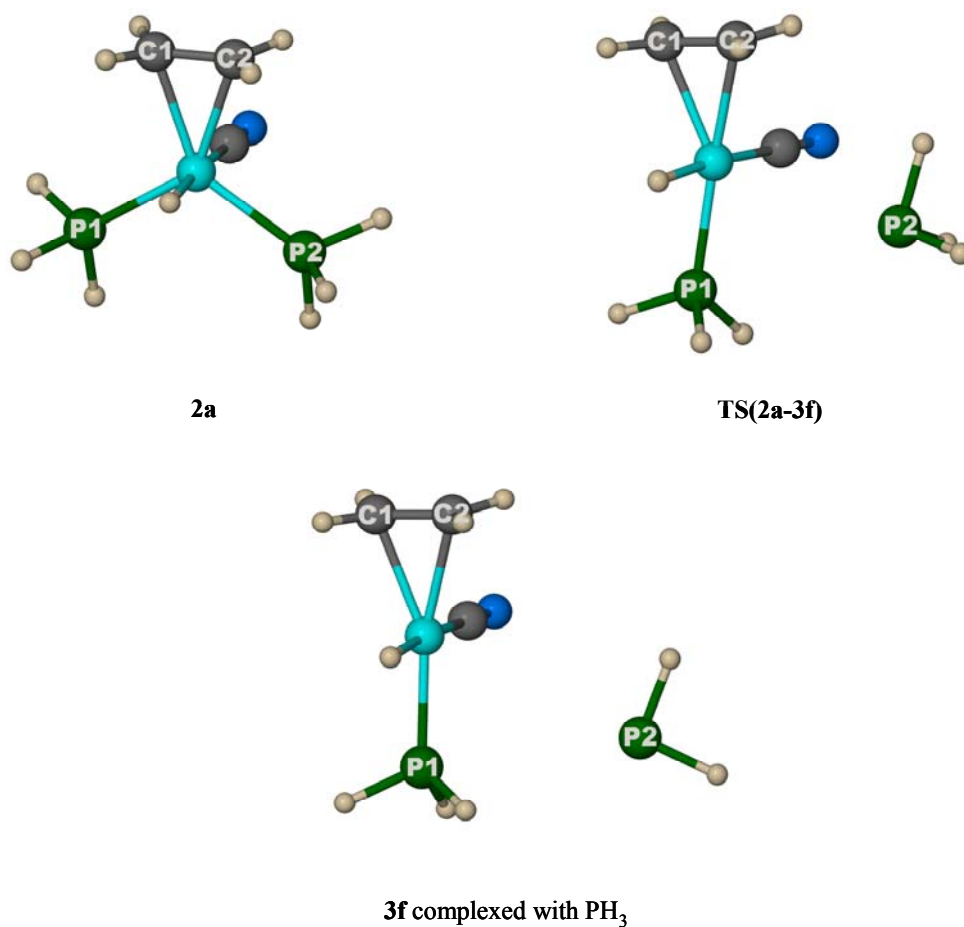


Figure 23. Minimum structures, transition structures and van der Waals complexes for ligand dissociation from **2a** and **2e**

Table 29. Selected bond lengths (Å) and angles (°) for ligand dissociation of **2a**

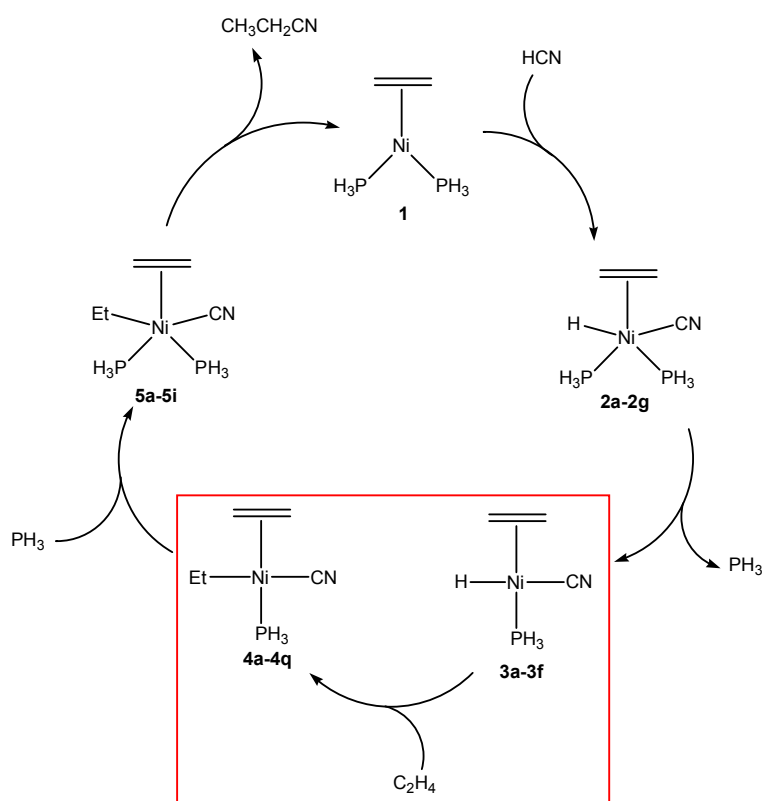
	TS(2a-3f)	3f-PH ₃
Ni-C1	2.175	2.182
Ni-C2	2.170	2.181
Ni-H	1.507	1.511
Ni-CN	1.920	1.915
Ni-P1	2.187	2.187
Ni-P2	3.390	4.160
C1-C2-Ni-H	-80.8	-89.7

Table 30. Energies for the ligand dissociation of **2a** relative to **2a**

Complex	Energy [kcal/mol]
2a	0.00
TS(2a-3f)	9.48
3f-PH₃	9.22
3f + PH₃	11.00

(c) (Ethylene)Ni(H)(CN)PH₃ (3a-3f) to (Ethylene)Ni(ethyl)(CN)PH₃ (4a-4q)

The association of a second molecule of ethylene with **3** (Scheme 13) can yield **4** in two ways.



Scheme 13. The catalytic cycle, showing the position of the transition from **3** to **4**

From the perspective of electron counting, it is most likely that the second molecule of ethylene will associate with the 16-electron complex **3** to give an 18-electron intermediate, followed by insertion of (either) ethylene into the Ni-H bond to give the 16-electron complex **4**. If migration of the coordinated ethylene takes place before association of the second ethylene molecule, a 14-electron intermediate will result, which seems unlikely (McKinney, 1986). However, from the structural point of view, migration before association (or at least a concerted mechanism) looks more plausible.

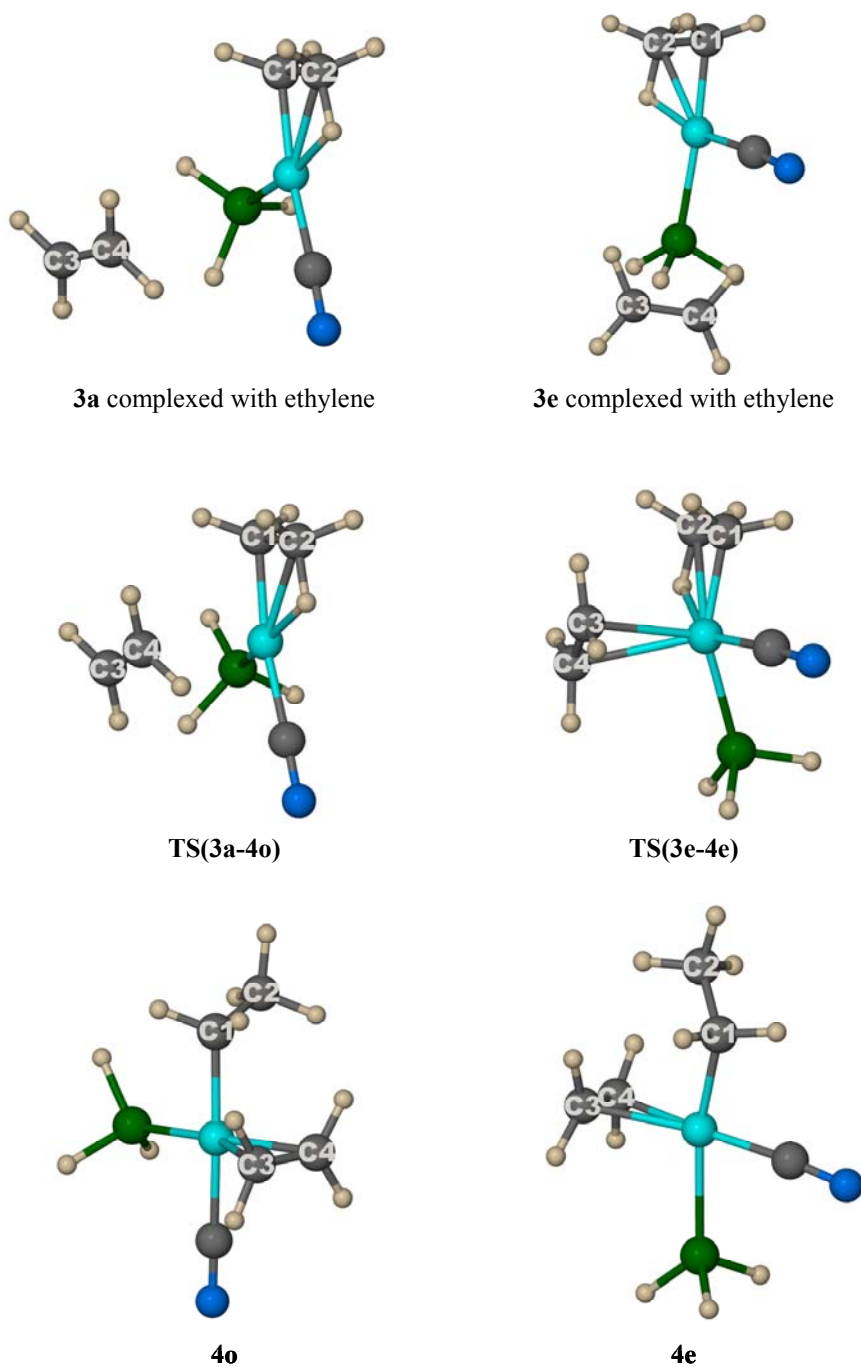
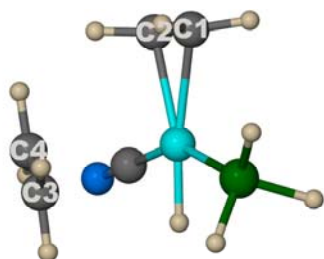


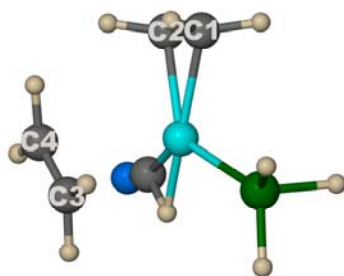
Figure 24. Transition structures for the association of ethylene to **3a** and **3e**

The interaction between Ni and H in **3a** and **3e** could be regarded as agostic with H bonded to C of ethylene when bond distances are considered in **3a** and **3e**. To test both hypotheses, potential energy surface scans were performed in which ethylene was allowed to approach **3a**, **3c** and **3e**. (The complexes with the C-C-axis of ethylene out of the plane were not considered because in each instance the out-of-plane

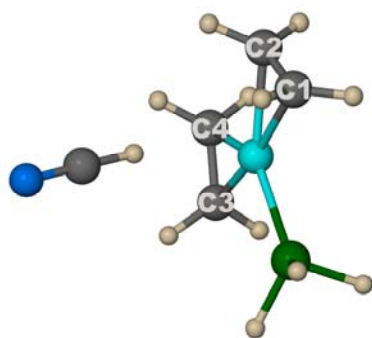
complex has higher energy than its in-plane counterpart and the transition can take place *via* a simple ethylene rotation, as described in Section 3(c).)



3c complexed with ethylene



TS(3c-6)



6

Figure 25. Transition structure of **3c** to **6**

The first mechanism is possible for all three of the selected isomers, whereas the second mechanism cannot occur for **3c** because the coordinated ethylene and hydrogen are not in the *cis* orientation. The results obtained point decisively to the

second mechanism – that of insertion before, or concurrent with, association. The transition states are shown in Figure 24. In the case of **3c**, association of the second ethylene molecule does take place, but with the simultaneous reductive elimination of hydrogen cyanide, to form **6** – bis(ethylene)-phosphine nickel – as shown in Figure 25.

Table 31. Comparative data for the transition of **3** to **4**, with bond lengths in Å and angles in °

	3a complexed with ethylene	TS(3a-4o)	4o
Ni-C1	1.914	1.913	1.970
Ni-C2	2.198	2.225	2.890
Ni-C3	4.454	3.101	2.190
Ni-C4	3.625	3.179	2.184
Ni-H	1.768	1.804	3.887
C2-H	1.167	1.160	1.100
C2-C1-Ni-CN	-0.5	-9.5	-50.0
C4-C3-Ni-CN	61.2	85.0	91.5
	3e complexed with ethylene	TS(3e-4e)	4e
Ni-C1	1.889	1.921	1.969
Ni-C2	2.190	2.371	2.980
Ni-C3	5.215	2.327	2.173
Ni-C4	5.055	2.482	2.179
Ni-H	1.761	2.008	3.940
C2-H	1.172	1.133	1.100
C2-C1-Ni-CN	-179.6	159.0	137.3
C4-C3-Ni-CN	-37.8	-142.7	-171.2

Comparative structural data for the transition of **3a** to **4o**, and of **3e** to **4e** is summarized in Table 31. Note that for **3a** and **3e**, Ni-C2 is longer than Ni-C1 and that the hydrogen atom is closer to C2 than to Ni – which already indicates a strong interaction between C2 and hydrogen. Structural data for the transition of **4c** to **6** is presented in Table 32. Note the shortening of the Ni-C (except Ni-CN) bonds throughout. A search on the Cambridge Crystallographic Database yielded a number of complexes with similar structure – one containing nickel (Nickel, 1994) and two containing platinum (Chetchuti, 1981; Howard, 1982). Most notable, however, is the structure from the group of Krüger (1972) – bis(ethylene)-tricyclohexylphosphine

nickel – which is shown in Figure 26. Selected parameters of bis(ethylene)-tricyclohexylphosphine nickel are summarized in Table 33 for comparison with **6**. It is evident from Table 33 that the Ni-C bond lengths in the crystal are much more variable than the calculated lengths, but that the calculated lengths are somewhat longer on average (Ni-C = 2.043 ± 0.001 Å for **6**; Ni-C = 2.013 ± 0.023 Å for the crystal structure). Correspondence of the other parameters is very good.

Table 32. Information for **3c** to **6**; and bis(ethylene)-tricyclo-hexylphosphine nickel, with bond lengths in Å and angles in °

	3c	TS(3c-6)	6	bis(ethylene)-tricyclo-hexylphosphine nickel
Ni-C1	2.190	2.068	2.043	2.016
Ni-C2	2.191	2.082	2.041	1.986
Ni-C3	4.175	2.837	2.044	2.009
Ni-C4	3.458	2.713	2.042	2.042
Ni-H	1.463	1.628	2.422	---
Ni-CN	1.857	1.938	3.481	---
H-CN	1.969	1.193	1.080	---
C2-C1-Ni-PH ₃	178.9	162.9	177.5	177.9
C4-C3-Ni-PH ₃	158.6	162.7	-177.4	-177.3

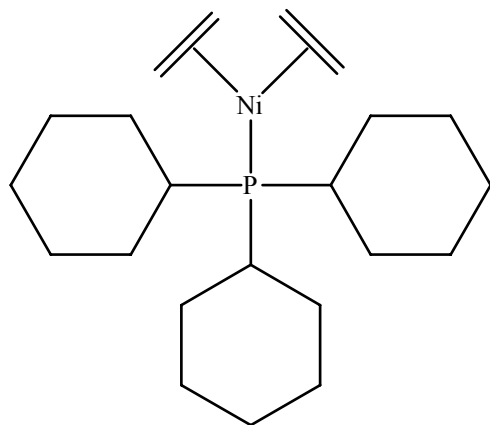


Figure 26. Structure of bis(ethylene)-tricyclo-hexylphosphine nickel (Krüger, 1972)

The energies relative to **4e** + HCN for the transitions between **3a** and **4o**, **3e** and **4e**, and **4c** and **6** are presented in Table 33. Note that the energy for **TS(3c-6)** is slightly lower than the energy of **3c**. However, the free energy of **3c** is about 2 kcal/mol lower than that of **TS(3c-6)**.

Table 33. Relative energies of **3** to **4** or **6** relative to **3e** + Ethylene

Complex	Energy [kcal/mol]	Complex	Energy [kcal/mol]
3a + Eth	1.29	TS(3a-4o)	0.83
3c + Eth	14.44	TS(3c-6)	13.48
3e + Eth	0.00	TS(3e-4e)	1.68
3a -Eth	0.64	4o	-4.37
3c -Eth	13.81	4e	-4.69
3e -Eth	-2.63	6	---

The orbitals for donation from ethylene and back-donation to ethylene for complex **6** are shown in Figure 27. A symmetric electron density was expected, based on the almost equal bond lengths obtained in the geometry optimization. However, Figure 27 shows that this is clearly not the case, especially with respect to the back-donation from Ni to ethylene.

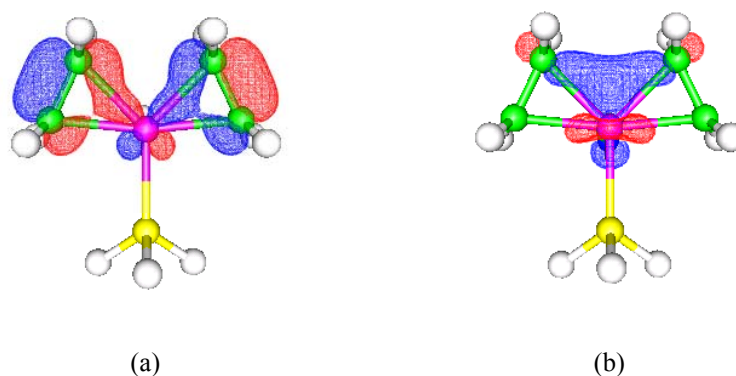
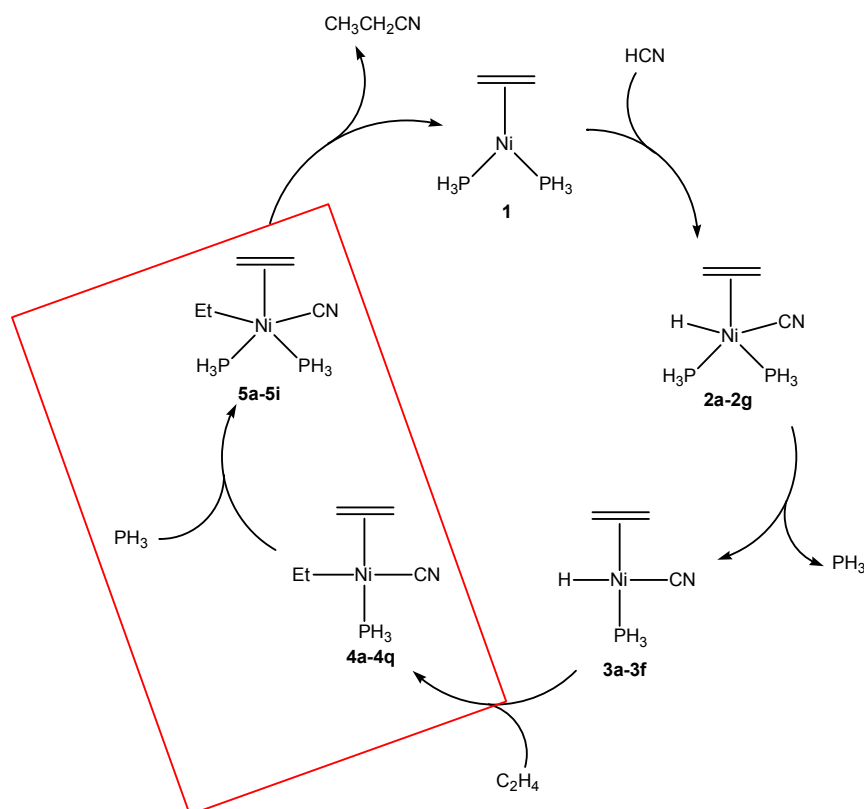


Figure 27. MOs for **6** denoting (a) donation from ethylene to Ni (b) back-donation from Ni to ethylene.

(d) (Ethylene)Ni(ethyl)(CN)PH₃ (4a-4q) to (Ethylene)Ni(ethyl)(CN)(PH₃)₂ (5a-5i)

Association of a ligand with the 16-electron complex **4** yields the 18-electron complex **5** (Scheme 13). There are quite a few possible transition structures for the reaction, but despite a number of attempts, only one transition structure could be found – that of the association of phosphine with **4o** to give **5a**.



Scheme 13. The catalytic cycle showing the position of the transition of **4** to **5**

The transition structure was obtained by doing a potential energy surface scan for the lengthening of the Ni-P bond. Optimization of the maximum energy structure and the two minima yielded **TS(4o-5a)**, **5a** and the **4o-PH₃** van der Waals complex. The relevant structures are shown in Figure 28 and selected parameters summarized in Table 34. It is interesting that transition structures for ligand association/dissociation could only be obtained for **5a** and **2a**, the only configurations of **5** and **2** (with the exception of their higher energy conformers) to have their two phosphine ligands in equivalent positions. The initial expectation was that this is the case because these are the only configurations where PH₃ can become apical in a square pyramidal geometry without substantial rearrangement of the original complex, but visual inspection of the other configurations of both **5** and **2** shows that this is not the case. Perhaps it is due to energetic factors. Only further investigation will tell.

The energies relative to **5a** (0.00 kcal/mol) are: 5.91 kcal/mol for **4o-PH₃** and 6.89 kcal/mol for **TS(4o-5a)**. For **4o** and PH₃ at infinite separation, the energy is 6.80 kcal/mol.

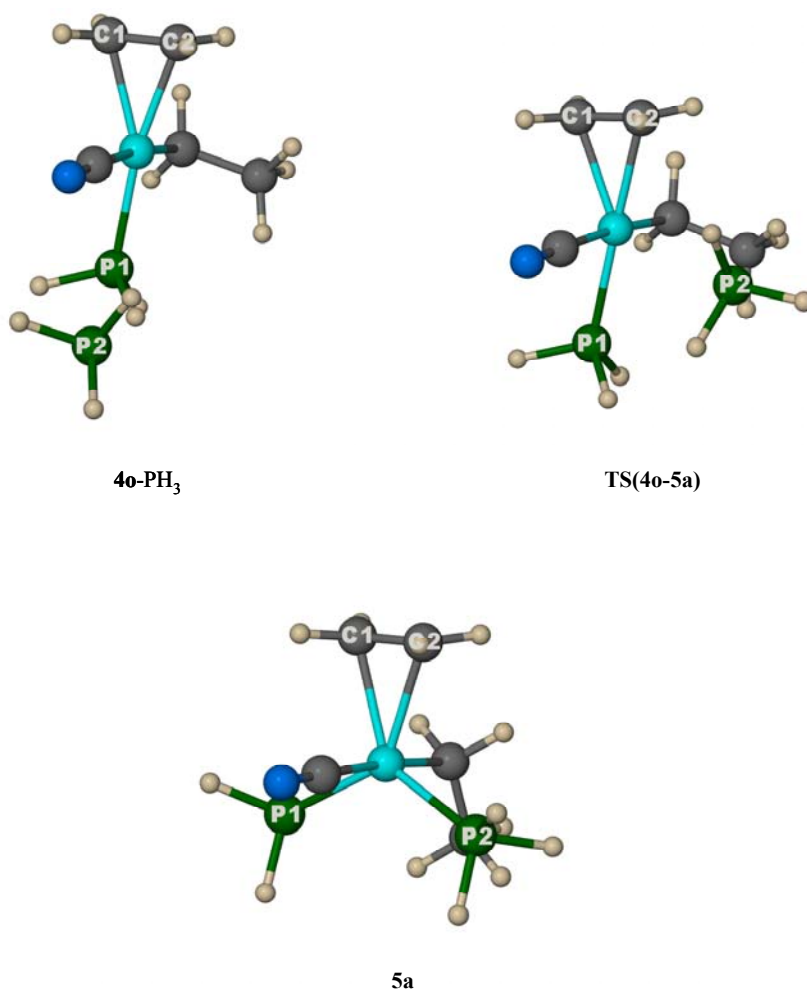


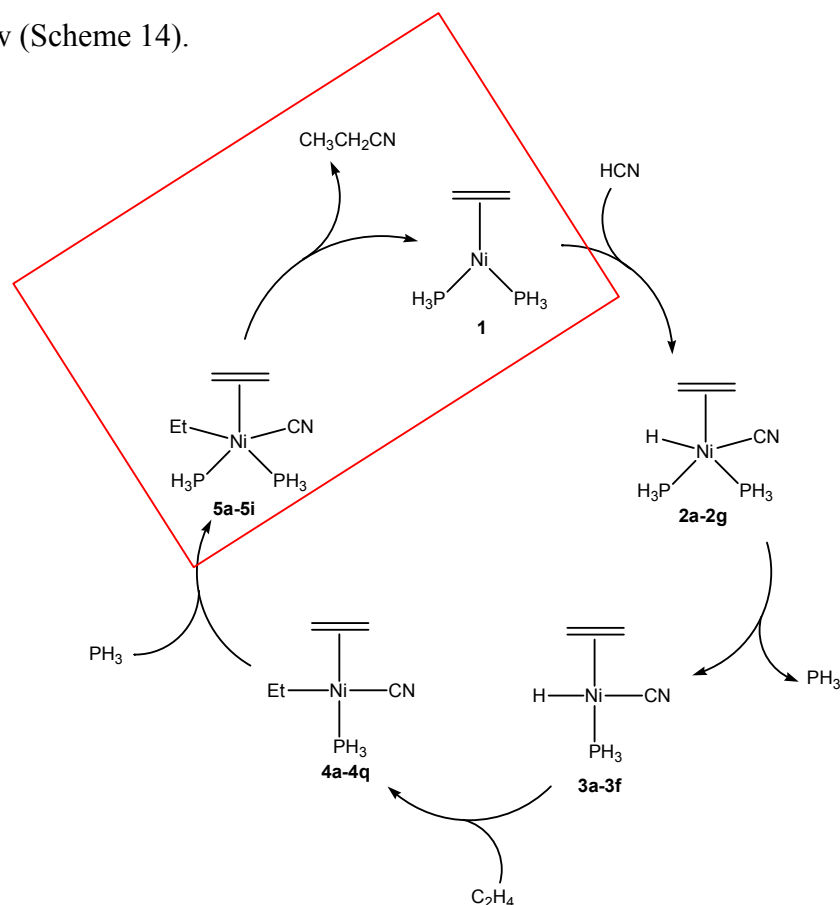
Figure 28. Transition from **4o** to **5a**

Table 34. Selected bond lengths (Å) and angles (°) for **4o-PH₃** and **TS(4o-5a)**

	4o-PH₃	TS(4o-5a)
Ni-C1	2.190	2.178
Ni-C2	2.184	2.173
Ni-P1	2.219	2.222
Ni-P2	5.367	3.530
Ni-CN	1.945	1.952
Ni-Et	1.970	1.973
C1-C2-Ni-P2	-114.9	-159.3

(e) (Ethylene)Ni(ethyl)(CN)(PH₃)₂ (**5a-5i**) to (Ethyl)Ni(PH₃)₂ (**1**)

Reductive elimination of ethyl cyanide from **5** gives complex **1**, to start the cycle anew (Scheme 14).



Scheme 13. The catalytic cycle showing the position of the transition of **5** to **1**

Elimination can take place either from **5d** or **5g**, which corresponds with the view that intramolecular reductive eliminations can only take place if the eliminating groups are *cis* to each other (McKinney, 1986). The transition structures are shown in Figure 29 and selected bond lengths in Table 34.

Table 34. Selected bond lengths (Å) for the transition of **5** to **1**

	5d	TS(5d-1)	1-EtCN	TS(5g-1)	5g
Ni-C3	1.996	2.193	3.789	2.192	2.016
Ni-CN	1.894	1.852	3.867	1.842	1.882
C3-CN	2.642	1.922	1.467	1.956	2.638

Note the increase in the Ni-C3 bond lengths and the decrease in the Ni-CN bond lengths from the minimum to the transition structures in both cases – the opposite to what happens in the transition from **1** to **2**.

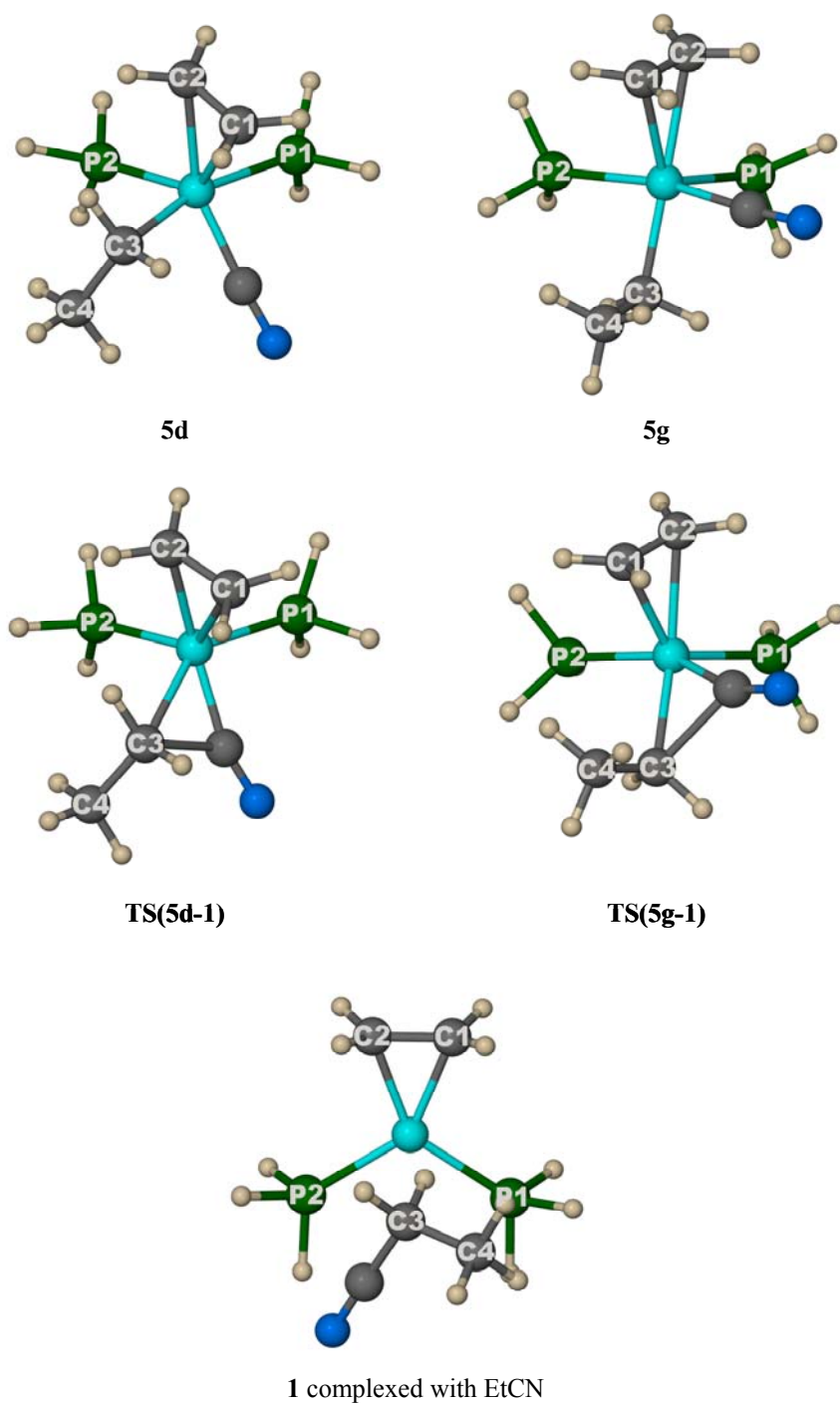


Figure 29. Transition states for **5** to **1**

The energies relative to **1** + EtCN of the transition states and minima are summarized in Table 35. Note that the van der Waals complex of **1** with ethylene cyanide has a slightly higher energy (0.68 kcal/mol) than the sum of the energies of **1** and ethylene cyanide.

Table 35. Energies for **5** to **1** relative to the added energies of **1** and ethylene cyanide

Complex	Energy [kcal/mol]	Complex	Energy [kcal/mol]
5d	28.27	TS(5g-1)	41.24
5g	30.61	1-EtCN	0.68
TS(5d-1)	39.63	1 + EtCN	0.00

A CDA analysis was done and the data is summarized in Tables 36 and 37.

Table 36. Charge components for selected MOs of **TS(5d-1)**, **TS(5g-1)** and **1-EtCN**

Complex	MOs	<i>d</i>	<i>b</i>	<i>r</i>
TS(5d-1)	Phosphine1 to Ni	0.128	0.021	-0.066
	Phosphine2 to Ni	0.159	-0.007	-0.318
TS(5g-1)	Ethylene to Ni	0.078	0.002	-0.011
	Phosphine1 to Ni	0.137	0.014	0.322
	Phosphine2 to Ni	0.145	0.008	-0.227
1-EtCN	Ethylene to Ni	0.187	0.016	-0.189
	Ni to Ethylene	0.011	0.305	-0.122
	Phosphine to Ni	0.243	0.007	0.156
	Phosphine to Ni	0.228	0.022	0.029

Table 37. Total amounts of donation and back-donation for **TS(5d-1)**, **TS(5g-1)** and **1-EtCN**

Complex	Donor	<i>d</i>	<i>b</i>	<i>r</i>
TS(5d-1)	Ethylene	0.471	0.168	-0.255
	Phosphine	0.843	0.210	-0.682
TS(5g-1)	Ethylene	0.428	0.152	-0.259
	Phosphine	0.762	0.197	-0.724
1-EtCN	Ethylene	0.558	0.337	-0.271
	Phosphine	0.807	0.337	-0.371

The total amounts of donation for the transition structures are similar to those of their derived minimum structures (**TS(5d-1)** was compared to **5e** since their structures are similar except for the orientation of ethyl). Donation from ethylene to Ni could not be localized to a specific orbital for this structure.

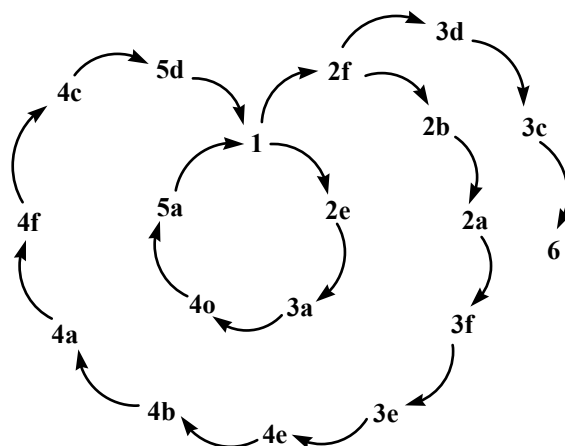
6. The Full Cycle

This section deals with the full catalytic cycle, and specifically the energetics of the cycle. In the first subsection the possible pathways that were obtained are discussed.

A comparison of the effects of progressive corrections to the electronic energies of the species is discussed next, followed by a brief description of the impact of different methods of calculating relative energies when dealing with intermolecular transitions (as discussed in Section 3).

(a) Possible pathways

The possible ways in which the catalytic cycle can proceed are shown in Scheme 14.



Scheme 14. Possible pathways for the catalytic cycle

In this work, two pathways were identified and characterized – an inner and an outer pathway – as well as an unproductive pathway leading *via* **2f**, **3d** and **3c** to **6**. The biggest difference between the two pathways is that the inner pathway is a more direct route to close the loop. The outer pathway is subject to more than one intramolecular rotation at two of the five steps in order to orient the molecule correctly for the next step. Of course, all these structures probably represent reactive and unstable species that cannot be isolated and characterized experimentally. These calculations give an idea of their relative stabilities.

(b) The effect of ZPE, thermal vibrational energy, rotation and translation, and entropy

The energy obtained by solving the Schrödinger equation is the electronic energy of a species. Zero-point vibrational energy corrections may be added to this. To obtain the enthalpy, further corrections for thermal vibrational energy as well as for rotational and translational energies has to be made. Finally, the entropy term may be added to obtain the free energy (G) for that species. All these quantities are after from the frequency calculation of a molecule optimized at the same level of theory and basis set

(Ochterski, 2000). This has been done for both the inner and the outer pathways and the results are graphically presented in Figures 30 and 32, as well as in Tables 38 and 39.

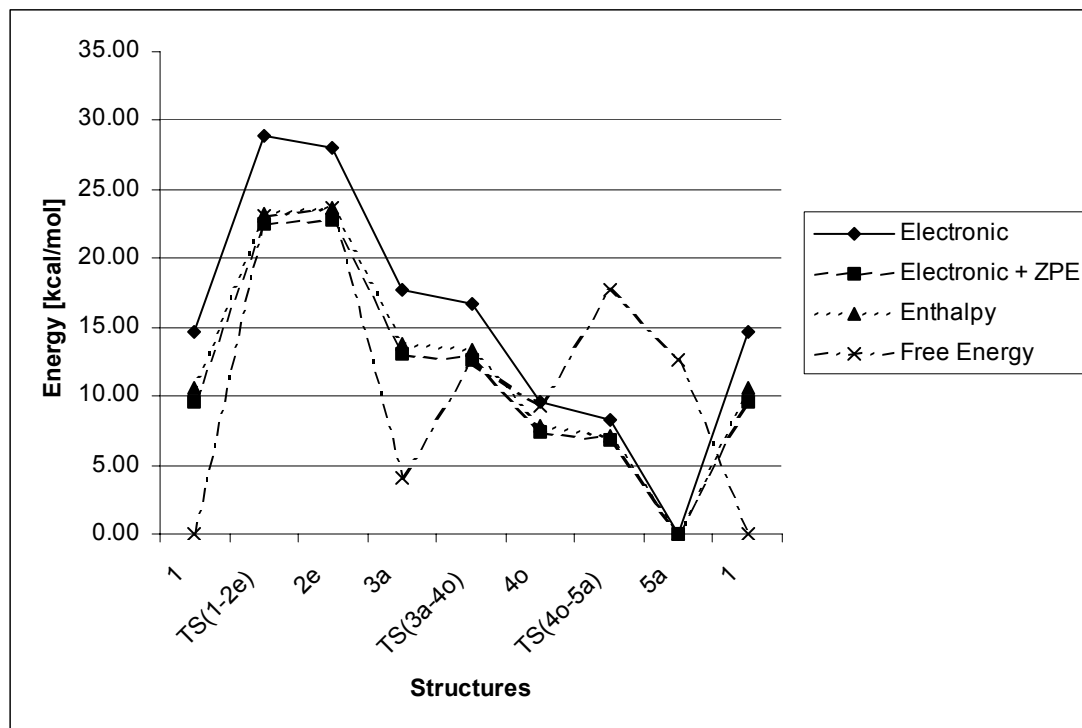


Figure 30. Energy profile for the inner pathway. The energy of the structure denoted as **1** on the horizontal axis of the graph is the sum of the energies of complex **1**, HCN and ethylene. For **2e**, it is the sum of the energies of complex **2e** and ethylene, and so forth.

Table 38. Relative energies of geometries participating in the inner pathway in kcal/mol

	Electronic Energy ^a	Electronic + ZP Energy ^b	Enthalpy ^c	Free Energy ^d
1 ^e	14.64	9.63	10.60	0.00
TS(1-2e)	28.85	22.54	23.27	23.10
2e	27.96	22.86	23.62	23.67
3a ^f	17.77	13.09	13.74	4.01
TS(3a-4o)	16.65	12.64	13.34	12.52
4o	9.56	7.47	7.84	9.30
TS(4o-5a)	8.24	6.84	7.15	17.74
5a	0.00	0.00	0.00	12.68

^{a, b, c} Energies relative to **5a**; ^d Energies relative to **1**; ^e See caption of Figure 30; ^f No transition structures from either **2e** to **3a**, or from **5a** to **1** have been found, see text for details

Turning first to Figure 30 (also refer to Table 38), the solid line represents the electronic energy changes only. The highest point on the cycle is at **TS(1-2e)**, with a relative (to **5a**) energy of 28.85 kcal/mol. The electronic energy barrier to **TS(1-2e)** from **1**, *i.e.* the barrier for the oxidative addition of HCN to **1**, is 14.21 kcal/mol. After oxidative addition, the energy decreases by 10.19 kcal/mol to **3a** (no transition structure for the dissociation of PH₃ from **2e** to form **3a** could be found). The electronic energy of the transition structure connecting **3a** and **4o** is lower than that of **3a** by 1.12 kcal/mol and higher than that of **4o** by 7.09 kcal/mol. Association of PH₃ to **4o** leads to the structure of the cycle with the lowest electronic energy. Again, the electronic energy of the transition structure is intermediate between those of **4o** and **5a**, being 1.32 kcal/mol lower than the former and 8.24 kcal/mol higher than the latter. No direct transition from **5a** to **1** or to any other configuration of **5** leading to **1** could be obtained, thus the energy barrier for reductive elimination in the inner pathway is not known. The dashed line in Figure 30 represents the sum of the electronic energies and the corresponding ZPE corrections. The trend is the same as for the electronic energy, except that the energy of **TS(1-2e)** is now somewhat lower than that of **2e**. This problem has been addressed in Section 5(a). The curve representing the enthalpy closely follows that of the ZPE-corrected-only energy, as expected. The free energy curve, however, differs quite substantially from the other three. (At this point, it should be noted that the symmetry of the molecules involved – specifically the highest-valued rotation axis – plays a role in the magnitude of the entropy. Since no symmetry constraints were used in the optimization of these geometries, the entropy values are somewhat overestimated. The highest axis of rotation for any of these geometries is two-fold, so the degree of over estimation will be a factor of $RT \ln 2$, which is small enough not to affect the general conclusions.) The lowest point on the curve is now encountered at **1**. The free energy increases by 23.10 kcal/mol to **TS(1-2e)** and then by an additional 0.57 kcal/mol to reach **2e**. This discrepancy is mostly due to the ZPE correction, as discussed earlier. The free energy of **2e** is 19.66 kcal/mol higher than that of **3a**, the next minimum structure in the cycle. This large decrease in free energy is due to the entropy effects accompanying the dissociation of PH₃ from **2e**. The free energy of **3a** is 5.29 kcal/mol lower than that of **4o**, with a barrier of 8.51 kcal/mol for the association of a second molecule of ethylene to **3a**. Due to the association of PH₃ to **4o**, the free energy of **5a** is 3.38 kcal/mol higher than that of **4o**. The barrier has a

height of 8.44 kcal/mol. Finally, the free energy decreases with the elimination of propionitrile, so that the free energy of **1** is 12.68 kcal/mol lower than that of **5a**. Unfortunately, as mentioned before, the barrier height between **5a** and **1** could not be calculated. The highest free energy barrier encountered for the inner pathway is therefore between **1** and **2**, or for the oxidative addition of HCN to **1**. However, since all the energy barriers could not be found, most notably the barrier for the reductive elimination of ethyl cyanide from **5a**, or more likely some other configuration of **5** that could follow from **5a** (elimination directly from **5a** is unlikely since the ethyl and cyanide groups are not in a *cis* configuration to one another), this conclusion cannot be seen as final. However, it is evident that the effects of entropy play a large role in the free energy profile of this reaction. This should give a better indication of occurring changes that determine the kinetics of the reaction than a simple electronic point of view. The entropy variation is graphically displayed in Figure 31.

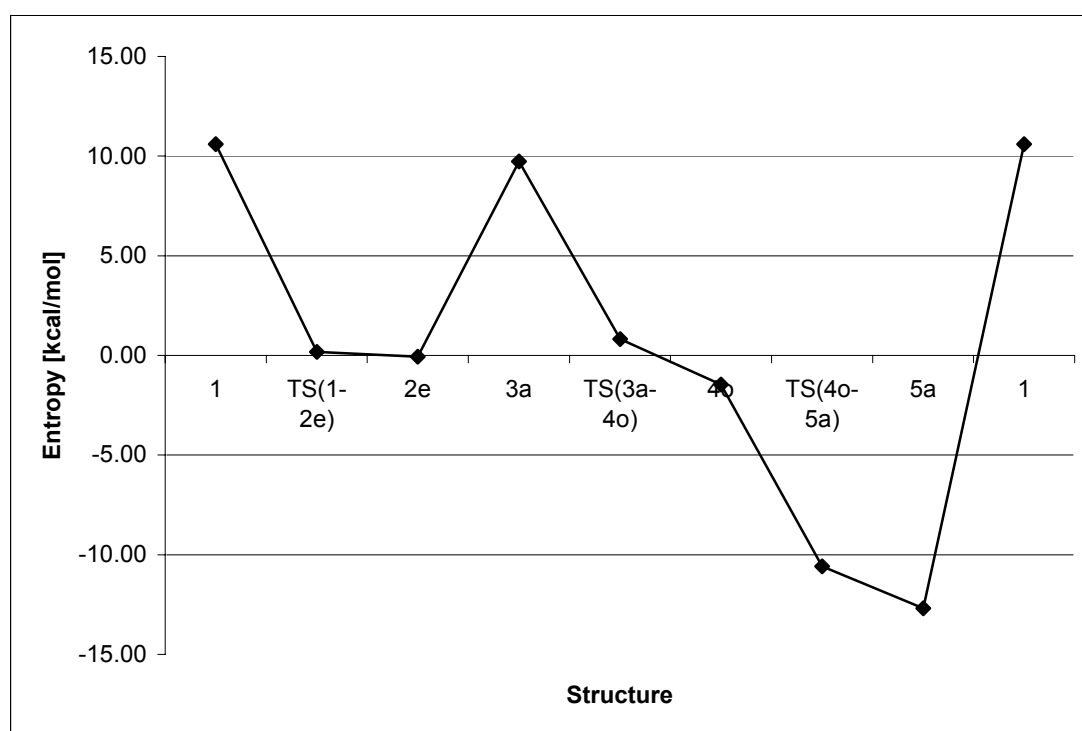


Figure 31. Entropy changes for the inner pathway in kcal/mol

The entropy decreases upon oxidative addition of HCN to **1**, as expected. The dissociation of a ligand from **2e** to form **3a** causes an increase in entropy, with the subsequent association of ethylene causing a decline. The entropy decreases even further when association of phosphine yields **5a**, followed by an increase as reductive elimi-

nation of propionitrile leads back to **1**. This variation is in line with expectation for ΔS^\ddagger -variation without complications such as electrostriction.

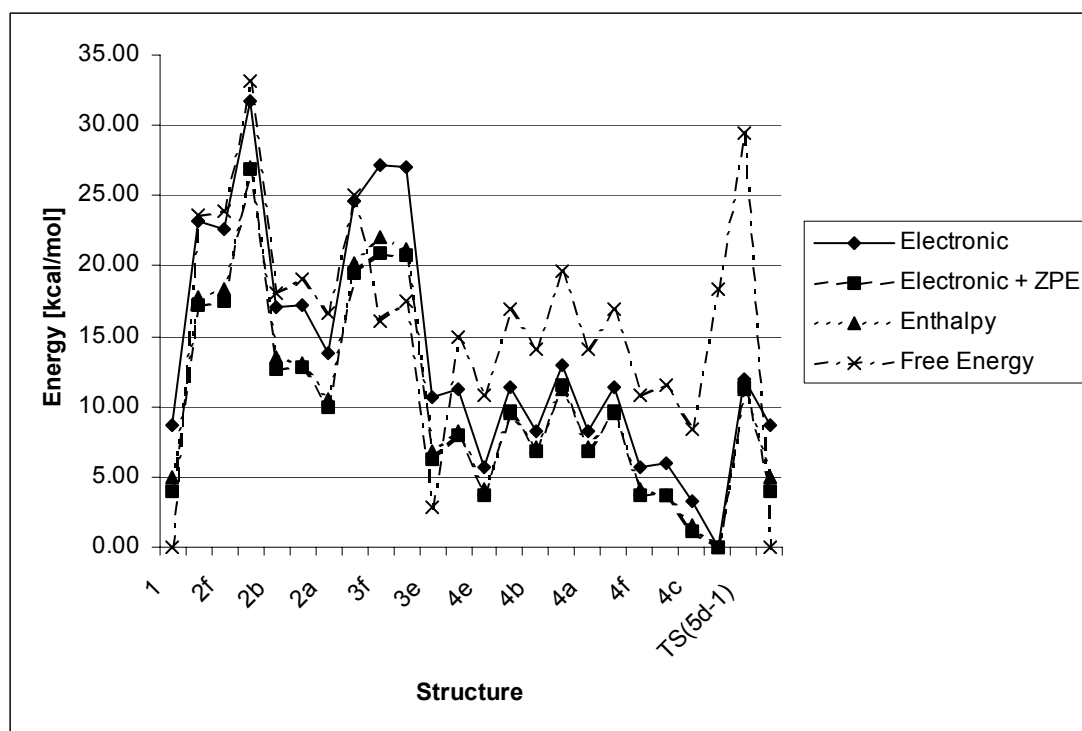


Figure 32. Energy profile for the outer pathway. The energy of the structure denoted as **1** on the x-axis of the graph is the sum of the energies of complex **1**, HCN and ethylene. For **2f**, it is the sum of the energies of complex **2f** and ethylene, and so forth.

Turning now to the outer pathway, (Figure 32; also refer to Table 39), the electronic energy barrier for the oxidative addition is 14.50 kcal/mol – very much comparable with the 14.21 kcal/mol obtained for the inner pathway. However, the intramolecular rearrangement of **2f** to form **2b** has an electronic energy barrier of 9.09 kcal/mol, placing **TS(2f-2b)** the highest point on the electronic energy curve. The energy descends to **2a** via **2b** and then increases again by 13.37 kcal/mol to **3f**. There is no electronic energy barrier for the dissociation of the ligand. Complex **3f** rearranges to **3e** (at 16.61 kcal/mol lower than **3f**) via rotation of ethylene. Although the electronic energy of **TS(3f-3e)** is 0.24 kcal/mol lower than that of **3f** (a situation worsened by the addition of the vibrational corrections), the entropy compensates for the discrepancy, as discussed below. Association of ethylene to **3e** yields **4e** at 4.88 kcal/mol lower in electronic energy. Various intramolecular rearrangements lead to **4c** and subsequent association of PH_3 lowers the electronic energy by 3.30 kcal/mol to give **5d** at the

lowest point of the cycle. The transition structure connecting **4c** and **5d** could not be obtained. Reductive elimination of propionitrile with a barrier of 12.00 kcal/mol closes the cycle.

Table 39. Relative energies of geometries participating in the outer pathway in kcal/mol

	Electronic Energy ^a	Electronic + ZP Energy ^b	Enthalpy ^c	Free Energy ^d
1^e	8.66	4.04	4.94	0.0
TS(1-2f)	23.16	17.18	17.84	23.62
2f	22.67	17.56	18.39	23.92
TS(2f-2b)	31.76	26.96	27.10	33.12
2b	17.11	12.72	13.55	18.02
TS(2b-2a)	17.25	12.79	13.10	19.04
2a	13.86	10.00	10.47	16.63
TS(2a-3f)	24.67	19.45	20.17	25.01
3f	27.23	20.95	21.99	16.15
TS(3f-3e)	26.99	20.75	21.15	17.52
3e	10.62	6.20	6.82	2.81
TS(3e-4e)	11.18	7.90	8.25	14.88
4e	5.74	3.65	4.08	10.84
TS(4e-4b)	11.40	9.61	9.50	16.98
4b	8.21	6.82	7.09	14.10
TS(4b-4a)	12.99	11.53	11.25	19.69
4a	8.21	6.82	7.09	14.09
TS(4a-4f)	11.40	9.61	9.50	16.98
4f	5.74	3.65	4.07	10.83
TS(4f-4c)	5.95	3.72	3.73	11.51
4c^f	3.30	1.16	1.61	8.33
5d	0.00	0.00	0.00	18.34
TS(5d-1)	12.00	11.35	11.20	29.42

^{a, b, c} Energies relative to **5a**; ^d Energies relative to **1**; ^e See caption of Figure 32; ^f No transition structure from **4c** to **5d** has been found, see text for details

The curve for the sum of the electronic energy and the ZPE correction as well as that for the enthalpy follow the same trend as the electronic energy curve, with the only exception being that the relative energy of **TS(1-2f)** is now slightly lower than that of **2f** for the same reason as discussed for the inner pathway. As for the inner pathway, the free energy curve is quite different from the other three, indicating that entropy effects are important. See also Figure 33 for a graphical representation of the entropy

changes. The most important differences are the following: the free energy of **3f** is now lower than that of **TS(3f-3e)**. The association of ethylene to **3f** is accompanied by an entropy decrease, so that the free energy curve from **4e** to **4c** lie higher than the other three curves. This corresponds exactly to what happens according to the inner pathway, although the effect is not as dramatic.

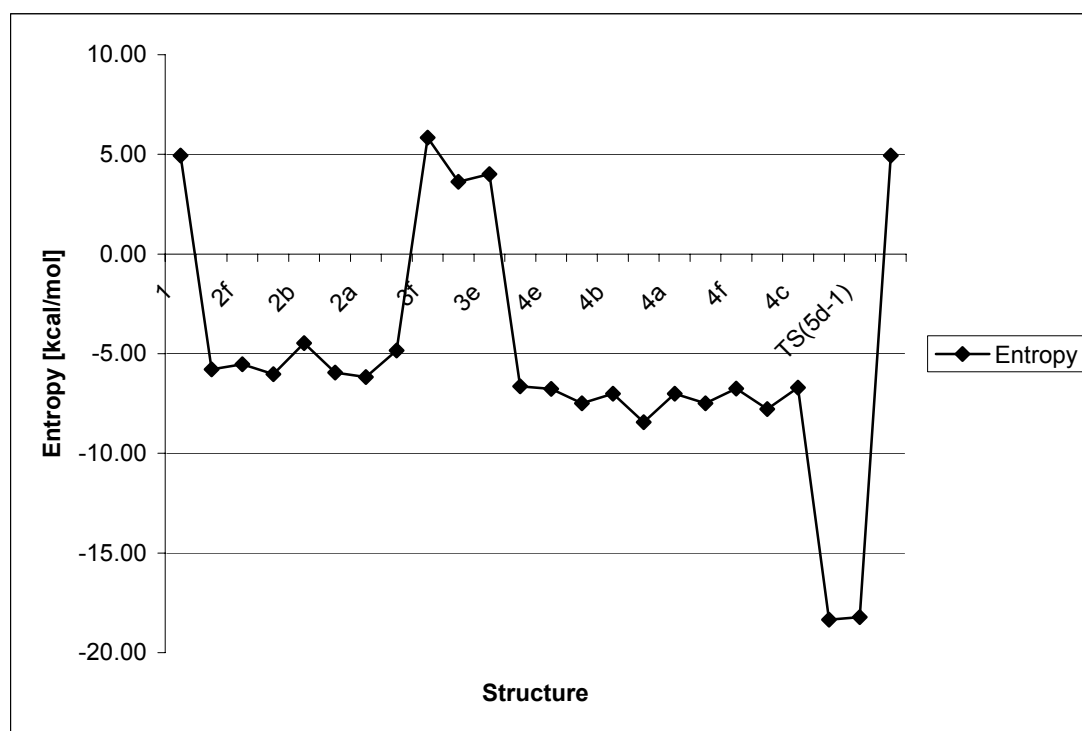


Figure 33. Entropy changes for the outer pathway in kcal/mol

The entropy decreases even more with the association of phosphine to give **5d**, but, as expected, increases again with the reductive elimination of propionitrile. The free energy barrier to this last step is 11.08 kcal/mol. This is somewhat lower than the 14.50 kcal/mol free energy barrier for the oxidative addition of HCN, implying that the oxidative addition of HCN is the rate-determining step in the gas phase. This result is contrary to the experimental claims (Tolman, 1985; McKinney, 1986), and suggests that solvent effects may play an important, but yet unaccounted for role in the mechanism of this reaction. To the best knowledge of the author, only one study has considered the effects of solvents on this process (Taylor and Swift, 1972). According to the authors, the solvent significantly influences both the reaction rate and the linear/branched selectivity. Higher linear/branched ratios are obtained with relatively nonpolar solvents, such as *p*-cresol, than with solvents of higher polarity, such as ace-

tonitrile. The linear/branched ratio is probably inversely proportional to the dielectric constant of the solvent, because the selectivity of *p*-cresol decreases with time, as the formation of nitriles increases the overall dielectric constant of the reaction medium. It is also likely that – especially in a polar solvent – the oxidative addition of HCN takes place stepwise, with addition of H⁺ followed by addition of CN⁻. This possibility is given credibility by the fact that HNi[P(O-*p*-tolyl)₃]₃⁺ has been observed spectroscopically at a low temperature (Eaton, 1984).

The reaction rate is higher in phenolic solvents than in other solvents such as acetonitrile, but the applicable mechanism is not understood. Further work is needed in this area, both experimentally and computationally.

(c) The favored pathway

The question now is whether the two model pathways are equally likely to occur, or whether one will be favored. This can be determined by regarding the velocity of the cycle that is given by

$$v \approx A' \exp[-(E_{aj} + E_j) / RT] = A' \exp(-\delta E / RT)$$

where E_j is the energy of the species with the lowest energy and E_{aj} is the energy of the species with the highest energy (a transition structure) and the quantity

$$\delta E = E_{aj} + E_j$$

is known as the energetic span (Shaik, 2005). Generally, reducing the energetic span of a catalytic cycle increases the turnover number, making for more effective catalysis. The energetic spans for the two pathways are summarized in Table 40. The negligence of the energies for the intermolecular transition structures do not have an impact on the energetic span of either pathway.

Table 40. Energetic spans (kcal/mol) for both pathways

	Electronic	Electronic + ZPE	Enthalpy	Free Energy
Inner	28.85	22.86	23.62	23.67
Outer	31.76	26.96	27.10	33.12

For the inner pathway, the energy maximum occurs at **TS(1-2e)** for the electronic energy and at **2e** in the other three cases. The outer pathway has its maximum at **TS(2b-2f)** for all four energy approximations. The outer pathway has a higher energetic span in all cases, but of course, it is only the free energy that is decisive. Here, the differ-

ence in energetic span between the inner and the outer pathways is 9.45 kcal/mol. This means that the inner pathway is likely to be favored over the outer pathway.

(d) The unproductive pathway

The energy profile for the unproductive pathway illustrated in Scheme 14 is shown in Figure 34.

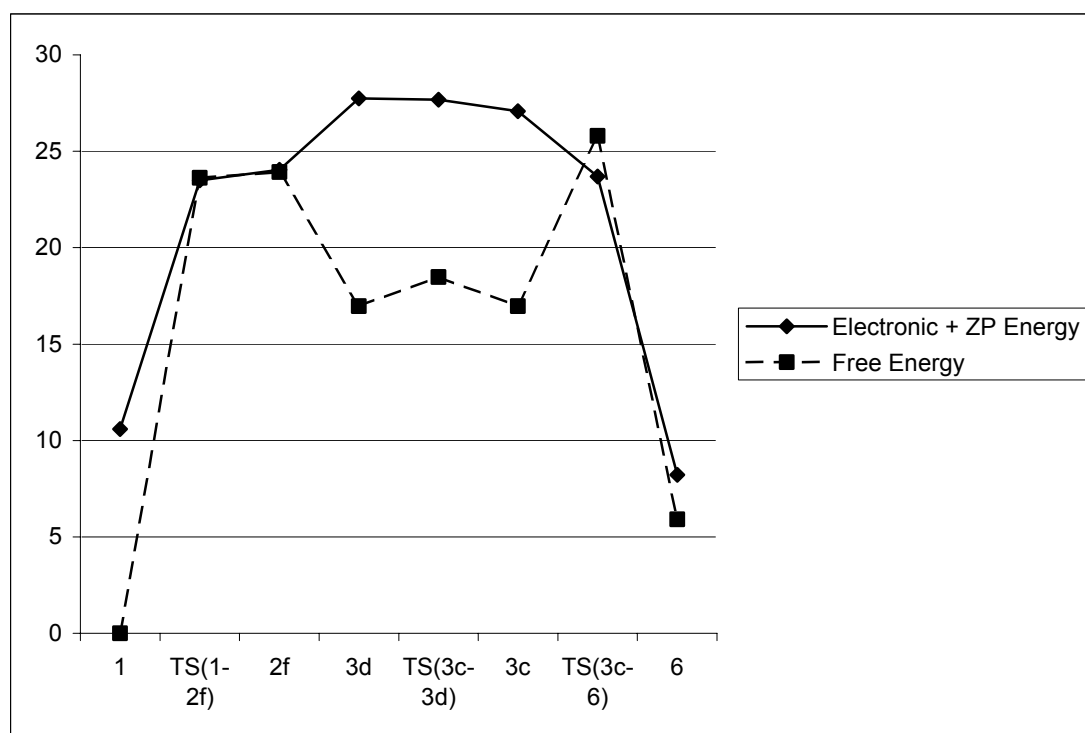


Figure 34. The energy profile of the unproductive pathway. The energy of the structure denoted as **1** on the x-axis of the graph is the sum of the energies of complex **1**, HCN and ethylene. For **2f**, it is the sum of the energies of complex **2f** and ethylene, and so forth.

Comparing this graph with the one in Figure 32, it can be seen that **2f** can either undergo a transition to **2b** or it can undergo ligand dissociation to form **3d**. The free energy activation barrier for the transition to **2b** is 9.20 kcal/mol. Unfortunately, the barrier for ligand dissociation from **2f** could not be obtained, but is expected to be ~5-10 kcal/mol, based on the values obtained for ligand dissociation from **2a** and ligand association to form **5a**. Thus, the unproductive pathway is unlikely to be favored by much, if at all, over the outer pathway. Moreover, any **3d** that does form will easily isomerize to **3c**, given the low free energy barrier between them. Since it has been shown that the energies of both **3a** and **3e** are lower than that of **3c** by a margin of ~14 kcal/mol, and given that isomerization between these species is quicker than the cata-

lytic reaction (McKinney, 1985), it is highly unlikely that **6** will form at all. It should, nevertheless, be interesting if this species could be observed experimentally. To this author's knowledge, this has never been achieved.

(e) The effect of van der Waals stabilizing energy

Thus far, all energies were represented by using the infinite separation mode of representation (see Section 3). However, it is both unrealistic to treat the components of the system at each step as if there are no interactions between them and erroneous to assume that if two or more structures are minima on separate PESs, they will remain as a minimum on a single PES. Therefore, for the inner pathway (Figure 35) the van der Waals energies have also been included where available.

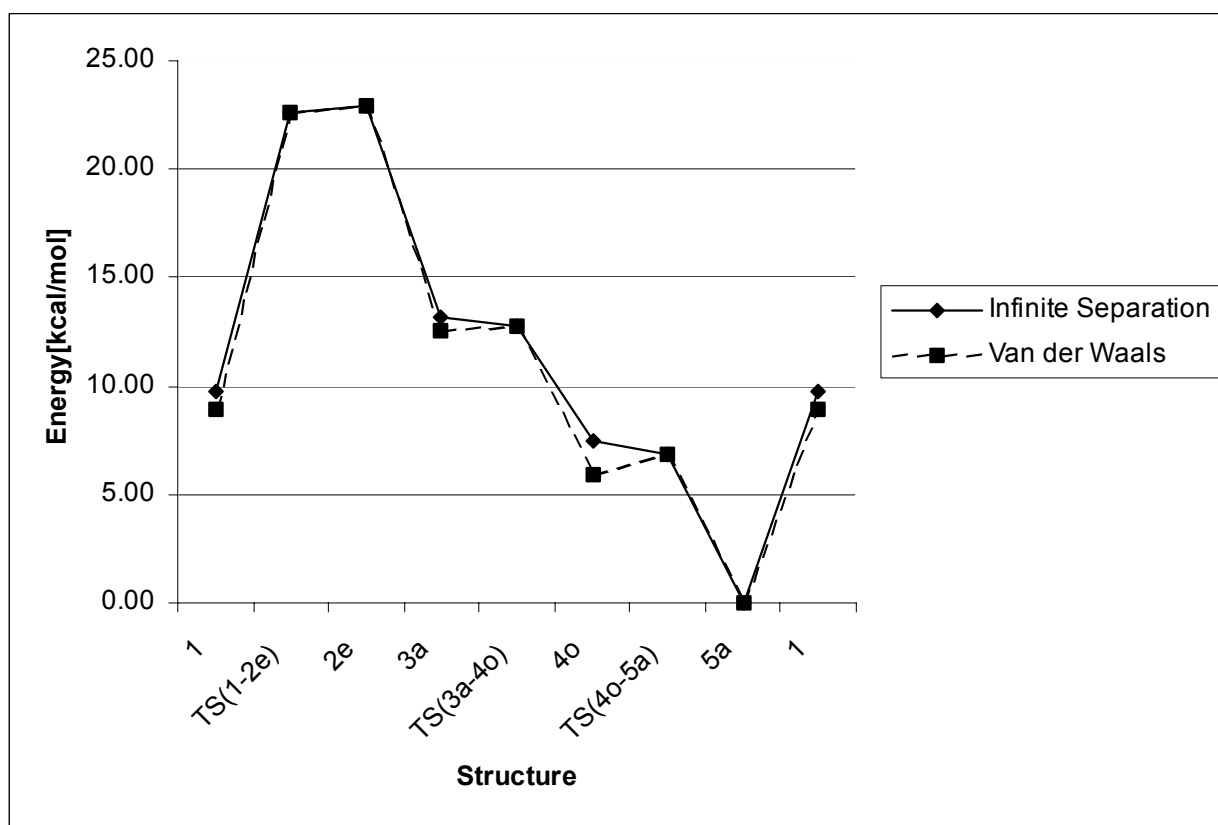


Figure 35. Energy profile for the inner pathway using two modes of representation. For the mode of infinite separation, the energy of the structure denoted as **1** on the x-axis of the graph is the sum of the energies of complex **1**, HCN and ethylene. For **2e**, it is the sum of the energies of complex **2e** and ethylene, and so forth. For the mode of van der Waals energies, the energy of **1** is the sum of the energies of the van der Waals complex **1**-HCN and ethylene, that of **3a** the sum of the energies of **3a**-ethylene and phosphine, and that of **4o** the energy of **4o**-PH₃.

This mode is not as consistent as the first mode, but perhaps more realistic in terms of interacting chemical systems. The differences between the two modes of representation are not dramatic (Figure 35), but significant. The energies of **1** (the sum of the energies of **1** and HCN was replaced with the energy of **1**-HCN), **3a** (the sum of the energies of **3a** and ethylene was replaced by the energy of **3a**-ethylene) and **4o** (the sum of the energies of **4o** and PH₃ was replaced by the energy of **4o**-PH₃) are lowered, while all the other energies remain the same. Although these energy differences are small, nevertheless, they are sufficient to show that the association and dissociation of both phosphine and ethylene are accompanied by distinct transition structures. If it were possible to calculate the geometry and energy of a van der Waals complex consisting of not only two, but all the participating molecules at each point on the cycle, the picture would be even more convincing.

7. Conclusion

This computational study represents a first step in analyzing hydrocyanation of ethylene catalyzed by Ni-complexes by computational means. It was found that the computational results support the mechanism suggested by Tolman and his co-workers (1985) to a large extent. However, the use of computational methods has uncovered new aspects of this reaction system and has also highlighted areas where more experimental work may aid in the understanding of the system.

Understanding of three aspects of this system have been especially enhanced: (i) the participation of only two out of the three possible isomers of the square planar (ethylene)NiHCNL (**3**) in the catalytic cycle; (ii) the fact that oxidative addition is rate-determining in the gas phase, indicating the decisive role of solvent effects; (iii) and the large role played by entropy-effects in the energetics of this reaction, even in the absence of a solvent.

It was found that the only isomers of **3** that participate in the cycle are those two that have ethylene and H coordinated in *cis*-positions relative to one another, so that migration-insertion of ethylene into the Ni-H bond can take place before, or concomitant with, association of a second molecule of ethylene. In no instance could a structure be obtained in which the ethylene that inserted into the Ni-H bond was the incoming molecule. The mechanism is most likely a concerted one, since the formation of a 14-electron fragment (as would be the case were the mechanism a stepwise one) is highly improbable. In the case of the third isomer, association of ethylene leads to the reduc-

tive elimination of HCN and formation of bis(ethylene) nickel phosphine (**6**). However, the energetics of this process probably precludes the formation of **6** and thus far, it has not been observed experimentally in the context of this reaction system.

As shown, oxidative addition of HCN to **1** has a free energy barrier of ~ 4 kcal/mol higher in the gas phase than that of the reductive elimination of propionitrile from **5d**, making oxidative addition the rate-determining step for the outer pathway in the gas phase. Unfortunately, the barrier for reductive elimination could not be obtained for the inner pathway, so that it is unknown whether the same effect would have been observed there. However, this evidence points to the importance of solvent effects in the liquid phase where this reaction is done. Yet, very little has been published in this regard. As mentioned, the reason that the reductive elimination of propionitrile has been experimentally determined as the rate-determining step, is because a polar solvent will increase the acid strength of HCN, making the addition of HCN a two-step ionic process (Tolman, 1985). This might lower the energy barrier decisively. Attempts have been made to replicate this process in gas phase calculations, but they were unsuccessful. It is evident, though, that more work is necessary to elucidate the role of solvents, both computationally and experimentally, especially in the light of the discussion on the effect of phenolic solvents in the work of Taylor and Swift (1972).

It was shown that the effect of entropy is quite pronounced for certain steps of the reaction pathway, especially ligand association and dissociation. Of course, this is not unexpected. However, it is interesting that entropy-effects are even significant in certain intramolecular transitions, such as the transition from **3f** to **3e**.

This study has also raised a few questions that require further investigation. Firstly, the orbitals of phosphine that donate to Ni seem to be centered on Ni itself, which seems rather strange. More work needs to be done to resolve this anomalous result. Secondly, it was only possible to find convincing transition structures for ligand dissociation from **2a** and for ligand association to **5a**. What these two geometries have in common, is that they have both ligands in equivalent positions – *i.e.* they are symmetric with respect to their ligands. This is certainly not expected, and apart, perhaps, from symmetry considerations, there is no obvious reason why this should be so.

This study should be seen as a basis for further computational work on the hydrocyanation of olefins. Apart from the necessary work on solvent effects that were mentioned earlier, the model cycle should also be modeled with a more sterically demanding ligand, since it is known that the steric effects induced by the ligands probably

play a much larger role than their electronic effects (Tolman, 1985). It is true that some work has been done in ligand design, most notable by Van Leeuwen and his co-workers (2004), but they have focused on optimizing ligand bite angles for chelates and mostly on the step of reductive elimination. Thirdly, substrates other than ethylene need to be studied. Sabo-Etienne and his co-workers (2004) have studied the isomerization of coordinated butadiene (see Chapter 2 for details), but again, attention should be paid to the entire cycle. Ideally, it should be possible to obtain, most realistically by means of ONIOM calculations or something similar, optimal ligand-substrate combinations – *i.e.* it could be possible to design ligands to ease the hydrocyanation of substrates for which the conventional ligands are not successful.

Finally, one general conclusion that may be drawn from the present investigation concerns the issue of the representation of relative energies. It was shown that the relative energies of any (catalytic) reaction system may be represented by a number of ways. If all transitions are intramolecular, there is never any ambiguity, since all the species are on the same PES. However, if some of the transitions are intermolecular, the implicit assumption that two structures which are minima on their own separate PESs, will remain a minimum when placed on the same PES at infinite separation, may be erroneous. For this reason, transition structures that may result from, for example ligand dissociation of ML_n , are seldom reported. This is because the energy of the minimum obtained by adding the energies of ML_{n-1} and L will be higher than that of the transition structure. However, if the geometry of the correct van der Waals complex of ML_{n-1} and L could be obtained, that energy will be lower than that of the transition structure. This has been shown for the catalytic cycle under discussion, where the information has been available. The bottom line is that the mode of representation of infinite separation is biased towards presenting the relatively larger molecules in a cycle as having relatively lower energies. It should be kept in mind that real molecules do interact with one another and that it is possible to represent that in calculations – something that might not be feasible experimentally.

V. EFFECTS OF LEWIS ACID CO-CATALYSTS – A PRELIMINARY DISCUSSION

1. Introduction

The addition of a Lewis acid (LA) co-catalyst can have a marked effect on both the selectivity and the rate of catalytic hydrocyanation of olefins, as discussed previously in Chapter 2. The effect obtained depends on the LA employed. It has been shown, with the isolation and characterization of $\text{HNi}[\text{P}(\text{O}-o\text{-tolyl})_3\text{CN}-\text{BPh}_3$ (Tolman, 1985), that LAs such as BPh_3 can coordinate to a nucleophilic center such as a nitrogen atom in the cyanide group of the catalyst. In this manner, the catalyst lifetime is increased, because, when using Ni-catalysts, the formation of insoluble $\text{Ni}(\text{CN})_2$ is prevented. AlCl_3 and ZnCl_2 can accelerate the reaction, whereas BPh_3 slows it down (Tolman, 1984). However, addition of BPh_3 does favor the formation of linear nitriles, presumably due to its steric bulk (Tolman, 1986). The addition of LAs is also thought to enhance the rate of the ionic pathway by increasing the acid strength of HCN when coordinating to nitrogen, thus facilitating addition of H^+ to the Ni catalyst precursor (Tolman, 1985).

The purpose of this chapter is to present some *preliminary* work on the effect of selected LAs on the inner pathway of the full cycle. It is essential to note that the data obtained thus far is not comprehensive and that any forthcoming conclusions are very tentative.

2. Computational details

For general computational details, see section 2 of Chapter 4. The basis set used for all geometry optimizations and frequency calculations (from which the zero-point energy corrections were obtained) is the ECP LANL2DZ (Dunning, 1976; Hay, 1985a-c) on Ni, 6-311G** on N, B and Al, the LANL2DZ ECP augmented with a polarization f -function optimized for Zn (exponent=3.031) according to the method of Frenking (1993) on Zn, and 6-31G(d) (Hehre, 1986) on all other atoms.

3. Results and Discussion

(a) The effect of Lewis acid co-catalysts on the H-CN bond

According to the second bond length variation rule of Gutmann (1978), the coordination of a LA to the nitrogen atom of HCN should result in a shortening of the H-CN bond and a concomitant lengthening of the C≡N bond. According to the present calculations, this is not what happens when BH₃, AlCl₃ and ZnCl₂ coordinate to HCN (Table 1). The only H-CN bond to shorten is that of HCN-BH₃ and by a very small amount. Moreover, the C≡N bond shortens somewhat, which is contrary to expectation. However, these changes are so small that they are probably negligible.

Table 1. Effect of the coordination of Lewis acids (LAs) on H-CN and C-N bond lengths of HCN

	HCN	HCNBH ₃	HCNAlCl ₃	HCNZnCl ₂
H-CN	1.071	1.070	1.074	1.073
C-N	1.152	1.146	1.144	1.146

The electron densities of the bond critical point of the H-CN bond remain constant whether a LA is coordinated or not. It is known that the charge transfer in donor-acceptor complexes containing HCN is very low (Gao, 2001), so this result is hardly surprising. Thus, it can be concluded that the coordination of a LA does not have a significant effect on the acid strength of HCN, keeping in mind, however, that these results were obtained in the gas phase and that solvent effects may certainly play a role. Nonetheless, the result is surprising and counter-intuitive. Unfortunately, nothing could be found in the literature on the effect of coordinating Lewis acids on weak acid strengths. The bonding energies for the bonding of a LA to HCN are 17.29 kcal/mol, 22.69 kcal/mol and 15.93 kcal/mol for BH₃, AlCl₃ and ZnCl₂, respectively. These energies may well be large enough to decrease the energetic span of the cycle.

(b) The effect of Lewis acids on the geometries and energetics of the inner pathway

Geometry and energy optimizations were done for combinations of the minimum energy structures of the inner pathway and selected Lewis acids. The LAs selected were BH₃, AlCl₃ and ZnCl₂, the latter two being chosen because of their accelerating effect on the rate of the reaction.

Addition of a Lewis acid to **2e** does have a noticeable effect on the geometry of the complex (Table 2 and Figure 1) and influences especially the bond lengths.

Table 2. Comparative geometries of **2e** and **2e-LA** complexes, with bond lengths in Å and angles in °

	2e	2e-BH₃	2e-AlCl₃	2e-ZnCl₂
Ni-C1	2.175	2.181	2.203	2.199
Ni-C2	2.146	2.160	2.187	2.181
Ni-P1	2.335	2.319	2.305	2.308
Ni-P2	2.327	2.330	2.335	2.344
Ni-CN	1.885	1.896	1.891	1.889
Ni-H	1.459	1.458	1.462	1.464
C-N	1.170	1.158	1.161	1.163
N-LA	---	1.555	1.918	2.054
C-Ni-C	37.1	36.9	36.4	36.5
P-Ni-P	101.6	101.0	100.6	99.9
P1-Ni-H	85.6	83.0	81.1	82.2
P2-Ni-CN	86.2	88.7	90.1	89.9
C-N-LA	---	178.7	171.0	148.4

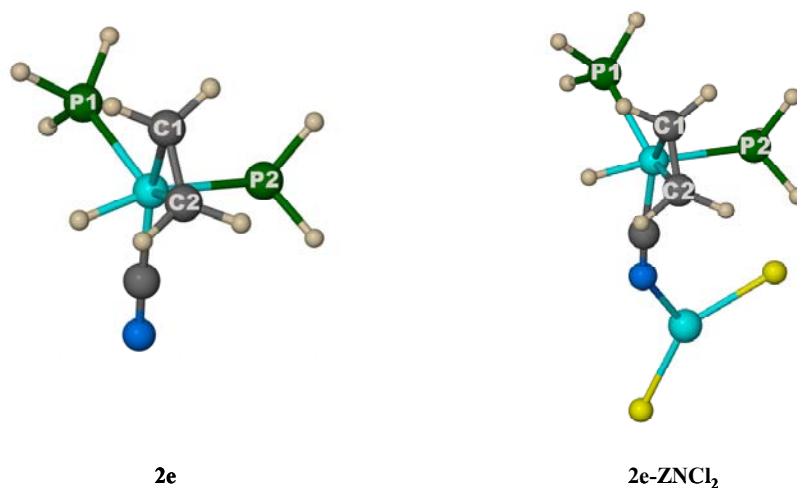


Figure 1. **2e** and **2e-ZnCl₂**

In all cases a slight lengthening of the Ni-ethylene bonds occur, the effect being the largest when the LA is AlCl₃ and the least when the LA is BH₃. The Ni-P1 bond

shortens in all the instances, whereas the Ni-P2 bond lengthens somewhat. The Ni-H bond lengthens very slightly in all the cases. Both the C-Ni-C and P-Ni-P angles decrease by a small amount for all the Lewis acids, but never by more than $\sim 1.5^\circ$. The P1-Ni-H angle decreases by an average amount of 3.6° and the P2-Ni-CN angle increases by an average amount of 2.9° . The Ni-CN bond becomes somewhat longer and the C-N bond shortens. The N-LA bond distance for BH_3 is the shortest at 1.555 \AA and is the longest for ZnCl_2 at 2.054 \AA , as expected. Overall, AlCl_3 and ZnCl_2 seem to have the largest effect on the geometry of **2e**. Interestingly, while the C-N-LA angle for **2e-BH₃**, and **2e-AlCl₃** vary between 171° and 179° , the C-N-Zn angle of **2e-ZnCl₂** is 148.4° . Based on available crystal structures, this is not out of the ordinary. For crystal structures with a Ni-C-N-B arrangement, the C-N-B angle varies between 174.6° and 177.5° , well within the range obtained here (Brunkan, 2004; Lancaster, 1999; Zhou, 2001). For crystal structures with a Ni-C-N-Zn arrangement, the C-N-Zn angle varies between 148.0° and 163.4° (Cernak, J., 1990, 1992; Wilting, 2005; Yuge, 1994), with one example found at 179.1° (Buttner, 1994). Thus, it seems that the smaller C-N-Zn angle is the norm, rather than the exception and the results obtained here confirm the available data. No crystal structures with a Ni-C-N-Al moiety could be found.

The comparative data for the geometries of **3a** and **3a-LA** are summarized in Table 3.

Table 3. Comparative geometries of **3a** and **3a-LA** complexes with bond lengths in \AA and angles in $^\circ$

	3a	3a-BH₃	3a-AlCl₃	3a-ZnCl₂
Ni-C1	1.909	1.903	1.903	1.903
Ni-C2	2.194	2.196	2.193	2.196
Ni-P	2.156	2.166	2.180	2.189
Ni-H	1.763	1.771	1.767	1.772
Ni-CN	1.900	1.911	1.907	1.909
CN	1.164	2.189	1.160	1.163
N-LA	---	1.551	1.925	2.062
C1-Ni-C2	42.1	42.0	42.0	42.0
N-C-LA	---	179.5	172.0	146.2
C1-C2-Ni-H	180.0	180.0	180.0	180.0

Figure 2 shows **3a** and **3a-ZnCl₂**. The changes induced in the geometry of **3a** by the coordination of the LAs are similar in magnitude to what was seen for **2e**. The Ni-C1 bonds are shortened somewhat, whereas the Ni-C2 bonds became a bit longer.

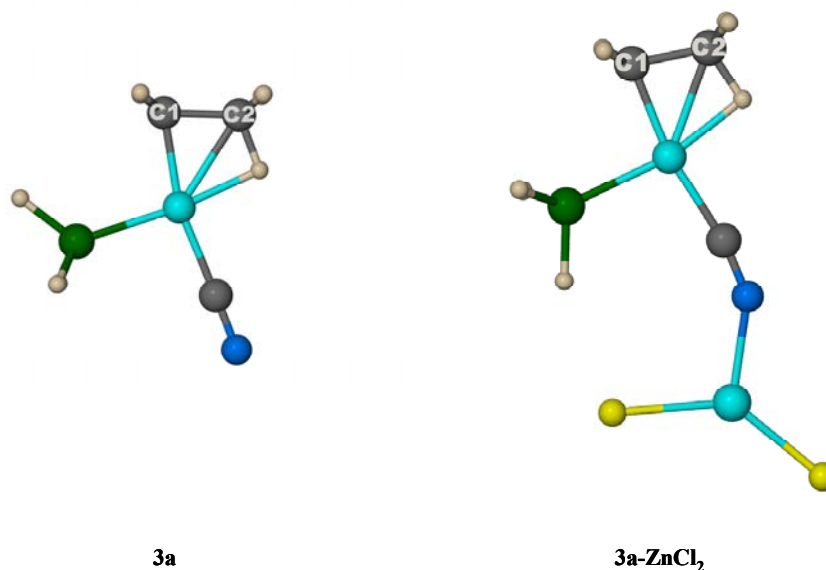


Figure 2. **3a** and **3a-ZnCl₂**

The Ni-H bond also lengthened somewhat, with the result that ethylene with hydrogen are now more like an ethyl group than when **3a** has no LA coordinated to it. The angle C1-Ni-C2 and the dihedral angle C1-C2-Ni-H are virtually unchanged. The Ni-CN bond also lengthened, while the CN bond shortened in all the cases except BH₃ where it became somewhat longer. Again, the N-ZnCl₂ bond is the longest of the N-LA bonds, at 2.062 Å, and the N-BH₃ bond the shortest, at 1.551 Å. It should be noted that there are two possible orientations for ZnCl₂ relative to **3a** – in the same plane as **3a** or perpendicular to the plane defined by **3a**. Both possibilities were explored, but the only one, which led to, an energy minimum is with ZnCl₂ in the same plane as **3a**. As before, the C-N-LA angles vary between 170° and 179° for **3a-BH₃**, **3a-BPh₃** and **3a-AlCl₃**, with the C-N-Zn angle of **3a-ZnCl₂** at 146.2°.

Table 4 shows the comparative data for the geometries of **4o** and **4o-LA**. Comparison with the data for **3a** shows similar trends, with two exceptions: The Ni-Et bonds become shorter (in contrast with the lengthened Ni-H bonds) and the Ni-C2 bonds became longer, due to the absence of coordinated hydrogen. The N-ZnCl₂ bond is the longest of the N-LA bonds and the N-BH₃ the shortest.

Table 4. Comparative geometries of **4o** and **4o-LA** complexes with bond lengths in Å and angles in °

	4o	4o-BH₃	4o-AlCl₃	4o-ZnCl₂
Ni-C1	2.184	2.195	2.209	2.214
Ni-C2	2.189	2.199	2.212	2.217
Ni-P	2.216	2.229	2.241	2.235
Ni-CN	1.943	1.956	1.956	1.951
Ni-Et	1.970	1.963	1.962	1.968
C-N	1.170	1.159	1.161	1.163
N-LA	---	1.553	1.926	2.062
C-N-LA	---	179.9	176.3	152.6
C1-C2-Ni-CN	91.3	90.8	89.9	91.0
CH₃-CH₂-Ni-P	-80.1	-80.9	-82.9	-91.2

Again, two orientations for ZnCl₂ are possible, but based on the results obtained for **3a**, it was assumed that only the in-plane orientation of ZnCl₂ would yield a minimum energy conformation. The geometries of **4o** and **4o-ZnCl₂** are shown in Figure 3. Note again the much smaller C-N-Zn angle when compared to the corresponding angles of the other complexes.

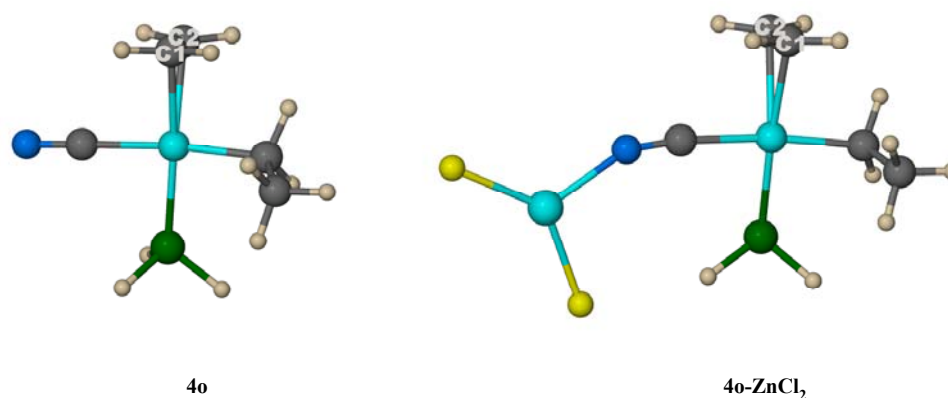


Figure 3. **4o** and **4o-ZnCl₂**

The comparative energy data for **5a** and the **5a-LA** complexes are summarized in Table 5.

Table 5. Comparative geometries of **5a** and **5a-LA** complexes

	5a	5a-BH₃	5a-AlCl₃	5a-ZnCl₂
Ni-C1	2.252	2.277	2.311	2.292
Ni-C2	2.252	2.277	2.311	2.290
Ni-P1	2.258	2.269	2.276	2.272
Ni-P2	2.258	2.269	2.276	2.282
Ni-Et	2.000	1.998	1.999	2.000
Ni-CN	1.950	1.953	1.942	1.948
C-N	1.170	1.159	1.161	1.163
N-LA	---	1.556	1.919	2.062
C-N-LA	---	179.9	176.9	154.8
C1-C2-Ni-P1	4.9	2.3	0.2	0.3
CH ₃ -CH ₂ -Ni-P1	61.8	62.5	64.3	63.6

Quite pronounced lengthening of the Ni-C bonds, as well as the Ni-P bonds occur. Both the NiEt and Ni-CN bonds shortened. The most notable change is the shortening of the C-N bond as a result of the formation of the N-LA bond. The geometries of **5a** and **5a-ZnCl₂** are shown in Figure 4.

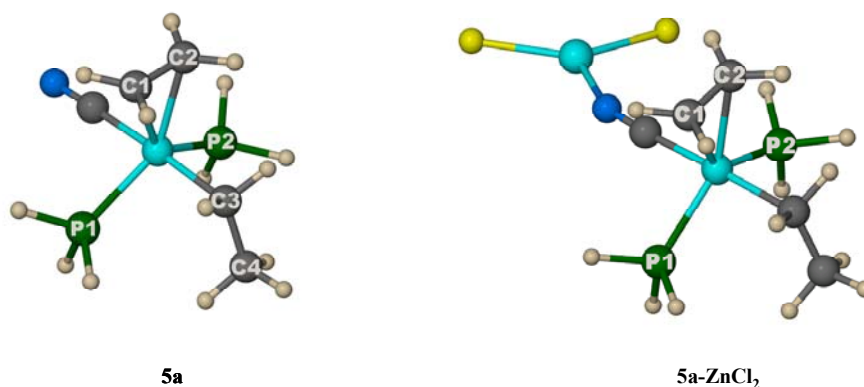


Figure 4. **5a** and **5a-ZnCl₂**

Even though the geometry changes induced by the coordination of the Lewis acids are quite pronounced, it is not possible to draw any conclusions from them at this stage.

Table 6 shows the relative (to the lowest energy species of each series) enthalpies and free energies for each of the minimum energy structures of the inner pathway without a LA; and the same structures coordinated to BH₃, AlCl₃ and ZnCl₂.

Apart from complex **1** (+ HCN-LA + Ethylene), the addition of the LA does not have a large influence on the relative enthalpies of the species involved, with complex **5a** having the lowest relative energy in all cases. With complex **1** the Lewis acid is really bonded to HCN, and it was shown earlier that the bonding energies are quite variable, as is reflected in this data too. This shows that as far as bonding energies are concerned, the addition of a LA has a much larger effect on free HCN in the gas phase than it has on CN⁻ bonded to Ni.

Table 6. Enthalpies and free energies (in kcal/mol) of the minimum energy structures of the inner pathway without a LA; and coordinated to BH₃, AlCl₃ and ZnCl₂. Energies are relative to the lowest energy species in each case.

		No LA	BH ₃	AlCl ₃	ZnCl ₂
1 + HCN-LA*	ΔH	10.60	22.40	35.10	30.00
	+ Ethylene ΔG	0.00	9.20	20.53	15.01
2e -LA	ΔH	23.62	23.40	22.90	22.18
	+ Ethylene ΔG	23.67	20.83	36.65	19.46
3a -LA + PH ₃	ΔH	13.74	12.94	13.96	12.35
	+ Ethylene ΔG	4.01	0.00	0.00	0.00
4o -LA + PH ₃	ΔH	7.84	7.43	8.50	7.49
	ΔG	9.30	5.53	6.32	6.28
5a	ΔH	0.00	0.00	0.00	0.00
	ΔG	12.68	9.83	8.85	15.01

*The notation X-LA denotes that X and LA are bonded to each other, except in the column denoted No LA.

The trends for the free energies are much more variable. Firstly, the presence or absence of any LA has a large effect on the free energy of all the species apart from **5a**, although it is clear that the effect is again the largest for **1**. Moreover, addition of a LA shifts the lowest energy point in the reaction from **1** to **3a**. Among the LAs, the variation in energy is also quite pronounced, although there is no consistent trend.

4. Conclusion

The preliminary data shows that all three LAs investigated have a similar effect on the energetics of the cycle in the gas phase. The only exception is complex **1** and this is due to the variable bonding energy of the different LA-HCN combinations.

It should be noted that the omission of the transition structures from the energetic analysis was deliberate. Apart from the problems of calculating the relative energies consistently (see Chapter 4), obtaining the Lewis acid complexes as transition structures are not straightforward. However, in order to make any definite conclusions on the role of the Lewis acids, it is essential to obtain these structures and work in that regard is still ongoing. Again, the very preliminary nature of this part of the study is emphasized.

The behavior of HCN with Lewis acids is unexpected. It is commonly accepted that the coordination of a Lewis acid to the nitrogen of HCN should increase the acidity of HCN, but, based on the electron density at the bond critical point of the H-C bond, this does not seem to occur. This phenomenon certainly warrants further investigation.

VI. CONCLUSIONS

This computational study supports the experimental work done on the hydrocyanation of ethylene. The most important conclusions can be summarized as follows:

- Migration-insertion of ethylene into the Ni-H bond takes place before, or concomitant with coordination of a second molecule of ethylene in the third step of the proposed cycle
- Oxidative addition of HCN is rate-determining in the gas phase, whereas reductive elimination of propionitrile is rate-determining in the liquid phase, pointing to the importance of solvent effects
- Entropy-effects play a decisive role in the gas-phase energetics of this reaction

The most important questions raised by this study are

- Why does the orbitals of phosphine that donate to Ni seem to be centered on Ni itself?
- Why could transition structures for ligand dissociation/association only be obtained from structures that are symmetric with respect to phosphine?
- Why does the strength of the H-CN bond – and therefore the acidity of HCN – not seem to be affected by the coordination of a Lewis acid, is counter to expectation?

These questions raise issues of a general nature. Despite thorough searches of the literature, no light could be shed on these phenomena and they certainly warrant further investigation.

Further work needs also to be done in the following areas:

- Experimental results and computations are needed to better understand the effects of different solvents on the rate and selectivity of this reaction. The effects of phenolic solvents are not understood at all and investigation in that direction should yield interesting results.
- More complete computational studies involving the role of solvents are also necessary to model the two-step oxidative addition that depends on the polarity of the solvent and cannot be replicated in the gas phase. This will enable comparison between the one-step and the two-step processes.

- Further computational modeling is necessary for sterically demanding ligands; it has been suggested that the steric effects of the “non-active” ligands are much more important than their electronic effects in homogeneously catalyzed hydrocyanation.

Finally, it was pointed out that there are different modes of representation of relative energies: an infinite separation approach and a Van der Waals approach. The infinite separation approach tends to bias relative energies towards lower energies for larger molecules by not taking into account the interactions between molecules. The Van der Waals approach does take into account the interactions between molecules. These interactions are more quantifiable computationally than experimentally – at least for systems with only two interacting entities. The literature typically reports combinations of these two approaches, without discriminating between the two explicitly. Such an approach could lead to ambiguity and it is important that the distinction be made explicitly.

REFERENCES

- Arndt, P., Baumann, W., Spannenberg, A., 2003. *Angew. Chem., Int. Ed.* **42**, 1414.
- Arthur, P., Jr., England, D.C., Pratt, B.C., 1954. *J. Am. Chem. Soc.* **76**, 5364.
- Bäckvall, J.-E., Andell, O.S., 1981. *J. Chem. Soc. Chem. Commun.*, 1098.
- Bader, R.F.W., 1990. *Atoms in Molecules: A Quantum Theory*, Clarendon Press, Oxford. See also www.chemistry.mcmaster.ca/aimpac
- Barbour, L.J., 2003. *J. Supramol. Chem.* **1**, 189.
- Becke, A.D., 1983. *J. Chem. Phys.* **98**, 5648.
- Becke, A.D., 1988. *Phys. Rev. A* **38**, 3098.
- Bickelhaupt, F.M., Ziegler, T., Schleyer, P.v.R., 1995. *Organometallics* **14**, 2288.
- Bottoni, A., Carvajal, M.A., Miscione, G.P., 2005. *Organometallics* **24**, 2086.
- Brookhart, M., Svejda, S.A., 1999. *Organometallics* **18**, 65.
- Brown, E.S., Rick, E.A., 1969. *J. Chem. Soc. Chem. Commun.*, 112.
- Brown, E.S., Rick, E.A., Mendicino, F.D., 1972. *J. Organomet. Chem.* **38**, 37.
- Brown, E.S., 1974. *Asp. Homogen Catal.* **2**, 57.
- Brunkan, N.M., Brestensky, D.M., Jones, W.D., 2004. *J. Am. Chem. Soc.* **123**, 223.
- Brunkan, N.M., Brestensky, D.M., Jones, W.D., 2004. *J. Am. Chem. Soc.* **126**, 3627.
- Cernak, J., Potocnak, I., Chomic, J., 1990. *Acta Crystut. C* **46**, 1098.
- Cernak, J., Potocnak, I., Petricek, V., 1992. *J. Inclusion Phenom. Macrocyclic Chem.* **14**, 73.
- Chatt, J., Duncanson, L.A., 1953. *J. Chem. Soc.*, 2939.
- Chaumonnot, A., Lamy, F., Sabo-Etienne, S., 2004. *Organometallics* **23**, 3363.
- Cheung, A.S.-C., Tong, G.S.M., Jeung, G.H., 2003. *J. Chem. Phys.* **118**, 9224.
- Chetchuti, M.J., Herbert, J.A., Howard, J.A.K., 1981. *J. Chem. Soc., Dalton Trans.*, 284.
- Cotton, F.A., Wilkinson, G., 1998. *Advanced Inorganic Chemistry, 5th Ed.*, Wiley, New York.
- Cramer, C.J., 2002. *Essentials of Computational Chemistry: Theories and Models*, Wiley, New York.
- Dewar, J.S., 1951. *Bull. Soc. Chim. Fr.* **18**, C71.
- Dillen, J.L.M., 1995. *J. Comput. Chem.* **16**, 595.
- Drinkard, W.C., Eaton, D.R., Jesson, J.P., 1970. *Inorg. Chem.* **9**, 329.
- Druliner, J.D., 1984. *Organometallics* **3**, 205.

- Dunning, T.H., Jr., Hay, P.J., 1976. *Modern Theoretical Chemistry* (Ed. Schaefer III, H.F.) Vol 3, Plenum, New York.
- Eaton, C.R., McGlinchey, M.J., Moffat, K.A., 1984. *J. Am. Chem. Soc.* **106**, 8110.
- Erker, G., Fromberg, W., Angermund, K., 1986. *Chem. Commun.*, 372.
- Ermer, O., 1981. *Aspekte von Kraftfeldrechnungen*, Bauer-Verlag, Munich.
- Favero, G., Turco, A., 1976. *J. Organomet. Chem.* **105**, 389.
- Favero, G., Gaddi, M., Morvillo, A., 1978. *J. Organomet. Chem.* **149**, 395.
- Foresman, J.B., Frisch, Æ., 1996. *Exploring Chemistry with Electronic Structure Methods*, Second Ed., Gaussian, Pittsburgh.
- Frenking, G., Höllwart, A., Böhme, M., 1993. *Chem. Phys. Lett.* **208**, 237.
- Frenking, G., Dapprich, S., 1995. *J. Phys. Chem.* **99**, 9352.
- Frenking, G., Torrent, M., Solà, M., 2000. *Chem. Rev.* **100**, 439.
- Frisch, M. J., Trucks, G. W., Schlegel, H. B., Scuseria, G. E., Robb, M. A., Cheeseman, J. R., Montgomery, Jr., J. A., Vreven, T., Kudin, K. N., Burant, J. C., Millam, J. M., Iyengar, S. S., Tomasi, J., Barone, V., Mennucci, B., Cossi, M., Scalmani, G., Rega, N., Petersson, G. A., Nakatsuji, H., Hada, M., Ehara, M., Toyota, K., Fukuda, R., Hasegawa, J., Ishida, M., Nakajima, T., Honda, Y., Kitao, O., Nakai, H., Klene, M., Li, X., Knox, J. E., Hratchian, H. P., Cross, J. B., Adamo, C., Jaramillo, J., Gomperts, R., Stratmann, R. E., Yazyev, O., Austin, A. J., Cammi, R., Pomelli, C., Ochterski, J. W., Ayala, P. Y., Morokuma, K., Voth, G. A., Salvador, P., Dannenberg, J. J., Zakrzewski, V. G., Dapprich, S., Daniels, A. D., Strain, M. C., Farkas, O., Malick, D. K., Rabuck, A. D., Raghavachari, K., Foresman, J. B., Ortiz, J. V., Cui, Q., Baboul, A. G., Clifford, S., Cioslowski, J., Stefanov, B. B., Liu, G., Liashenko, A., Piskorz, P., Komaromi, I., Martin, R. L., Fox, D. J., Keith, T., Al-Laham, M. A., Peng, C. Y., Nanayakkara, A., Challacombe, M., Gill, P. M. W., Johnson, B., Chen, W., Wong, M. W., Gonzalez, C., and Pople, J. A., 2003. *Gaussian 03 (Revision B.05)*, Gaussian, Inc., Pittsburgh PA.
- Gao, J., Mo, Y., 2001. *J. Phys. Chem. A* **105**, 6530.
- Griffiths, D.J., 1995. *Introduction to Quantum Mechanics*, Prentice Hall, Upper Saddle River, New York.
- Guggenberger, L.J., 1973. *Inorg. Chem.* **12**, 499.
- Guggenberger, L.J., 1974. *Inorg. Chem.* **12**, 499.
- Gutmann, V., 1978. *The Donor-Acceptor Approach to Molecular Interactions*, Plenum Press, New York, p. 12.

- Hay, P.J., Wadt, W.R., 1985a. *J. Chem. Phys.* **82**, 270.
- Hay, P.J., Wadt, W.R., 1985b. *J. Chem. Phys.* **82**, 284.
- Hay, P.J., Wadt, W.R., 1985c. *J. Chem. Phys.* **82**, 299.
- Hehre, W.J., Radom, L., Schleyer, P.R., Pople, J.A., 1986. *Ab Initio Molecular Orbital Theory*, Wiley, New York.
- Hodgson, M., Parker, D., Taylor, R.J., 1988. *Organometallics* **7**, 1761.
- Horacek, M., Stepnicka, P., Kubista, J., 2004. *Organometallics* **23**, 3388.
- Horrocks, W.D., Jr., Taylor, R.C., 1963. *Inorg. Chem.* **2**, 723.
- Howard, J.A.K., Mitprachachon, P., Roy, A., 1982. *J. Organomet. Chem.* **235**, 375.
- Hubert, A.J., Puentes, E., 1983. *Catalysis in Cl Chemistry* (Ed: W. Keim), Reidel, Dordrecht.
- Huthmacher, K., Krill, S., 2002. in *Applied Homogeneous Catalysis with Organometallic Compounds Vol. 1* (Ed: B. Cornils), Wiley-VCH, Berlin, p.468.
- Ibers, J.A., Davis, B.R., Payne, N.C., 1969. *Inorg. Chem.* **8**, 2719.
- Jackson, W.R., Perlmutter, P., Elmes, P.S., 1984. in *Organic Synthesis Interdisciplinary Challenge* (Ed: H. Prinsbach), p. 55.
- Jackson, W.R., Thompson, R.J., Haarbarger, D., 1987. *Aust. J. Chem.* **40**, 1083.
- Jolly, P.W., Wilke, G., 1974. In *The Organic Chemistry of Nickel*, Vol. 1, Academic Press, New York.
- Kamer, P.C.J., Van Leeuwen, P.W.N.M., Reek, J.N.H., 2001. *Acc. Chem. Res.* **34**, 895.
- Keim, W., Behr, A., Bioul, J.P., 1982. *Erdöl, Kohle, Erdgas, Petrochemie* **35**, 436.
- Keim, W., 1990. *Angew. Chem., Int. Ed. Engl.* **29**, 235.
- Koch, W., Holthausen M.C., 2000. *A Chemist's Guide to Density Functional Theory*, Wiley-VCH, Weinheim.
- Krüger, C., Tsay, Y.-H., 1972. *J. Organomet. Chem.* **34**, 387.
- Laing, M., Kruger, G., Du Preez, A.L., 1974. *J. Organomet. Chem.* **82**, C40.
- Lancaster, S.J., Walker, D.A., Thornton-Pett, M., 1999. *Chem. Commun.*, 1533.
- Lautens, M., Ma, S., Chiu, P., 1997. *J. Am. Chem. Soc.* **119**, 6478.
- Lee, C., Yang, W., Parr, R.G., 1988. *Phys. Rev. B* **37**, 785.
- Levine, I.N., 2000. *Quantum Chemistry*, 5th Ed., Prentice Hall, Upper Saddle River, New York.
- Lewars, E., 2003. *Computational Chemistry: Introduction to the Theory and Applications of Molecular and Quantum Mechanics*, Kluwer, Dordrecht.

- Louie, J., Gibby, J.E., Farnworth, M.V., 2002. *J. Am. Chem. Soc.* **124**, 15188.
- McKinney, R.J., 1985a. *Organometallics* **4**, 1142.
- McKinney, R.J., Roe, D.C., 1985b. *J. Am. Chem. Soc.* **107**, 261.
- McKinney, R.J., Roe, D.C., 1986. *J. Am. Chem. Soc.* **108**, 5167.
- McKinney, R.J., Nugent, W.A., 1989. *Organometallics* **8**, 2871.
- Moloy, K.G., Marcone, J.E., 1998. *J. Am. Chem. Soc.* **120**, 8527.
- Montgomery, J., 2001. In *Science of Synthesis (Houben-Weyl Methods of Molecular Transformations)*, Vol. 1 (Eds: B.M.Trost, M. Lautens), Thieme, Stuttgart, 2001.
- Montgomery, J., 2004. *Angew. Chem., Int. Ed. Engl.* **43**, 3890.
- Nickel, T., Goddard, R., Krüger, C., 1994. *Angew. Chem., Int. Ed. Engl.* **33**, 879.
- Ochterski, J.W., 2000. *Thermochemistry in Gaussian*, www.gaussian.com/g_whitepap/thermo.htm
- Pearson, R.G., Meier, M., Basolo, F., 1969. *Inorg. Chem.* **8**, 795.
- Perdew, J.P., 1986. *Phys. Rev. B*, **33**, 3322.
- Puentes, E., Mamalis, I., Noels, A.F., 1983. *J. Catal.* **82**, 364.
- Radom, L., Chan, B., 2005. *J. Am. Chem. Soc.* **127**, 2443.
- Raetiger, J.W., Miedaner, A., Curtis, C.J., 2004. *J. Am. Chem. Soc.*, **126**, 5502.
- RajanBabu, T.V., Casalnuovo, A.L., 1996. *J. Am. Chem. Soc.* **118**, 6325.
- RajanBabu, T.V., Radetich, B., 1998. *J. Am. Chem. Soc.* **120**, 8007.
- Rzepa, H.S., Marshall, E.L., Gibson, V.C., 2005. *J. Am. Chem. Soc.* **127**, 6048.
- Sabo-Etienne, S., Chaumonnot, A., Lamy, F., 2004. *Organometallics* **23**, 3363.
- Scott, A.P., Radom, L., 1996. *J. Phys. Chem.* **100**, 16502.
- Schrauzer, G.N., 1960. *J. Chem. Soc.* **82**, 1008.
- Schunn, R.A., 1970. *Inorg. Chem.* **9**, 393.
- Shaik, S., Kozuch, S., Amatore, C., 2005. *Organometallics* **24**, 2319.
- Shriver, D.F., 1970. *Acc. Chem. Res.* **3**, 231.
- Szabo, A. Ostlund, N.S., 1989. *Modern Quantum Chemistry: Introduction to Advanced Electronic Structure Theory*, Dover Publications, Mineola, New York.
- Takano, K., Tsumura, H., Nakazawa, H., 2000. *Organometallics* **19**, 3323.
- Tatsumi, K., Nakamura, A., Komiya, S., 1984. *J. Am. Chem. Soc.* **106**, 8181.
- Taylor, B.W., Swift, H.E., 1972. *J. Catal.* **26**, 254.
- Thiel, W., Goossen, L.J., Koley, D., 2005. *Organometallics* **24**, 2398.
- Tolman. C.A., 1970a. *J. Am. Chem. Soc.* **92**, 2953.
- Tolman. C.A., 1970b. *J. Am. Chem. Soc.* **92**, 2956.

- Tolman, C.A., Gosser, L.W., 1970c. *Inorg. Chem.* **9**, 2350.
- Tolman, C.A., Seidel, W.C., 1970d. *Inorg. Chem.* **9**, 2354.
- Tolman, C.A., 1970e. *J. Am. Chem. Soc.* **92**, 4217.
- Tolman, C.A., 1970f. *J. Am. Chem. Soc.* **92**, 6777.
- Tolman, C.A., 1971. *Inorg. Chem.* **10**, 1540.
- Tolman, C.A., 1972a. *Chem. Soc. Rev.* **1**, 337.
- Tolman, C.A., 1972b. *Inorg. Chem.* **11**, 3128.
- Tolman, C.A., 1972c. *J. Am. Chem. Soc.* **94**, 2994.
- Tolman, C.A., Seidel, W.C., Gosser, L.W., 1974a. *J. Am. Chem. Soc.* **96**, 53.
- Tolman, C.A., Seidel, W.C., 1974b. *J. Am. Chem. Soc.* **96**, 2774.
- Tolman, C.A., 1974c. *J. Am. Chem. Soc.* **96**, 2780.
- Tolman, C.A., 1976a. *J. Organomet. Chem.* **117**, C30.
- Tolman, C.A., Druliner, J.D., English, A.D., 1976b. *J. Am. Chem. Soc.* **98**, 2156.
- Tolman, C.A., 1977. *Chem. Rev.* **77**, 313.
- Tolman, C.A., Seidel, W.C., Druliner, J.D., 1984. *Organometallics* **3**, 33.
- Tolman, C.A., McKinney, R.J., Seidel, W.C., 1985. *Adv. Cat.* **33**, 1.
- Tolman, C.A., 1986. *J. Chem. Ed.* **63**, 199.
- Van Leeuwen, P.W.N.M., Kamer, P.C.J., Reek, J.N.H., 2001. *Acc. Chem. Res.* **34**, 895.
- Van Leeuwen, P.W.N.M., 2004. *Homogeneous Catalysis: Understanding the Art*, Kluwer, Dordrecht.
- Vogt, D., Wilting, J., Müller, C., 2005. *Organometallics* **24**, 13.
- Wender, P.A., Nuss, J.M., Smith, D.B., 1997. *J. Org. Chem.* **62**, 4908.
- Wender, P.A., Smith, T.E., 1998. *Tetrahedron* **54**, 1255.
- Wilke, G., Jolly, P.W., Heimbach, P., 1970. *Adv. Organomet. Chem.* **8**, 29.
- Wilke, G., 1988. *Angew. Chem., Int. Ed. Engl.* **27**, 185.
- Wilting, J., Muller, C., Hewat, A.C., 2005. *Organometallics* **24**, 13.
- Wulfsberg, G., *Principles of Descriptive Inorganic Chemistry*, Brooks/Cole, Monterey, CA.
- Yuge, H., Iwamoto, J., 1994. *J. Chem. Soc. Dalton Trans.*, 1237.
- Zhou, J., Lancaster, S.J., Walker, D.A., 2001. *J. Am. Chem. Soc.* **126**, 223.
- Ziegler, T., Autschbach, J., 2005. *Chem. Rev.* **105**, 2695.

Key

Red: Inner pathway

Black: Outer pathway

Blue: Unproductive Pathway

